2014

The Biogeochemistry of iron, zinc and cobalt in the Atlantic Ocean: the Atlantic Meridional Transect and UK GEOTRACES sections

Wyatt, Neil

THE BIOGEOCHEMISTRY OF IRON, ZINC AND COBALT IN THE ATLANTIC OCEAN: THE ATLANTIC MERIDIONAL TRANSECT AND UK GEOTRACES SECTIONS

by

NEIL JOHN WYATT

A thesis submitted to the University of Plymouth
in partial fulfilment for the degree of

DOCTOR OF PHILOSOPHY

School of Geography, Earth and Environmental Sciences
Faculty of Science and Environment

January 2014

THE BIOGEOCHEMISTRY OF IRON, ZINC AND COBALT IN THE ATLANTIC OCEAN: THE ATLANTIC MERIDIONAL TRANSECT AND UK GEOTRACES SECTIONS

Neil John Wyatt

Between 40 % and 50 % of the Earth's primary production occurs in marine environments, primarily by phytoplankton. The trace metal micronutrients iron, zinc and cobalt are known to exert a significant biological control on phytoplankton productivity by serving as essential active centres in enzymatic processes such as inorganic carbon, nitrogen and phosphorus acquisition. The distributions and biogeochemistries of iron, zinc and cobalt therefore, have the potential to impact upon the global carbon cycle and hence climate. This research involves investigations into the biogeochemical cycling of iron, zinc and cobalt in the Atlantic Ocean.

Iron measurements were conducted during October and November 2009 to determine the distribution and biogeochemistry of iron in the upper water column of the Atlantic Ocean along an Atlantic Meridional Transect (*AMT*-19). In addition, deck board incubation experiments were performed to establish the role of iron in controlling rates of di-nitrogen (N_2) fixation in the North Atlantic. The distribution patterns and biogeochemistries of iron, zinc and cobalt in the South Atlantic at 40° S were determined during the UK GEOTRACES Section GA10 cruises of October 2010 and December 2011 to January 2012.

Iron distributions in North Atlantic surface waters were primarily controlled by the transport and deposition of atmospheric dust particles. In the North Atlantic, elevated surface dissolved iron concentrations (0.50 - 1.65 nM) were associated with wet and dry deposition of Saharan dust between 4 and 29° N. To the south of 4° N, surface dissolved iron concentrations were markedly reduced (0.14 nM) indicating that high precipitation rates in the Inter-Tropical Convergence Zone (4 - 10° N) formed a barrier to the large-scale transport of Saharan dust particles, thus iron, to the South Atlantic. Here, the low surface dissolved iron concentrations were balanced by a total dissolvable iron flux out of the surface mixed layer (3.2 μmol m^{-2} y^{-1}) that was comparable to atmospheric input estimates. Nitrogen fixation rates in the North Atlantic were highest (0.3 – 1.1 nmol L^{-1} d^{-1}) where surface dissolved iron concentrations were elevated (1.02 nM) and decreased with increasing latitude as iron decreased. Hence, iron variability in the North Atlantic was sufficient to influence nitrogen fixation over a large spatial scale.

In the South Atlantic Ocean at 40° S, the vertical and horizontal distributions of dissolved zinc and cobalt showed distinct gradients associated with the water masses present. Zinc concentrations ranged from 15 pM in open ocean surface waters to 8 nM in Antarctic Bottom Waters, whilst cobalt ranged from 2 pM to 80 pM in intermediate waters and was scavenged in deeper waters. Growth limiting mixed layer zinc concentrations resulted from the lack of a direct return path for zinc to the South Atlantic pycnocline with Sub-Antarctic Mode Water. Low zinc in this return path was identified by a linear correlation between zinc and soluble reactive phosphorus that showed a kink at ~ 500 m, much deeper than that observed in other oceanographic regimes. A seasonal study in the Southeast Atlantic revealed that the depletion of zinc over spring-summer periods resulted in an increase in the nutritional importance of cobalt and a shift towards phytoplankton with a cellular preference for cobalt over zinc and/or the ability to co-substitute these two trace metals at the molecular level.

These key findings demonstrate the physico-chemical and biological influences that interact to control the distributions and biogeochemistries of iron, zinc and cobalt across diverse oceanographic regimes of the Atlantic Ocean, provide the first examination of zinc and cobalt biogeochemistries along the productive 40° S parallel and highlight the need for additional research in this region.

CONTENTS

FIGURES

TABLES

ACRONYMS

Analytical / Experimental

Fe	Iron
Zn	Zinc
Co	Cobalt
Cd	Cadmium
Al	Aluminium
dFe	Total dissolved iron
TDFe	Total dissolvable iron
CSV	Cathodic stripping voltammetry
FIA	Flow injection analysis
FI-CL	Flow injection with chemiluminescence detection
FI-FL	Flow injection with fluorescence detection
FI-spec	Flow injection with spectrophotometric detection
ICP-MS	Inductively Coupled Plasma Mass Spectrometry
LDPE	Low density polyethylene
HDPE	High density polyethylene
HCl	Hydrochloric acid
UHP	Ultra high purity
UpA	Ultra pure acid
SpA	Super pure acid

Oceanographic

AMT	Atlantic Meridional Transect
BATS	Bermuda Atlantic Time-series Station
CO_2	Carbon dioxide
CTD rosette	Conductivity, temperature and density probes mounted on a frame that holds water column sampling

	bottles
DIC	Dissolved inorganic carbon
DOC	Dissolved organic carbon
PIC	Particulate inorganic carbon
POC	Particulate organic carbon
GEOTRACES	An international study of marine biogeochemical cycles of trace elements and their isotopes
GEOTRACES GD	GEOTRACES deep (1000 m) seawater reference samples
GEOTRACES GS	GEOTRACES surface seawater reference samples
SAFe	Sampling and Analysis of Fe
SAFe D	SAFe deep (1000 m) seawater reference samples
SAFe S	SAFe surface seawater reference samples
SOLAS	Surface Ocean Lower Atmosphere Study
HNLC	High Nutrient, Low Chlorophyll
ITCZ	Intertropical Convergence Zone
N_2	Dinitrogen
O_2	Oxygen
PAR	Photosynthetically active radiation

Biogeochemical Provinces and water masses

NADR	North Atlantic Drift Region
NATL	North Atlantic Gyre
NATR	North Atlantic Tropical Gyre
WTRA	Western Tropical Atlantic
SATL	South Atlantic Gyre
SSTC	South Sub-Tropical Convergence
AAIW	Antarctic Intermediate Water
AABW	Antarctic Bottom Water

LCDW	Lower Circumpolar Deep Water
NADW	North Atlantic Deep Water
UCDW	Upper Circumpolar Deep Water
SAMW	Sub-Antarctic Mode Water
SASW	Sub-Antarctic Surface Water
STSW	Sub-Tropical Surface water
WSDW	Weddell Sea Deep Water

AUTHORS DECLARATION

At no time during the registration for the degree of Doctor of Philosophy has the author been registered for any other University award without prior agreement of the graduate committee.

Work submitted for this research degree at the University of Plymouth has not formed part of any other degree either at the University of Plymouth or at any other establishment.

This study was financed with the aid of a studentship from the Natural Environmental Research Council (Studentship number NE/G52388X/1) at the University of Plymouth and carried out in collaboration with Plymouth Marine Laboratory.

The work in this thesis was primarily the work of the author unless acknowledged otherwise. Relevant scientific seminars and conferences were attended at which work was presented, research cruises were undertaken, external institutions were visited for experience and knowledge transfer and several papers prepared for publication.

Word count of main body of thesis

49,688 words

Signed……..

Date…….

ACKNOWLEDGEMENTS

I am eternally grateful to my supervisors, Prof. Maeve Lohan, Prof. Paul Worsfold and Dr. Andrew Rees. In particular to Maeve, your guidance, support and faith in me over the course of my study has been inspirational. Thank you Paul for your analytical and editorial expertise and also your calming influence. A huge thank you to Andy for supervising me during my first steps into the world of science at sea.

I would like to say a big thank you to the members of the Biogeochemistry Research Centre past and present. A special thanks to Angie and Rachel for passing on their trace metal expertise and to Jane Eagling for guiding me through both the great and the more difficult times. Thanks to Luke, Dave, Kate, Claire, Matt, Simon, Patricia, and all others I have missed, for your friendship, laughs and support.

My gratitude to the people I've been lucky enough to meet on research cruises, conferences and during laboratory exchanges for your friendship and the opportunities you have given me. My thanks to the captains and crews of the ships involved during my research for their excellent shipboard support. To Andy Arnold, Claire Williams and Jeremy Clark, thank you for sharing your technical expertise at the University of Plymouth.

To my family: Mum and Dad, for everything… I could not have done this without you. Your love, support and wisdom have never wavered through the ups and downs and I am indebted to you. I love you. Thank you Jo for being an incredible housemate and Hayley for being a wonderful girlfriend.

This funding for the research conducted in this thesis was provided by a National Environmental Research Council whilst my thanks also extend to the Marine Institute at the University of Plymouth for financial help towards attending conferences and training workshops.

PUBLICATIONS

Peer reviewed

Wyatt, N.W., Milne, A., Woodward, E.M.S., Rees, A.P., Browning, T.J., Bouman, H.A., Worsfold, P.J. & Lohan, M.C. (2014), **Biogeochemical cycling of dissolved zinc along the GEOTRACES South Atlantic transect GA10 at 40º S**, *Global Biogeochemical Cycles*, DOI: 10.1002/2013GB004637.

Other publications

Wyatt, N. (2009**), Carbon Biogeochemistry Workshop, Bergen, Norway**. Challenger Wave: Newsletter of the Challenger Society for Marine Science, April 2009, p7.

PRESENTATIONS AND CONFERENCES ATTENDED

Jan 2009: Integrated Marine Biogeochemistry and Ecosystem Research (IMBER) Conference, University of Plymouth, Plymouth, UK. The effects of high CO_2 on the fixed nitrogen inventory of the Western English Channel (poster presentation).

Feb 2009: European Project on Ocean Acidification (EPOCA) workshop, Bergen, Norway. The effects of high CO_2 on the fixed nitrogen inventory of the Western English Channel (poster presentation).

Apr 2009: Plymouth Ocean Acidification Meeting, University of Plymouth, UK. The effects of climate change on iron speciation and rates of nitrogen fixation (oral presentation).

Sep 2012: 15th biennial Challenger Conference for Marine Science, University of East Anglia, Norwich, UK (attended).

Dec 2012: 4th Annual Biogeochemistry Research Conference, University of Plymouth, UK. The distribution of dissolved zinc in the South Atlantic as part of the UK GEOTRACES Programme (oral presentation).

Dec 2012: Plymouth Marine Science and Education Foundation Conference, Plymouth Marine Laboratory Marine Matters Centre, Plymouth, UK. The distribution of dissolved zinc in the South Atlantic as part of the UK GEOTRACES Programme (oral presentation).

CO-AUTHORED PRESENTATIONS

Mar. 2012: Dall'Olmo, G., Boss, E., Behrenfeld, M., Westbury, T., Wyatt, N.J., Lohan, M.C., Rees, A.P. Optical scattering during AMT-19: horizontal, temporal and vertical variability. Invited talk, University of Plymouth, UK (oral presentation).

Sep. 2012: Worsfold, P.J., Ussher, S., Shelley, R.U., Séguret, M., Wyatt, N.J., Cabedo-Sanz, P., Clough, R., Nimmo, M., Lohan, M.C. Investigating the chemistry of the oceans using flow injection with luminescence detection. 12th International Conference on Flow Analysis. Thessaloniki, Greece (keynote lecture).

Feb. 2013: Lohan, M.C., Wyatt, N.J., Milne, A., Woodard, E.M., Schlosser, C., Klar, J. Biogeochemical cycling of dissolved zinc and cobalt along 40° S GEOTRACES transect. Ocean Sciences. New Orleans, USA (oral presentation).

Aug. 2013: Lohan, M.C., Wyatt, N.J., Milne, A., Woodward E.M. Biogeochemical cycle of dissolved zinc and cobalt in the South Atlantic. Goldschmidt. Florence, Italy (oral presentation).

RESEARCH EXPERIENCE

Oct. 2008: Laboratory-based teaching methods and practice course (code: ENV5101) at the University of Plymouth, UK.

Feb. 2009: European Project on Ocean Acidification (EPOCA) workshop: Fundamentals of carbon biogeochemistry, Bergen, Norway. A three day workshop detailing theoretical and practical approaches to carbon biogeochemistry measurements, data reporting and archiving.

Oct. – Dec. 2009: Atlantic Meridional Transect (AMT – 19) cruise. An investigation of iron distribution in the upper water column and its control on nitrogen fixation rates.

Dec. 2011 – Jan. 2012: UK GEOTRACES section GA10 cruise. An investigation of the biogeochemical cycling of dissolved zinc in the South Atlantic Ocean at 40^{o} S.

Jun. 2012: Oversaw visiting scientist, James Moffett, University of Southern California. Demonstration of the determination of total dissolved zinc in seawater by FI-FL detection.

Dec. 2012: Oversaw visiting scientists, Raimund Rentel, University of Stellenbosch, & Thato Mtshali, CSIR & University of Stellenbosch. Aid was given towards the set-up of a FI-CL system for the determination of total dissolved iron in seawater.

Chapter 1

Biogeochemical cycling of iron, zinc and cobalt

1.1. Introduction

Marine phytoplankton are responsible for between 40 to 50 % of the photosynthetic carbon fixation (primary production) on Earth (Field *et al.*, 1998; Behrenfeld *et al.*, 2006). This is remarkable given that their biomass only amounts to ~ 1 - 2 % of the total global plant carbon (Falkowski, 1994). The magnitude of phytoplankton primary production comes from their ability to direct virtually all harvested light energy towards photosynthesis, and therefore the entire marine population can replace itself each week (Falkowski, 2002; Morel and Price, 2003). In contrast, land plants must invest large amounts of energy to build roots, wood and leaves and take an average 20 years to replace themselves (Falkowski, 2002). It is the rapid life cycle of phytoplankton that is key to their profound effect on the oceanic and global carbon cycles and climate regulation.

The process by which carbon dioxide (CO_2) fixed in photosynthesis is transferred to the ocean interior, and is either recycled or stored permanently in the deep ocean, is referred to as the biological pump. A simplified conceptual model of the principle components of the biological pump is presented in Figure 1.1. Phytoplankton carbon fixation removes CO_2 from the euphotic zone and converts it into organic material. Together with nutrients and trace elements, organic carbon forms the carbohydrates, lipids, and proteins that constitute bulk organic matter (de La Rocha, 2003). Phytoplankton either become senescent and sink out as aggregates, or are consumed by herbivorous zooplankton that egest faecal material. Particulate organic carbon (POC) may then be decomposed and remineralised back to CO_2 by bacteria or further consumed by animals. Most of this recycling occurs in the upper few hundred metres of the oceans, where the CO_2 is instantly available to be photosynthesized or

absorbed back into the atmosphere (Martin *et al.*, 1987; Falkowski *et al.*, 2000). Most influential to climate is the POC that sinks into the deep ocean before it decays. Approximately 15 - 25 % of the CO_2 fixed in the sunlit ocean sinks with settling phytoplankton into the ocean interior where it is released by oxidation through heterotrophic respiration and stored for several hundreds of years (Falkowski *et al.*, 1998; Laws *et al.*, 2000; Falkowski, 2002).

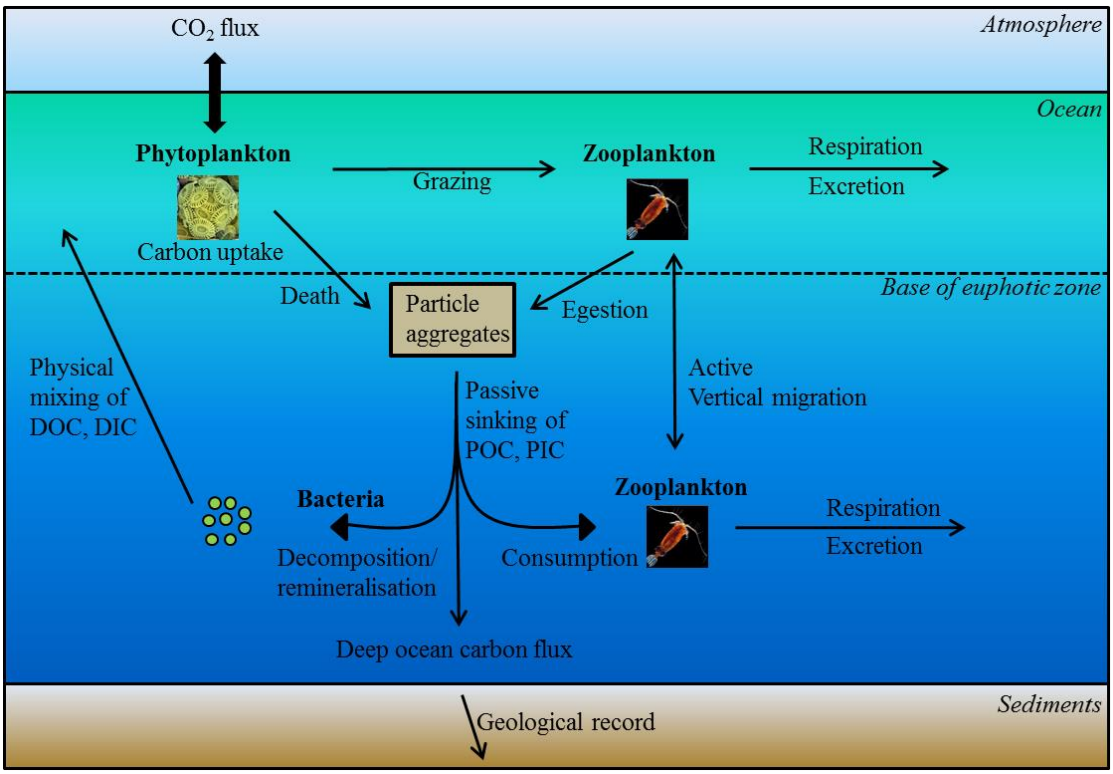

Figure 1.1. Conceptual model showing the main processes involved in the oceanic biological pump. Adapted from de la Rocha (2003).

The residence time of CO_2 in the deep oceans is a result of the lack of mixing between cold and dense deeper waters with warmer waters above. Eventually however, most of the nutrients released in the deep oceans find their way back to the sunlit ocean via upwelling and other ocean currents where they can stimulate primary productivity

(Palter *et al.*, 2010). Approximately 1 % of the deep ocean carbon flux settles to the sea floor before it can be recycled back to the upper ocean where it becomes incorporated into the fossil record.

The oceanic biological pump could not operate without an external supply of nutrients that are essential to phytoplankton growth (Morel and Price, 2003). In the absence of the biological pump, Falkowski *et al.* (2000) estimate CO_2 concentrations in the atmosphere would be between 150 - 200 parts per million (ppm) higher than their current value of 390 – 395 ppm (Dlugokencky and Tans, 2013). Much of the focus when investigating the biological pump and carbon cycling is placed on the macronutrients nitrate, phosphate and silicate (*e.g.* Tyrrell, 1999; Mather *et al.*, 2008) due to their importance in cellular photosynthesis, respiration, metabolism and structure. Macronutrient concentrations in the oceans are usually reported in the micromolar (μM) range, although surface depletion in some oceanic regions may reduce concentrations to nanomolar (nM) levels (Mather *et al.*, 2008).

A number of trace elements, particularly first row transition metals (iron, zinc, cobalt, manganese, vanadium, chromium, nickel and copper), and some second row transition metals (molybdenum, cadmium), are also essential for the growth of phytoplankton though their involvement in such processes as inorganic carbon, nitrogen and phosphorus acquisition and transformation (Bruland *et al.*, 1991; Morel *et al.*, 2003; Morel and Price, 2003). Although there is limited quantitative information regarding enzymatic processes in phytoplankton cells and their corresponding trace element requirements, Table 1.1 lists the known biochemical functions that are thought to correspond to major trace metal requirements in marine phytoplankton.

Table 1.1. Essential trace metals and their function in important biochemical processes by phytoplankton in the oceans. Adapted from GEOTRACES Planning Group (2006).

Biochemical function	**Trace metal**
Carbon concentration/acquisition	Zn, Co, Cd
Carbon fixation	Fe, Mn
Respiration	Fe
N_2 fixation	Fe, Mo
Denitrification	Fe, Cu
Nitrate reduction	Fe, Mo
Assimilatory nitrite reduction	Fe
Ammonia oxidation / nitrification	Fe, Mo, Cu
Vitamin B_{12} synthesis	Co
Remineralisation pathways	Fe, Zn
Organic nitrogen utilisation	Fe, Cu, Ni
Organic phosphorus utilisation	Zn
Silica uptake	Zn, Cd
Calcification	Co, Zn
Superoxide dismutase	Fe, Mn, Zn, Cu, Ni
Methane oxidation	Cu
Plastocyanin	Cu
Formation of volatile species	Fe, Cu, V
Photopigment synthesis	Fe and others

Whilst there is no clear definition of trace elements, generally their concentrations are less than 10 µM (Bruland and Lohan, 2003; Sohrin and Bruland, 2011) and usually in the nM to picomolar (pM) range (*e.g.* Lai *et al.*, 2008; Milne *et al.*, 2010). The average oceanic concentrations of selected macronutrients and trace elements along with their oceanic residence times are shown in Table 1.2.

At the molecular level, the mechanisms by which macronutrients and trace elements function as active centres or structural factors in enzymes is termed bioinorganic chemistry, whilst at the scale of ocean basins, the interaction of physical, chemical and biological processes that determine the cycling of these elements is the

subject of marine biogeochemistry. With regards to carbon fixation, phytoplankton growth, the biological pump and climate regulation, the fields of bioinorganic chemistry and marine biogeochemistry are critically linked by the extremely low concentrations of trace elements in surface waters, which results from their quasi-complete biological utilisation and incorporation into sinking organic matter (Morel *et al.*, 2003; Morel 2008).

Table 1.2. The concentrations and residence times of macronutrients and selected trace metals in the open ocean. Note the oceanic mixing time is 500 - 1000 y^{-1}. Adapted from Bruland and Lohan, 2003 and www.mbari.org/chemsensor/pteo.htm (28.8.2013).

Nutrient	Average oceanic concentration (10^{-9} mol kg^{-1})	Oceanic concentration range (10^{-9} mol kg^{-1})	Residence time (y)
Macronutrients			
Silicate (H_4SiO_4)	100000	500 - 180000	20000
Nitrate (NO_3^-)	30000	10 - 45000	3000
Phosphate (HPO_4^{2-})	2000	1 - 3500	69000
Trace elements			
Fe	0.54	0.02 - 2	200
Zn	5.4	0.05 - 9	51000
Co	0.20	0.04 – 0.3	340
Mn	0.36	0.08 - 5	60
V	39	30 - 36	50000
Cr	4.0	3 - 5	8000
Ni	8.2	2 - 12	6000
Cu	2.4	0.5 – 4.5	5000
Cd	0.62	0.001 - 1	50000

1.2. Biogeochemistry of iron, zinc and cobalt

1.2.1. Biological functions of iron, zinc and cobalt

The key to understanding the role of the global oceans in climate regulation lies in our understanding of the biological functions of trace metals in the modern oceans and what controls their distributions (de Baar and La Rocha, 2003). Figure 1.2A illustrates how the numerous enzymatic processes of the nitrogen cycle involve metalloenzymes with different trace metal requirements, whilst Figure 1.2B shows the principal trace metal requirements for carbon, nitrogen and phosphorus acquisition.

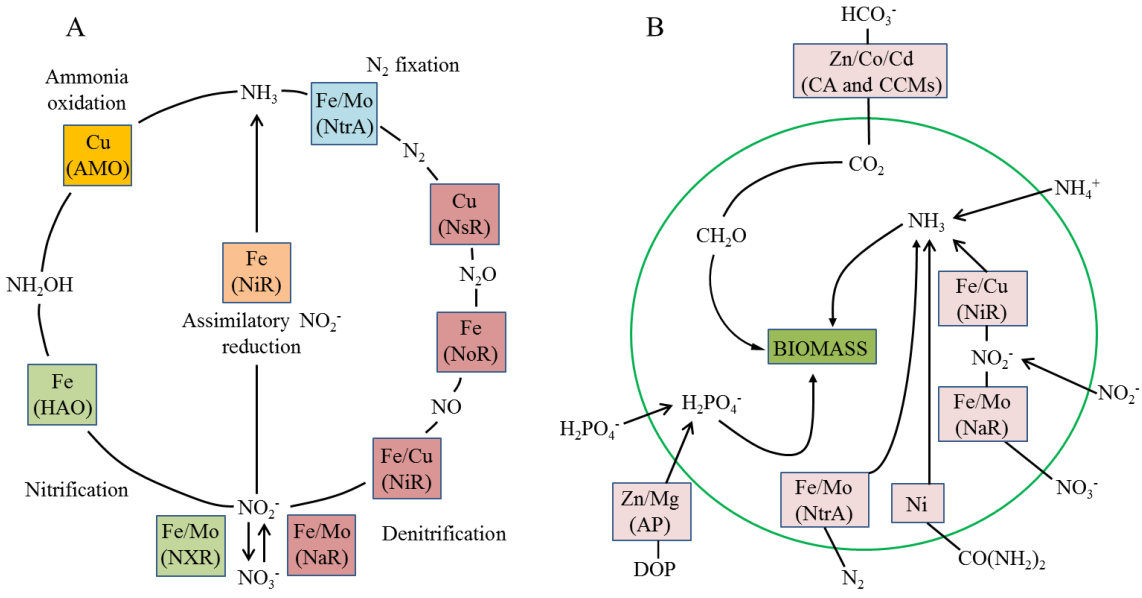

Figure 1.2. (A) The nitrogen cycle indicating the metal cofactors in each enzymatically catalysed step and the associated enzymes. Each group of reactions is colour coded: nitrogen fixation (blue); denitrification (pink), nitrification (green), ammonia oxidation (orange) and assimilatory nitrite reduction (beige). (B) The principle cellular metal requirements for carbon, nitrogen and phosphorus acquisition and assimilation by phytoplankton and associated enzymes. Enzyme abbreviations in alphabetical order: AMO: ammonia monooxygenase; AP: alkaline phosphatase; CA: carbonic anhydrase; CCM: carbon concentrating mechanisms; HAO: hydroxylamine oxidoreductase; NaR: nitrate reductase; NiR: nitrite reductase; NoR: nitric oxide reductase; NsR: nitrous oxide reductase; NtrA: nitrogenase; NXR: nitrite oxidoreductase. Adapted from Morel and Price (2003).

Iron

Iron (Fe) plays a central role in the light reactions of photosynthesis (Morel *et al.*, 2003), during which, Fe is an essential component in the reaction centres of photosystems I and II. Together, the photosynthetic apparatus of oxygenic phototrophic organisms contain about two thirds of the total Fe requirement (Raven, 1990). The low productivity in Fe depleted regions of the oceans is primarily due to low efficiency of the light reaction of photosynthesis. Respiration, which accounts for the remaining third, also becomes inefficient at low dissolved Fe concentration resulting in heterotrophic bacteria being able to convert less of the carbon they consume into biomass (Tortell *et al.*, 1996).

Iron is also a necessary enzymatic component in virtually all stages of the nitrogen cycle (Fig. 1.2A). The most pervasive effect of Fe on the nitrogen cycle is probably the limitation of di-nitrogen (N_2) fixation, which requires Fe in nitrogenase. Due to the difficult reduction of N_2 to ammonium (NH_4^+), nitrogen fixing phytoplankton are thought to require two to five times more Fe than phytoplankton growing on reduced nitrogen (Flynn and Hipkin, 1999; Sanudo-Wilhelmy *et al.*, 2001; Kustka *et al.*, 2003a,b). Low Fe may also inhibit the activities of nitrogen reductase enzymes both in the assimilatory pathway of phytoplankton and in the dissimilatory pathway of denitrifying bacteria (Averill, 1996) (Fig. 1.2A). The effect of low Fe concentration on nitrate reductase is of particular importance to diatoms as these larger phytoplankton cannot grow on the low ambient ammonium (NH_4^+) concentration and must instead reply on the acquisition of nitrate (NO_3^-) (Morel and Price, 2003). For diatoms growing at an average N:C ratio of 1:6, the reduction of NO_3^- to NH_4^+ is estimated to require 60 % more Fe than phytoplankton growing on ammonium (Raven

et al., 1992). The multiple roles for Fe in the cycling of carbon and nitrogen has led biogeochemists to argue that Fe is the most important, but by no means the only, essential bioactive trace metal in the oceans (Bruland *et al.*, 1991).

Zinc

Although the cellular concentration of zinc (Zn) is typically lower than that of Fe (Ho *et al.*, 2003), the number of known Zn metalloenzymes appears to be much larger than that of Fe metalloenzymes (Maret, 2002). Zinc is critical for the acquisition of inorganic carbon in marine phytoplankton as the carbon-concentrating mechanism involves the Zn metalloenzyme carbonic anhydrase (CA) (Price and Badger, 1989; Badger, 2003; Kupriyanova and Pronina, 2011). The CA metalloenzyme catalyses the chemical reaction responsible for the conversion of bicarbonate (HCO_3^-) to CO_2 prior to carbon fixation.

As is the case for nitrogen, organic compounds form a significant source of phosphorus for some species of marine phytoplankton (Mather *et al.*, 2008). In most species, the Zn metalloenzyme alkaline phosphatase (AP) is principally involved in cleaving the phosphate group from its organic moiety prior to uptake (Fig. 1.2B). Shaked *et al.* (2006) have calculated that the additional Zn demand of the haptophyte *Emiliania huxleyi* grown on organic phosphorus amounted to 16 % of the cellular quota. Thus, low Zn concentrations may therefore limit the ability of phytoplankton to synthesize AP resulting in a biochemical dependency on both Zn and inorganic phosphate (Jakuba *et al.*, 2008; Saito *et al.*, 2008).

Cobalt

It is argued that the bioinorganic chemistry of cobalt (Co) is complicated by two issues; (I) the potential biochemical substitution of Co, Zn and Cd as the metal centres in enzymes, and (II) the influence of the chemical speciation of each of these trace metals on their bioavailability to phytoplankton (Saito *et al.*, 2004). However, whilst some organisms can substitute these metals (*e.g.* centric diatoms and haptophytes), there are others, particularly the phototrophic picocyanobacteria (*Prochlorococcus and Synechococcus*), and some diatoms species, that have an absolute cellular requirement for Co (Sunda and Huntsman, 1995a; Saito *et al.*, 2002; Saito and Goepfert, 2008).

Like Zn, the primary role of Co in most phytoplankton is to serve as a metal centre in CA, which catalyses inorganic carbon acquisition. In some taxa, CA can inter-replace Co with Zn or Cd as a metal centre (*e.g.* Morel *et al.*, 1994; Lane *et al.*, 2005). Yee and Morel (1996) studied Zn and Co substitution in CA for the marine diatom *Thalassiosira weissflogii* and concluded that these elements could substitute in CA, but that the enzyme possessed a higher affinity for Zn. A cellular preference for Zn has also been reported for the diatoms *T. pseudonana* and *T. oceanica* and the haptophyte *Phaeocystis antarctica*, whilst for *Emiliania huxleyi* a preference for Co has been observed (Sunda and Huntsman, 1995a; Saito and Goepfert, 2008). Thus, the activity of CA under low Zn or Co conditions can be restored by biochemical substitution. If, however, both elements were simultaneously low then biochemical substitution co-limitation may occur (Saito *et al.*, 2008).

Cobalt is also a requirement for vitamin B_{12} (cobalamin) *de novo* synthesis. Vitamin B_{12} is a Co-containing organometallic molecule that only can only be synthesised by select bacteria and archaea and yet is an essential vitamin for almost all

phytoplankton (Droop, 1974; 2007). Cobalt serves as a metal centre insider the coring ring of vitamin B_{12} and thus their biogeochemical cycles are critically linked (Bertrand *et al.*, 2007; Taylor and Sullivan, 2008). Low Co concentrations in some regions of the world's oceans could therefore limit the production of vitamin B_{12} by heterotrophic and phototrophic bacteria as reported for the North Atlantic Ocean (Panzeca *et al.*, 2008) and the Ross Sea (Bertrand *et al.*, 2007). In the Ross Sea, primary production has previously been shown to be seasonally limited by Fe availability (Martin *et al.*, 1990a; Coale *et al.*, 2003) but the recent argument for independent nutrient co-limitation by Fe and Co-containing vitamin B_{12} provides a greater understanding of the nutritional controls on phytoplankton growth and production in this region (Bertrand *et al.*, 2007).

1.2.2. Nutrient co-limitation

The idea of simultaneous limitation by more than one element (co-limitation) is an important and yet often misunderstood concept. The notion detracts away from the two paradigms of nutrient limitation: (I) Liebig's Law of the Minimum (de Baar, 1994), whereby the overall yield of phytoplankton biomass is limited by one element at a time, aside from light and (II) Blackman limitation (Saito *et al.*, 2008), where growth rate is reduced rather than yield. However, research over the last 20 years has revealed that these two concepts can interact, whereby CO_2, macronutrients and trace metals can co-limit phytoplankton growth and yield (Sunda and Huntsman, 1992; 1995a,b; Arrigo, 2005; Coles and Hood, 2007; Fu *et al.*, 2008; Saito and Goepfert, 2008; Feng *et al.*, 2010).

The surface oceans are particularly susceptible to nutrient co-limitation because of the simultaneous scarcity of many elements, the complex speciation of trace elements and CO_2 and the various uptake and intracellular pathways that these chemicals are involved in (Morel and Price, 2003; Saito *et al.*, 2008). Hence, an alternative approach to Liebig/Blackman-style limitation is required to provide a realistic understanding of nutrient co-limitation in the surface ocean. In an attempt to reconcile the concept of nutrient limitation of primary productivity in aquatic environments, Saito *et al.* (2008) proposed that co-limitation can be divided into one of three categories.

Independent nutrient co-limitation

This type of nutrient co-limitation describes two elements that are generally biochemically mutually exclusive, but are both found in the surface ocean at such low concentrations as to be potentially limiting. An example of independent nutrient co-limitation is the Sargasso Sea, where both nitrate and phosphate are considered to co-limit the gross autotrophic community (Moore *et al.*, 2008).

Biochemical substitution co-limitation

This type of nutrient co-limitation describes two elements that can substitute to perform the same biochemical role within an organism. There are two permutations of this type of nutrient co-limitation: (I) where two or more elements substitute effectively within the same enzyme, *e.g.* Zn, Co and Cd in the metalloenzyme CA (*e.g.* Lane *et al.*, 2005; Xu *et al.*, 2008) (Table 1.1 and Fig. 1.2), and (II) where two enzymes perform the same biochemical function, each utilising a different element, *e.g.* there are four known varieties of super oxide dismutase (enzymes required to detoxify cellular superoxide)

distinguished by containing either Fe, Mn, Ni or both Zn and Cu in their metal centres (Wolfe-Simon *et al.*, 2005) (Table 1.1).

Biochemical dependant co-limitation

This type of nutrient co-limitation refers to the limitation from one element that results from the inability to acquire another. An example of dependant co-limitation occurs once again in the Sargasso Sea where low Zn concentrations inhibit AP activity and the ability of phytoplankton to acquire dissolved organic phosphate (Shaked *et al.*, 2006; Jakuba *et al.*, 2008).

1.2.3. Trace metals and productivity

In most oceanic regions, primary production is limited by macronutrients and light (*e.g.* Maranon *et al.*, 1999; Arrigo, 2005; Mather *et al.*, 2008). The observation that phytoplankton communities were lower than expected in regions where macronutrients were replete led early workers to hypothesise that Fe, and other trace metals, may be limiting phytoplankton growth in these regions and their ability to remove available macronutrients (Gran, 1931; Hart, 1934).

Despite these early observations, the significance of Fe in these High Nutrient Low Chlorophyll (HNLC) regions was not determined until the late 1980's following the development of clean sampling and handling techniques (Bruland *et al.*, 1979). The first oceanographically consistent Fe determinations were published by Landing and Bruland (1987), Martin and Gordon (1988) and Martin *et al.* (1989) as part of the VERTEX programme. These findings indicated that dissolved Fe (dFe) concentrations in Eastern Pacific surface waters were < 1 nM, an order of magnitude lower than

previously reported. In addition to the vertical concentration profiles obtained at this time, ship-board experiments using Fe additions to surface seawater revealed the existence of Fe limitation in the HNLC regions of the sub-Arctic and Equatorial Pacific (Martin *et al.*, 1991) and Southern Ocean (Martin *et al.*, 1990a). These HNLC regions account for between 30 and 40 % of the surface waters in the world's oceans (Moore *et al.*, 2002; Boyd and Ellwood, 2010) (Fig. 1.3).

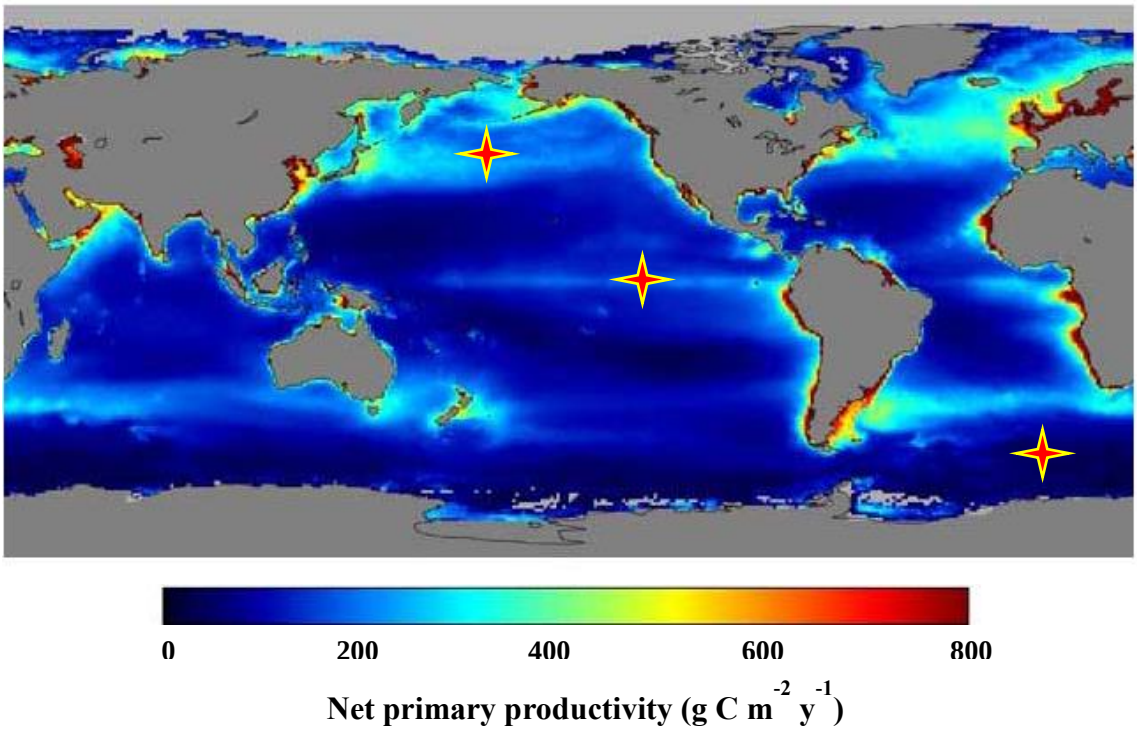

Figure 1.3. Distribution of net primary productivity in the oceans with the major HNLC regions marked with stars. HNLC regions are replete with macronutrients but exhibit low rates of primary production. Adapted from NASA Earth Observatory (www.nasa.gov/centers/ goddard/news /top- story/2003/0815oceancarbon.html; accessed 2.9.2013).

In accordance with this, John Martin published the "Iron Hypothesis" in 1990 (Martin, 1990), which explicitly suggested that an increase in Fe input to HNLC regions, via atmospheric dust deposition, could stimulate primary productivity and carbon export with significant impacts for the global climate. This hypothesis was based on an inverse

relationship found between CO_2 and Fe concentrations (inferred from aluminium data) in the Vostok ice cores.

Since 1993, 12 mesoscale *in situ* Fe fertilization experiments have been conducted covering the three major HNLC regions (de Baar *et al.*, 2005; Boyd *et al.*, 2007). The experiments have included IronEx I and II in the Equatorial Pacific (Martin *et al.*, 1994; Coale *et al.*, 1996), SEEDS I and II in the sub-Arctic Pacific (Tsuda *et al.*, 2003; 2007), as well as SOFeX North and South, and SOIREE in the Southern Ocean (Boyd *et al.*, 2000; Coale *et al.*, 2004). Observations from these studies showed that whilst an increased Fe supply may directly enhance primary productivity, the time scales (< 2 months) and spatial dimensions (a few tens of km) of fertilization experiments do not permit the fate of Fe induced POC export to the interior ocean to be assessed (de Baar *et al.*, 2005; Boyd *et al.*, 2007; Watson *et al.*, 2008). Thus, few fertilization experiments to date have firmly proven the export of POC, albeit modest, to deeper waters (Bidigare *et al.*, 1999; Buesseler *et al.*, 2004; Smetacek *et al*., 2012). This has led Watson *et al.* (2008) to argue that only by combining observations with modelling studies can we effectively assess the evolution of an Fe induced phytoplankton bloom and the efficiency of Fe fertilization experiments in sequestering CO_2. When a modelling approach was applied to SOIREE (Watson *et al.*, 2000), results suggested that Fe additions could result in an enhanced, but modest, POC export flux. In addition, modelled results by Moore *et al.* (2002) suggest that an increase in atmospheric Fe inputs, to a situation where Fe was non-limiting in global surface waters, would result in enhanced POC export. In this modelled scenario, almost three times the POC export occurs at non-limiting surface Fe concentrations (16.5 Gt C y^{-1}) compared

with the absence of an atmospheric input (5.8 Gt C y^{-1}), with increases mainly occurring in HNLC regions.

Whilst the long term sequestration of atmospheric CO_2 through ocean artificial Fe fertilization remains poorly constrained, the role of Fe for carbon export continues to be evaluated with the focus of recent studies turning to the natural Fe fertilization of the surface ocean, which can be observed over greater time scales (Pollard *et al.*, 2009; Achterberg *et al.*, 2013). Results from the CROZEX natural Fe fertilization experiment indicate that annual POC fluxes from a naturally Fe fertilized region of the sub-Antarctic Southern Ocean are two to three times larger than then POC fluxes from and adjacent HNLC area not fertilized by Fe (Pollard *et al.*, 2009). In addition, Blain *et al*. (2008) showed that natural Fe fertilisation of surface waters above the Kerguelen Plateau was 10 – 150 times more efficient at exporting carbon below 200 m than artificial Fe fertilization experiments.

Whilst Fe is perhaps the most important of all the bioactive trace metals with regards to its influence on oceanic primary productivity, and has therefore historically received the most attention, it has recently become clear that the availability of other trace metals, such as Zn, may be important in regulating primary productivity. For example, the low chlorophyll concentrations of the oligotrophic Sargasso Sea are thought to result from growth limiting Zn and Co concentrations and the subsequent inhibition of dissolved organic phosphorus acquisition (Shaked *et al.*, 2006; Jakuba *et al.*, 2008). In addition, a number of culture studies have found phytoplankton growth to be limited by several trace metals, including Fe, Zn, Co, at the range estimated for surface seawater (*e.g.* Sunda and Huntsman, 1992; 1995a,b; de la Rocha *et al.*, 2000; Saito and Goepfert, 2008).

As discussed by Morel (2008), the phenomenon of trace metal limitation arises from the complex co-evolution of planktonic life forms and ocean chemistry, whereby the biological utilisation of trace metals has evolved to closely match their fluxes to the surface ocean. The simplest way to look at how phytoplankton and ocean chemistry interact to influence the limitation of ocean productivity is to compare the stoichiometric composition of the two. Using phosphate to normalise essential trace elements, Morel (2008) report the following stoichiometric formulae:

Deep Pacific Ocean: $P_{1000}\,Fe_{0.22}\,Zn_{3.1}\,Cu_{0.75}\,Cd_{0.33}\,Mn_{0.10}\,Co_{0.07}$ Eq. 1.1

Pacific phytoplankton: $P_{1000}\,Fe_{4.1}\,Zn_{2.4}\,Cu_{0.45}\,Cd_{0.54}\,Mn_{0.35}\,Co_{0.2}$ Eq. 1.2

While these formulae are only approximate, it is clear that the stoichiometric coefficients of the trace metals (defined as their mole ratio to P) are for the most part within the same order of magnitude in both the deep ocean and phytoplankton biomass. Thus, in steady state, phytoplankton uptake of, and limitation by, trace elements in the surface ocean must resemble their total supply, i.e. upward vertical flux, recycling flux and atmospheric flux (which is small for most trace metals except Fe) (Morel, 2008).

The two exceptions to this are Fe and Co, which are one order of magnitude lower in the deep ocean (Eq's 1.1 and 1.2). Both of these elements are susceptible to removal by scavenging processes in ocean interior (Bruland and Lohan, 2003; Measures *et al.*, 2012). Hence, when nutrient rich deep water is returned to the surface ocean via upwelling or other ocean currents, the ratio of dissolved Fe and Co to the accompanying macronutrients is significantly below that required for biological uptake (Eq. 1.1 and 1.2), which could limit phytoplankton growth.

In the case of Fe, the difference between the phytoplankton and deep ocean stoichiometric coefficients may be explained by the large atmospheric flux relative to other trace metals. In the case of Co, which has a minimal atmospheric input, the difference may reflect metal substitution in phytoplankton enzymatic processes and/or efficient recycling in the surface ocean. For example, the four-fold lower Zn:Co ratio in phytoplankton compared to the deep ocean suggests that the kinetics of metal uptake in the surface ocean leads to a greater uniformity of these metals in phytoplankton than the deep ocean, reducing the potential for growth limitation (Morel, 2008). Zinc is not scavenged at depth due to its high solubility in seawater and therefore elevated Zn concentrations may be returned to the surface ocean with upwelling and other ocean currents (Bruland and Lohan, 2003; Jakuba *et al.*, 2012). If the upward fluxes of Zn and Co are proportional to their concentrations in deep water multiplied by the rate of vertical mixing, then the upward flux of Zn is 44 times greater than the upward flux of Co. Similarly, if their rates of incorporation into phytoplankton biomass are proportional to their concentrations in the biomass multiplied by their average growth rate, the incorporation of Zn into phytoplankton biomass is only a factor of 12 greater than that of Co. It therefore appears that Co may be recycled more efficiently than Zn in the surface ocean (Morel, 2008), possibly reducing the effects of Zn limitation through metal co-substitution in regions lacking in a steady input of Zn to surface waters.

Determining the relative importance of factors such as external inputs, surface ocean recycling, the biological pump, metal substitution and ocean chemistry on global ocean primary productivity requires more data than presently available. A region by region analysis is required that takes into account the variable stoichiometry of phytoplankton adapted to different oceanographic conditions. This is exemplified in

Figure 1.4, which shows trace metal cellular quotas of four marine eukaryotic phytoplankton, clearly highlighting the trace element variability between phyla in both oceanic and coastal regimes.

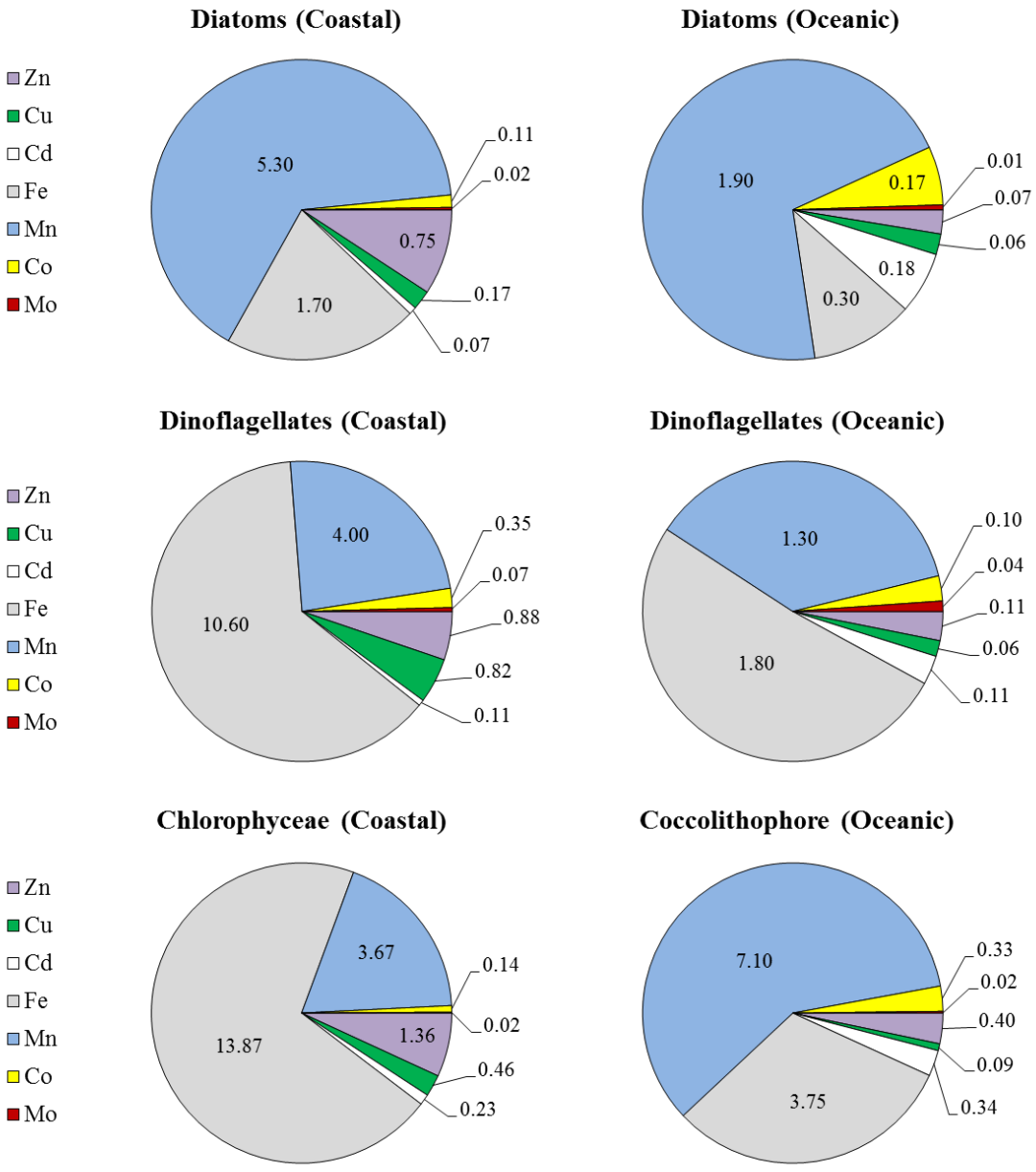

Figure 1.4. The average cellular trace element quotas in four eukaryotic phytoplankton phyla. Elements are normalized to phosphorus (mmol mol^{-1}). Adapted from Ho *et al.* (2003).

Such variability includes the potential for trace metal induced changes in phytoplankton community structure and ecosystem functions, such as primary production, which, given the current concerns over atmospheric CO2 concentrations, is vitally important to climate regulation.

In addition to limiting net community primary productivity, it has become apparent in recent years that trace metals, such as Fe, Zn and Co, also play vital intermediary roles in oceanic nutrient cycling due to their involvement in processes, such as N_2 fixation (Mills *et al.*, 2004; Coles and Hood, 2007; Moore *et al.*, 2009) and organic phosphorus acquisition (Shaked *et al.*, 2006; Jakuba *et al.*, 2008; Saito and Goepfert, 2008) (Table 1.1 and Fig. 1.2). For example, N_2 fixation in surface waters of the western tropical North Atlantic, which can provide up to 70 % of the nitrogen demand during bloom conditions (Carpenter *et al.*, 1999) is considered to be controlled by Fe availability (Moore *et al.*, 2009). However, the notion that N_2 fixation is universally controlled by Fe is being replaced by a more complex understanding that allows for limitation by other nutrients such as phosphate (Arrigo, 2005), or even co-limitation by Fe and phosphate (Mills *et al.*, 2004). The concept of Fe and P co-limitation of N_2 fixation is particularly relevant in certain locations, such as the oligotrophic surface waters of the North Atlantic and North Pacific (Karl *et al.*, 1997; Mills *et al.*, 2004).

Similarly, Zn serves as a cofactor in several extracellular phosphatases, which allow phytoplankton to acquire phosphate from organic phosphorus compounds (Shaked *et al.*, 2006) in oligotrophic ocean regions. At low Zn concentrations or availability, the synthesis of these Zn containing metalloenzymes may be limited, leading to Zn-P co-limitation of phytoplankton growth. Such Zn-P co-limitation has

been reported recently for the oligotrophic Sargasso Sea (Jakuba *et al.*, 2008), a region where the overall autotrophic community appears to be co-limited by N and P (Moore *et al.*, 2008). Considering that the dissolved organic phosphorus pool is reported to support 20 % of primary production in the North Atlantic sub-tropical gyre (Mather *et al.*, 2008), the Zn-P limitation of phytoplankton growth may exert an important influence on the efficiency of the oceanic biological pump.

1.2.4. Oceanic distributions of iron, zinc and cobalt

Open ocean dissolved Fe, Zn and Co concentrations are presented in Tables 1.3, 1.4 and 1.5 respectively. Note that the chemical dissolved form in these Tables is operationally defined by physical size fractionation. In some studies listed below it is defined as < 0.2 µm and in others < 0.45 µm. Both of these fractions will include the truly soluble fraction (operationally defined as < 0.02 µm) and part of the colloidal fraction (0.02 - 1 µm) of each metal.

Table 1.3. Dissolved iron concentrations in the open ocean (dissolved defined as either < 0.2 µm or < 0.4 µm).

	Fe Concentrations (nM)		
Ocean	**Surface (0 – 25 m)**	**Depth (> 500 m)**	**References**
Atlantic			
NE Atlantic	0.14 – 0.6	0.2 – 2	Ussher *et al.* (2007)
NW Atlantic	0.73 – 1.35	0.55 – 1.18	Fitzsimmons *et al.* (2013)
NW Atlantic (Sargasso Sea)	0.3 – 1.6	0.2 – 0.7	Shelley *et al.* (2012)
N Atlantic gyre (W)	0.2 – 1.6	2 (200 m)	Ussher *et al.* (2013)
Tropical N Atlantic (4 – 18° N)	0.1 – 1.3	≤ 2 (200 – 800 m)	Measures *et al.* (2008)
Equatorial Atlantic	0.1 – 0.2	0.6 – 1	Measures *et al.* (2008)
S Atlantic gyre	0.05 – 0.3	0.4 – 0.7	Noble *et al.* (2012)
SW Atlantic	0.2 – 0.4	0.27 – 0.47	Bergquist and Boyle (2006)
SE Atlantic (Benguela OMZ)	0.1 – 0.3	0.4 – 2.2	Noble *et al.* (2012)
Pacific			
Sub-Arctic Pacific	0.1 – 0.3	0.6 – 1.6	Uchida *et al.* (2013)
N Pacific gyre	0.37	0.22 – 0.45	Bruland *et al.* (1994)
Equatorial Pacific	0.2 – 0.9	1 - 2	Slemons *et al.* (2010)
S Pacific gyre	0.09 – 0.2	0.07 – 0.29 (300 – 400 m)	Blain *et al.* (2008)
SE Pacific (Chilean OMZ)	0.08 – 0.32	0.33 – 1.61 (300 – 400 m)	Blain *et al.* (2008)
Southern Ocean			
Atlantic sector (sub-Antarctic)	0.17 – 0.3	0.28 - 0.65	Klunder *et al.* (2011)
Pacific sector	0.09 – 0.35	0.15 – 0.32 (300 m)	Measures and Vink (2001)
Indian sector	0.1 – 1.05	0.12 – 2.08 (300 – 750 m)	Planquette *et al.* (2008)
Australian sector	0.05 – 0.7	0.09 – 0.45 (300 m)	Sedwick *et al.* (2008)
Weddell Sea	0.08 – 0.41	0.3 – 0.8	Klunder *et al.* (2011)
Ross Sea	0.1 – 2.3	0.1 – 0.3	Sedwick and DiTullio (1997)
Indian			
Arabian Sea	0.09 – 0.36	0.77 – 1.52	Nishioka *et al.* (2013)
Indian (central)	0.02 – 0.09	0.15 – 2.06	Nishioka *et al.* (2013)

Table 1.4. Dissolved zinc concentrations in the open ocean (dissolved defined as either < 0.2 µm or < 0.4 µm).

	Zn Concentrations (nM)		
Ocean	**Surface (0 – 25 m)**	**Depth (> 500 m)**	**References**
Atlantic			
NE Atlantic	0.28 – 0.64	0.70 – 2.03	Ellwood and van den Berg (2000)
NE Atlantic (incl. European shelf)	0.07 – 4.8		Kremling and Streu (2001)
NW Atlantic	0.08 – 1.32		Jakuba *et al*. (2008)
Greenland Sea	0.5 – 5.25		Pohl *et al*. (1993)
Pacific			
Sub-Arctic Pacific	0.10 – 1.15	6.82 – 10.30	Jakuba *et al*. (2012)
Bearing Sea (HNLC)	0.06 – 0.2		Leblanc *et al*. (2005)
NE Pacific	0.08 – 0.37	4.58 – 9.63	Bruland (1980)
NE Pacific	0.04 – 0.90	3.43 – 14.4 (200 – 400 m)	Lohan *et al*. (2002)
Southern Ocean			
Atlantic sector	0.8 – 5.3 (< 40 m)	4.5 – 8.0	Löscher (1999)
Pacific sector (HNLC)	0.006 – 0.06		Ellwood (2004)
Australian sector	0.20 – 0.45	0.6 – 3.4	Ellwood (2008)
Ross Sea	0.24 – 2.81	4.88 – 7.11 (200 – 375 m)	Fitzwater *et al*. (2000)
Indian			
S Indian	0.02 – 0.24	0.30 – 3.86	Gosnell *et al*. (2012)

Table 1.5. Dissolved cobalt concentrations in the open ocean (dissolved defined as either < 0.2 µm or < 0.4 µm).

	Co Concentrations (pM)		
Ocean	**Surface (0 – 25 m)**	**Depth (> 500 m)**	**References**
Atlantic			
NE Atlantic	33	31 - 41	Ellwood and van den Berg (2001)
NW Atlantic (Sargasso Sea)	18 – 63	30 – 70	Shelley *et al.* (2012)
N & S (E) Atlantic (open ocean inc. gyres)	36 – 53[a]		Bowie *et al.* (2002a)
N & S (E) Atlantic (upwelling and shelf)	47 – 93[a]		Bowie *et al.* (2002a)
SW Atlantic (upwelling and shelf)	73[a]		Bowie *et al.* (2002a)
S Atlantic gyre (central)	6 – 25	60 – 100	Noble *et al.* (2012)
SE Atlantic (Benguela OMZ)	40 – 110	30 – 155	Noble *et al.* (2012)
Pacific			
Gulf of Alaska	< 10 - > 20		Martin *et al.* (1989)
NE Pacific	109 - 119	24 - 59	Knauer *et al.* (1982)
NW Pacific	95	22 - 58	Wong *et al.* (1995)
N Pacific (near Hawaii)	10 - 20	40 - 80	Noble *et al.* (2008)
Southern Ocean			
Atlantic sector	7 – 36	24 – 73	Bown *et al.* (2011)
Australian sector	10 - 30	20 - 55	Ellwood (2008)
Ross Sea	31 - 51		Bertrand *et al.* (2007)

[a]Unfiltered samples

In order to discuss the distributions of Fe, Zn and Co in the oceans it is necessary to consider them in terms of their chemical behaviour throughout the water column. The vertical distribution of trace metals in seawater can be categorised into four broad classifications based on the sources and sinks to the water column trace metal inventory: conservative, nutrient-like, scavenged-type, and hybrid-type (Bruland and Lohan, 2003).

Nutrient-like

Trace elements with nutrient-like distributions are dominated by the internal cycles of biologically derived particulate material (*e.g.* Zn). Consequently, the concentrations of these elements are depleted at the surface due to biological assimilation and increase in sub-surface waters (Bruland and Franks, 1983; Löscher, 1999; Lohan *et al.*, 2002) as sinking organic particulate matter undergoes decomposition and remineralisation in the interior ocean (Fig. 1.1). In addition, nutrient-like elements are not readily scavenged in the deep ocean and thus their concentrations increase with the thermohaline circulation of oceanic deep waters (Bruland and Lohan, 2003). The concentrations of these elements are therefore, greater in the older waters of the deep Indian and Pacific Oceans relative to the Atlantic. Nutrient- like elements typically have intermediate oceanic residence times ($10^3 – 10^5$ y) (Table 1.2) because a portion the sinking particulate organic matter settles to the sea floor where it becomes incorporated into the fossil record (Fig. 1.1).

Scavenged-type

Scavenged elements are extremely particle reactive (*e.g.* aluminium), rapidly sorb onto sinking particulate material and thus have short oceanic residence times (~ 10^2

– 10^3 y). External processes markedly change the concentrations of scavenged elements because their fluxes are large relative to the internal mixing rate. In general, the concentrations of these elements exhibit maxima near major sources such as rivers, atmospheric deposition events, bottom sediments and hydrothermal vents (*e.g.* Vink and Measures, 2001; Statham *et al*., 2005; Measures *et al.*, 2008). Owing to continued particle scavenging, the concentrations of scavenged metals tend to decrease with thermohaline circulation of deep waters, thus concentrations in the deep Pacific are generally lower in the deep Pacific than in the deep Atlantic.

Hybrid-type

Some trace metals, such as Fe and Co, have distributions that are strongly influenced by both recycling and relatively intense scavenging processes. As with nutrient-type metals, hybrid elements may be depleted in open ocean surface waters such as HNLC regions and appear to be regenerated with depth. However, in oligotrophic waters, particularly in regions of high atmospheric dust deposition, hybrid trace metals can exhibit surface water maxima more indicative of scavenged elements (Johnson *et al.*, 1997; Measures *et al.*, 2008). In deeper waters (below ~ 1000 m), hybrid trace metal concentrations remain relatively constant, balanced by rates of organic particle remineralisation and particulate scavenging (Johnson *et al.*, 1997). As "hybrid-type" is a relatively new term to describe oceanic trace metal vertical profiles, the oceanic residence time of trace metals that fall into this category show large variability. The residence time for Fe, as an example, is estimated to be 100 – 200 y (Table 1.2), considerably less than the oceanic mixing time and therefore, the deep waters of the Pacific are not enriched with Fe relative to the deep waters of the Atlantic (Johnson *et al.*, 1997; Bruland and Lohan; 2003).

Iron

Concentrations of dissolved Fe (dFe) in open ocean surface waters generally range from 0.02 to 1 nM and reach maximum concentrations of ~ 2 nM in deeper waters (Table 1.3). Figure 1.5 provides a comparison the vertical dFe profiles from high latitudes of the HNLC North Atlantic and North Pacific. Also shown in Figure 1.5 are the dFe data from the upper 1000 m of the highly stratified North Atlantic gyre.

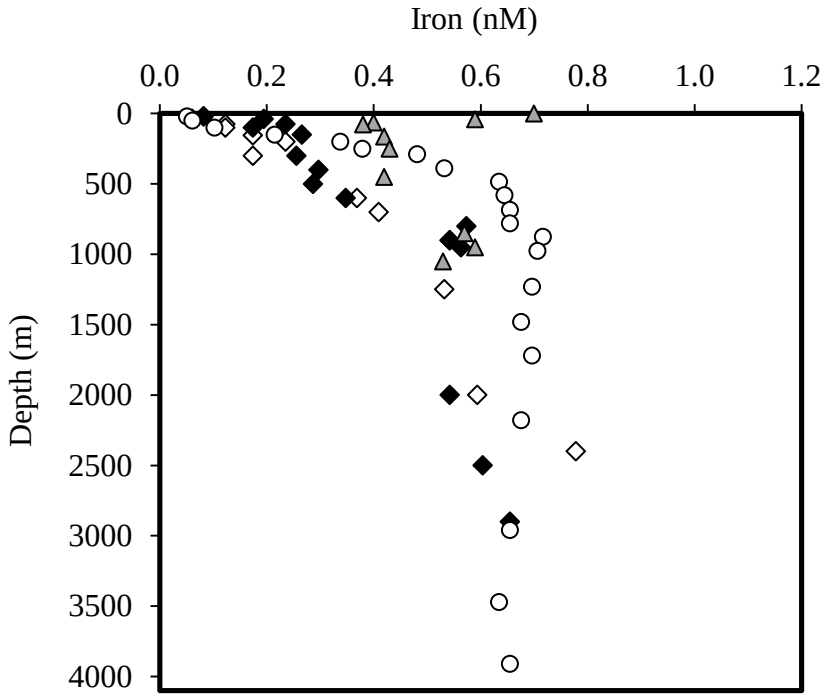

Figure 1.5. Vertical profiles of dissolved iron from high latitudes of the North Atlantic (white and black diamonds) (59° N, 20° W and 47° N, 20° W; data from Martin *et al.*, 1993) and the North Pacific (circles) (50° N, 145° W; data from Martin *et al.*, 1989). Also shown are dissolved iron data from the upper 1000 m of the highly stratified North Atlantic gyre (triangles) (30° N, 45° W; data from Bergquist and Boyle, 2006).

In the North Atlantic and North Pacific profiles, the lowest dFe concentrations (< 0.2 nM) are observed in the upper 100 m of the water column due to biological uptake. Within intermediate waters (~ 200 – 1500 m), the dFe concentrations increase

as organic material is decomposed and Fe remineralised. Below 1000 m, the dFe profiles from the Atlantic and Pacific are not significantly different. It is hypothesised that the lack of inter-basin fractionation between the Atlantic and the Pacific Oceans may result from the organic speciation of dFe by strong Fe-binding ligands that act to reduce the scavenging rate at dFe concentrations less than 0.6 nM (Johnson *et al.*, 1997). These ligands have been found in both the Atlantic and Pacific at concentrations near 0.6 nM and are thought to be the principal mechanism maintaining the hybrid-type dFe profile.

As observed from the North Atlantic gyre profile in Figure 1.5, surface waters in oligotrophic gyres can exhibit surface dFe maxima, often above 1 nM in regions associated with large atmospheric Fe fluxes (*e.g.* Shelley *et al.*, 2012; Fitzsimmons *et al.*, 2013; Ussher *et al.*, 2013) (Table 1.3). Here, the vertical dFe profiles can often resemble a scavenged-type trace metal, a phenomenon that Bruland *et al.* (1994) attributed to rapid remineralisation of organic material in a strongly stratified surface mixed layer. In such conditions there is little vertical transport of organic matter to the interior ocean or macronutrients to the surface mixed layer, resulting in an accumulation of trace metals, such as Fe, from atmospheric dust deposition to the surface ocean.

Zinc

Dissolved Zn (dZn) concentrations in the open ocean range from 0.01 – 1 nM in surface waters to ~ 10 nM in deep waters (Table 1.4). As with Fe, the vertical distributions of dZn in the HNLC high latitude North Atlantic and Pacific oceans are compared in Figure 1.6A. Zinc concentrations are lowest (< 0.5 nM) in the upper 100 m, depleted by biological assimilation and export. Concentrations of dZn as low as 40 pM have been reported for the HNLC northeast Pacific (Lohan *et al.*, 2002). In deep waters,

dZn reaches a constant concentration that can be up to 100 times greater than observed at the surface (Martin *et al.*, 1989). As such, mechanisms that return dZn and other nutrient-like elements from the deep ocean to the surface waters, such as upwelling and other ocean currents, provide an important control on surface ocean primary productivity (Sarmiento *et al.*, 2004; Ellwood, 2008; Palter *et al.*, 2010).

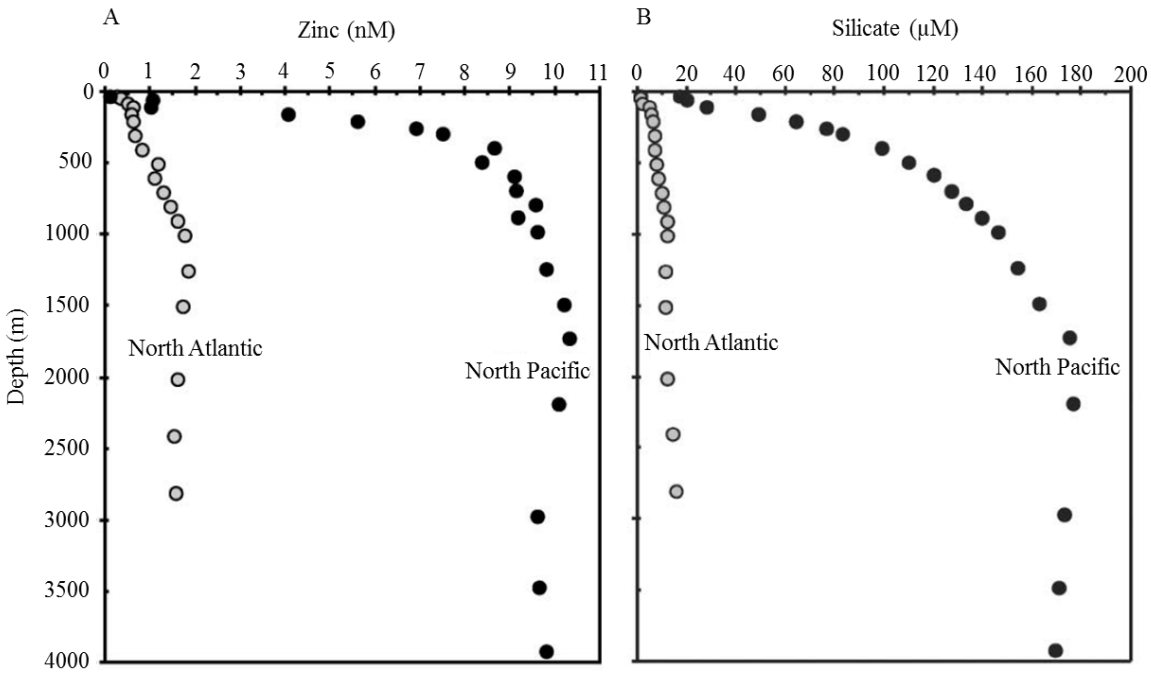

Figure 1.6. Vertical profiles of dissolved (A) zinc and (B) silicate observed at high latitudes of the North Atlantic (59° N, 20° W; data from Martin *et al.*, 1993) and North Pacific (50° N, 145° W; data from Martin *et al.*, 1989). Adapted from Bruland and Lohan, (2003).

In contrast to dZn, the free Zn ion (Zn^{2+}) concentration in deeper waters can be > 1000 times higher than in surface waters Bruland *et al.* (1991). The difference between the dissolved and free ion Zn concentrations is thought to be linked to the presence of Zn-binding ligands in excess of the dZn concentration at depths above ~ 300 m, thus a high degree of organic speciation helps maintain Zn in solution.

As observed in Figure 1.6A, Zn concentrations display a strong inter-basin fractionation, typical of nutrient-type trace metals. In intermediate mesopelagic waters, the inter-basin differences may reflect the phyico-chemical processes occurring in the water column, such as organic matter remineralisation, re-supply by advection and mixing. Below 1000 m, as deep waters follow the main path of thermohaline circulation their Zn concentrations gradually increase through organic matter remineralisation so that their deep North Pacific values are a factor of 5 higher than observed in the deep North Atlantic (Bruland and Lohan, 2003) (Table. 1.4).

As widely reported, the oceanic dZn profile is similar to that of dissolved silicate (*e.g.* Bruland *et al.*, 1978; Lohan *et al.*, 2002; Croot *et al.*, 2011) (Fig. 1.6B), thought to be a result of the presence of Zn in silicate uptake transport proteins (Grachev *et al.*, 2005; 2008; Danilovtseva *et al.*, 2009) (Table 1.1). Hence, deep water silicate concentrations increase by a factor of 10 between the North Atlantic and Pacific oceans. The dissolved Zn and silicate data available for oceanic deep waters (< 1000 m) has led Marchitto *et al.* (2000) to propose a global linear relationship between dZn and silicate: [Zn] (nM) = 0.052[Si] (μM) + 0.79 that can be used to estimate deep water dZn concentrations in the absence of trace metal data but available silicate data.

Cobalt

In the open ocean, dissolved Co (dCo) generally falls into the hybrid-type category since its oceanic distributions are often controlled by a combination of nutrient-like processes in surface waters and scavenging processes in intermediate and deep waters (Noble *et al.*, 2008; Saito *et al.*, 2010; Bown *et al.*, 2011; Shelley *et al.*, 2012). These scavenging processes prevent the accumulation of dCo in deep waters

with thermohaline circulation (Saito and Moffett, 2002). Figure 1.7 compares the dCo vertical profiles from the HNLC high latitude North Atlantic and Pacific Oceans.

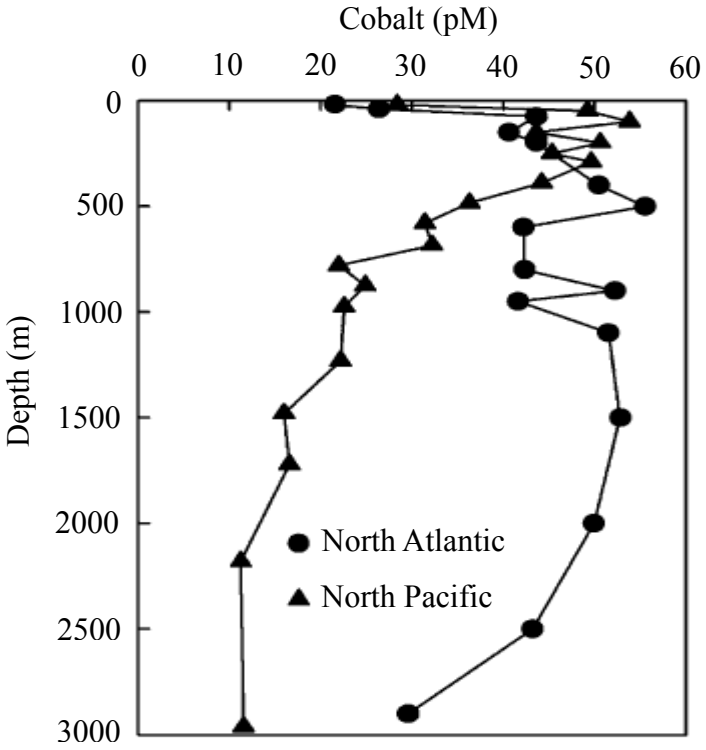

Figure 1.7. Vertical profiles of dissolved cobalt from high latitudes in the North Atlantic (47° N, 20° W; data from Martin *et al.*, 1993) and North Pacific (50° N, 145° W; data from Martin *et al.*, 1989). Adapted from Morel (2008).

In surface waters, dCo concentrations generally range from 1 to 40 pM (Table 1.5) and reach maximum values of 50 – 150 pM in intermediate mesopelagic waters coinciding with minimum oxygen concentrations (Saito and Moffett, 2002; Bown *et al.*, 2011; Noble *et al.*, 2012). These elevated concentrations may result from increased remineralisation rates and low scavenging rates under low oxygen conditions (Noble *et al.*, 2012). In addition, organic speciation may promote the stabilisation of the soluble Co(II) redox state favoured by oxygen minimum zones. For example, in the low oxygen waters of the mesopelagic Southeast Atlantic, Bown *et al.* (2012) reported that > 75 %

of the dCo was stabilised by organic complexes. Below the mesopelagic Co maximum, concentrations decrease with further depth to between 10 and 40 pM (Knauer *et al.*, 1982; Martin *et al.*, 1989; 1993; Saito and Moffett, 2002). Like Fe, deep water Co concentrations do not increase with thermohaline circulation through the deep ocean basins and instead, tend to decrease between the deep Atlantic and deep Pacific (Fig. 1.7) owing to continued particle scavenging.

1.3.1. Sources and sinks of trace metals to the oceans

Trace metals that enter the world's oceans are derived from either the continental crust or the oceanic crust. Much of the material transported to the oceans is mobilised during natural crustal weathering or volcanic activity. In addition, pollutant material is mobilised during a variety of anthropogenic activities including industrial and agricultural practices or weathering processes such as acid rain erosion. A conceptual model of the marine biogeochemical cycle for the trace metals Fe, Co and Zn is represented in Figure 1.8.

The principle routes by which both natural and anthropogenically derived trace metals reach the oceans are fluvial (river) and atmospheric transport. Trace metals are delivered to the oceans from the oceanic crust via weathering of basalt rocks and high-temperature hydrothermal activity (Chester, 2003). Processes removing trace metals from the oceans include active biological uptake by phytoplankton and passive scavenging onto living and dead particulate material (Johnson *et al.*, 1997; Wu *et al.*, 2001; Bruland and Lohan, 2003). Whilst a large portion of this particulate material,

along with its associated trace metals, is internally recycled, the ultimate sink of trace metals is generally marine sediments following particle export.

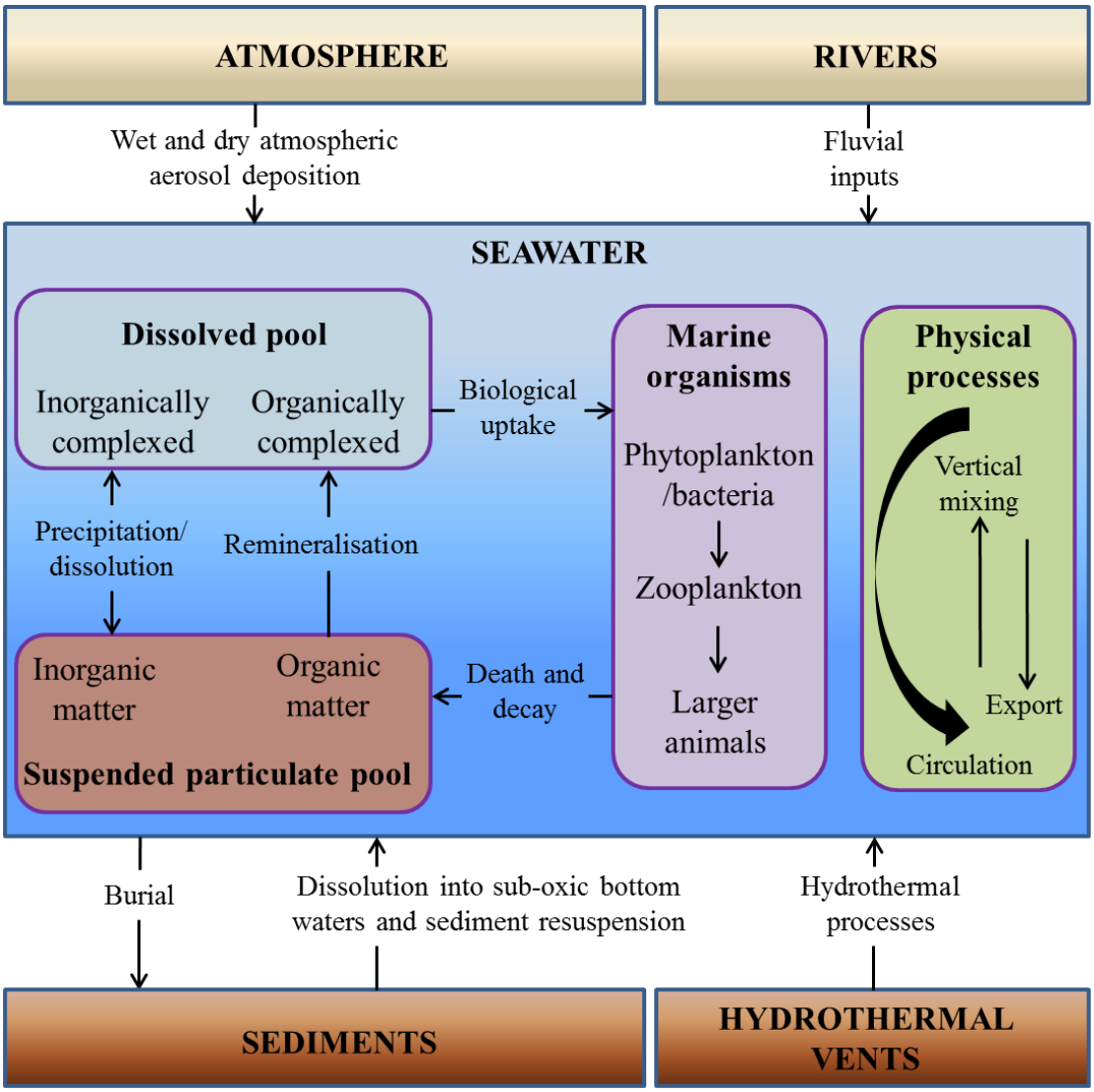

Figure 1.8. Conceptual model showing the main processes involved in the biogeochemical cycling of iron, cobalt and zinc in the oceans and major input and removal mechanisms.

Whilst the processes and mechanisms described above are common for all trace metals, the relative importance of these pathways varies considerably between the elements, both spatially and temporally (Table 1.6). For example, the atmospheric

transport and deposition of dust-derived Fe is greatest in lower latitudes, and greater in the Atlantic Ocean than in the Pacific, Indian or Southern Oceans (Jickells *et al.*, 2005).

Table 1.6. The elemental flux of some bioactive metals to the world's oceans from the major sources; units, mol y^{-1}. Adapted from Chester (2003).

Element	Fluvial gross flux (particulate + dissolved)	Atmospheric gross flux (particulate + soluble)	Fluvial net particulate flux	Atmopsheric particulate flux	Fluvial net dissolved flux	Atmospheric soluble flux	Hydro-thermal dissolved flux
Al	54×10^{12}	0.31×10^{12}	5.4×10^{12}	0.24×10^{12}	6.0×10^{10}	1.2×10^{10}	6.0×10^{8}
Fe	13.3×10^{12}	0.065×10^{12}	1.3×10^{12}	0.06×10^{12}	2.3×10^{10}	0.28×10^{10}	19×10^{10}
Co	056×10^{10}	0.004×10^{10}	0.05×10^{10}	0.003×10^{10}	0.013×10^{10}	0.68×10^{7}	68×10^{5}
Zn	6.0×10^{10}	0.25×10^{10}	0.6×10^{10}	0.17×10^{10}	1.4×10^{10}	0.08×10^{10}	0.32×10^{10}
Mn	30×10^{10}	0.14×10^{10}	2.9×10^{10}	0.1×10^{10}	0.55×10^{10}	0.04×10^{10}	3.4×10^{10}
Cu	2.5×10^{10}	0.06×10^{10}	0.24×10^{10}	0.04×10^{10}	0.5×10^{10}	0.01×10^{10}	13×10^{8}

1.3.2. Atmospheric deposition

The atmospheric transport and deposition of continentally derived lithogenic particles (commonly referred to as dust) is a major source of trace metals to the oceans (Duce and Tindale, 1991; Jickells *et al.*, 2005; Ussher *et al.*, 2013). In regions of the ocean far from fluvial or hydrothermal influences, atmospheric dust deposition may be the only source of trace metals, thus having a significant effect on surface ocean biogeochemistry.

Dust becomes entrained in the troposphere when high velocity winds blow across regions of erodible surfaces such as deserts. This dust is transported to the oceans where it enters through dry and wet deposition mechanisms (Helmers and Schrems, 1995; Sarthou *et al.*, 2003). The distance that dust particles are transported is generally dependant on the particle size and the rate of gravitational settling (Maring *et al.*, 2003; Kallos *et al.*, 2006). For example, the residence time of dust particles in the troposphere

ranges from days for particles > 2.5 µm, to weeks for smaller particles (Perry *et al.*, 1997; Maring *et al.*, 2003; Kallos *et al.*, 2006).

Atmospheric dust concentrations, and hence the dry and wet deposition of dust to the oceans, are highly variable both spatially and temporally and yet are relatively well understood (Prospero and Lamb, 2003; Jickells *et al.*, 2005). For instance, Jickells *et al.* (2005) have estimated that the world's oceans receive an annual atmospheric dust input of approximately 450 T g yr^{-1} (x 10^{12} g y^{-1}). The spatial variability of this annual dust flux is shown in Figure 1.9. Of this dust flux, the North Atlantic receives approximately 43 % (194 Tg y^{-1}) due to the influence of the seasonally oscillating Saharan dust plume between 0 and 30° N. In contrast, the South Atlantic receives only 4 % (18 Tg y^{-1}) of the global dust flux, the Indian Ocean 25 % (113 Tg y^{-1}), the Pacific Ocean 21 % (95 Tg y^{-1}) and the Southern Ocean 6 % (27 Tg y^{-1}).

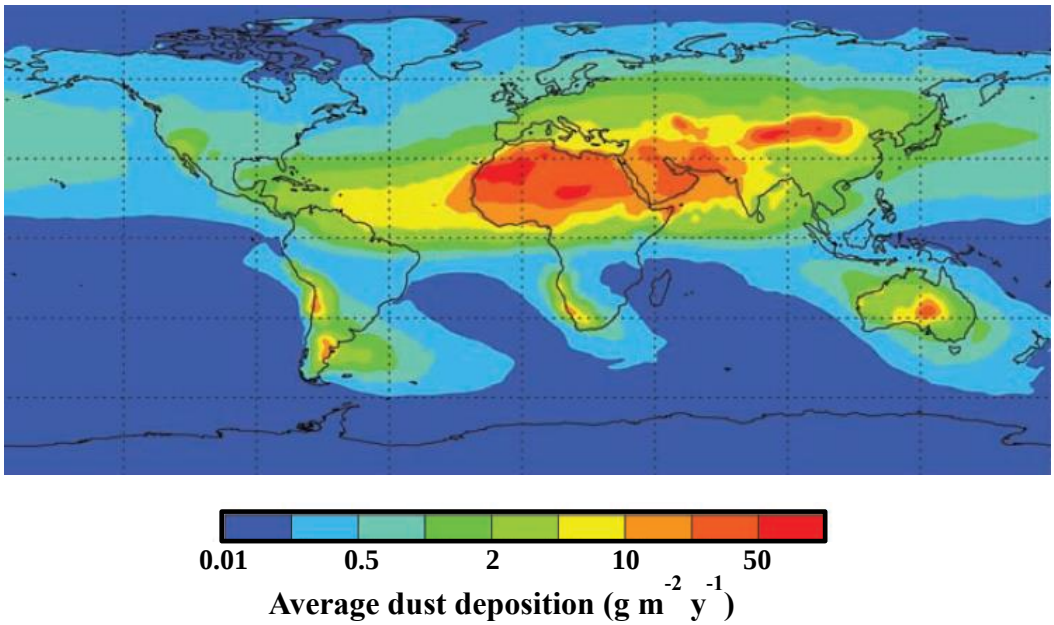

Figure 1.9. Atmospheric dust fluxes to the world's oceans based on a composite of three published modelling studies. Total atmospheric dust inputs to the oceans = 450 Tg y^{-1}. Percentage inputs to the ocean basins are as follows: N. Atlantic, 43 %; S. Atlantic, 4 %; N. Pacific, 15 %; South Pacific, 6 %; Indian, 25 %; and Southern Ocean, 6 %. Taken from Jickells *et al.* (2005).

Calculations by Chester (2003) have estimated the atmospheric particulate flux of selected trace metals to the world's oceans and these values are shown in Table 1.6. The particulate Fe flux of 0.06 x 10^{12} mol y^{-1} is several orders of magnitude greater than the values estimated for both Co and Zn, which is not surprising considering their relative abundance in the earth's continental crust; Fe = 3.5 %, Zn = 0.0071 % and Co = 0.0017 % (Taylor and McLennan, 1985; McLennan, 2001). However, only a fraction of the trace metals associated with atmospherically transported dust are soluble in seawater and therefore bioavailable to phytoplankton and bacteria (Spokes and Jickells, 1996; Baker and Croot, 2010; Thuróczy *et al.*, 2010).

The solubility of aerosol trace metals remains a key uncertainty in our understanding of marine trace metal biogeochemical cycles and their links with trace metal metabolism, primary production and the global carbon cycle. The uncertainties surrounding aerosol trace metal solubility result from the diverse range of techniques used in solubility estimates (Baker *et al.*, 2006; Sholkovitz *et al*., 2012) and from the complex interactions that occur in both the atmosphere and oceans which alter trace metal solubility. Such interactions include aerosol source/mineralogy, atmospheric chemical/photochemical processing, aerosol size, the type of deposition (dry or wet), seawater dissolved metal concentrations, seawater metal-binding ligand concentrations and biological influences from phytoplankton and bacteria and grazing effects (Desboeufs *et al.*, 1999; 2005; Baker and Jickells, 2006; Baker and Croot, 2010; Sholkovitz *et al.*, 2012). As a consequence, the fractional solubility of aerosol trace metals such as Fe, Zn and Co show great variation between oceanic regions (*e.g.* Baker *et al.*, 2006; Thuróczy *et al.*, 2010; Shelley *et al.*, 2012; Sholkovitz *et al.*, 2012; Mason,

2013) with average open ocean solubility's of 4.6 %, 45 %, and 22.5 % respectively (Chester, 1996; Fan *et al.*, 2006).

Based on the atmospheric trace metal particulate fluxes detailed in Table 1.6 and the average aerosol solubility for Fe, Zn and Co reported above, the estimated soluble atmospheric flux of Fe to the oceans is 0.28 x 10^{10} mol y^{-1}, whilst for Zn the soluble flux is 0.08 x 10^{10} mol y^{-1} (Table 1.6). Both of these values are several orders of magnitude higher than the soluble atmospheric Co flux of 0.68 x 10^{7} mol y^{-1}. An example of the soluble atmospheric Fe flux to the world's oceans estimated using a three-dimensional model of dust entrainment, transport, deposition and solubility is shown in Figure 1.10 (Behrenfeld *et al.*, 2009).

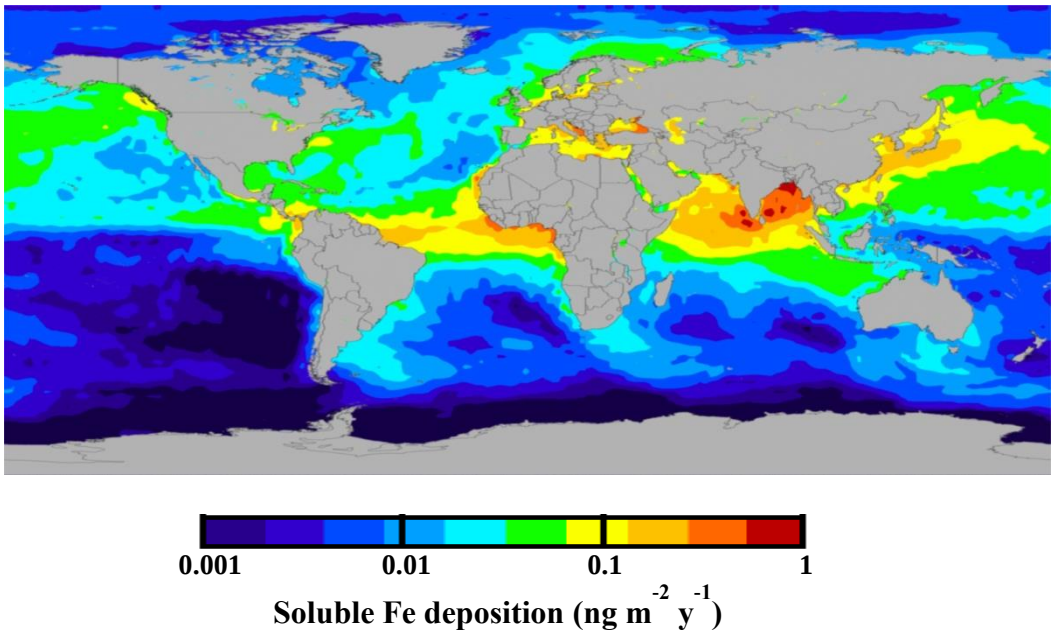

Figure 1.10. Atmospheric soluble iron deposition to the world's oceans estimated using a three-dimensional model of dust entrainment, transport, deposition and solubility. Taken from Behrenfeld *et al.* (2009).

1.3.3. Fluvial inputs

Much of the particulate material mobilised during both natural and anthropogenic weathering of the continental crust is transported to the land-sea margin by rivers (Boyle *et al.*, 1974). As can be seen from Table 1.6, the gross fluvial flux (particulate + dissolved) therefore totally dominates the supply of trace metals to the oceans. Fluvial inputs however, are not considered a dominant source of trace metals to remote open ocean regions. What is also clear from Table 1.6 is that the difference between the fluvial gross and net fluxes is much larger than the atmospheric equivalent. This large difference is due to complex processes occurring in the estuarine environment.

Estuaries are mixing zones for fresh and saline water which results in complex boundary conditions in the estuarine mixing zone. As a result, riverine trace metals are subject to a variety of chemical, physical and biological processes that act as a filter (Sholkovitz and Copland, 1981; Turner and Millwood, 2002; Fitzsimons *et al.*, 2011). The most important processes that occur in the estuarine mixing zone are desorption, adsorption and complexation, which interact to affect the partition of trace metals between the solution and suspended particulates (Sholkovitz and Copland, 1981; Santschi *et al.*, 1997; Fitzsimons *et al.*, 2011).

Once in the mixing zone, trace metals are desorbed from the riverine suspended particulates due to the increased competition for binding sites from major seawater cations, such as Mg^{2+} and Ca^{2+}, that increase in concentration concomitant with increasing salinity, thereby enhancing the dissolved trace metal pool (van der Weijden *et al.*, 1977; Li and Chan, 1979). The adsorption of dissolved trace metals by seawater inorganic anions and cations, such as Cl^-, SO_4^{2-}, Mg^{2+} and Ca^{2+}, followed by

sedimentation in the estuarine mixing zone, removes trace metals from the dissolved pool and therefore significantly reduces the gross fluvial input of trace metals to the marine environment (Sholkovitz and Copland, 1981; Escoube *et al.*, 2009) (Table 1.6). This process is thought to remove up to 80 % of Fe at seawater Ca^{2+} concentrations but only 3 % of Co from river water at seawater Ca^{2+} concentrations. Crucially, the pioneering studies of Sholkovitz and Copland (1981) found that organic complexation increases the concentrations of dissolved trace metals at high salinities. The organically complexed trace metals can then be transported from the estuaries into the coastal oceans (Powell and Wilson-Finelli, 2003). In addition to chemical processing, the extent to which trace metals are removed is also a function of the river flow rate, tidal cycle and the size of the suspended particulate material to which the metal is adsorbed. For example, smaller sized particles are more readily retained in suspension during tidal cycles and at times of high flow rates, and thus may escape the mixing zone.

The complex nature of the estuarine mixing zone, coupled with the spatial and temporal differences in riverine trace metal inputs makes it difficult to accurately determine the net flux of dissolved trace metals to the marine environment. Simple estimates based on the estimated global fluvial particulate flux of 15500 Tg y^{-1} (Chester, 2003) may afford us an insight. According to Judson (1968), it is probable that approximately 90 % of the particulate material transported by rivers is trapped in estuaries. This would result in a global fluvial net particulate flux of 1550 Tg y^{-1}. By following the same procedure it is possibly to estimate the fluvial net particulate flux of trace metals to the world's oceans (Table 1.6) based on the gross flux estimates reported by Chester (2003). Subsequently, these authors calculated the dissolved fluvial flux of Fe and Zn to be 0.54 – 2.3 x 10^{10} mol y^{-1} and 0.04 – 1.4 x 10^{10} mol y^{-1} respectively

whilst the flux of Co is lower at 0.011 – 0.013 x 10^{10} mol y^{-1}. It should be noted that for Zn, the fluvial net dissolved flux exceeds the net particulate flux, a situation that may arise when estuarine processes lead to the addition of dissolved components from the particulate phase. For example, Li *et al.* (1984) reported that the desorption of Zn increased with salinity but reported minimal Zn coagulation during estuarine mixing of the Hudson and Mississippi rivers.

1.3.4. Hydrothermal inputs

The discovery of hydrothermal vents on the deep ocean floor in the 1970's has transformed our understanding of the sources and sinks of trace metals to the oceans. High concentrations of trace metals, including Fe, Co and Zn, have been reported in the vicinity of these vents (Fouquet *et al.*, 1993; Boyle *et al.*, 2005; Statham *et al.*, 2005; Hardardóttir *et al.*, 2009; Saito *et al.*, 2013). In fact, the trace metal concentrations in these high temperature, reducing fluids have been reported to be enriched by 7 – 8 orders of magnitude (German and Von Damm, 2003).

The trace metal composition of hydrothermal vent fluids is controlled by a number of complex chemical and physical interaction that vary in both time and space (Tivey, 2007). For example, concentrations of Fe, Co and Zn in hydrothermal fluids venting from mid-ocean ridge sites range from 7 – 18700 µM, 0.02 – 1.43 µM and 79 – 780 µM respectively (Tivey, 2007; Hardardóttir *et al.*, 2009). Given the high concentrations of Fe in hydrothermal fluids, and the fact that the global hydrothermal dissolved Fe flux (2.3 – 19 x 10^{10} mol y^{-1}) is greater than the combined dissolved Fe flux from fluvial and atmospheric sources (Table 1.6), it is not surprising that recent

attention has focused on hydrothermal Fe as an important source of oceanic dissolved Fe (Statham *et al.*, 2005; Boyle and Jenkins, 2008; Toner *et al.*, 2009; Saito *et al.*, 2013). Bennett *et al.* (2008) estimate that submarine venting may account for between 12 – 22 % of the global deep-ocean dissolved Fe budget. Furthermore, Tagliabue *et al.* (2010) argue that as hydrothermal dissolved Fe fluxes are constant over millennial timescales they may buffer the global oceanic dissolved Fe inventory against short-term (decadal) fluctuations in atmospheric dust deposition. Thus, hydrothermal Fe inputs may have a significant role in long-term climate regulation. However, recent results from Saito *et al.* (2013) suggest that the global Fe contributions from hydrothermal vents may be significantly higher than previously thought owing to a greater contribution from vents along slow-spreading ridges (previous assumed to be less significant than fast spreading ridges and therefore relatively unexplored). These authors calculated Fe contributions over the South Atlantic slow spreading ridge were 80 fold higher than reported for a plume emanating from faster spreading ridges in in the Southeastern Pacific.

Hardardóttir *et al.* (2009) have also recently sampled mid-Atlantic ridge hydrothermal systems close to Iceland and report Fe and Zn concentrations of 154 – 2431 µM and 79 – 393 µM respectively. These concentrations were several orders of magnitude higher than the concentrations observed in shallower waters above the vent (Fe = 0.8 µM and Zn = 0.3 µM) due to precipitation caused by boiling during ascent. Interestingly, Co concentrations in the hydrothermal fluids were below the limit of detection (< 0.2 µM) indicating, as shown in Table 1.6, that hydrothermal activity is not a major source of Co to the oceans. This hypothesis is supported by the findings of Noble *et al.* (2012) who report no hydrothermal input of Co along the same cruise track as Saito *et al.* (2013).

1.3.5. Sedimentary supply, upwelling, vertical mixing and lateral transport

Although atmospheric deposition is believed to be the principle mechanism by which trace metals enter the surface waters of the open ocean (see section 1.3.2), there are a number of regions where dust deposition is low (Fig. 1.9), such as the South Atlantic, the South Pacific and the Southern Ocean (Mahowald *et al.*, 1999; Jickells *et al.*, 2005). In these regions, alternative mechanisms may be as significant as the atmospheric trace metal flux. For example, recent estimates suggest that the sedimentary supply of dFe to the global ocean is similar to that of atmospheric deposition (Moore and Braucher, 2008). The sedimentary supply results from either reductive dissolution of Fe under low oxygen conditions, which has been shown to markedly increase the concentration of dFe in hypoxic bottom waters along the western coasts on North and South America (Bruland *et al.*, 2005; Lohan and Bruland, 2008), or on a smaller scale, from the flux of non-reduced pore waters (Radic *et al.*, 2011; Homoky *et al.*, 2013). In addition, Saito *et al.* (2004) estimate that the dCo flux associated with the Peru upwelling region of 19.9 x 10^6 mol y^{-1} is large enough to replenish 11 % of the entire Pacific dCo inventory. This flux is nearly three times the atmospheric soluble Co flux calculated by Chester (2003) (Table 1.6). Thus, the upwelling of metal-rich water at continental margins followed by lateral transport can provide an important mechanism for the supply of trace metals to the surface ocean and phytoplankton (*e.g.* Lohan and Bruland, 2008; Bruland *et al.*, 2005).

In the North Pacific, Lippiat *et al.* (2011) report mesoscale anticyclonic eddies that are an important mechanism for the transport of elevated Fe from the Fe-rich but nitrate-poor Alaska Coastal Current to the HNLC central Gulf of Alaska. These authors suggest that these eddies can provide a source of Fe to this HNLC region, thereby

promoting and sustaining primary productivity within the eddy over its lifespan (> 3.5 y). Similarly, the upwelling and vertical mixing of intermediate and deep waters, particularly at high latitudes, provides a significant return path for trace metals to the surface ocean. For example, observations by Klunder *et al.* (2011) and Croot *et al.* (2011) indicate that upwelling and mixing provide the principle supply of Fe and Zn respectively to surface waters of the Southern Ocean. It is therefore possible that the upward branch of the Meridional Overturning Circulation (MOC) may be a significant return pathway for trace metals to thermocline waters at low latitudes, as is the case for the macronutrients (Sarmiento *et al.*, 2004; Palter *et al.*, 2010).

1.3.6. Regeneration

The process of internal recycling is particularly relevant to the nutrient-like trace metals such as Zn and to those that show aspects on nutrient-like behaviour (*e.g.* Fe and Co). Like the macronutrients, trace metals undergo multiple cycles of assimilation into biogenic particulate material within the surface ocean and release though decomposition and remineralisation at depth (Bruland and Lohan, 2003) (Fig. 1.8).

For the purpose of this section, it may be informative to follow the example of Bruland and Lohan (2003) and describe the internal cycling of Fe and Co in terms of Zn cycling. Due to the specific cellular requirement for Zn by important biochemical functions (Table 1.1 and Fig. 1.2), dZn is rapidly taken up into phytoplankton cells where it may reside for a day or two before the cells are consumed by herbivorous zooplankton (Hutchins and Bruland, 1994). In the open ocean, the majority of Zn and other trace metals will be remineralised in the surface ocean where it will perhaps

undergo 10 further uptake and remineralisation cycles (Hutchins *et al.*, 1993; Hutchins and Bruland, 1994). For Fe, whose internal cycle has been studied to a greater extent than Zn, the high cellular demand of phytoplankton phyla (Fig. 1.4) coupled with the rapid recycling within the microbial food-web has been termed the 'Ferrous wheel' (Kirchman, 1996). There is also evidence that Co is efficiently recycled in the surface ocean (Noble *et al.*, 2008; Bown *et al.*, 2011), and to a greater extent than Zn (Morel, 2008).

Zinc is eventually exported from the surface ocean to the interior ocean as part of the oceanic biological pump. Here, Zn is released back into the dissolved pool by either remineralisation of organic particulate matter and/or the oxidation of inorganic particulate matter (Bruland and Lohan, 2003). In the case of Fe, particle recycling in deeper waters is particularly important where Fe inputs from the surface or below are high (Planquette et al., 2009; Fitzsimmons *et al*., 2013; Ussher *et al*., 2013). In such scenarios, the recycling of particulate material with high Fe:C ratios, followed by upwelling, may provide an important source for dFe to surface waters as shown for the tropical North Atlantic (Ussher *et al*., 2013) and Crozet Islands (Planquette *et al*., 2009).

Within a few hundred to a thousand years, the dZn can be returned to the surface ocean through upwelling where the cycle can repeat itself numerous times during the course of its oceanic residence time (Table 1.2) before being removed to the sediments.

1.3.7. Removal mechanisms

The principle removal mechanisms for Fe and Co in the open ocean include active biological uptake and passive scavenging onto living and dead sinking particulate

material (Johnson *et al.*, 1997; Wu *et al.*, 2001; Bruland and Lohan, 2003). Diatoms are particularly important for the removal of Fe because of their high cellular requirement (Fig. 1.4) and their important role in new and export production (Smetacek, 1999). Some species of diatoms have a luxury uptake capability that allows then to store Fe at concentrations 10 – 30 times that required for maximum growth (Sunda and Huntsman 1995b; Chen *et al*., 2011), a mechanism that allows them to accumulate excess Fe during periods of high Fe availability. For Co, another important removal mechanism appears to be biotic Co-Mn co-oxidation. For instance, due to their similar redox speciation, both Co and Mn can be co-oxidised via a common microbial pathway in regions of high microbial Mn-oxidising activity (Moffett and Ho, 1996). If the concentrations of Co or Mn oxides are also high, such as in regions with an advective margin source, then the subsequent co-precipitation can remove Co from the water column (Tebo *et al.*, 1984; Moffett and Ho, 1996). For Zn, being a nutrient-like trace metal, the principle removal process is also biological uptake (Saito *et al.*, 2010; Jakuba *et al.*, 2012).

Whilst a large portion of trace metals removed from the water column by biological assimilation is internally recycled (see section 1.3.6), the ultimate sink of trace metals is generally marine sediments (Fig. 1.8). Once finally buried in the sediments, it may be hundreds of millions of years before these trace metals make their way back to ocean via atmospheric, fluvial or hydrothermal sources.

1.4. The Atlantic Ocean

The Atlantic Ocean, the second largest of the five major ocean basins, is characterised by contrasting biogeochemical provinces from polar to tropical, oligotrophic gyres to upwelling. Each of these provinces experiences different trace metal input and removal mechanisms. Due to global air mass circulation, the Atlantic Ocean receives almost half the annual input flux of continentally derived mineral dust (Jickells *et al.*, 2005), a significant source of trace metals to surface waters of the open ocean (Buck *et al.*, 2010a; Shelley *et al.*, 2012; Ussher *et al.*, 2013). Owing to the distribution of the major continental land masses, the North Atlantic receives the majority of this input flux, predominately from the Sahara Desert, whilst the South Atlantic receives the lowest flux of all the major ocean basins (Jickells *et al.*, 2005).

Trace metal studies in the Atlantic Ocean benefit from a number of time-series data. For example, situated in the Sargasso Sea, the Bermuda Atlantic Time-Series (BATS) station has been repeatedly sampled over the last few decades providing a large quantity of trace metal biogeochemistry data, *e.g.* the controls on dissolved Fe and Co concentrations in surface waters (Shelley *et al.*, 2012). At the basin scale, the Atlantic Meridional Transect (*AMT*) (www.*AMT*-uk.org) time series programme has occupied hydrographic stations along a 12,000 km gyre centred transect between 50° N and 50° S for almost 20 years. In that time, 22 cruises have taken place that have allowed the biogeochemical cycles of important bioactive elements such as Fe and aluminium to be investigated (*e.g.* Bowie *et al.*, 2002a; Moore *et al.*, 2009; Ussher *et al.*, 2013).

GEOTRACES is an on-going international research programme which aims to improve the understanding of biogeochemical cycles and distribution of trace elements and their isotopes in the global oceans at an unprecedented scale. The central focus of

the programme is a series of cruises (GEOTRACES Sections) that cover the global oceans from the surface waters to the ocean floor. The completed GEOTRACES Sections along with the planned Sections are shown in Figure 1.11. The UK contribution to the GEOTRACES programme is helping to rapidly increase the observational data from the Atlantic Ocean and thereby adding to our understanding of global trace metal cycling.

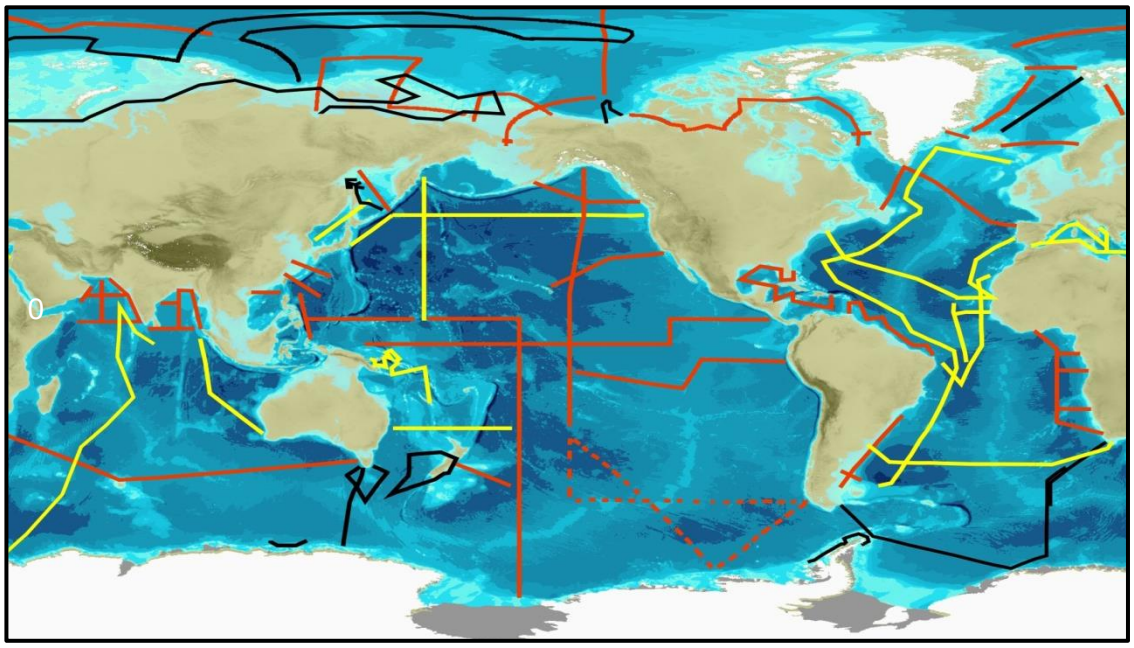

Figure 1.11. GEOTRACES study Sections including completed Sections (yellow), Sections completed as part of the GEOTRACES contribution to the International Polar Year, planned Sections (red). Taken from www.geotraces.org (13.9.2013).

In addition to the *AMT* and GEOTRACES programmes, there are several other major international oceanographic programmes that are constantly adding to our knowledge of trace metal cycling in the Atlantic Ocean. These include the Surface Ocean Lower Atmosphere Study (SOLAS) and Climate Variability and Predictability (CLIVAR), which samples to 1000 m.

Presently, much of the attention in the Atlantic Ocean has focused on Fe and aluminium owing to importance of Fe in climate regulation and Al as a proxy for mineral dust (*e.g.* Vink and Measures, 2001; Bowie *et al.*, 2002a; Measures *et al.*, 2008; Dammshäuser *et al.*, 2011; Fitzsimmons *et al.*, 2013; Ussher *et al.*, 2013). In comparison, relatively little is known about the biogeochemical cycling of Zn and Co in the Atlantic. The *AMT* and GEOTRACES programmes therefore provide an excellent opportunity to build on the work of previous oceanographic campaigns and improve our current understanding of Fe biogeochemistry, and further our understanding of Zn and Co biogeochemistry.

1.5. Aims and objectives

The aims of the work presented in this thesis were to investigate the distribution of Fe, Zn and Co in the Atlantic Ocean and to determine how physical, chemical and biological interactions influence their cycling in very different ocean environments. In order to achieve this, samples were collected on three UK led research cruises. *AMT*-19 was a large-scale transect between 50° N to 40° S in the Atlantic Ocean that sampled across diverse biogeochemical provinces, including the North and South oligotrophic gyres and the equatorial upwelling regime, and areas of high and low atmospheric dust deposition fluxes. The UK GEOTRACES Section A10 consisted of two separate research cruises located in the South Atlantic along the 40° S parallel, a region where a number of possible inputs and processes occur including atmospheric deposition (South American dust plume), fluvial inputs (Rio de la Plata estuary), surface currents (Agulhas Current and Brazil-Malvinas Current), Southern Ocean mode waters, and

hydrothermal venting (mid-Atlantic ridge), but where there is little understanding of the supply and biogeochemical cycling of trace metals.

Flow injection techniques, using both chemiluminescence (FI-CL) and fluorescence (FI-FL) detection systems, were optimised to determine these trace metals at picomolar to nanomolar concentration in samples from both coastal and open ocean regimes. These FI methods were used to measure total dissolved Fe and total dissolvable Fe during *AMT*-19 and dissolved Co and Zn as part of the UK GEOTRACES section A10 programme (cruises D357 and JC068).

The key objectives were therefore:

(I) Optimisation of sensitive, robust, flow injection systems capable of detecting dissolved Fe, Zn and Co, as well as total dissolvable Fe, at low concentrations (pM) in seawater samples, suitable for both laboratory and shipboard use.

(II) Analyse GEOTRACES and SAFe intercalibration standards and to submit the results to the GEOTRACES Standards and Intercalibration Committee in order to improve the consensus values for dissolved Fe, Zn and Co.

(III) Investigate the sources and biogeochemical cycling of Fe to the upper water column (≤ 150 m) of the North and South Atlantic Ocean, focusing on atmospheric dust deposition, biological Fe uptake and remineralisation.

(IV) Determine the distribution and biogeochemical cycling of Zn and Co throughout the entire water column of the South Atlantic Ocean along the 40° S parallel.

(V) Investigate the seasonal impacts of Zn and Co concentrations in the Southeast Atlantic Ocean on their utilisation by phytoplankton, and how these trace metals influence phytoplankton community structure.

(VI) Interpret Fe, Zn and Co data in conjunction with other hydrographic parameters to further our understanding of their biogeochemical cycling in the Atlantic Ocean and publish the findings in peer reviewed journals.

In order to present the results associated with the stated aims and objectives, this thesis will be presented in the following format:

Chapter 2

Describes the analytical methods employed during this study. This chapter introduces the concept of flow injection as an analytical tool for dissolved Fe, Zn and Co analyses and describes the chemiluminescence and fluorescence reaction mechanisms used. This is followed by a detailed description of the flow injection techniques used to determine dissolved Fe, Zn and Co in seawater samples. Finally this chapter describes the analytical methods used to determine biological N_2 fixation rates and pH in seawater.

Chapter 3

Iron data are presented from the Atlantic Meridional Transect (cruise *AMT*-19) between 50° N and 40° S during October and November 2009. The sources of dissolved Fe and total dissolvable Fe data are discussed in the context of the physico-chemical and biological properties that influence their distributions in the upper water column (≤ 150 m). Key focus is on the atmospheric supply of Fe to the Atlantic and estimates of the aerosol Fe deposition flux to surface waters of each geographical province are

presented and discussed. This chapter concludes with calculations of the residence time for Fe in surface waters of the Atlantic Ocean.

Chapter 4

Investigates the biogeochemical cycle of Zn in the South Atlantic at, 40° S, as part of the UK GEOTRACES programme. Initially, the distribution of Zn is described and related to ancillary hydrographic data and macronutrient distributions to associate its distribution with the water masses present at this latitude. Strong correlations between Zn and the macronutrients silicate and phosphate are presented and used to discuss the biological role for Zn in the South Atlantic. Finally, this chapter presents evidence for the lack of a direct return path for Zn from the Southern Ocean to 40° S as part of thermohaline overturning circulation. This chapter is based on a paper of the same name accepted for publication in Global Biogeochemical Cycles (DOI: 10.1002/2013GB004637) that includes a novel Zn* tracer for low Zn Southern Ocean waters that forms part of Chapter 6 in this thesis.

Chapter 5

Presents a seasonal study of Co and Zn biogeochemical cycling in the South Atlantic Ocean, at 40° S, as part of the UK GEOTRACES programme. The purpose of this research was to establish how the concentrations of these elements influenced phytoplankton communities in this productive region. To complement the Zn distributions described in Chapter 4, Co distributions are described for the entire South Atlantic at 40° S, whilst Co and Zn distributions are also described for two additional transects in the Southeast Atlantic Ocean and related to ancillary hydrographic data and macronutrient distributions. Metal-phosphate correlations in the upper water column are

presented as evidence for trace metal utilisation and the relative nutritional role of Co and Zn in the South Atlantic is described. Finally, Co and Zn distributions are considered alongside phytoplankton diversity to determine how seasonal changes in metal concentration may alter community structure.

Chapter 6

The final chapter provides a holistic summary based on the key findings presented in the previous chapters and includes recommendations for future research directions. Specifically, a new Zn* tracer is presented that can be used to map the transport of zinc with Sub-Antarctic Mode Water to pycnocline waters of the world's oceans.

Chapter 2

Methods

2.1. Introduction

To improve our understanding of the role of bioactive trace metals (*e.g.* Fe, Zn and Co) in global oceanic biogeochemical cycles, it is necessary to obtain high resolution and accurate measurements of these metals in seawater. However, the extremely low concentrations of Fe, Zn and Co (sub-nanomolar) in the open ocean present a significant analytical challenge. Firstly, the presence of various metal components on research vessels provides a constant threat of contamination during sample collection. Secondly, for the shipboard determination of Fe, Zn and Co, only a limited number of methods are sufficiently portable and sensitive enough to perform such analyses, including adsorptive cathodic stripping voltammetry (CSV) (Ellwood and van den Berg, 2000; Buck and Bruland, 2007) and flow injection analysis (FIA) (Lohan *et al.*, 2006; Shelley *et al.*, 2012; Gosnell *et al.*, 2012; Ussher *et al.*, 2013). These methods typically have detection limits in the picomolar concentration range and have enabled accurate, in-situ determination of very low metal concentrations.

In order to determine Fe, Zn and Co in seawater, there is a need for reliable sampling and handling protocols and sensitive, accurate and rapid analytical techniques suitable for ship- and laboratory-based use. The international GEOTRACES programme has adopted standard protocols for sampling and handling of trace metal seawater samples (http://www.geotraces.org/science/ intercalibration/222-sampling-and-sample-handling-protocols-for-geotraces-cruises; de Baar *et al.*, 2008). Furthermore, inter-laboratory calibration is particularly important for assessing the accuracy and suitability of analytical methods for determining trace metals in seawater. The GEOTRACES programme is co-ordinating this effort to ensure that the results from different ship- and

laboratory-based methods can be compared in a meaningful way (www.geotraces.org/science/intercalibration).

2.2. Cleaning protocols

The extremely low concentrations of Fe Zn and Co in seawater and the various sources of contamination from dust particles and manufactured items make it necessary to adopt strict protocols related to cleaning and sample handling prior and during analysis. Table 2.1 summarises the cleaning procedures followed, adapted from the aforementioned GEOTRACES protocols, for the cleaning of plasticware used in all experiments during this study. Low density polyethylene (LDPE) containers (Nalgene) were used for both sample collection and solution (reagents, standards) preparation. Sample bottles followed a three stage cleaning procedure whereas reagent and standard bottles followed a two stage cleaning procedure.

Table 2.1. Cleaning protocols for plasticware.

Step	Procedure
Stage 1. *In general laboratory*	
1	Rinse 3 times with distilled water
2	Immerse in 3 M HCl (Fisher, reagent grade) for 1 week
3	Rinse 3 times with distilled water
4	Rinse 3 times with UHP water
Stage 2. *In clean air (class-100) laboratory*	
1	Immerse in 0.5 M HCl (Fisher, trace metal grade) for 1 week
2	Rinse 3 times with UHP water
Stage 3. *For sample bottle storage*	
1	Fill with UHP water and acidify to 0.024 M with HCl (Romil, SpA grade)
2	Triple bag in clean polyethylene bags and store in clean plastic container

UHP = ultra-high purity (≥ 18.2 MΩ cm, Elgastat Maxima)

2.3. Flow Injection Analysis

Flow injection (FI) is an excellent analytical tool for various chemical analyses which can be coupled to a range of detection systems (Zagatto *et al.*, 2012). These techniques have some major advantages over other methods including portability, robustness, low sample and reagent consumption, minimal sample handling and rapid analysis time (of the order of minutes) (Bowie *et al.*, 1998; Obata *et al.*, 1993; Nowicki *et al.*, 1994; Cannizzaro *et al.*, 2000). These benefits, coupled with excellent sensitivity and detection limits, make FI systems particularly well suited to in situ oceanographic trace metal analyses (*e.g.* Bowie *et al.*, 2002b; Lohan *et al.*, 2006; Shelley *et al.*, 2012). In addition, FI methods, coupled with suitable detection systems, allow near real-time data acquisition and analytical windows over a range as much as three orders of magnitude (Xu *et al.*, 2005), and therefore the ability to modify research strategies in response to changes in local environmental conditions, *e.g.* phytoplankton abundance or trace metal inputs. Additionally, it is useful to have FI systems on-board ship to minimise the possibility of contamination and/or sample degradation.

FI systems are ideally suited for use with kinetic catalytic methods, which use the analyte of interest as part of a reaction, resulting in highly sensitive analytical techniques (Measures *et al.*, 1995; Aguilar-Islas *et al.*, 2006; Brown and Bruland, 2008). Flow injection-catalytic methods utilise a number of different (portable) detection systems for the determination of trace metals in seawater, *e.g.* flow injection with spectrophotometric detection (FI-spec) (Measures *et al.*, 1995; Weeks and Bruland, 2002; Lohan *et al.*, 2006); flow injection with chemiluminescence detection (FI-CL) (Obata *et al.*, 1993; Bowie *et al.*, 2002b; Shelley *et al.*, 2010); flow injection with fluorimetric detection (FI-FL) (Nowicki *et al.*, 1994; Brown and Bruland, 2008; Gosnell

et al., 2012). Alternatively, FI systems can be coupled with laboratory-based detection systems such as inductively coupled plasma mass spectrometry (ICP-MS). The main advantage of ICP-MS detection over the portable systems is the ability to perform simultaneous multi-element determinations (Hurst *et al.*, 2008; Milne *et al.*, 2010; Boye *et al.*, 2012). One disadvantage of ICP-MS detection is that the instrumentation is not portable and therefore not suitable for use on board research vessels.

Owing to the extremely low concentrations of dissolved Fe, Zn and Co in the open ocean (dFe = 0.02 – 2 nM, *e.g.* Klunder *et al.*, 2011; Ussher *et al.*, 2013; dZn = 0.01 – 10 nM, *e.g.* Lohan *et al.*, 2002; Gosnell *et al.*, 2012; dCo = 1 – 120 pM, *e.g.* Bown *et al.*, 2011; Shelley *et al.*, 2012) and the complexity of the seawater matrix (which contains the major seawater ions at concentrations up to 10^9 greater than dissolved Fe, Zn and Co), it is essential to include a pre-concentration and matrix removal step where the analyte of interest is separated from the major seawater cations (Na^+, K^+, Mg^{2+}, Ca^{2+} and Sr^{2+}). This can be achieved using a chelating resin. One of the most utilised chelating resins for trace metal analyses contains immobilized 8-hydroxyquinoline (8-HQ). Resin immobilised 8-HQ has affinity for binding several metals, it does not swell and can be regularly exposed to molar concentrations of acids and bases (Landing *et al.*, 1986). Furthermore, extraction onto resin immobilized 8-HQ columns is pH dependant, allowing some chemical control over which trace metals are bound (Sohrin *et al.*, 1998). However, resin immobilised 8-HQ is not commercially available and its synthesis is time consuming and complicated (Landing *et al.*, 1986; Dierssen *et al.*, 2001), leading to inter-laboratory performance variability. Commercially available chelating resins are therefore preferable, because the quality of the resin is reproducible and because their use simplifies system set-up. Commercially

available resins that have been used to determine trace metals in seawater include a nitriloacetic acid-type (NTA) chelating resin (Lohan *et al.*, 2005a; 2006), an ethylenediaminetetraacetic acid-type (EDTA) resin (Sohrin *et al.*, 2008) and the commonly used Toyopearl resin (Warnken *et al.*, 2000; de Baar *et al.*, 2008; Milne *et al.*, 2010; Klunder *et al.*, 2011; Shelley *et al.*, 2010; Castrillejo *et al*., 2013). In this study, the Toyopearl AF-Chelate-650 M resin was used, the characteristics of which are presented in Table 2.2. The Toyopearl resin is a non-swelling, methacrylic polymer bead (Toyopearl HW-65) which contains iminodiacetate (IDA) functional groups. The IDA functional groups serve as a tridentate ligand for complexing metal cations (Warnken *et al.*, 2000). One of the main advantages of Toyopearl is the greater binding capacity compared with resin immobilised 8-HQ (35 ± 10 µeq mL^{-1} versus 10 µeq mL^{-1} respectively).

Table 2.2. The characteristics of Toyopearl AF-Chelate-650M resin (Tosoh-Bioscience, 2010).

Bead	HW-65
Chelating group	Iminodiacetic acid (IDA)
Chelating group structure	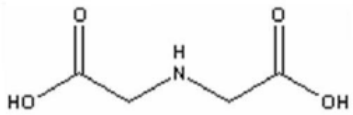
Ion exchange capacity	35 ± 10 µeq mL^{-1}
Particle size	65 µm
Pore size	1000 Å
Exclusion limit	5 x 10^6 Dalton
Shelf life	10 years

2.3.1. Chemiluminescence detection

Chemiluminescence (CL) refers to the emission of light (luminescence) from chemical reactions and is observed in solid, liquid and gas phases (Lin and Yamada, 2003; Barni *et al.*, 2007). Flow injection-chemiluminescence (FI-CL) methods utilise this chemical reaction to quantitatively determine the concentration of an analyte in solution following its catalytic reaction with a chemiluminescent molecule. The popularity of CL as a detection system relates to its high sensitivity, speed of response and the simple instrumentation required (a photomultiplier tube, PMT). In contrast to fluorimetry and absorption methods, no light source is required for CL detection.

There are two principle modes of chemiluminescent emission, direct and indirect, which mainly occur during oxidation reactions or free radical recombination (Barni *et al.*, 2007). Direct chemiluminescence can be represented by:

$$A + R \rightarrow I^{*} \rightarrow PRODUCTS + LIGHT \qquad \text{Eq. 2.1.}$$

Where A is the analyte (*e.g.* Fe), R is the chemiluminescent reagent (*e.g.* luminol) and I* is an excited state intermediate (*e.g.* aminophthalate dianion). Decay of an excited intermediate to a lower energy state product yields light-emitting photons. In cases where the excited state is an inefficient emitter, its energy may be transferred to a sensitizer (F) for light emission to be observed. This is termed indirect chemiluminescence and is represented by:

$$A + R \rightarrow I^{*} + F \rightarrow [F]^{*} \rightarrow PRODUCTS + LIGHT \qquad \text{Eq. 2.2.}$$

The light emitted is detected by a PMT with the quantum yield of photons related to the efficiency of the reaction.

Iron

One of the most sensitive and widely used chemiluminescent molecules for the detection of Fe in seawater is luminol (5-amino-2,3-dihydrphthalazine-1,4-dione) (Obata *et al.*, 1993; Bowie *et al.*, 1998; Achterberg *et al.*, 2001; Ussher et al, 2007; Klunder *et al.*, 2011). However, the mechanism via which the oxidation of luminol results in direct CL is still relatively poorly understood despite a major effort by Merényi and co-workers in the 1980's (Merényi *et al.*, 1990). A more recent understanding of the probable mechanism is reported by Barnett and Francis (2005a) and Barni *et al.* (2007) and is summarised in Figure 2.1.

The major CL generating mechanism for luminol in aqueous solutions occurs in three steps. The primary oxidation (1) of luminol in a basic medium (pH 8 – 14, Barni *et al.*, 2007) occurs via the de-protonation of luminol to monoanionic and dianionic forms and their subsequent oxidation by OH^-, or its radical derivatives, to form luminol radical intermediates. The key intermediate α-hydroxy-hydroperoxide (α-HHP) is formed from the secondary oxidation (2) of the luminol radical, either directly by superoxide (O_2^-) oxidation of the monoanion radical or via the production of the intermediate diazaquinone followed by its oxidation with monodissociated hydrogen peroxide (HO_2^-). The final decomposition step (3) occurs via the de-protonation of the α-HHP (p*K* 8.2 Merényi *et al.*, 1990) to the monoanion form and its subsequent split to form N_2 and an electronically excited aminophthalate (3-APA*). The generation of light occurs during the de-excitation of 3-APA* to the ground state (3-APA) (White and Bursey, 1964; White *et al.*, 1964; Gunderman and McCapra, 1987) at 425 nm (Rose and Waite, 2001).

The decomposition step is dependant solely on the pH of the solution once the α-HHP has been formed, with optimal CL efficiency observed at pH 10.5 due to increased monoanion formation (O'Sullivan *et al.*, 1995).

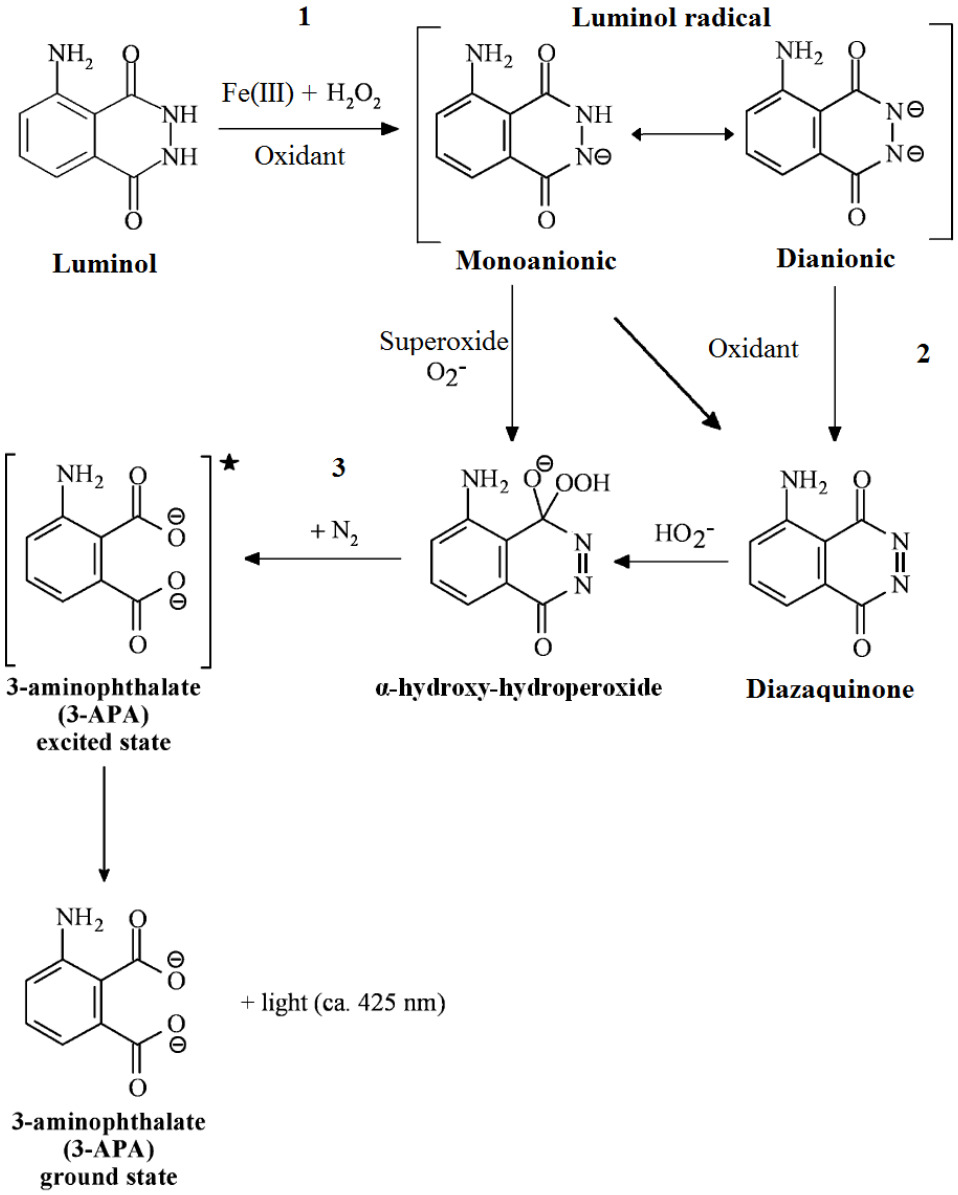

Figure 2.1. The reaction mechanism for luminol chemiluminescence (adapted from Barni *et al.*, 2007).

Cobalt

Oxidation – reduction reactions involving Co and organic polyhydric phenols such as pyrogallol (1,2,3-trihydrobenzene) are particularly efficient producers of indirect CL (Stieg and Nieman, 1977; Yamada *et al.*, 1983; Miller and Ingle, 1981; Evmiridis *et al.*, 2007). Such reactions are modifications of the Trautz-Schorigin Reaction (TSR, Trautz and Schorigin, 1905), which involves the oxidation of gallic acid (3,4,5-trihydroxybenzene) by hydrogen peroxide in a basic medium (pH 8 – 12, Slawinska and Slawinski, 1975) to produce CL emission in the visible region (580 – 850 nm). During this oxidation process, an excited singlet oxygen molecule ($^1O_2^*$) is formed and the light emission occurs via intermolecular energy transfer as well as simple excimer emission (Bowen, 1964; Kearns, 1971; Evmiridis *et al.*, 2007).

An example of the TSR where either pyrogallol or gallic acid is oxidised by hydrogen peroxide to produce light emission is shown in Figure 2.2. The reaction proceeds as a gradual multi-stage process involving coloured intermediates. The polyphenol (1) is oxidised to its orthoquinone (2), which can either polymerize or, after further dehydrogenation and loss of carbon, couple with another molecule of pyrogallol to give purpurogallin (3). This 7-membered ring then undergoes hydroperoxide-mediated ring cleavage. The final oxidation products (4 – 7) are tropolone, oxylate, a brown, low-molecular weight, water soluble polymer of unknown structure and carbon dioxide (Slawinska and Slawinski, 1975). Generation of the excited singlet oxygen molecule ($^1O_2^*$) can occur either in the polymerisation step or during the ring cleavage step. The emission spectrum consists of two bands – an intense, narrow, red emission band between 630 – 645 nm during the polymerization step and a weaker blue emission

band in the range 440 – 510 nm resulting from the oxidative cleavage of the polyphenol (Bowen, 1964; Slawinska and Slawinski, 1975; Stieg and Nieman, 1977).

Flow injection methods have been developed to determine dissolved Co (dCo) in seawater using gallic acid (Sakamoto-Arnold and Johnson, 1987) and more recently pyrogallol (Cannizzaro *et al.*, 2000; Shelley *et al.*, 2010) as the polyphenol in the TSR, with pyrogallol found to be 40 % more sensitive than gallic acid (Cannizzaro *et al.*, 2000).

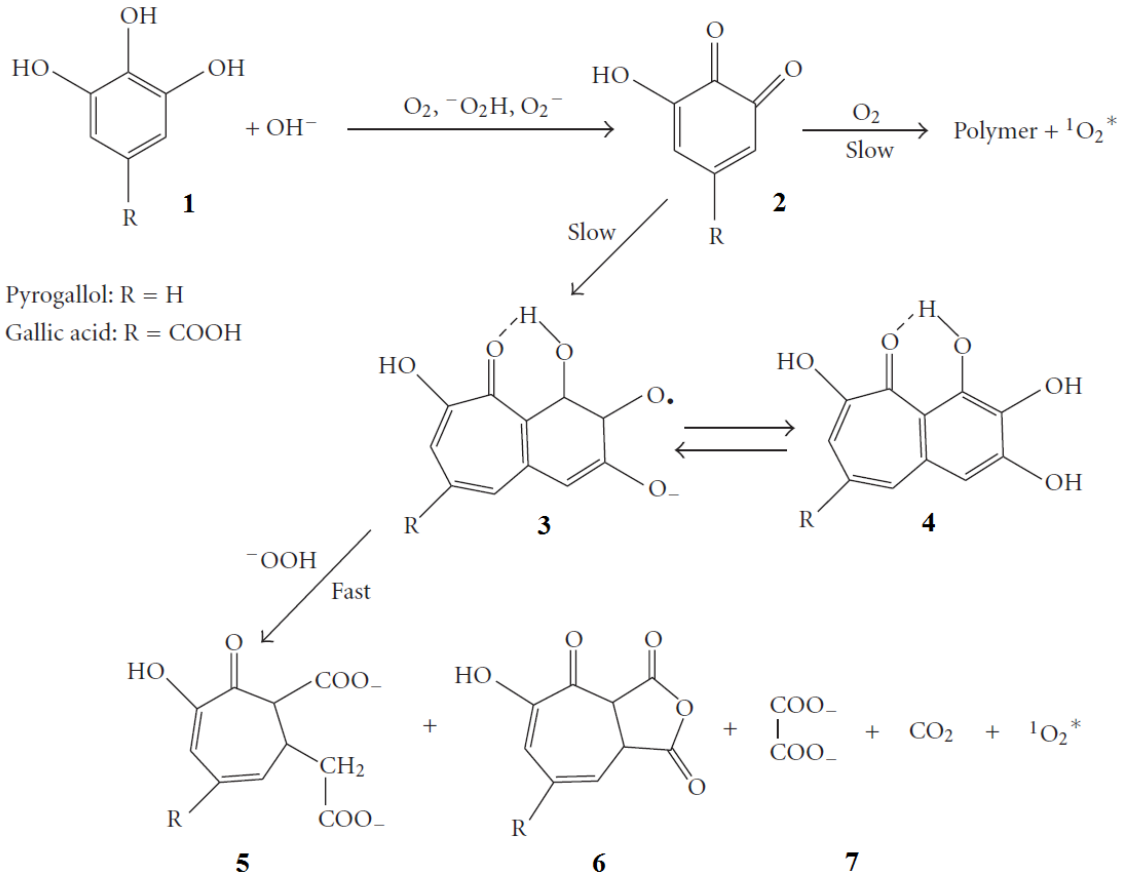

Figure 2.2. Trautz-Schorigin Reaction for the oxidation of pyrogallol and gallic acid by hydrogen peroxide (adapted from Evmiridis *et al.*, 2007).

2.3.2. Fluorescence detection

Fluorescence (FL) can be distinguished from CL according to the way in which the molecule is promoted to the excited state. Whilst the CL excited state is generated through chemical reactions, the fluorescence excited state is generated by ultraviolet/visible radiation from a high intensity light source (*e.g.* xenon or mercury arc lamps) (Diaz-Garcia and Badia-Laiño, 2005a). Fluorescence techniques, like CL techniques, are sensitive to environmental conditions (*e.g.* solvent type, the presence of quenchers, pH, ionic strength and temperature) that may alter the rate and/or intensity of the FL reaction (Barnett and Francis, 2005b; Diaz-Garcia and Badia-Laiño, 2005a). Fluorescence detection systems offer the capability to isolate wavelengths, select source intensity, excitation beam size and location (Trojanowicz, 2000; Barnett and Francis, 2005b), and therefore, often allow for better performance characteristics such as selectivity and reproducibility, compared with CL (Diaz-Garcia and Badia-Laiño, 2005a). However, the complexity of FL instrumentation makes this technique prone to source noise and light scattering, which may reduce the detection limits compared with those achievable with CL (Barnett and Francis, 2005b).

A method to improve FL detection limits, along with increasing selectivity, is by FL derivatization procedures through which weakly fluorescent or non-fluorescent compounds are converted into highly fluorescent products (Diaz-Garcia and Badia-Laiño, 2005b). For FL derivatization based on the formation of metal complexes, the ligand must have the capacity to covalently bond with the metal ion through at least two functional groups (Diaz-Garcia and Badia-Laiño, 2005b). Common functional groups that are available for metal ions to attach to include primary amines (*e.g.* sulphonamides and carboxamides), thiols, aldehydes and ketones (Diaz-Garcia and Badia-Laiño,

2005c). The major means of exciting the chelates is by using the absorption bands of these metal chelates. Under optimal reaction conditions, some organic compounds are highly stable and selective for certain metal ions (Diaz-Garcia and Badia-Laiño, 2005b).

Zinc

Zinc chelators based on a quinoline sulphonamide core, such as *p*-tosyl-8-aminoquinoline (pTAQ), are currently the most widely used Zn-activated fluorophores (see Falcon *et al.*, 1993; Nowicki *et al.*, 1994; Fahrni and O'Halloran, 1999; Snitsarev *et al.*, 2001; Pluth *et al.*, 2011). Much of the early work was reported in the Russian literature but it appears that Bozhevol'nov and co-workers (Bozhevol'nov and Serebriakova, 1961, Serebriakova *et al.*, 1964) were the first to introduce pTAQ as a reagent for the spectrophotometric determination of Zn(II). These authors determined that the derivatives of the quinoline sulphonamide compounds I and II (Fig. 2.3) gave the most intense fluorescence in the presence of Zn by formation of 1:2 (Zn:ligand) complexes. Subsequently, Fredrickson *et al.* (1987) investigated a number of commercially available quinoline derivatives for visualising and assaying Zn in human tissues, and achieved the best results with pTAQ (Fig. 2.3). However, it is only recently that the structure, thermodynamics and stoichiometry of pTAQ and related fluorophores have been examined (Fahrni and O'Halloran, 1999; Nasir *et al.*, 1999; Kimura and Aoki, 2001; Meeusen *et al.*, 2011; Nowakowski and Petering, 2011).

At neutral pH, the free ligand pTAQ exhibits little fluorescence. The de-protonation of the sulphonamide occurs with a p*K* of 9.63 (Fahrni and O'Halloran., 1999) followed by the coordination and covalent bonding of Zn(II) by the two sulphonamide nitrogen atoms. Hence, they bind Zn(II) in a 1:2 metal to ligand ratio as reported in the early literature. The formation of the 1:2 complex (binding constant log

β_2 18.24) is favoured over the formation of the 1:1 complex (log β_1 8.43) by nearly 3 orders of magnitude (Nasir *et al.*, 1999). The chelation of Zn(II) is accompanied by the appearance of an intense fluorescence emission spectrum with excitation and emission maxima of 360 nm and 490 nm respectively (Meeusen *et al.*, 2011).

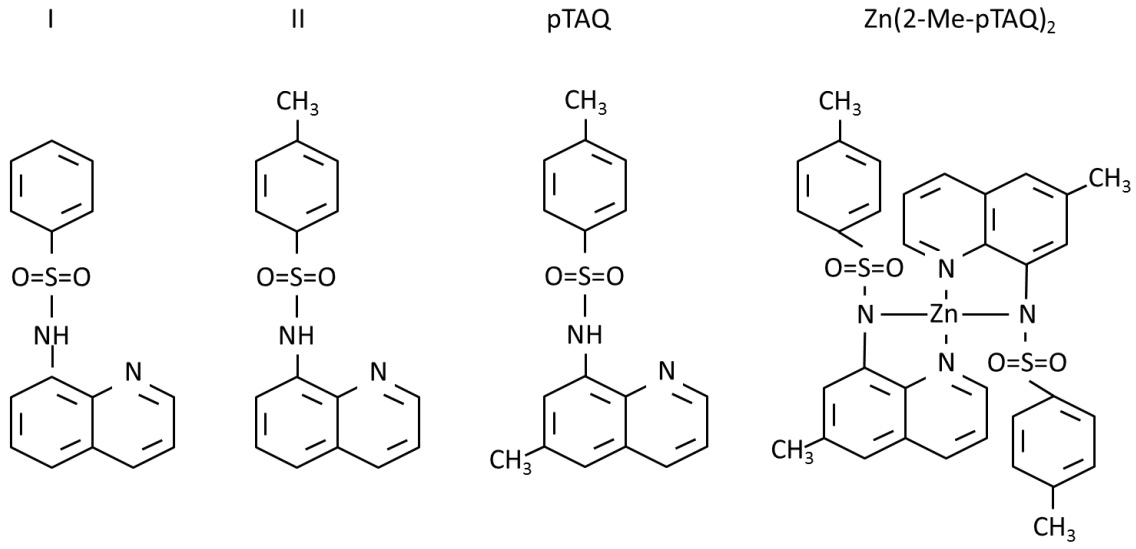

Figure 2.3. Structure of quinoline sulphonamide derivatives I & II, the indicator ligand *p*-tosyl-8-aminoquinoline (pTAQ) and the 2:1 fluorescent complex it forms with zinc (adapted from Fahrni and O'Halloran, 1999 and Snitsarev *et al.*, 2001).

2.3.3. Operational definitions for iron, zinc and cobalt species

In order to understand the processes that control trace metal biogeochemistry, the species that are determined must be clearly defined. Typically the physico-chemical form of a given metal determined in a seawater sample is defined by the sample pre-treatment process. Size fractionation is particularly important due to the wide variety of metal species that exist in seawater, including the particulate, dissolved, soluble and colloidal fractions. The chemical forms of Fe defined by physical size fractionation are shown as an example in Figure 2.4. Traditionally, the filtration size cut-off for the

dissolved Fe fraction (sample passing through a 0.2 – 0.4 µm membrane filter) was chosen based on the biological role of Fe and the need to exclude living cells that may alter the dissolved phase (Bowie and Lohan, 2009). However, some picophytoplankton exist in the 0.2 – 0.5 µm size fraction, hence membrane or cartridge filters with a pore size of 0.2 µm are now recommended (Bowie and Lohan, 2009).

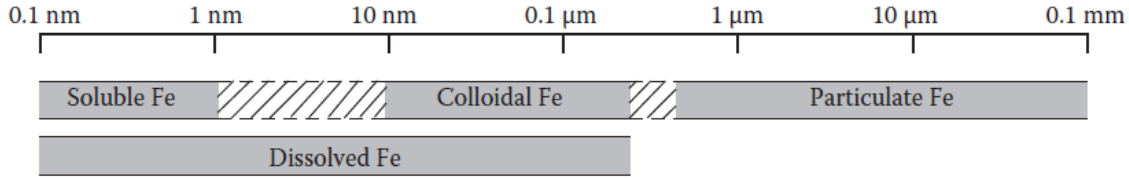

Figure 2.4. The chemical forms of iron in seawater defined by traditional physical size fractionation where dissolved iron = < 0.45 µm (taken from Bowie and Lohan, 2009). The hatched areas indicate the overlap where colloidal iron can exist in the particulate or soluble size fractions.

The recent development of ultra-filtration techniques has allowed improved characterisation of different size fractions of Fe (Wu *et al.*, 2001; Ussher *et al.*, 2004; Frew *et al.*, 2006; Bowie and Lohan, 2009). Additionally, the acidification of samples affects the speciation of redox elements such as Fe and Co and therefore when comparing concentrations it is important to note the size fraction and also the sample preparation being used. For example, recent studies have demonstrated that the acidification of filtered seawater samples to < pH 1.8 is required to release all dissolved Fe (dFe) from Fe-binding ligands (Lohan *et al.*, 2005a; Johnson *et al.*, 2007; Bowie and Lohan, 2009). Over long term storage at pH < 1.8, some of the dFe will be reduced to Fe(II) (Lohan *et al.*, 2005a; Ussher *et al.*, 2005). The addition of an oxidising or reducing agent is therefore required prior to analysis to determine total dissolved Fe. For dCo, acidification to < pH 1.8 is not sufficient to fully liberate organically

complexed Co and samples need an additional ultraviolet (UV) irradiation step (Shelley *et al.*, 2010).

During this study, dissolved Fe(II+III) (dFe), dissolved Zn (dZn) and dissolved Co(II+III) (dCo) were operationally defined as the fraction which passed through a 0.2 µm filter and were determined following acidification (0.024 M HCl). Total dissolvable Fe(II+III) (TDFe) was defined as the total Fe in an unfiltered seawater sample and acidified in a similar manner but left for a minimum 6 months before analysis.

2.4. Aims and Objectives

The aims and objectives of the work described in this chapter were to:

1. Optimize a FI-CL method for the determination of dFe and TDFe in seawater (based on Obata *et al.*, 1993; de Baar *et al.*, 2008; Klunder *et al.*, 2011). This technique was used to investigate the distribution and biogeochemistry of Fe in the upper 200 m of the Atlantic Ocean as part of the Atlantic Meridional (*AMT*) Transect (Chapter 3). Dissolved Fe concentrations typically occur in the open ocean between 0.02 – 2 nM and therefore, the target detection limit was 0.02 nM with < 5% relative standard deviation (RSD). The accuracy of this method was validated by determination of dFe in SAFe reference samples.

2. Optimize a FI-FL method for the determination of dZn in seawater (based on Nowicki *et al.*, 1994; Gosnell *et al.*, 2012). This technique was used to investigate the distribution and biogeochemistry of Zn in the South Atlantic Ocean as part of the UK GEOTRACES programme (Chapter 4). Dissolved Zn

concentrations typically occur in the open ocean between 0.02 – 9 nM and therefore, the target detection limit was 0.015 nM with < 5 % RSD. The accuracy of this method was validated by determination of dZn in SAFe reference samples.

3. Optimize a FI-CL method for the determination of dCo in seawater (based on Shelley *et al.*, 2010). This technique was used to investigate the distribution and biogeochemistry of Co in the South Atlantic Ocean as part of the UK GEOTRACES programme (Chapter 5). Dissolved Co concentrations typically occur in the open ocean between 5 – 120 pM and therefore, the target detection limit was 1pM with < 5 % RSD. The accuracy of this method was validated by determination of dCo in SAFe and GEOTRACES reference samples.

2.5. Determination of dissolved iron in seawater

This section describes the optimization of a FI-CL detection system capable of measuring seawater dFe and TDFe concentrations in the 0.01 – 2 nM range based on the method of Obata *et al.* (1993) and the modifications of de Jong *et al.* (1998) and de Baar *et al.* (2008). As described in section 2.2, the extremely low concentration of Fe in the open ocean requires a pre-concentration and seawater matrix separation step for FI-CL detection. In this study the commercially available Toyopearl AF-Chelate-650 M resin was used to pre-concentrate Fe. This chelating resin has been successfully shown to selectively and quantitatively recover Fe from seawater in the range pH 3.5 – 5 (*e.g.* de Baar *et al.*, 2008; Klunder *et al.*, 2011).

2.5.1. FI-CL manifold

A schematic diagram of the FI manifold used for the determination of Fe(III) is shown in Figure 2.5. It consisted of an 8-channel peristaltic pump (Minipuls 3, Gilson) set at 6.75 rpm to ensure the flow rates detailed in Figure 2.5, two micro-electronically actuated 6-port, 2 position injection valves (VICI, Valco Instruments), a photomultiplier tube (PMT, Hamamatsu H 6240-01) and a thermostatic water bath (Grant). The peristaltic pump tubing used was 2-stop accu-rated^{TM} PVC (Elkay) which was changed weekly. All other manifold tubing was 0.8 mm i.d. PFA Teflon (Cole-Palmer).

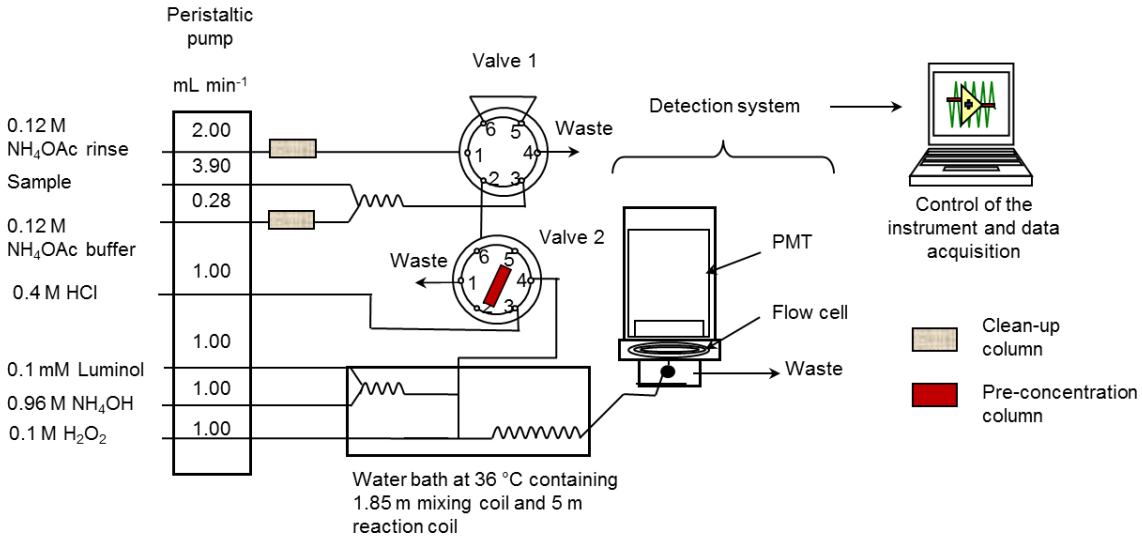

Figure 2.5. FI-CL manifold for the determination of iron(III) in seawater.

The FI manifold had two 1.85 m mixing coils (for the sample/buffer and luminol/buffer respectively) and one 5 m reaction coil. The luminol/buffer mixing coil and the reaction coil were maintained at 36 °C by placing them inside the water bath. Three acrylic columns (2 cm, internal volume 70 µL) were incorporated; one 'clean-up' column on both the sample buffer and column rinse lines to remove trace-metal impurities from

these solutions and a third attached as a sample loop in the injection valve for the pre-concentration of Fe from the sample seawater matrix. All columns were filled with approximately 50 µL of Toyopearl AF-Chelate-650 M resin (Tosohass) secured with porous high density polyethylene (HDPE) frits (BioVion F, 0.75 mm). The direction of flow through the clean-up columns was uni-directional and so these columns required reversing every few days to prevent the resin becoming compacted. This was not required for the pre-concentration column, which was loaded and eluted in opposite flow directions. The data acquisition module (Ruthern Instruments) and valve control software (LabVIEW v. 7.1) were operated using a laptop computer (Dell). To minimise contamination, the FI system was flushed daily, and following manifold alterations (*e.g.* pump tubing or connector replacement), with 0.5 M HCl solution. To further minimise contamination all reagent lines and the sample line were maintained inside a Class-100 laminar flow hood.

2.5.2. Reagents

All chemicals were obtained from Fisher Scientific unless otherwise stated and used as received. The reagents were prepared inside a Class-100 laminar flood hood using ultra-high purity (UHP) water (≥ 18.2 MΩ cm, Elgastat Maxima). The critical reagent in this method is luminol (5-amino-2,3-dihydrophthalazine-1,4-dione) which emits CL following its catalytic oxidation by H_2O_2 in the presence of Fe. The 0.3 mM luminol reagent was prepared by dissolving 0.177 g luminol in 10 mL UHP water that contained 0.1 g of fully dissolved sodium hydroxide (NaOH) to give a 0.1 M stock. Three mL of luminol stock was diluted to 1 L with UHP water and 60 µL of triethylenetetramine (TETA) was added to eliminate the interference from copper ions

(Lunvongsa *et al*., 2006). The luminol oxidizing agent, 0.1 M H_2O_2, was prepared by diluting 11.34 mL H_2O_2 (30 %, Merck) in 1 L UHP water. The reaction buffer, 0.96 M ammonia solution (NH_4OH) (Romil), was prepared by diluting 168 mL ammonia solution (SpA, Romil) in 1 L UHP water to attain a CL reaction pH of 9.8 - 10. The 0.12 M ammonium acetate (NH_4OAc) sample buffer and column rinse solutions were prepared by diluting 100 mL ammonia solution (SpA, Romil) plus 30 mL acetic acid (SpA, Romil) to 250 mL with UHP water to give a 2 M stock. Next, 60 mL of stock solution was diluted to 1 L with UHP water and the pH adjusted to 4.0 with acetic acid. Acidified seawater samples were buffered in-line (pH 3.5 – 3.7). The eluent, 0.4 M hydrochloric acid (HCl), was prepared by diluting 33.3 mL super-pure, sub-boiling distilled 12 M HCl (SpA, Romil) to 1 L with UHP water.

2.5.3. Procedure

The procedures and valve timings used in the Fe FI-CL method are documented in Table 2.3. The FI system was washed daily with 0.5 M HCl for 30 min in order to wash all trace-metal impurities from the manifold tubing and column resins. The reagents were then allowed to flow through the manifold for 30 – 40 min to ensure stabilization of the CL baseline. All seawater samples received a 50 µL addition of 0.012 M H_2O_2 (30 % Merck) one hour prior to analysis in order to reverse any reduction of Fe(III) to Fe(II) during sample storage (Lohan *et al.*, 2005a; Johnson *et al.*, 2007).

The system started in the sample loading position whereby Fe in the buffered seawater sample was recovered (pH 3.5 – 4) onto the pre-concentration column for 60 s (~ 4 mL total). Valve 1 was then switched to its second position and the pre-

concentration column rinsed with NH_4OAc for 40 s. During the load and rinse steps the eluting acid bypassed the pre-concentration column, mixing with the reaction reagents flowing towards the PMT to generate the baseline CL signal. Following the column rinse step, valve 2 switched to its second position and the eluting acid passed through the column for 30 s in the opposite flow direction to that of the loading and rinse steps, thus liberating Fe(III) from the chelating resin into the reagent stream travelling towards the PMT. The CL reaction occurred at 36 °C and pH 10 within the 5 m reaction coil immediately prior to entering the PMT. Each sample was run in triplicate with one complete analytical cycle taking 6.5 min.

Table 2.3. Valve timings and position for the iron(III) FI-CL method.

Procedure	Time (s)	Valve positions (V1/V2)
Sample preparation		Load/Elute
Sample load	60	Load/Load
Column rinse	40	Rinse/Load
Column eluent	30	Rinse/Elute

The analytical system was calibrated daily using standards (additions of 0.2 – 2 nM) made daily in low-iron seawater (Atlantic Ocean surface seawater collected and filtered (0.2 μm) at 37° 52’ S, 41° 05’ W; dFe 0.17 ± 0.09 nM), and which was acidified to pH 1.7 (0.024 M HCl, SpA, Romil) prior to use. An example of a typical calibration graph for dFe and TDFe determination is presented in Figure 2.6.

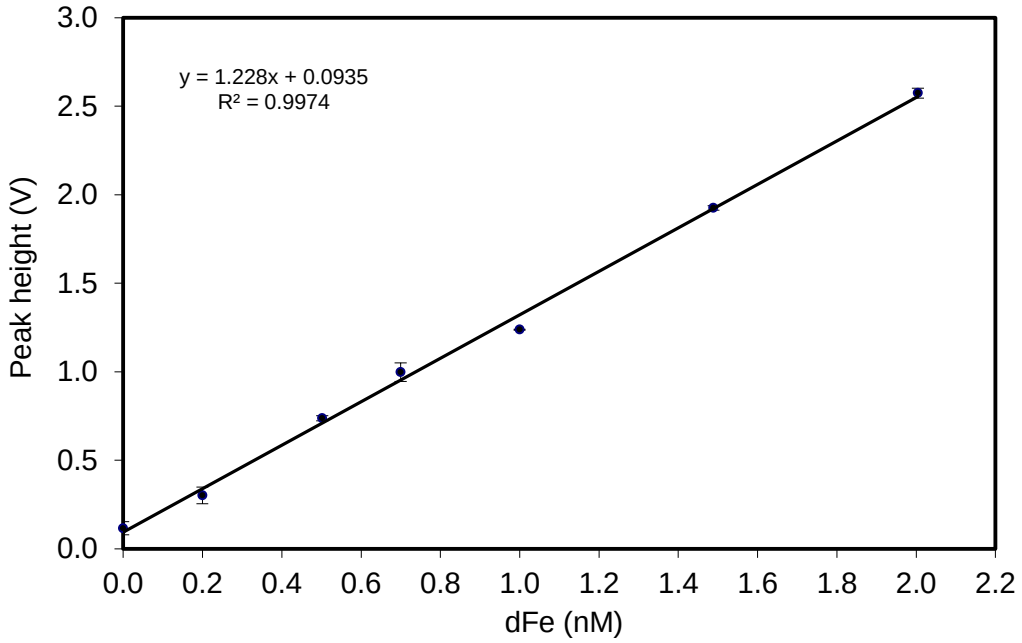

Figure 2.6. A typical calibration graph for the determination of dissolved iron and total dissolvable iron. Error bars represent one standard deviation of three replicate measurements of the same standard.

The stock standards were prepared in UHP water acidified to pH 2 (0.012 M HCl, SpA, Romil) by serial dilution of a 17.9 mM Fe atomic absorption standard solution (Spectrosol). The stock and working standards received a 50 µL addition of 0.012 M H_2O_2 (30 % Merck) to ensure that all Fe in the standards remained in the oxidized Fe(III) form. The same addition was made to the seawater samples one hour prior to analysis in order to reverse any reduction to Fe(II) during sample storage (Lohan *et al.*, 2005a; Johnson *et al.*, 2007). Calibrations were run at the beginning of each sequence of analysis and concentrations calculated form peak heights. Standard graphs were linear ($r^2 > 0.98$) over the calibration range.

2.5.4. Analytical figures of merit

Blanks and detection limits

The major blank contribution to the Fe(III) FIA method arises from the reagents that can be pre-concentrated onto the column resin (i.e. the NH_4OAc sample buffer and column rinse solutions). Any Fe present in these solutions can potentially contribute to the analytical signal and therefore a clean-up column containing Toyopearl resin was incorporated into both reagent lines (Figure 2.5). The combined blank signal that includes Fe leached from both the pump and manifold tubing upstream of the pre-concentration column, as well as reagents loaded onto the column, was investigated daily prior to each system calibration by running a complete analytical cycle without a sample. The mean blank concentration was 0.25 ± 0.05 nM (n = 15). The detection limit for each analytical run was estimated as the Fe concentration corresponding to 3 times the standard deviation of the blank signal for that calibration. The mean detection limit was 0.03 ± 0.02 nM (n = 15).

Accuracy and precision

The accuracy of this FI method for determining dFe and TDFe in seawater was validated by the quantification of dFe in surface water (S) and 1000 m water (D1) collected in the North pacific during the SAFe programme (Johnson *et al.*, 2007). The concentrations of dFe (± 1 std. dev.) measured in the SAFe reference samples during this study (S = 0.14 ± 0.08 nM; D1 = 0.74 ± 0.10 nM; n = 15) were in good agreement with the consensus values (± 1 std. dev.) obtained for the same sample by other laboratories using different analytical techniques (S = 0.09 ± 0.07 nM; D1 = 0.67 ± 0.07 nM, http://www.geotraces.org/science/intercalibration/322-standards-and-reference-

materials). The SAFe reference samples were analysed alongside all seawater samples for which Fe data are presented in this thesis (see Chapter 3). The analytical precision of the method was determined from repeat analysis of the SAFe (S) sample during one analytical cycle. The uncertainty, expressed as the relative standard deviation (RSD) of the mean for a particular analysis was ± 1.8 % (n = 3). Samples that had an RSD > ± 5 % were re-analysed.

2.5.5. Discussion

The Fe FI-CL method described here is selective, has a low limit of detection (0.03 ± 0.02 nM) and is portable, making it particularly well suited to the determination of Fe in oceanographic regimes.

One modification to the published method made in this work was the use of a weakly acidified NH_4OAc rinse solution. Previous FI-CL methods that have used Toyopearl resin for Fe determination in seawater (Klunder *et al.*, 2011) have used UHP water as a column rinse step. This is in contrast to FI methods that utilise Toyopearl to pre-concentrate other transition metals (*e.g.* Mn and Co) which suggest the need for a buffered column rinse step (Aguilar-Islas *et al.*, 2006; Shelley *et al.*, 2010). The buffered rinse step, usually a buffer with a similar pH to that of the in-line buffered seawater sample, performs two functions. Firstly, the buffer acts as a column rinse solution removing the major seawater cations that can interfere in the determination of Fe and other trace metals when using CL detection (Hopkinson *et al.*, 2007, Shelley *et al.*, 2010). Secondly, it is important to match the pH of the rinse solution to the pH of the eluent. Failure to do so leads to a depression in the baseline prior to the analytical

peak as the rinse solution dead volume (ca. 70 µL) in the pre-concentration column, once valve 2 is switched from rinse to elute, will also be mixed into the reagent stream to give a lower CL emission signal detected by the PMT. Lohan *et al.* (2006) described how such a depression was observed using a UHP rinse solution when determining dFe using an NTA-type chelating resin. These authors concluded that a 1.5 M NH_4OAc rinse solution adjusted to pH 3.5 was ideal because its ionic strength matched the ionic strength of the elution acid and removed the depression from the baseline signal. Furthermore, at this pH any Fe bound to the NTA-resin would not be removed during the rinse step. Willie *et al.* (2001) demonstrated that a 0.1 M NH4OAc rinse solution, buffered in the pH range 3 – 5, was sufficient to eliminate seawater interfering cations whilst still retaining the analyte on a Toyopearl chelating resin. Studies by Shelley *et al.* (2010) have shown that a further reduction in the ionic strength of this NH_4OAc solution to 0.05 M did not result in reduced sensitivity when analysing dCo. It was therefore important for this study to compare a UHP rinse solution against a buffered rinse solution (0.12 M NH_4OAc) to assess the effect on calibration sensitivity and analytical peak shape during the determination of dFe. The results are presented in Figure 2.7. The addition of a buffered rinse step resulted in a minimal reduction in sensitivity (UHP, $y = 1.50x + 0.28$, $r^2 = 0.99$; 0.05 M NH_4OAc, $y = 1.42x + 0.21$, $r^2 = 0.99$) and no change in blank contribution (0.22 nM for these tests). The buffered rinse completely removed the baseline depression prior to the analytical signal and reduced the baseline output to 4.2 mV from 6.6 mV. This resulted in an improved signal-to-noise ratio and therefore made it easier to quantify analytical peaks. The 0.12 M NH_4OAc rinse solution was therefore used instead of a UHP water rinse.

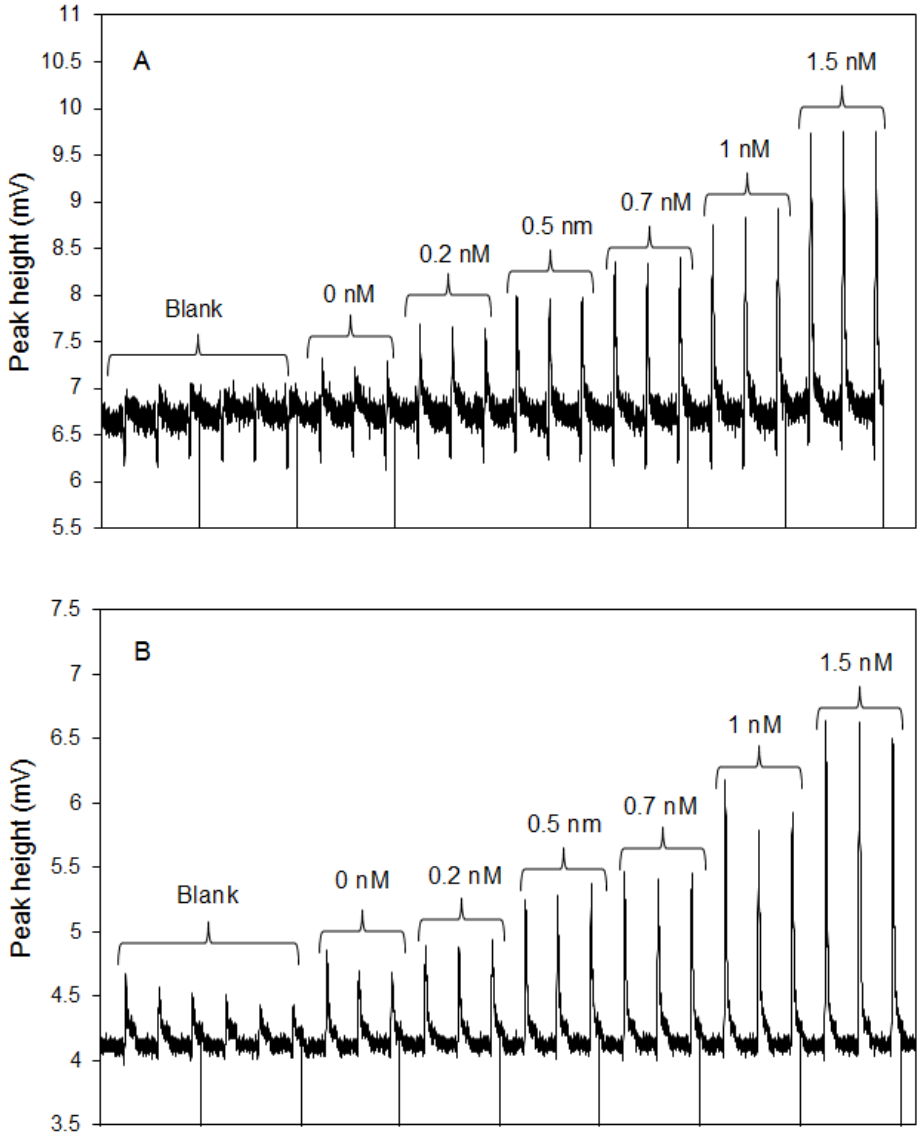

Figure 2.7. Elution peaks of dissolved iron in seawater (dFe 0 – 1.5 nM) with (A) a UHP rinse step and with (B) a 0.12 M NH4OAc rinse step.

2.6. Determination of dissolved cobalt in seawater

Flow injection chemiluminescence methods have been developed for determining dCo in coastal and estuarine samples (Sakamoto-Arnold and Johnson, 1987; Cannizzaro *et al.*, 2000), but to date only one method describes the determination of dCo in open ocean seawater (Shelley *et al.*, 2010) with the accuracy and precision that

is required from the international trace metal community. Subsequently, this method has been used to investigate the biogeochemical cycle of dCo in the South Atlantic and Southern Ocean (Bown *et al.*, 2011) and in the Sargasso Sea (Shelley *et al.*, 2012).

This section describes the optimization of a FI-CL detection system that is capable of measuring seawater dCo concentrations in the 2 – 100 pM range, thereby improving on the detection limits of Shelley *et al.* (2010). Given that Co is an essential micronutrient for carbon acquisition for key phytoplankton genera (*e.g. Prochlorococcus, Synechococcus*), this reduction in detection limit will ultimately provide further insights into the role of dCo in controlling ocean primary productivity and the global carbon cycle.

2.6.1. FI-CL manifold

A schematic of the FI manifold used for the determination of Co(II) is shown in Figure 2.8. It consisted of three peristaltic pumps (Minipuls 3, Gilson; colour coded in Figure 2.8), one micro-actuated 10-port valve (VIVI, Valco Instruments), one micro-electronically actuated 6-port valve (VIVI, Valco Instruments), one solenoid switching valve, a photomultiplier tube (PMT, Thorn EMI) and a thermostatic water bath (Grant). The advantage of working with three pumps was that they could be controlled separately through the computer software, allowing the sample, buffer and rinse pumps to be switched off when not in use, thus reducing the sample requirement and reagent consumption. The peristaltic pump tubing used was 2-stop accu-rated^{TM} PVC (Elkay) which was changed weekly. All other manifold tubing was 0.8 mm i.d. PFA Teflon (Cole-Palmer). The FI manifold had one 1.85 m mixing coil to mix the sample and

buffer, one 3 m mixing coil to mix the pyrogallol and reaction buffer, and one 'French Knitted' 5 m reaction coil. The pyrogallol/reaction buffer mixing coil and the reaction coil were maintained at 67 °C by placing them inside the water bath.

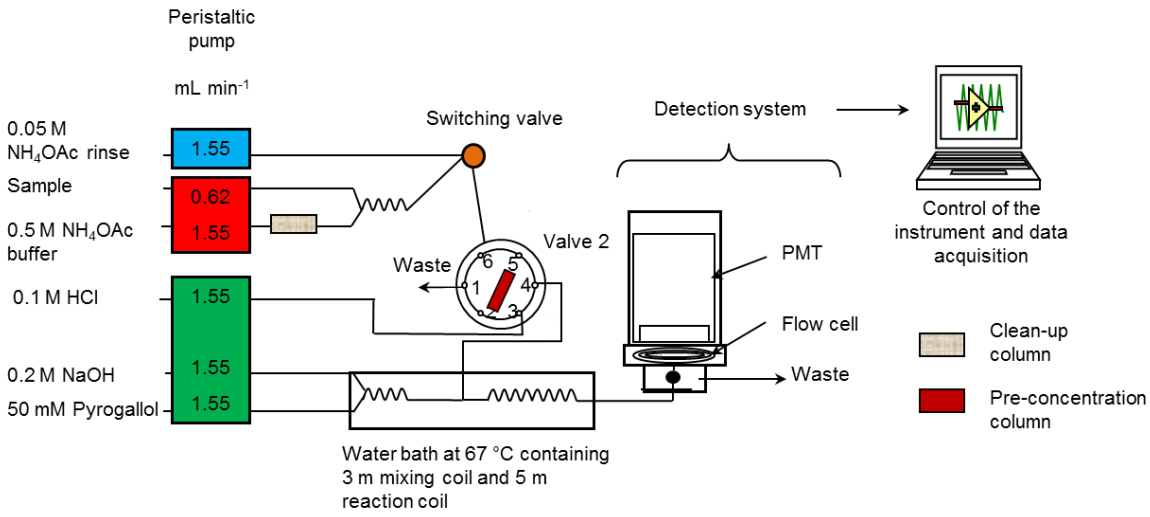

Figure 2.8. Three pump FI-CL manifold for the determination of cobalt(II) in seawater. The three pumps are coloured: rinse pump = blue, sample pump = red, reagent and eluent pump = green.

Unlike the Fe- and Zn-FI manifolds, only two columns (2 cm acrylic, internal volume 70 µL) were needed for the Co-FI manifold. The first was a clean-up column incorporated into the sample buffer line to remove trace metal impurities from this solution. This column was necessary as the detection limit of FI methods is quite often limited by the blank signal (Bowie and Lohan, 2009). The second column was attached as a sample loop in the injection valve for the pre-concentration of Co from the sample seawater matrix. Both columns were filled with approximately 50 µL of Toyopearl AF-Chelate-650 M resin (Tosohass) secured with porous HDPE frits (BioVion F, 0.75 mm). It was not necessary to include a clean-up column on the weak, ammonium acetate rinse

line as previous studies have shown that the determination of Co in seawater is almost free of contamination (Cannizzaro *et al.*, 2000) and the molarity of this solution is sufficiently low. The data acquisition module (Ruthern Instruments) and valve control software (LabVIEW v. 7.1) were operated was using a laptop computer (Hewlett Packard). To minimise contamination, the FI system was flushed daily, and following manifold alterations (*e.g.* pump tubing or connector replacement), with 0.5 M HCl solution. To further minimise contamination all reagent lines and the sample line were maintained inside a Class-100 laminar flow hood.

2.6.2. Reagents

All chemicals were obtained from Fisher Scientific unless otherwise stated and used as received. The reagents were prepared inside a Class-100 laminar flood hood using ultra-high purity (UHP) water (≥ 18.2 MΩ cm, Elgastat Maxima). The critical reagent in this method is pyrogallol (1,2,3-trihydrobenzene) which emits CL following its catalytic oxidation by H_2O_2 in the presence of Co. The 50 mM pyrogallol reagent was prepared by sonicating 6.30 g of pyrogallol and 9.12 g of cetyltrimethylammonium (CTAB) in 500 mL UHP water. When the pyrogallol and the CTAB were fully dissolved, 100 mL of 30 % H_2O_2 was added and the solution diluted to 1 L with UHP water. The pyrogallol reagent was prepared the day before use but it must be noted that this reagent was only stable for 48 h. The reaction buffer, 0.2 M NaOH, was prepared by dissolving NaOH (8.0 g L^{-1}, Sigma-Aldrich) in 1 L of solution (20 % v/v methanol (MeOH, Acros Organics), 80 % v/v UHP water) to attain a CL reaction pH of 10.4. The 0.5 M NH_4OAc sample buffer was prepared by diluting 100 mL ammonia solution (SpA, Romil) plus 30 mL acetic acid (SpA, Romil) to 250 mL with UHP water to give a

2 M stock. Next, 250 mL of stock solution was diluted to 1 L with UHP water and the pH adjusted to 7.2 with acetic acid. Acidified seawater samples were buffered in-line to between pH 5.2 – 5.5. The 0.05 M NH_4OAc column rinse solution was also prepared from a 2 M NH_4OAc stock by diluting 50 mL in 1 L UHP water and adjusting the pH to 5.5 with acetic acid. The eluent, 0.1 M hydrochloric acid (HCl), was prepared by diluting 8.33 mL of 12 M ultra-pure sub-boiling distilled HCl (SpA, Romil) to 1 L with UHP water.

2.6.3. Procedures

The procedures and valve timings used in the Co FI-CL method are documented in Table 2.4. The peristaltic pumps were set at: 6 rpm = rinse pump, 6 rpm = sample pump, 9 rpm = reagent pump to attain the flow rates shown in Figure 2.8. The FI system was washed daily with 0.5 M HCl for 30 min in order to wash all trace metal impurities from the manifold tubing and column resins. The reagents were then allowed to flow through the manifold for 30 – 40 min to ensure stabilization of the CL baseline. The system started in the sample loading position whereby Co in the buffered seawater sample was recovered (pH 5.2 – 5.5) onto the pre-concentration column for 220 s (~ 2.3 mL total). When loading was complete the sample pump was turned off and the rinse pump turned on. The pre-concentration column was rinsed for 50 s to remove the interfering alkaline earth ions Mg(II) and Ca(II) (Shelley *et al.*, 2010). The solenoid switching valve allowed flow from these two pumps to be controlled. Next the eluting acid passed through the column for 60 s in the opposite flow direction to that of the loading and rinse steps, thus liberating Co from the chelating resin into the reagent stream travelling towards the PMT. The reagent and eluent pump remained on

throughout the analytical cycle in order to maintain a constant CL baseline. The CL reaction occurred at 67 °C and pH 10.4 within the 5 m reaction coil immediately prior to entering the PMT. Each sample was run in triplicate with one complete analytical cycle taking 16.5 min.

Table 2.4. Valve timings and position for the cobalt(II) FI-CL method.

Procedure	Time (s)	Valve positions (solenoid/6-port)
Sample preparation		Load/Elute
Sample load	220	Load/Load
Column rinse	50	Rinse/Load
Column eluent	60	Rinse/Elute

The analytical system was calibrated daily by the linear regression of standard additions, an example of which is presented in Figure 2.9. The stock standards were prepared in UHP water acidified to pH 1.7 (0.024 M HCl, SpA, Romil) by serial dilution of a 1000 mg L^{-1} atomic absorption standard Co(II) (Romil). Working standards (additions of 0 – 80 pM) were prepared daily in low-Co seawater (Southwest Atlantic Ocean surface seawater collected from a towed fish and filtered (0.2 µm); dCo 16.5 ± 5.2 pM, n = 15), which was acidified to pH 1.7 (0.024 M HCl, SpA, Romil) prior to use. Calibrations were run at the beginning of each sequence of analysis and concentrations calculated form peak heights. Standard graphs were linear ($r^2 > 0.99$) over the calibration range.

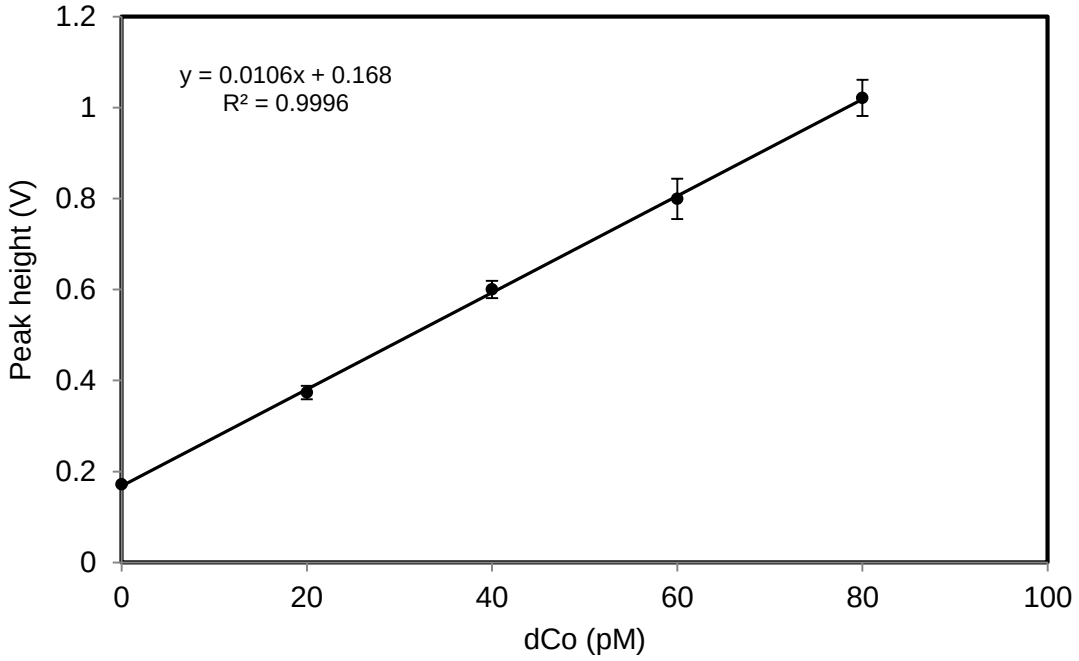

Figure 2.9. A typical calibration curve utilised for the determination of dissolved cobalt. Error bars represent one standard deviation of three replicate measurements of the same standard.

2.6.4. UV-irradiation

It is well known that, like several other bioactive trace metals, a large fraction (> 90 %) of dCo in seawater is complexed by uncharacterized organic ligands (Donat and Bruland, 1988; Saito and Moffett, 2001; Ellwood and van den Berg, 2001; Bown *et al.*, 2012). However, in contrast to organic Fe and Zn complexes which appear to fully dissociate following acidification to pH 1.7 (Lohan *et al.*, 2005a; Johnson *et al.*, 2007; Bowie and Lohan, 2009), the results of UV-irradiation experiments using a variety of analytical techniques to determine dCo (*e.g.* Donat and Bruland, 1988; Vega and van den Berg, 1997; Noble *et al.*, 2008; Milne *et al.*, 2010, Shelley *et al.*, 2010) indicate that organic Co complexes do not fully dissociate at this pH. This may be due to the presence of strong, Co-binding organic ligands in seawater that have high stability constants ($K_s = 10^{16.3}$, Saito and Moffett, 2001; Saito *et al.*, 2005) compared with the

reported K_s values for strong Fe-binding ligands ($K_s = 10^{13.08}$, Rue and Bruland, 1995) and for strong Zn-binding ligands ($K_s = 10^{9\text{-}11}$, Ellwood and van den Berg, 2000; Lohan *et al.*, 2005b; Croot *et al.*, 2011). Shelley *et al.* (2010) compared acidified seawater samples, collected as part of the SAFe programme (Johnson *et al.*, 2007), that had received UV-irradiation to those which had not, using FI-CL. The reported dCo concentration in samples UV-irradiated for 3 h (40.9 ± 2.6 pM, $n = 9$) was found to be almost double the concentration measured in non-irradiated samples (25.4 ± 1.2 pM, $n = 8$) demonstrating the fact that UV-irradiation is essential for the determination of dCo in seawater by FI-CL.

During this study, seawater samples were UV-irradiated in acid-washed quartz vials for 2 h using a 400 W medium-pressure Hg lamp (Photochemical Reactors). Further experiments have shown that a 2 h irradiation time is sufficient to fully release all dCo from the organic complexes associated with seawater (A. Milne, 2013, personal. comm.). After UV-irradiation, samples were left for a minimum 12 h prior to analysis in order to eliminate UV-generated free radicals that might interfere with the pyrogallol CL reaction.

2.6.5. Analytical figures of merit

Blanks and detection limits

The key analytical figures of merit are shown in Table 2.5. In contrast to the FI methods for Fe and Zn determination described previously, the Co FI-CL method has a low risk of reagent contamination as Co is sparsely used in laboratory environments and represents only ~ 0.002 % of the earth's crust as opposed to the ~ 3.5 % that Fe

constitutes (McLennan, 2001). Additionally, the potential for a blank contribution from other metal ions has been proven unlikely when determining dCo in seawater using FI-CL methods (Sakamoto-Arnold and Johnson, 1987; Cannizzaro *et al.*, 2000).

Table 2.5. Key analytical figures of merit for FI-CL determination of dissolved cobalt.

Parameter	This study	Bown *et al.* (2011)	Shelley *et al.* (2010)	Cannizzaro *et al.* (2000)	Sakamoto-Arnold & Johnson (1987)
Detection limit (pM)	1.98	3.72	4.50	5.0	8.0
Blank (pM)	None detected	5.90 ± 1.24	4.2 ± 1.5	None detected	None detected
RSD (%)	2.3 (n = 4)	4.1 (n = 6)	4.0 (n = 3)	2.1 (n = 3)	5.0 (n = 80)

The reported blank signals for Co FI-CL systems are therefore extremely low (Table 2.5). The blank signal was investigated daily prior to each system calibration by running a complete analytical cycle with UHP water running through the sample line. In contrast to recently published FI-CL systems for the determination of Co (*e.g.* Shelley *et al.*, 2010; Bown *et al.*, 2011), this study observed no detectable blank signal. The detection limit of this method was estimated as the Co concentration corresponding to 3 times the standard deviation of the lowest standard signal for that calibration, resulting in a detection limit of 1.98 ± 0.87 pM (n = 15). This detection limit is an improvement on those previously reported for FI-CL dCo determination (Table 2.5).

Accuracy and precision

The accuracy of this FI method for determining dCo in seawater was assessed by the quantification of dCo in surface water (S) and 1000 m water (D1, D2) collected in

the oligotrophic North Pacific during the SAFe programme (Johnson *et al.*, 2007) and also 2000 m water (GD) collected in the North Atlantic as part of the international GEOTRACES programme. The concentration of dCo (± 1 std. dev.) measured in the SAFe and GEOTRACES reference samples during this study (S = 4.09 ± 0.36 pM, *n* = 3; D1 = 44.26 ± 1.03 pM, *n* = 4; D2 = 48.46 ± 0.04 pM, *n* = 2; GD = 73.04 ± 3.51 pM, *n* = 5) were in excellent agreement with the consensus values obtained for the same samples by other laboratories using different analytical techniques (S = 5.4 ± 2.2 pM; D1 = 43.0 ± 5.6 pM; D2 = 45.4 ± 3.8 pM; GD = 65 ± 8 pM, http://www.geotraces.org/science/ intercalibration/322-standards-and-reference-materials). The reference samples were UV-irradiated and analysed alongside all seawater samples for which Co data are presented in this thesis (see Chapter 5). The analytical precision of the method was determined from repeat analysis of the SAFe D2 reference sample during one analytical cycle. The RSD of the mean was ± 2.3 % (*n* = 4). Samples that had an RSD > ± 5 % during this study were re-analysed.

In addition to the reference samples mentioned above, this study also analysed a number of North Pacific GEOTRACES samples that are still being treated as "unknown" until more data has been gathered. This process is an important part of the GEOTRACES intercalibration exercise that aims to achieve the best sampling and handling protocols, thus best possible analytical accuracy, for the suite of elements measured by the international trace metal community. What is clear from the data currently submitted to the intercalibration study and from Co UV-irradiation studies (Shelley *et al.*, 2010) is that the UV-irradiation step is vital to accurately quantify dCo in reference and other seawater samples.

2.6.6. Discussion

The Co FI-CL method described here is selective, portable, has short analysis time and a limit of detection lower (1.98 pM) than previously reported FI methods (Table 2.5). This makes this technique particularly well suited to in situ measurements of the low dCo concentrations observed in the open ocean. In contrast to previous Co-FI methods (Cannizzaro *et al.*, 2000; Shelley *et al.*, 2010; Bown *et al.*, 2011), this study used a three pump manifold which allowed the sample and rinse pumps to be turned off when not in use, thus reducing reagent consumption. Using this system, this study observed no detectable blank signal. One reason for this may be the use of super-pure ammonium solution and acetic acid (Romil) in the preparation of the NH_4OAc sample buffer and column rinse reagents as opposed to the ammonium acetate crystals (Fisher Scientific) used by Shelley *et al.* (2010), thus reducing the amount of Co loaded onto the pre-concentration column during the column rinse step. It should be noted that neither study incorporated a clean-up column in the pre-concentration column rinse line. This study showed that the removal of the blank signal should lead to enhanced sensitivity and allow for a lower detection limit (Table 2.5).

2.7. Determination of dissolved zinc in seawater

This section describes the optimization of a FI-FL detection system that is capable of measuring seawater dZn concentrations in the 0.015 – 10 nM range based on the methods of Nowicki *et al.* (1994), Nolting *et al.* (2000) and Gosnell *et al.* (2012). These studies are the only reported methods that utilise FI-FL for the determination of dZn in seawater. Other studies used either cathodic stripping voltametric techniques (*e.g.*

Bruland, 1989; Lohan *et al.*, 2002; Ellwood and van den Berg, 2000; Croot *et al.*, 2011) or land-based ICP-MS methods (*e.g.* Milne *et al.*, 2010; Jakuba *et al.*, 2008). However, FI-FL methods are particularly well suited to shipboard investigations of oceanic dZn distribution and therefore beneficial to this study.

2.7.1. FI-FL manifold

A schematic of the FI manifold used for the determination of Zn is shown in Figure 2.10. It consisted of an 8 channel peristaltic pump (Minipuls 3, Gilson) set at 7 rpm to ensure the flow rates detailed in Figure 2.10, two micro-electronically actuated 6-port, 2 position injection valves (VICI, Valco Instruments), a fluorimeter (RF-10Axl, Shimadzu) with excitation and emission wavelengths set to 377 nm and 495 nm respectively, and a chart recorder (Kipp and Zonen). The peristaltic pump tubing used was 2-stop accu-rated^{TM} PVC (Elkay) which was changed weekly. All other manifold tubing was 0.8 mm i.d. PFA Teflon (Cole-Palmer).

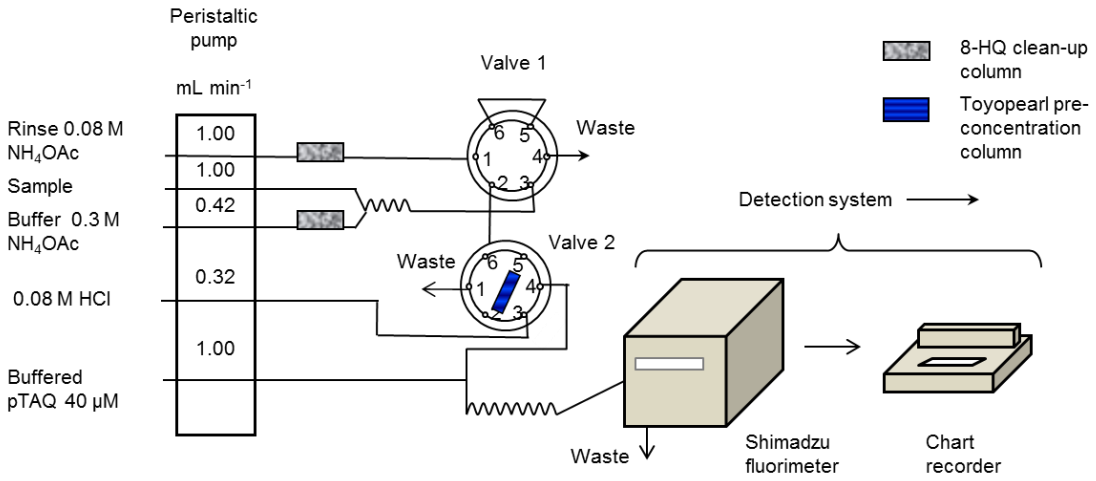

Figure 2.10. FI-FL manifold for the determination of zinc in seawater.

The FI manifold had one 1.85 m mixing coil for the sample/buffer and one 'French Knitted' 40 cm reaction coil prior to the fluorimeter. As described for the Fe manifold, three 2 cm columns, containing Toyopearl AF-Chelate-650 M resin, were incorporated in-line; one acrylic 'clean-up' column on both the sample buffer and column rinse lines to remove trace metal impurities from these solutions and a third chlorotrifluoroethylene (CTFE) column (GlobalFIA) attached as a sample loop in the injection valve for the pre-concentration of Zn from the sample seawater matrix. The acrylic columns were secured with porous HDPE frits (BioVion F, 0.75 mm) whilst the CTFE column was secured with porous polyethylene frits (GlobalFIA, 20 µm pore size). The valve control software (VICI, Valco Instruments) was operated using a laptop computer (Mercury). To minimise contamination, the FI system was flushed daily, and following manifold alterations (*e.g.* pump tubing or connector replacement, with 0.1 M HCl solution). To further minimise contamination all reagent lines and the sample line were maintained inside a Class-100 laminar flow hood.

2.7.2. Reagents

All chemicals were obtained from Fisher Scientific unless otherwise stated and used as received. The reagents were prepared inside a Class-100 laminar flood hood using ultra-high purity (UHP) water (≥ 18.2 MΩ cm, Millipore). The FL producing reagent in this method is p-tosyl-8-aminoquinoline (pTAQ, Sigma-Aldrich) which forms a stable fluorescent complex with dZn(II). The 40 µM pTAQ reagent was prepared by dissolving 0.291 g of pTAQ into 20 mL of non-ionic surfactant base Triton X-100 (poly(oxyethylene)isooctylphenol) to form a 0.05 M pTAQ stock. Triton is required as pTAQ is insoluble in water between the pH range 3 - 11 (Inman *et al.*, 1989)

making direct use of it in UHP water impossible. Several stock solutions were made 2 months in advance of their use to ensure the complete dissolution of the pTAQ. From the stock, 800 µL of pTAQ was added to a 1L solution containing 25 mL of 2 M sodium hydroxide (NaOH) and 100 mL of 0.5 M boric acid (H_3BO_3) to form the 40 µM working reagent. The boric acid solution was prepared by dissolving 31 g of H_3BO_3 into 1 L of microwave warmed UHP water. Due to the viscous nature of the Triton, shaking the 40 µM working pTAQ reagent produced bubbles that could travel through the manifold to the detector. The reagent was therefore prepared in advance and allowed to settle overnight before use. The 0.3 M NH_4OAc sample buffer and the 0.08 M NH4OAc column rinse solutions were prepared by diluting 200 mL ammonia solution (SpA, Romil) plus 60 mL acetic acid (SpA, Romil) to 500 mL with UHP water to give a 2 M stock. Next, 150 mL of stock solution was diluted to 1L with UHP water to form the 0.3 M sample buffer whilst 40 mL of stock solution was diluted to 1 L with UHP water to form the 0.08 rinse solution. The NH_4OAc sample buffer and column rinse reagents were adjusted to pH 6.0 and 5.5 respectively with acetic acid. Acidified seawater samples were buffered in-line to pH 5.2 by mixing with the sample buffer solution. The eluent, 0.08 M hydrochloric acid (HCl), was prepared by diluting 6.7 mL super-pure, sub-boiling distilled 12 M HCl (SpA, Romil) to 1 L with UHP water.

2.7.3. Procedures

The procedures and valve timings used in the Zn FI-FL method are documented in Table 2.6. The FI system was washed daily with 0.1 M HCl for 30 min in order to wash all trace-metal impurities from the manifold tubing and column resins. The reagents were then allowed to flow through the manifold for 30 – 40 min to ensure

stabilization of the FL baseline. The system was stabilized in the elute position and the elution acid passed over the pre-concentration column. The analytical cycle started when valve 2 switched and the buffered seawater sample passed over the pre-concentration column where Zn was recovered (pH 5.2) for either 120 s (~2 mL total) or 240 s (~ 4 mL total) depending on the calibration concentration range being used (Table 2.6). The pre-concentration column was then rinsed for either 30 or 60 s.

Table 2.6. Valve timings and position for the zinc(II) FI-FL method.

Procedure	Calibration range 0 – 1 nM	Calibration range 0 - 10 nM	Valve positions (V1/V2)
Sample preparation			Load/Elute
Sample load	120 s	240 s	Load/Load
Column rinse	30 s	60 s	Rinse/Load
Column eluent	60 s	60 s	Rinse/Elute

During the load and rinse steps the eluting acid bypassed the pre-concentration column and mixed with the buffered pTAQ reagent flowing towards the fluorimeter to generate the baseline FL signal. Following the column rinse step the eluting acid passed through the column for 60 s in the opposite flow direction to that of the loading and rinse steps, thus liberating Zn from the chelating resin into the reagent stream travelling towards the fluorimeter. The FL reaction occurred at pH 8.7 within the 40 cm reaction coil immediately prior to entering the fluorimeter. Each sample was run in triplicate with one complete analytical cycle taking either 10.5 min or 18 min depending on the calibration concentration range.

The analytical system was calibrated daily by standard additions, examples of which are presented in Figure 2.11. The large range of dZn concentrations observed in a typical open ocean vertical Zn profile (0.01 nM to 8 nM) made it necessary to use two separate six-point calibrations in order to analyse all samples with the highest possible accuracy. For samples collected above 1000 m, a calibration range 0 - 1 nM Zn is suitable, whereas for depths ≥ 1000 m a calibration range of 0 – 10 nM Zn is appropriate.

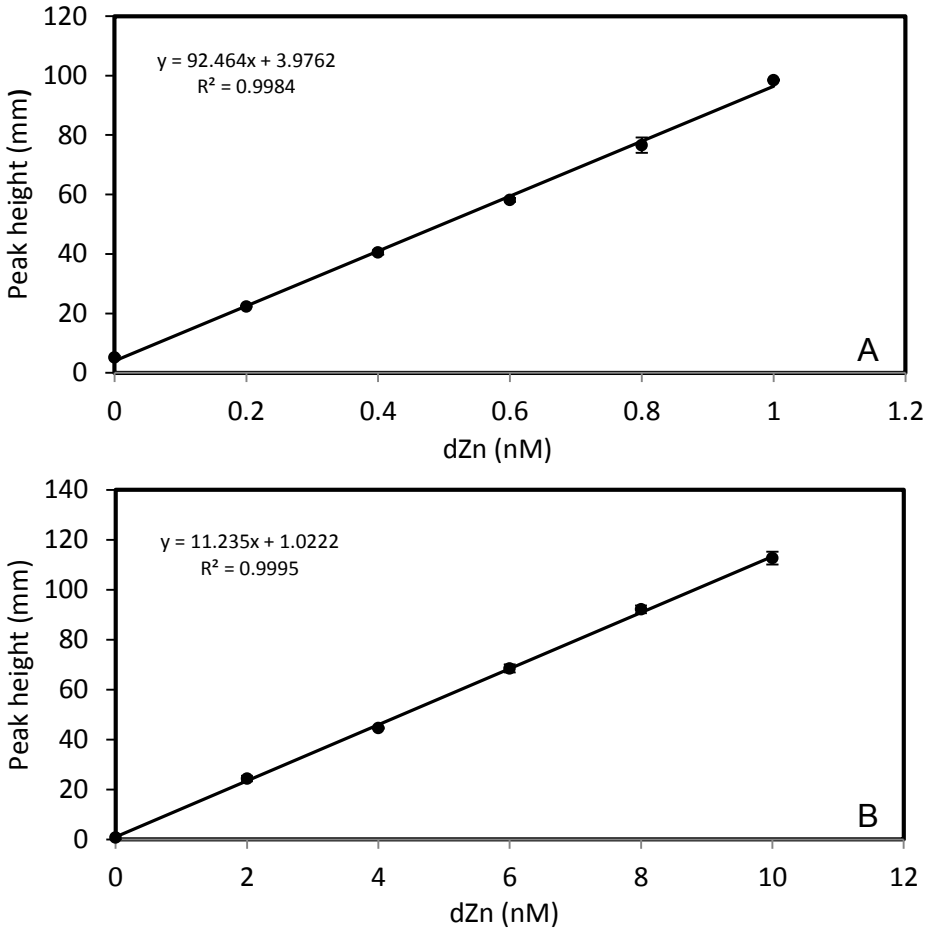

Figure 2.11. Typical calibration curves for the utilised for the determination of dissolved zinc in the range (A) 0 – 1 nM and (B) 0 – 10 nM. Error bars represent one standard deviation of three replicate measurements of the same standard.

Two stock standards were required, 0.3 µM and 3 µM, which were prepared in UHP water acidified to pH 1.7 (0.024 M HCl, SpA, Romil) by serial dilution of a 1000 mg L^{-1} Zn(II) atomic absorption standard solution (Romil). Working standards were prepared daily in 'low-zinc' seawater (Atlantic Ocean surface seawater collected regularly from the vicinity of the chlorophyll maximum and filtered (0.2 µm); dZn 0.08 ± 0.05 nM, *n* = 10), which was acidified to pH 1.7 (0.024 M HCl, SpA, Romil) prior to use. Calibrations were run at the beginning of each sequence of analysis and concentrations calculated from peak heights. Standard graphs were linear ($r^2 > 0.99$) over the calibration ranges.

2.7.4. Cadmium interference

Due to its proximity to Zn in the periodic table, dissolved cadmium (dCd) also forms a fluorescent complex with pTAQ that has an optimal emission at pH 9.2 and therefore interferes with the fluorescent signal produced by Zn using this FI-FL method (Inman *et al.*, 1989; Nowicki, *et al.*, 1994; Gosnell *et al.*, 2012). Unlike the interfering cations of seawater, the problem of dCd interference is not removed by rinsing the column with NH_4OAc solution and a correction is therefore necessary. Previous Zn FI-FL studies have reported very different levels of dCd interference when using pTAQ as the luminescent molecule, ranging from 30 % (Gosnell *et al.*, 2012) to 70 % (Nowicki *et al.*, 1994). Concentrations of dCd in seawater exist at approximately one-tenth the concentration of dZn (Bruland *et al.*, 1978; Bruland, 1980). Thus dCd interference could be between 3 and 7 % of the total zinc concentration which, if not corrected for, could equate to an overestimation of deep water dZn concentrations by up to 0.6 nM.

The potential interference of dCd on the observed dZn signal was investigated by spiking low-zinc seawater with known Zn and Cd concentrations, singularly and in combination (standard stocks were 1000 mg L^{-1} atomic absorption standard Zn(II) and Cd(II) solutions, Romil). The standard matrix and the percentage interference from dCd are displayed in Table 2.7.

Table 2.7. The additions of zinc and cadmium singularly and in combination to determine the total equivalent zinc concentration and the percentage cadmium interference.

Added Zn (nM)	Added Cd (nM)	Total equivalent Zn ± 1 std. dev. (nM)	Cd interference (%)
1	0	0.95 ± 0.03	-
0	1	0.66 ± 0.02	69.0
2	0	2.06 ± 0.02	N/A
0	2	1.24 ± 0.04	60.1
10	0	9.96 ± 0.08	-
0	10	6.46 ± 0.03	64.9
2	2	3.35 ± 0.01	67.6
2	10	8.64 ± 0.13	66.4

Standards of 1 nM, 2 nM and 10 nM Cd yielded fluorescence equivalent to 0.66 nM, 1.24 nM and 6.46 nM Zn respectively. A combination of 2 nM Cd plus 2 nM Zn yielded fluorescence equivalent to 3.35 nM Zn, and a combination of 10 nM Cd plus 2 nM Zn yielded fluorescence equivalent to 8.64 nM Zn. Thus, the fluorescent signal from dCd observed during this study averaged ~ 66 % that of the equivalent dZn emission. This interference is comparable to the 70 % reported by Nowicki *et al.* (1994) and higher than the 30 % reported by Gosnell *et al.* (2012). With dCd concentrations in the ocean

approximately 10 % that of dZn concentrations, the correction used during this study was 6.6 %. The dCd concentrations used for this correction were estimated from measured phosphate concentrations and the well-known oceanic relationship between the two elements (see Boyle, 1988; Cullen, 2006; Lane *et al.*, 2009). This relationship can generally be described by two distinct linear relationships with a kink at ~1.3 µmol L^{-1} PO_4^{3-} (Boyle, 1988; de Baar *et al.*, 1994; Löscher *et al.*, 1997) using the equation:

$$[Cd]\ (nM) = 0.21\ [PO_4^{3-}]\ (\mu M) \qquad \text{Eq. 2.3.}$$

for PO_4^{3-} concentrations <1.3 µM and:

$$[Cd]\ (nM) = 0.40\ [PO_4^{3-}]\ (\mu M) - 0.25 \qquad \text{Eq. 2.4.}$$

for PO_4^{3-} concentrations ≥ 1.3 µM. Ideally these corrections should be made using measured Cd concentrations due to the significant regional variability in the surface water Cd:PO_4^{3-} ratio, thought to be the result of Fe limitation of phytoplankton growth (Cullen, 2006). Seawater samples collected from depths shallower than 200 m required no correction as the correction value was generally below the detection limit of the Zn FI-FL method.

2.7.5. Analytical figures of merit

Blanks and detection limits

In common with the Fe FI-CL method described in the previous section, the major blank contribution to the Zn FIA method arises from the reagents that can be pre-

concentrated onto the column resin (i.e. the NH_4OAc sample buffer and column rinse solutions). Therefore a clean-up column containing Toyopearl resin was incorporated into both reagent lines (Figure 2.10). The blank signal was investigated daily prior to each system calibration by running a complete analytical cycle with acidified UHP water running through the sample line. The mean blank concentration was 0.27 ± 0.06 nM (n = 12). The daily detection limit was estimated as the Zn concentration corresponding to 3 times the standard deviation of the blank signal for that calibration, resulting in a detection limit of 0.014 ± 0.017 nM (n = 12).

Accuracy and precision

The accuracy of this FI method for determining dZn in seawater was assessed by the quantification of dZn in surface water (S) and 1000 m water (D2) collected in the oligotrophic North Pacific during the SAFe programme (Johnson *et al.*, 2007). The concentration of dZn (± 1 std. dev.) measured in the SAFe reference samples during this study (S = 0.06 ± 0.02 nM, n = 7; D2 = 7.72 ± 0.09 nM, n = 12) were in good agreement with the consensus values obtained for the same sample by other laboratories using different analytical techniques (S = 0.064 ± 0.019 nM; D2 = 7.66 ± 0.28 nM, http://www. geotraces.org/science/intercalibration/322-standards-and-reference-materials). The SAFe reference samples were analysed alongside all seawater samples for which Zn data are presented in this thesis (see Chapter 4). The analytical precision of the method was determined from repeat analysis of a random seawater sample. The RSD of the mean was ± 2.6 % (n = 10). Samples that had an RSD > ± 5 % were reanalysed.

2.7.6. Discussion

The Zn FI-FL method described here is well suited to *in situ* open ocean measurements of dZn owing to its portability, rapid analysis time, low limit of detection (14 pM) and large linear range (0 – 10 nM). The implementation of an automated sample selection valve would further facilitate the use of this method during shipboard studies and reduce the risk of contamination associated with transferring the sample line from one sample to the next.

A number of modifications were made to the dZn FI-FL method described by Gosnell *et al.* (2012). Firstly, this study used the commercially available resin Toyopearl AF-Chelate-650 M instead of resin immobilized 8-HQ. The synthesis of 8-HQ is both time consuming and complicated (Landing *et al.*, 1986; Dierssen *et al.*, 2001) leading to concerns about resin reproducibility. The Toyopearl resin has recently been successfully used in the FI-CL determination of both Fe (de Baar *et al.*, 2008; Klunder *et al.*, 2011) and Co (Shelley *et al.*, 2010) without any reported loss of sensitivity compared to the well documented 8-HQ resin. The Toyopearl resin was therefore preferred during this study to simplify preparation of the analytical system.

As with the Fe FI-CL system, a weakly acidified ammonium acetate rinse solution was chosen to remove interfering seawater cations from the pre-concentration column prior to elution. In addition, the NH_4OAc rinse eliminates the depression in the FL baseline prior to the analytical peak resulting from the differing ionic strengths of the rinse and elution solutions. The molarity of the rinse solution (0.08 M) in this study was half that used by Gosnell *et al.* (2012). By reducing the molarity of the ammonium acetate rinse solution to that of the HCl elution acid (0.08 M) no reduction in sensitivity was observed and therefore the method used lower reagent volumes.

Finally, the 0.5 M boric acid solution used in the 40 µM pTAQ preparation was half the concentration used by both Nowicki *et al.* (1994) and Gosnell *et al.* (2012). This eliminated back-pressure resulting from the build-up of boric acid crystals within the FI manifold. The reduction in the molarity of the boric acid solution resulted in a new reaction pH of 8.7 at which a stable Zn-pTAQ complex was formed. This modified reaction pH is higher than previously reported (pH 8.1) but still within the pH window of 5 - 9 reported by Nowicki *et al.* (1994) as having no effect on the fluorescence intensity of the Zn-pTAQ complex and no reduction in sensitivity (fluorescence emission) of the complex. However, it must be noted that this reaction pH of 8.7 is closer to the pH 9.2 considered to be the optimal reaction pH of the interfering Cd(II)-pTAQ complex (Inman *et al.*, 1989). This may in part explain why this study observed quite high Cd interference (66 % of equivalent Zn fluorescence).

2.8. Conclusions

The Fe, Co and Zn FI methods described in this chapter are portable, sensitive, selective, have low detection limits (30 pM, 2 pM and 15 pM respectively) and short analysis times (≤ 18.0 min per analytical cycle) making them particularly suitable for use in the laboratory and for shipboard analyses. These FI methods enable near real-time mapping of spatial and temporal trends in oceanic dissolved Fe, Co and Zn distributions, thus they have clear advantages over land-based ICP-MS and time-consuming CSV techniques.

The use of the commercially available Toyopearl AF-Chelate-650M resin throughout this study provided excellent analytical precision (RSD < 3 % for all three

FI methods) and simplified the preparation of the analytical systems. In addition, the use of an acidified ammonium acetate rinse, with an ionic strength similar to that of the elution acid, allowed the removal of interfering seawater cations from the pre-concentration column whilst also removing the baseline depressions observed with a UHP rinse. This led to an improved signal to noise ratio without significant loss of sensitivity (*e.g.* for Fe FI-CL $y = 1.50$ with UHP rinse and 1.42 with NH_4OAc rinse). A minor modification was made to the Zn FI-FL method, whereby the 0.5 M boric acid solution was half that reported elsewhere and, which resulted in a reaction pH of 8.7 at which the Zn-pTAQ complex was formed. The reduction in boric acid molarity eliminated back-pressure, resulting from the build-up of boric crystals within the FI manifold, and improved system performance.

The accuracy of the FI methods was validated by the quantification of SAFe and GEOTRACES reference seawater samples. An excellent agreement between the values obtained for these samples and the consensus values was observed for all three methods (*e.g.* SAFe D1 ($n = 15$) this study 0.74 ± 0.10 nM Fe, consensus value 0.67 ± 0.07 nM Fe; D1 ($n = 4$) this study 44.3 ± 1.0 pM Co, consensus value 43.0 ± 5.6 pM; SAFe S ($n = 7$) this study 60.0 pM ± 20 pM, consensus value 64 ± 19 pM.

The FI methods described in this chapter were successfully used to determine Fe throughout the Atlantic Ocean as part of the Atlantic Meridional Transect (see Chapter 3), and Zn and Co along the Atlantic 40° S latitudinal line as part of the UK GEOTRACES programme (see Chapters 4 and 5).

Chapter 3

Biogeochemistry of iron in the upper water column of the Atlantic Ocean: observations from the Atlantic Meridional Transect

3.1. Introduction

Iron (Fe) is an essential requirement for phytoplankton growth in the world's oceans, playing an important role in biochemical processes such as carbon and di-nitrogen (N_2) fixation (Morel and Price, 2003; Küpper *et al.*, 2008). Despite Fe being the fourth most abundant element in the earth crust, dissolved Fe (dFe) is often only present at trace concentrations (< 0.5 nM) in oxygenated surface waters of the open ocean (Moore and Braucher., 2008; Boyd and Ellwood, 2010; Tagliabue *et al.*, 2012). Consequently, Fe is considered to limit primary production in ~ 30 – 50 % of the world's surface waters, specifically the high nitrate, low chlorophyll (HNLC) regions of the Southern Ocean, sub-Arctic Pacific and equatorial Pacific (Moore *et al.*, 2002; 2004; Aumont *et al.*, 2003; Boyd and Ellwood, 2010).

However, for the majority of the Atlantic Ocean, the rate of primary production is largely controlled by the availability of inorganic macronutrients (N and P) (Marañón *et al.*, 2003; Gist *et al.*, 2009) delivered predominantly by (a) *in-situ* biological processes (*e.g.* N_2 fixation and remineralisation) or (b) physical processes (*e.g.* upwelling and lateral transport). The fixation of atmospheric N_2 is of particular importance to primary production being an important process in the delivery of new nitrogen to the euphotic zone (Tyrrell, 1999; Karl *et al.*, 2002). For example, N_2 fixation can provide up to 70 % of the nitrogen demand during bloom conditions in surface waters of the western tropical North Atlantic (Carpenter *et al.*, 1999). Iron limitation can restrict rates of N_2 fixation (Mills *et al.*, 2004; Coles and Hood, 2007; Moore *et al.*, 2009). Nitrogen fixing cyanobacteria have a cellular Fe requirement that is estimated to be between 2.5 and 5.2 times higher than phytoplankton relying on ammonium alone (Sanudo-Wilhelmy *et al.*, 2001). This high biological demand for

Fe by N_2 fixing phytoplankton, along with that of non-N_2 fixing phytoplankton, indicates that Fe concentrations can influence rates of N_2 fixation (Mills *et al.*, 2004; Coles and Hood, 2007; Moore *et al.*, 2009), and thus primary production within the Atlantic Ocean (Moore *et al.*, 2002; Moore *et al.*, 2006).

A major source of Fe to Atlantic surface waters is via the wet and dry deposition of atmospheric dust (Jickells *et al.*, 2005; Sarthou *et al.*, 2007; Buck *et al.*, 2010a; Evangelista *et al.*, 2010; Ussher *et al.*, 2013). The principle origin of this dust is Northwest Africa, from which an estimated 240 ± 80 Tg (10^{12} g) is transported west annually during the summer months (Kaufman *et al.*, 2005). Of this dust transport, approximately 140 ± 40 Tg are deposited into the Atlantic Ocean, the majority into waters underneath the Saharan dust belt (~ 0 - 30° N; Jickells *et al.*, 2005; Mahowald *et al.*, 1999; Kaufman *et al.*, 2005). Despite the fractional solubility of Fe in Saharan dust being only ≤ 1 % (Sedwick *et al.*, 2007; Buck *et al.*, 2010a), the elevated dust loadings to this region result in the highest surface Fe concentrations (Measures *et al.*, 2008; Fitzsimmons *et al.*, 2013; Ussher *et al.*, 2013) and N_2 fixation rates (Coles and Hood, 2007; Moore *et al.*, 2009) found in the Atlantic open ocean.

Another source of Fe to remote Atlantic surface waters is through vertical mixing. This mechanism reportedly provides between ~ 8 and 31 % of the total vertical dFe input flux (upward vertical dFe flux plus atmospheric dFe flux) to the Atlantic mixed layer (Ussher *et al.*, 2013). Vertical mixing is particularly important in the tropics where high sub-surface dFe concentrations of up to 2 nM are associated with remineralisation of Fe-rich organic matter formed in the dust laden surface ocean (Bergquist and Boyle, 2006; Measures *et al.*, 2008; Fitzsimmons *et al.*, 2013; Ussher *et al.*, 2013). The lateral advection of Fe from shelf regions to the remote

Atlantic open ocean is reported to be negligible (Laes *et al.*, 2007; Ussher *et al.*, 2007; Fitzsimmons *et al.*, 2013), whilst hydrothermal sources of Fe to the upper water column of the Atlantic are also reported to be minimal (Tagliabue *et al.*, 2010; Hardardóttir *et al.*, 2009).

The primary removal mechanism for Fe from the euphotic zone is through active biological uptake (Martin and Gordon, 1988) via N_2 fixation and primary production. In addition to active uptake, there is also passive adsorptive scavenging of Fe onto particles (both living and dead) that exist in surface waters (Johnson *et al.*, 1997; Wu *et al.*, 2001; Bruland and Lohan, 2003). However, dFe is strongly protected from scavenging by its complexation with strong Fe-binding organic ligands (> 99 %) (Rue and Bruland, 1995; Van den Berg, 1995).

The Atlantic is an important ocean to study the distribution and cycling of Fe for several reasons. Firstly, the Atlantic includes contrasting biogeochemical provinces such as the northern and southern hemisphere oligotrophic gyres, and temperate eutrophic shelf seas. Second, an extensive oxygen minimum zone (OMZ) extends westward from the North African coast to ~ 35° W with oxygen concentrations as low as 40 μmol kg^{-1} (Stramma *et al.*, 2008). This OMZ is maintained by a combination of coastal upwelling off Northwest Africa, which promotes biological oxygen consumption via respiration in the thermocline (Karstensen *et al.*, 2008), and sluggish ocean ventilation, which supplies oxygen (Stramma *et al.*, 2008). Finally, and arguably most importantly, the North Atlantic Ocean receives approximately half the dust entering the global ocean annually through wet and dry atmospheric deposition (Jickells *et al.*, 2005). Since Fe constitutes ~ 3.5 % of the mass of mineral matter (Taylor and McLennan, 1985), dFe

concentrations in the North Atlantic are likely to be higher than in other oceanic regions.

The Atlantic Meridional Transect (*AMT*) time series programme provides an ideal opportunity to improve our current understanding of Fe cycling in the upper Atlantic Ocean and the role of Fe on climate relevant biological processes. This chapter reports on the geographical distribution and biogeochemistry of Fe in the upper water column along a 12,000 km gyre-centred transect of the Atlantic Ocean. In this study, dFe and total dissolvable Fe (TDFe) data are discussed in the context of the biogeochemical and physical properties of the different geographic provinces in order to investigate the distribution and behaviour of Fe in the upper water column of the Atlantic Ocean between ~ 50° N and 40° S.

3.2. Materials and procedures

3.2.1. Sampling methods

Seawater samples were collected from the upper water column (0 - 150 m) at 29 oceanographic stations during the UK Atlantic Meridional Transect cruise between Falmouth, UK and Punta Arenas, Chile (*AMT*-19; Fig. 3.1). The cruise took place from 13th October - 28th November 2009 on board the R.R.S. *James Cook* (JC039). All sampling bottles were cleaned according to procedures adopted from the GEOTRACES sample handling protocols detailed in Chapter 2.2.

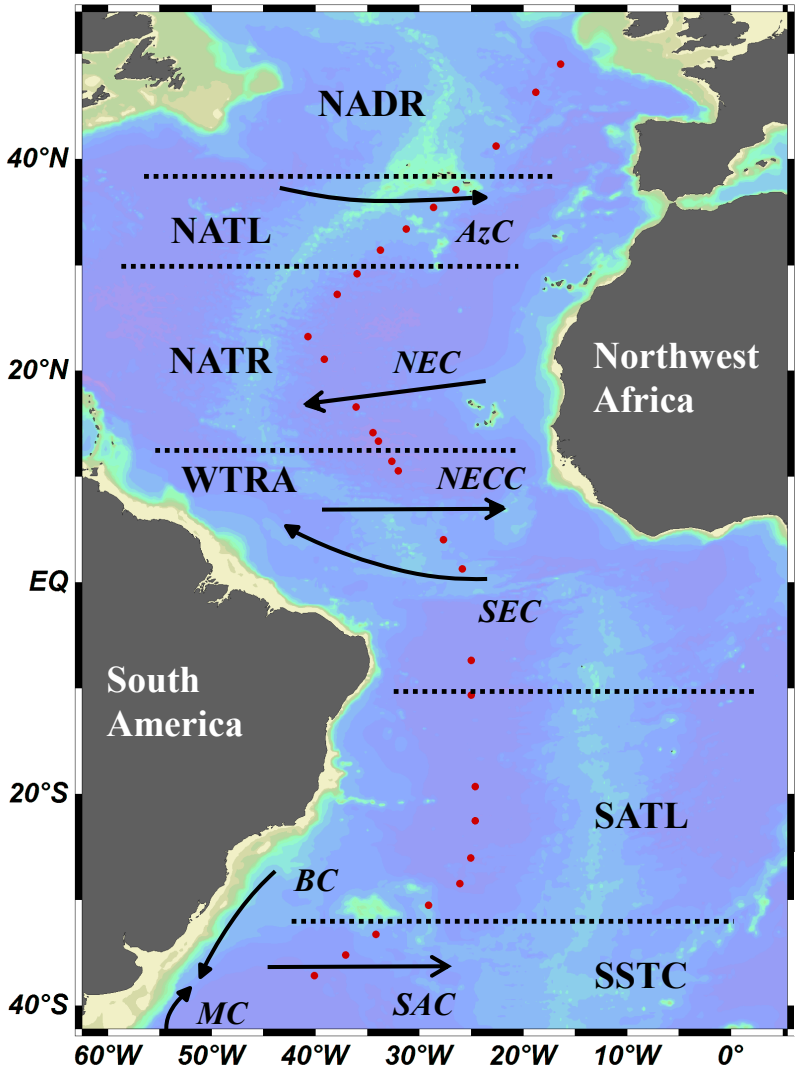

Figure 3.1. The stations (red dots) sampled for dissolved iron and total dissolvable iron during *AMT*-19. Geographic provinces are indicated as North Atlantic Drift (NADR), North Atlantic Gyre (NATL), North Atlantic Tropical Gyre (NATR), Western Tropical Atlantic (WTRA), South Atlantic Gyre (SATL) and South Sub-Tropical Convergence (SSTC). The major Atlantic currents shown are the Azores Current (AzC), the North Equatorial Current (NES), the North Equatorial Counter Current (NECC), the South Equatorial Current (SEC), the South Atlantic Current (SAC), the Brazil Current (BC) and the Malvinas Current (MC). Station metadata can be obtained from http://www.bodc.ac.uk/projects/uk/amt/. This figure was made using Ocean Data View (Schlitzer, 2012).

Seawater samples were collected using six 10 L trace metal clean Teflon coated OTE (Ocean Test Equipment) sampling bottles attached to a titanium CTD frame. The

sample bottles were remotely closed from the ship during the retrieval of the CTD into waters that had not previously been in contact with the frame. Upon recovery, the OTE bottles were transferred into a class 1000 clean air container and lightly pressurised with high purity nitrogen gas (BOC Gases), which was filtered in-line using a 0.2 µm polypropylene housed, glass microfiber filter (HEPA-CAP-36, Whatman). Seawater samples were collected for two different size fractions of Fe, defined as: dFe (< 0.2 µm) and TDFe (unfiltered seawater). Samples for dFe were filtered through 0.2 µm cellulose acetate membrane, polypropylene housed filter capsules (Sartobran-300, Sartorius) into 60 mL low density polyethylene (LDPE) bottles (Nalgene), whereas TDFe samples were collected directly from the OTE sampling bottles into 60 mL LDPE bottles. Each sample was acidified to pH 1.8 (0.024 M) by addition of 12 M hydrochloric acid (HCL, SpA, Romil) under a class 100 laminar flow hood. The sample bottles were sealed tightly and stored in polyethylene zip-lock bags for > 3 months before analysis on land.

3.2.2. Determination of iron in seawater

Dissolved Fe and TDFe were determined using flow injection with chemiluminescence detection (FI-CL) within a Class 1000 clean room facility (ISO 9001) at the University of Plymouth, UK. The FI method used in this study was based on the method originally described by Obata *et al.* (1993) and modified by de Jong *et al.* (1998) and de Baar *et al.* (2008). The detailed methodology is described in Chapter 2.5. Briefly, measurements were made based on the catalytic oxidation of luminol by hydrogen peroxide in the presence of Fe. This method detects Fe(III); therefore this study used a hydrogen peroxide oxidation step whereby each sample had an addition of H_2O_2 (30 % v/v, Merck, to make a final concentration of 10 nM) 1 h prior to the

determination of Fe(III) as recommended previously (Lohan *et al.*, 2005a; Johnson *et al.*, 2007). The sample was buffered in-line to pH 3.5 – 4.0 with 0.12 M ammonium acetate before being loaded onto a chelating iminodiacetic acid (IDA, Toyopearl AF-Chelate-650 M) pre-concentration column (Fig. 2.5). The column was rinsed with 0.12 M ammonium acetate to remove interfering cations of the seawater matrix before Fe was eluted from the column with 0.4 M HCl (SpA, Romil). The HCl eluent entered the reaction stream where it mixed firstly with a 0.3 M 5-amino-2,3-dihydrophthalazine-1,4-dione (luminol: Aldrich) solution containing 0.96 M ammonia hydroxide, and secondly with 0.1 M H_2O_2. Chemiluminescence emission was detected by a Hamamatsu low power photomultiplier tube (model H 6240-01) and recorded using LabVIEW v.7.1 software (Fig. 2.5).

The accuracy of the method was assessed daily by the determination of dFe in SAFe S and D1 seawater reference materials. The concentrations of dFe (± 1 std. dev.) measured in the SAFe reference samples (*S* = 0.14 ± 0.08 nM; D1 = 0.74 ± 0.10 nM; *n* = 15) were in good agreement with the consensus values (*S* = 0.09 ± 0.07 nM; D1 = 0.67 ± 0.07 nM).

3.2.3. Air mass back trajectories

Five day air mass back trajectories (AMBTs) were simulated for four North Atlantic stations using the NOAA Air Resources Laboratory Hybrid Single-Particle Lagrangian Integrated Trajectory Model (HYSPLIT, GDAS data set) (Draxler and Rolph, 2013; Rolph, 2013). These four stations represent the four geographic provinces (NADR, NATL, NATR and WTRA; Fig. 3.1) that together receive ~ 43 % of the dust

flux to the world's oceans (Jickells *et al.*, 2005). In contrast, the South Atlantic receives only ~ 4% of the dust flux and therefore is not represented here. Trajectory arrival heights of 400, 800 and 1500 m were selected. The 400 and 800 m arrival heights represent air masses that have arrived within the marine boundary layer, the part of the atmosphere that has direct contact with the ocean, and hence is where dust deposition occurs. The 1500 m arrival height represents air masses that originate at starting altitudes within the range of Saharan dust transport (1 – 5 km) (Prospero and Carlson, 1972; Prospero *et al.*, 1981).

3.2.4. Nitrogen fixation, primary productivity and chlorophyll-*a*

For rates of N_2 fixation, samples were collected pre-dawn at nine North Atlantic stations using the titanium CTD system. Seawater was collected from four light penetration depths (97, 33, 20 and 1 % of surface light irradiance), which were estimated from *in situ* irradiance profiles using an Alphatraka MkII transmissometer (Helsea Instruments). Sub-samples of 1 L were labelled with 1 mL of 99 % ^{15}N-N_2 (Isotech) and incubated on-board for 24 h under relevant light attenuating filter screens. Following incubation, the samples were filtered (0.7 µm Whatman GF/F) and the filters oven dried at 60° C overnight. Particulate nitrogen and ^{15}N atom % were determined at Plymouth Marine Laboratory, UK, using pre-calibrated (urea standards 0.1 – 0.75 µmol-N, PDZ-Europa Ltd.) stable isotope mass spectrometry (PDZ-Europa 20-20 and GSL; Owens and Rees, 1989) and the rates determined according to Montoya *et al.* (1996). Rates of N_2 fixation determined in this manner may prove to be an underestimation due to the unequal dissolution of the ^{15}N-N_2 bubble (Mohr *et al.*, 2010). Absolute rates may

alter between 1.4 (Mulholland *et al.*, 2012) and up to 6 times (Wilson *et al.*, 2012) with modified methodology and so rates reported here should be considered conservative.

For rates of primary productivity (Dr. Claire Widdicombe; PML), seawater was collected pre-dawn from six light penetration levels (between 97 % and 1 % surface irradiation) using standard 20 L Niskin bottles fitted to a stainless steel CTD rosette. Sub-samples of 75 mL were labelled with 10 µL of ^{14}C-HCO_3^{1-} and incubated on-deck for 12 – 14 h (local dawn to dusk) under relevant light attenuating filter screens. The experiments were terminated by sequential filtration through 2 µm polycarbonate and 0.2 µm Supor 200 membrane filters and fumed overnight with HCl prior to analysis onboard using a Packard Tricarb 2900 liquid scintillation counter. For chlorophyll-*a* determination (Dr. Claire Widdicombe; PML), samples were filtered (0.2 µm polycarbonate) and the filters extracted in 10 mL of 90 % acetone overnight at 4 - 20° C (Welschmeyer *et al.*, 1994). The chlorophyll-*a* extract was measured on a pre-calibrated (pure chlorophyll-*a* standard, Sigma) Turner Designs Trilogy 700 fluorimeter.

3.2.5. Nutrients, temperature, salinity and pH

The dissolved macronutrients silicate, phosphate and nitrate (determined as nitrate + nitrite) were determined on-board (Carolyn Harris; PML) using an AA III segmented-flow AutoAnalyser (Bran and Luebbe) following colorimetric procedures (Woodward and Rees, 2001). These were determined in all samples from the titanium CTD rosette and additionally from the stainless steel CTD rosette. Clean sampling and analysis procedures for macronutrients were adopted (Hydes *et al.*, 2010). Salinity, temperature and depth were measured using a Seabird 911+ CTD mounted to the rosette.

Dissolved O_2 was determined by a Seabird SBE 43 O_2 sensor. Salinity was calibrated on-board using an Autosal 8400B salinometer (Guideline) whilst dissolved O_2 was calibrated by photometric automated Winkler titration (Carritt and Carpenter, 1966).

Seawater pH was determined on-board on samples collected from the titanium CTD rosette by spectrophotometric methods described by Dickson *et al.* (2007), using the sulfonephthalein indicator dye *m*-cresol purple and a Perkin Elmer Lambda 35 spectrophotometer. A 2 mM stock solution was prepared by adding 0.977 g *m*-cresol sodium salt to 1 L UHP water. From this stock, 100 µL was added to seawater samples before and after a series of absorbance measurements. Initially, seawater sub-samples were allowed to acclimatise to room temperature (~ 21° C) over several hours. The absorbance measurements were conducted in 10 cm path-length quartz glass cells at three wavelengths: a non-absorbing wavelength (730 nm for *m*-cresol purple) and at the wavelengths corresponding to the absorbance maxima of the base (I^{2-}) and acid (HI^{-}) forms of the dye (578 and 434 nm respectively). The acid dissociation constant for *m*-cresol purple was calculated from the equations of Clayton and Byrne (1993) and pH expressed on the total hydrogen ion concentration scale. The pH values were corrected to ambient temperature using the CO_2SYS software programme (Lewis and Wallace, 1998) and temperature/salinity data from the titanium CTD.

3.3. Results

3.3.1. Hydrographic setting and macronutrient distributions

During this study, the Atlantic Ocean was partitioned into 6 geographic provinces (Fig. 3.1, Table 3.1) based on the physical circulation of the ocean described

by Longhurst (1998). This approach is intended to highlight the regional oceanographic processes that influence the distribution and biogeochemistry of Fe in the Atlantic. The provinces are as follows: North Atlantic Drift Region (NADR, 56 - 38º N), North Atlantic Gyre (NATL, 38 - 30º N), North Atlantic Tropical Gyre (NATR, 30 -12º N), Western Tropical Atlantic (WTRA, 12º N - 10º S), South Atlantic Gyre (SATL, 10 - 33º S), and South Sub-Tropical Convergence (SSTC, 33 - 55º S).

Table 3.1. Description of the biogeochemical provinces sampled during *AMT*-19. Adapted from Longhurst (1998).

Biogeochemical province	Acronym	Latitudinal range
North Atlantic Drift Region	NADR	56 – 38º N
North Atlantic Gyre	NATL	38 – 30º N
North Atlantic Tropical Gyre	NATR	30 – 12º N
Western Tropical Atlantic	WTRA	12º N – 10º S
South Atlantic Gyre	SATL	10 – 33º S
South Sub-Tropical Convergence	SSTC	33 – 55º S

Within these provinces, the thermohaline structure of the upper water column (Fig. 3.2) is determined by the water masses that occupy each region and the relative evaporation and precipitation rates. In the North Atlantic, the lowest upper water column temperatures (12 - 22° C) were observed within the NADR. Here, the water column displayed weak thermohaline stratification, characteristic of high wind stress in the NADR during boreal autumn (Longhurst, 1998).

Moving south into the NATL, the introduction of a warmer (20 - 26° C), more saline (*S* 36 – 37), tropical water mass that originated in the northern margins of the Azores Current (Aiken *et al.*, 2000) resulted in a mixed layer depth of between 40 and

50 m. This tropical water is also present throughout the NATR where high rates of evaporation result in salinity > 37. Consistent with previous *AMT* observations (Aiken *et al.*, 2000; Robinson *et al.*, 2006), this tropical water mass was observed to depths of ~ 150 m between 20 and 26° N during *AMT*-19.

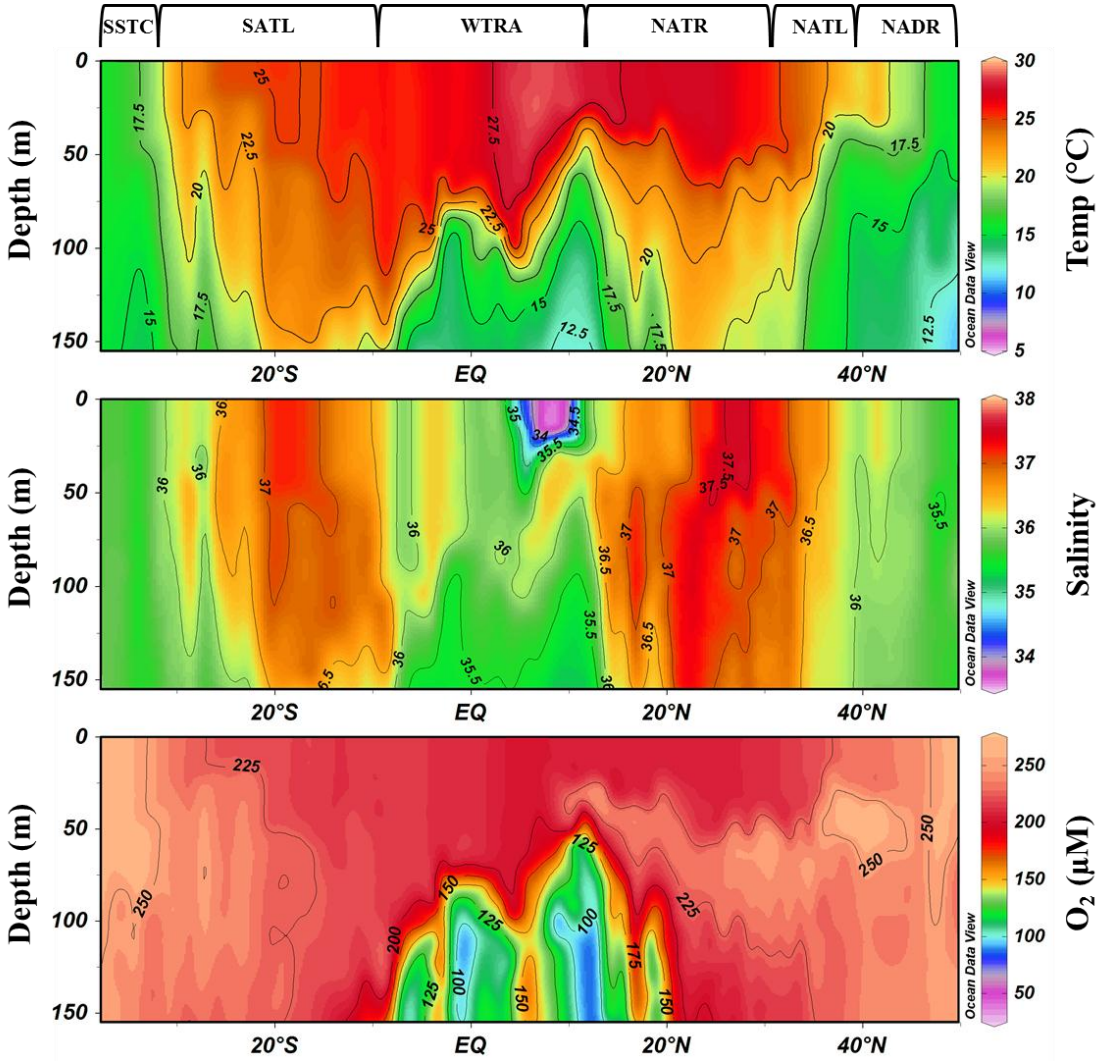

Figure 3.2. The distributions of temperature (top), salinity (middle) and dissolved oxygen (bottom) in the upper 150 m of the Atlantic Ocean during *AMT*-19, with the biogeochemical provinces marked above (refer to Table 3.1 for acronyms). This figure was made using Ocean Data View (Schlitzer, 2012).

Towards the southern extent of the NATR province, a plume of cooler (< 20° C), fresher (*S* < 36), low oxygen (< 150 µM) upwelled water was clearly visible below 60

m (Fig. 3.2). Strong upwelling off the Northwest African Margin results from the divergence between the North Equatorial Current and the North Equatorial Counter Current at ~ 10° N, and the divergence between the same Counter Current and the South Equatorial Current at ~ 2° S (Hastenrath and Merle, 1987; Longhurst, 1998; Aiken *et al.*, 2000; Fig. 3.1). Within this upwelled water, low oxygen concentrations are maintained by biological oxygen consumption via respiration in the thermocline (Karstensen *et al.*, 2008) and sluggish ocean ventilation (Stramma *et al.*, 2008). The North Atlantic OMZ extends from the Northwest African margin to ~ 35° W (Fitzsimmons *et al.*, 2013) and extended throughout the tropical Atlantic to the southern boundary of the WTRA during *AMT*-19. As a result, mixed layer depths in the WTRA varied between 30 and 75 m. Above the mixed layer, the WTRA surface waters displayed low salinity ($S < 36.5$) relative to the sub-tropical gyres, caused by dilution through an excess of precipitation over evaporation (Aiken *et al.*, 2000).

A surface salinity minimum ($S < 35$) was observed within the WTRA between 6 and 8° N to 30 m (Fig. 3.2), a common feature that can arise from either converging air masses and subsequent high precipitation rates in the Inter-Tropical Convergence Zone (ITCZ) (Bowie *et al.*, 2002a; Ussher *et al.*, 2013), or from Amazon Water transported eastwards across the Atlantic by the North Equatorial Counter Current (Aiken *et al.*, 2000). No elevation in surface silicate concentration (data not shown), which would be indicative of Amazon Water, was observed during *AMT*-19. In addition, two large rainfall events were recorded between 6 and 9° N during the cruise, indicating high rates of precipitation in the ITCZ as the cause of the WTRA salinity minimum.

As observed during earlier *AMT* studies (Robinson *et al.*, 2006), a gradual latitudinal decrease in sea surface temperature and salinity was observed in the SATL

(10 – 33º S) and into the SSTC (33 – 38º S); a manifestation of the decrease in evaporation rates associated with lower temperatures at higher latitudes. An increase in the westerly winds as the ship travelled south, coupled with increased downwelling associated with the anti-cyclonic circulation of the sub-tropical gyre (Longhurst, 1998; Ussher *et al.*, 2013), resulted in a deepening of the SATL mixed surface layer up to 75 m, and a fully homogenous upper water column (T ~ 16 °C, S ~ 35.5) in the SSTC.

The distribution of macronutrients along the transect (Fig. 3.3) revealed extremely low mixed layer concentrations (nitrate < 1µM and phosphate < 0.1 µM), depleted through biological uptake, and three distinct regions where concentrations below the mixed layer were elevated. Firstly, within the NADR, macronutrient concentrations were elevated below 60 m (nitrate 2.5 - 12 µM and phosphate 0.2 - 0.9 µM). These elevations continued into the northern section of the NATL before becoming depleted to concentrations less than 1 µM nitrate and 0.1 µM phosphate. Secondly, macronutrient concentrations were greatly elevated in waters associated with the equatorial upwelling (nitrate 2.5 - 23 µM and phosphate 0.2 - 1.5 µM). Finally, macronutrient concentrations in the SSTC were elevated below 100 m (nitrate 2.5 - 5 µM and phosphate 0.2 - 0.5 µM), values similar to those reported for the Southwest Atlantic at 40° S by Wyatt *et al.* (2013; *in press*) (see Chapter 4), and which may reflect mixing with high nutrient sub-Antarctic water associated with the Brazil-Malvinas Current convergence and the South Atlantic Current (Fig 3.1).

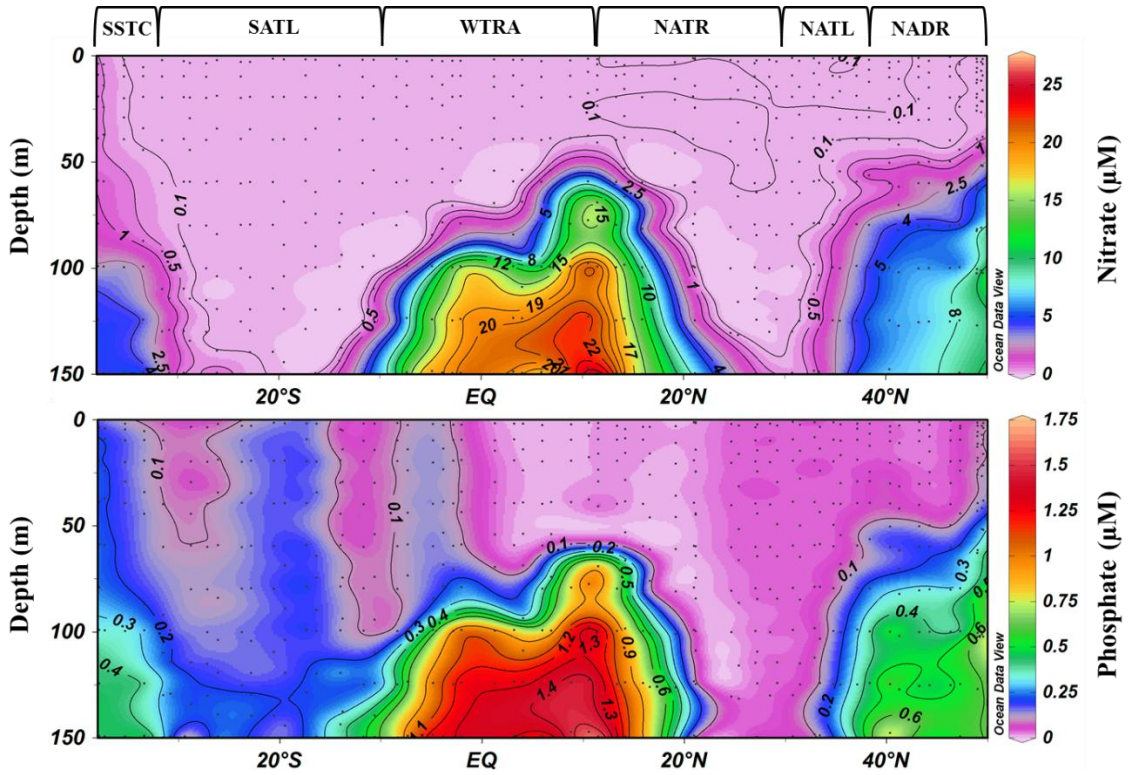

Figure 3.3. Concentrations of macronutrients (nitrate and phosphate) in the upper 150 m of the Atlantic Ocean during *AMT*-19 with the biogeochemical provinces marked above (refer to Table 3.1 for acronyms). This figure was made using Ocean Data View (Schlitzer, 2012).

3.3.2. Air mass regimes

Five-day AMBT's for the North Atlantic Ocean during *AMT*-19 (Fig. 3.4) show that the cruise track passed under three distinct air mass regimes; North Atlantic/European air in the NADR (Fig. 3.4A), North Atlantic/maritime air in the NATL and NATR (Fig. 3.4B and C respectively), and Saharan air in the WTRA (Fig. 3.4D). These air masses and their aerosol chemical constituents have been described elsewhere (*e.g.* Baker *et al.*, 2006; Buck *et al.*, 2010a,b). The 5-day AMBT's for the NADR at 46° N (Fig. 3.4A) showed a cyclonic atmospheric circulation pattern with trajectories that pass over Northwest Europe and Scandinavia. Buck *et al.* (2010a) report an aerosol Fe:Al molar ratio of 0.05 for North Atlantic/European air at 46° N (Table

3.2) that is significantly lower than the Saharan dust Fe:Al ratio of 0.26 (Formenti *et al.*, 2003), apparently a result of aerosol particles depleted in Fe.

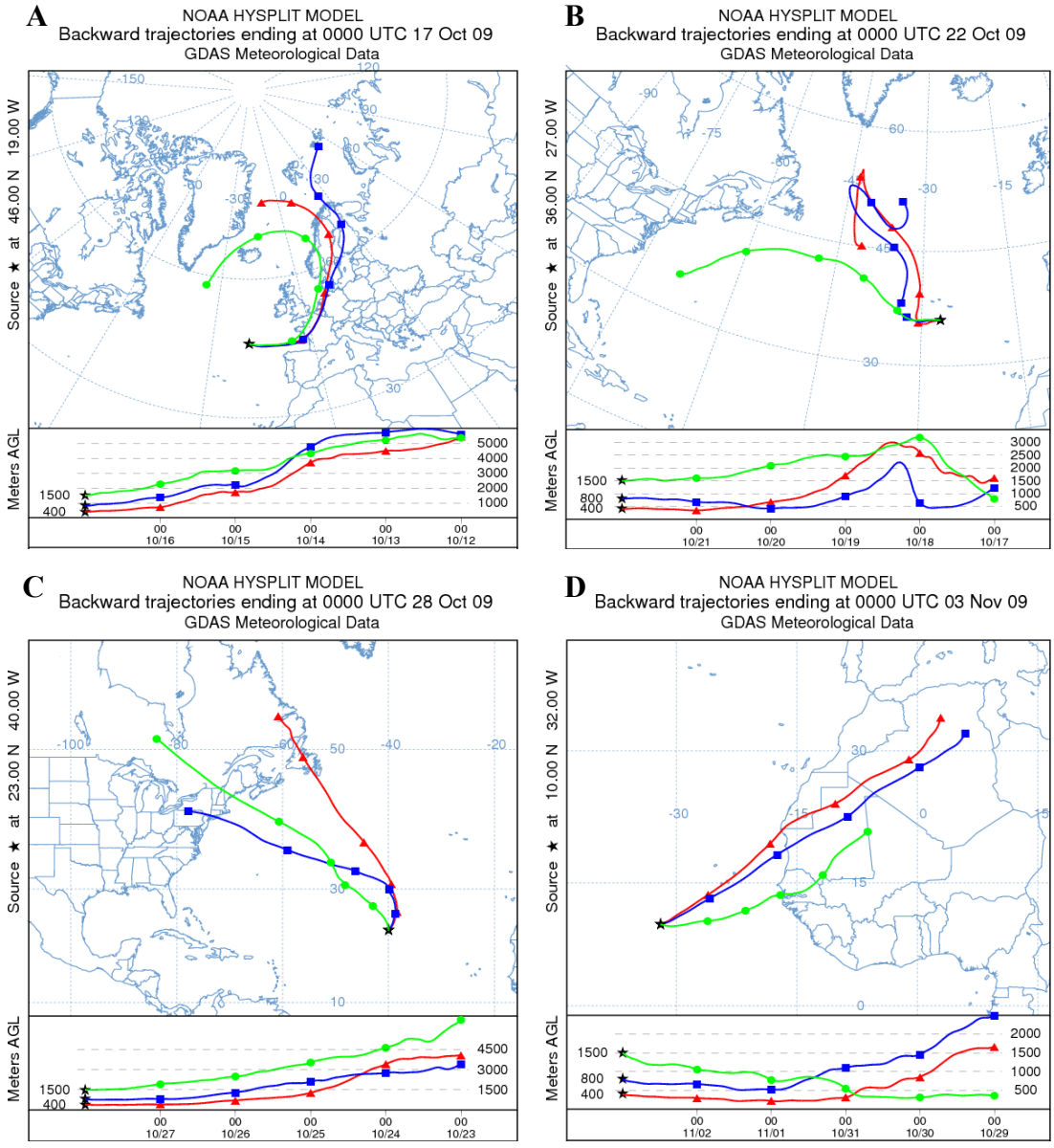

Figure 3.4. Five day (120 h) back-trajectory analysis for selected points along the *AMT*-19 cruise track: (A) NADR: 46° N 19° W, 17th October 2009, North Atlantic European air (B) NATL: 36° N 27° W, 22nd October 2009, North Atlantic/remote air (C) NATR: 23° N 40° W, 28th October 2009, North Atlantic maritime air (D) WTRA: 10° N 32° W, 3rd November 2009, Saharan air. Back trajectories converge at arrival heights of 400 m (red), 800 m (blue), and 1500 m (green) above the ship's position. Lower sections of each panel show variation in height (m above ground level) of each air parcel over the preceding 5 days.

Further to the south, the 5-day AMBT's for the NATL at 36° N (Fig. 3.4B) were of marine origin and appear to be influenced at their southern extent by prevailing westerly winds. However, extending the trajectories to ten days showed that the air masses originated over continental North America and may be influenced by polar and continental polar air masses. Here, the aerosol molar Fe:Al ratio of 0.40 (Table 3.2) was higher than that of Saharan dust, which when considered in conjunction with elevated aerosol manganese and vanadium to titanium ratios, has led Buck *et al.* (2010a) to suggest an anthropogenic influence on these air masses.

Table 3.2. Total aerosol iron, aluminium and silicate concentrations for samples collected during CLIVAR A16N. Adapted from Buck *et al.* (2010a).

Province	Latitude (°N)	Total aerosol Fe (pmol m^{-3})	Total aerosol Al (pmol m^{-3})	Total aerosol Si (pmol m^{-3})	Fe:Al molar ratio	Fe:Si molar ratio
NADR	46	30	620	DL	0.05	N/A
NATL	36	146	365	795	0.40	0.18
NATR	23	1904	6737	15007	0.28	0.13
WTRA	10	1755	6893	16077	0.25	0.11

DL = below detection limit

Similarly, the air regime within the NATR at 23° N (Fig. 3.4C) had 5-day AMBT's that originated above continental North America. Within the NATR, atmospheric transport appears to be strongly influenced by the Bermuda-Azores high pressure system (BAH) as the trajectories travel eastward before following an arc-like pattern as they decrease in altitude and converge with northeasterly trade winds. At this latitude, the aerosol Fe:Al molar ratio of 0.28 (Table 3.2) reported by Buck *et al.* (2010a) is similar to that of Saharan dust suggesting that Saharan dust entrained in the trade winds is an important source of Fe to the NATR.

The AMBT's for the WTRA at 10° N (Fig. 3.4D) begin to show air masses originating over the African continent. The Saharan air masses associated with the WTRA are dominated by the signature of Saharan dust particles with an aerosol Fe:Al molar ratio of 0.25 observed at 10° N (Buck *et al.*, 2010a) (Table 3.2). These air masses, along with Saharan dust, can be carried to the ocean surface by entrainment with descending northeasterly trade winds. (Buck *et al.*, 2010a).

3.3.3. Surface water iron distributions

The two chemical forms of Fe investigated during this study, defined by physical size fractionation (see Chapter 2.3.3), are shown in Figure 3.5. Here, dFe was operationally defined as the fraction which passed through a 0.2 μm filter, whilst TDFe was defined as the total Fe in an unfiltered seawater sample and includes the fraction of reactive Fe solubilised from particles following a 6 month weak acid (0.024 M HCl) leach.

Surface water (≤ 25 m) Fe distributions during *AMT*-19 displayed distinct regional differences between the North and South Atlantic (Fig. 3.5). Elevated surface Fe concentrations (dFe = 0.50 – 1.65 nM, TDFe = 0.80 – 1.68 nM) were observed within the NATR and the WTRA provinces between ~ 4 and 29° N, a latitudinal range in agreement with the known extent of the Saharan dust belt (0 – 30° N; Kaufman *et al.*, 2005). Within this latitudinal range, two distinct surface Fe maxima were observed (Fig 3.5). The first Fe maxima, located in the NATR between ~ 20 and 29° N (dFe = 0.68 – 1.02 nM, TDFe = 0.96 – 1.66 nM), was in the vicinity of elevated rates of surface N_2 fixation (0.3 – 1.1 nmol L^{-1} d^{-1}; see section 3.3.5, Fig. 3.6). Within this region, dFe

represented only 48 ± 26 % of the TDFe pool suggesting that atmospheric dry deposition of Fe-rich Saharan dust may be the principal source of Fe to the NATR. The second, located in the southern NATR, northern WTRA between ~ 4 - 14° N (dFe = 0.50 – 1.65 nM, TDFe = 0.83 – 1.68 nM), broadly coincided with the ITCZ surface salinity minimum (Fig. 3.2).

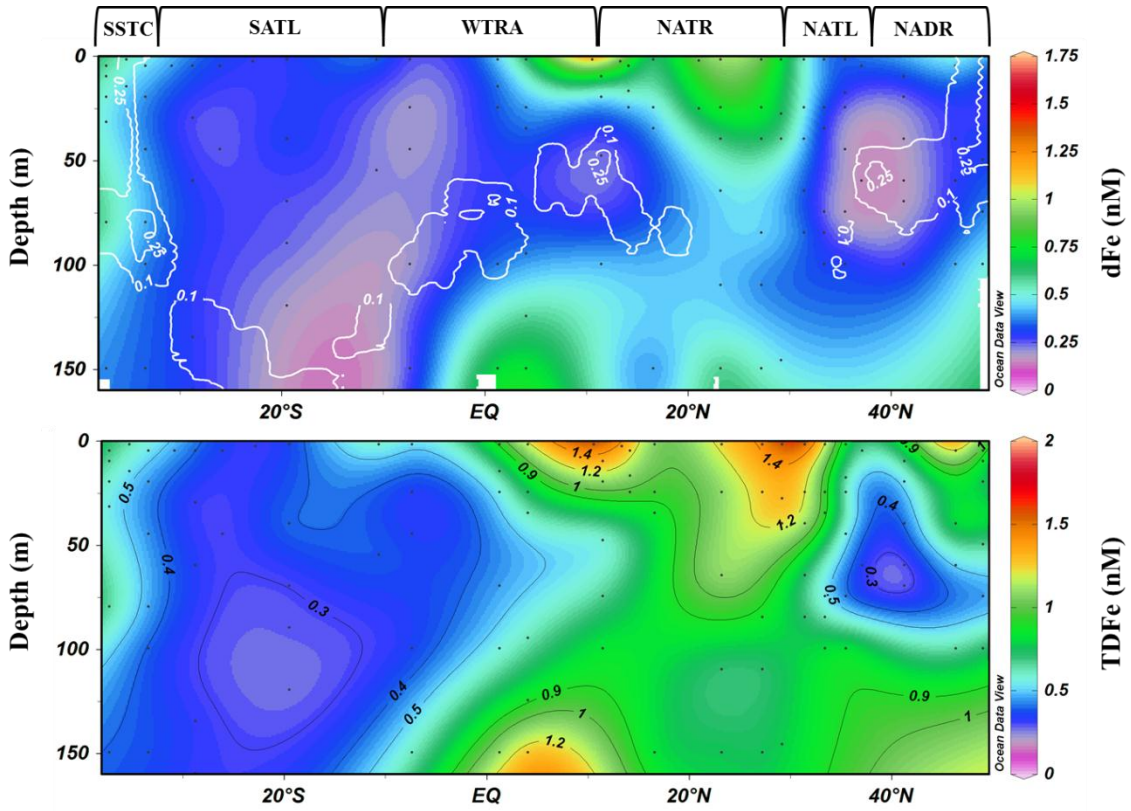

Figure 3.5. Concentrations of total dissolved iron overlaid with chlorophyll-*a* (mg m^{-3}; white contours) (top) and total dissolvable iron (bottom) in the upper 150 m of the Atlantic Ocean during *AMT*-19, with the biogeochemical provinces marked above (refer to Table 3.1 for acronyms). This figure was made using Ocean Data View (Schlitzer, 2012).

Here, dFe represented 60 ± 26 % of the TDFe pool indicating that Fe was more soluble in the ITCZ than in the NATR immediately to the north. In addition, both dFe and TDFe were significantly inversely correlated with salinity in ITCZ surface waters

(r^2 = 0.46 and 0.41 respectively; n = 13, $p < 0.05$). Together, these data suggest that the atmospheric wet deposition of more soluble Fe (Jickells and Spokes, 2001; Baker *et al.*, 2007) may be the dominant input mechanism to the ITCZ. The two North Atlantic Fe maxima were in excellent agreement with observations from other Atlantic transects (*e.g.* Bowie *et al.*, 2002a; Bergquist and Boyle, 2006; Measures *et al.*, 2008; Ussher *et al.*, 2013).

To the north of 30° N, surface Fe concentrations in the NATL (dFe = 0.16 – 0.55 nM, TDFe = 0.25 – 1.37) were lower (Fig. 3.5), likely due to a reduced Saharan dust input and stronger winter mixing in the NATL compared with weak seasonal mixing in the NATR (Longhurst, 1998). A slight surface dFe elevation of 0.58 nM was found in the NADR at ~ 46° N, near the approach to the European continental shelf, which corresponded to TDFe of 1.92 nM. As discussed further on, it is likely that this elevated Fe does not represent a shelf source and instead, may result from a small atmospheric dust deposition event.

The lowest surface Fe concentrations (dFe = 0.14 – 0.32 nM, TDFe = 0.29 – 0.71 nM) were found in the centre of the SATL (Fig. 3.5), where atmospheric dust inputs are minimal (Mahowald *et al.*, 1999; Jickells *et al.*, 2005), and increased southwards into the SSTC (dFe = 0.39 – 0.58 nM, TDFe = 0.43 – 0.71 nM) as STSW mixed with high Fe sub-Antarctic water associated with the Brazil-Malvinas Current convergence (Fig. 3.1). For the SATL and SSTC provinces combined, Fe existed predominately in the dissolved phase (dFe contributed 85 ± 5% towards the TDFe pool). Interestingly, Ussher *et al.* (2013) have shown that Fe in the SATL exists largely in the soluble size fraction (< 0.02 µm), which may be expected given the minimal atmospheric supply and increased dFe residence time (8 - 11 y) compared with the

North Atlantic provinces (0.4 – 3 y) reported by these authors. The difference in chemical forms of Fe between the North and South Atlantic can therefore be explained, for the most part, by the differences in atmospheric fluxes and by different biogeochemical processing of Fe in these surface waters.

3.3.4. Sub-surface iron distributions

The sub-surface (> 25 m) distribution of Fe also displayed strong latitudinal gradients (Fig. 3.5). In the North Atlantic, minimum sub-surface Fe concentrations (dFe = 0.06 – 0.20 nM, TDFe = 0.16 – 0.39 nM) were observed in the vicinity of the chlorophyll-*a* maximum (0.20 – 0.25 mg m^{-3}). Maximum sub-surface Fe concentrations (dFe = 0.79 nM, TDFe = 1.54 nM) were observed in the WTRA, coincident with an oxygen minimum of ~ 122 µM (Fig. 3.2). Observations of elevated dFe in this OMZ are consistent with similar studies in the North Atlantic (Bergquist and Boyle, 2006; Measures *et al.*, 2008; Fitzsimmons *et al.*, 2013; Ussher *et al.*, 2013). This suggests that the elevated dFe in the north Atlantic OMZ may be a steady-state feature, possibly sustained by remineralisation of Fe-rich organic matter formed in the surface mixed layer. Elevated sub-surface dFe concentrations were also found below 100 m in the northern NATR, southern NATL waters between 22 and 28° N (0.44 – 0.77 nM; Fig. 3.5). Here, the dFe fraction represented 69 ± 18 % of the TDFe pool and could therefore be a relic of a previous dust deposition event.

In the South Atlantic, sub-surface Fe concentrations in the SATL were relatively low and less variable (dFe = 0.15 - 0.39 nM, TDFe = 0.25 – 0.59 nM). The highest South Atlantic sub-surface Fe concentrations were observed in the SSTC (dFe =

0.33 – 0.61 nM, TDFe = 0.33 – 0.73 nM), in close proximity to the chlorophyll-*a* maxima (> 0.25 mg m^{-3}) at these stations (Fig. 3.5).

3.3.5. Nitrogen fixation in the upper water column

In the North Atlantic Ocean, the upper water column (115 m) integrated N_2 fixation rates were highest between 21 – 23° N (54 – 56 µmol m^{-2} d^{-1}; Fig. 3.6). These values were in excellent agreement with the ~ 50 µmol m^{-2} d^{-1} reported by Moore *et al.* (2009) at these latitudes for *AMT*-17, approximately 4° east of this study. The lowest rates of N_2 fixation in the upper water column (5 – 11 µmol m^{-2} d^{-1}) were observed at the northern most stations between 33 – 44° N, a latitudinal range where the concentrations of *Trichodesmium*, the major group of N_2 fixing phytoplankton in the oceans (Capone *et al.*, 1997), are reported to be minimal or absent (Tyrrell *et al.*, 2003).

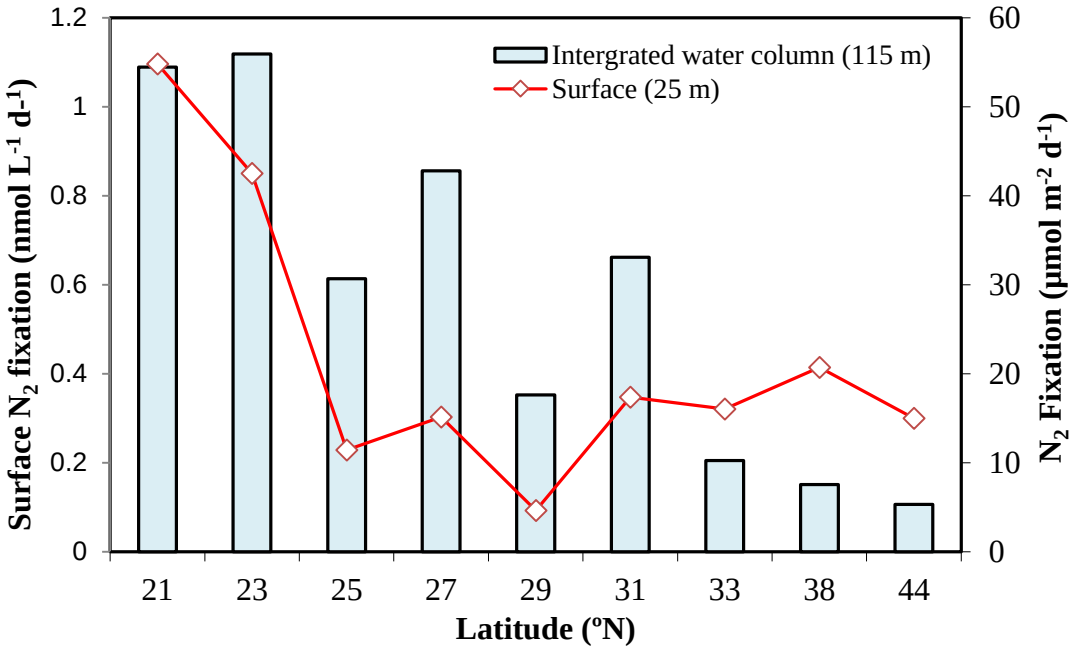

Figure 3.6. Average surface (25 m) and upper water column (115 m) integrated N_2 fixation rates from nine North Atlantic stations during *AMT*-19.

At individual stations, N_2 fixation was generally highest in surface waters (≤ 25 m), which agrees well with the vertical distribution of *Trichodesmium* in the water column of the North Atlantic (Tyrrell *et al.*, 2003). Within these surface waters, N_2 fixation ranged from 0.1 to 1.1 nmol L^{-1} d^{-1} (Fig. 3.6), values once again in close agreement with the range reported for *AMT*-17 at corresponding latitudes (Moore *et al.*, 2009). The highest surface rates (0.85 – 1.1 nmol L^{-1} d^{-1}) were observed between 21 – 23° N, whilst the lowest (0.1 – 0.2 nmol L^{-1} d^{-1}) were observed between 25 – 29° N. Instead, N_2 fixation between these latitudes was highest at ~ 40 m (0.2 – 0.7 nmol L^{-1} d^{-1}). It should be noted that lower surface rates were also observed during *AMT*-17 at ~ 28° N (Moore *et al.*, 2009). It has been suggested that active buoyancy regulation may allow *Trichodesmium* to migrate vertically (Villareal and Carpenter, 1990) and therefore the deeper depth of the N_2 fixation maximum between these latitudes may reflect the vertical migration of diazotrophs in response to Fe or macronutrient availability (Fig's 3.5 and 3.3).

3.3.6. pH distributions in the upper water column

The latitudinal distribution of seawater pH is shown in Figure 3.7. The surface (≤ 25 m) pH ranged from 8.00 to 8.14 along the transect with the highest values of 8.08 to 8.14 observed in the northern and southern extremes where chlorophyll-*a* concentrations were also high (> 0.25 mg m^{-3}; Fig. 3.5). This implies that the increase in pH may be driven by recent biological production, as also observed by Chierici *et al.* (2004) in the Atlantic sector of the Southern Ocean. The lowest surface pH values of between 8.00 and 8.05 were found in the SATL and may therefore reflect the low biological production in this province along with the control of temperature and salinity

on carbon dioxide saturation. Within the WTRA, a small decrease in surface pH of 0.03 was observed within the centre of the ITCZ that corresponded with reduced salinity of 34.2 (Fig. 3.2).

Within sub-surface waters (> 25 m), the highest pH values along the transect (8.07 – 8.24) were broadly associated with the chlorophyll-*a* maximum (Fig. 3.5). The lowest sub-surface pH values (7.99 – 8.03) were observed in the NATR between 22 and 28° N (Fig. 3.7). These low pH values appear to be associated with the introduction of a warm tropical water mass (Fig. 3.2) that is thought to originate in the northern margins of the Azores Current (Aiken *et al.*, 2000; Fig. 3.1), and which may have very different biogeochemical properties.

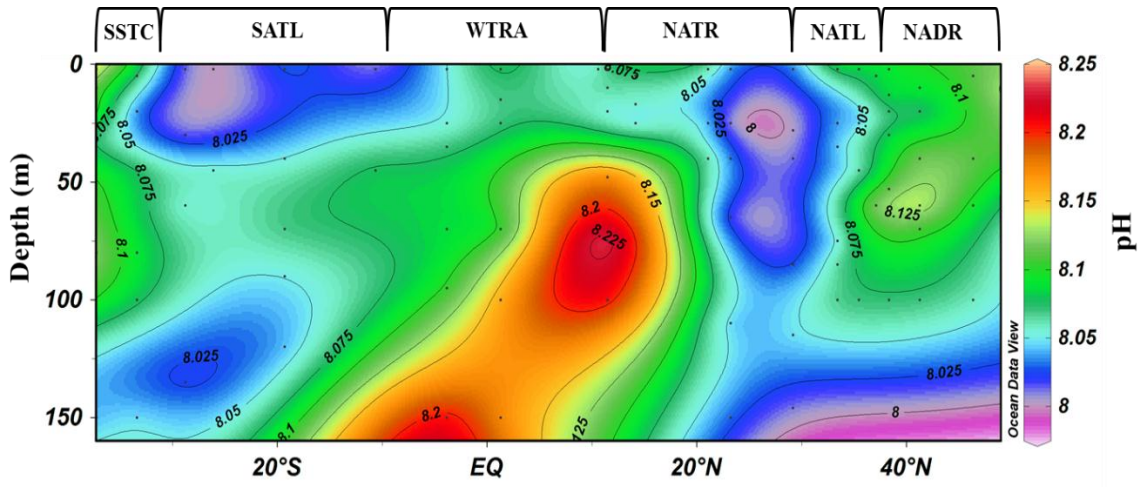

Figure 3.7. The latitudinal distribution of seawater pH along *AMT*-19. This figure was made using Ocean Data View (Schlitzer, 2012).

3.4. Discussion

3.4.1. Sources of iron to surface waters

Sources of Fe to Atlantic surface waters include atmospheric dust deposition, offshore advection of Fe-rich continental shelf waters and vertical mixing across the thermocline (Measures *et al.*, 2008; Ussher *et al.*, 2007; 2013). During *AMT*-19, NADR surface dFe concentrations of 0.17 to 0.58 nM were similar to the 0.14 to 0.60 nM reported by Ussher *et al.* (2007) for Northeast Atlantic surface waters ~ 240 km from the European continental shelf. These authors observed a dFe concentration gradient over a relatively short distance spanning the shelf break and concluded that minimal horizontal transport of dFe from the shelf to the open ocean occurred in this region, despite severe winter storms. The present study began trace metal sampling ~ 242 km from the European continental shelf and therefore, based on the observations of Ussher *et al.* (2007), assumes no dFe transport from the European shelf margin to the open Atlantic Ocean. The southernmost station sampled during *AMT*-19 was over 1000 km east the South American continental shelf, a distance that dFe surface gradients from shelf regions do not generally exceed (Elrod *et al.*, 2004; Ussher *et al.*, 2007). This study, therefore, only considers atmospheric deposition and upward vertical mixing as sources of Fe to surface waters of the Atlantic Ocean along the *AMT*-19 transect.

3.4.2. Atmospheric deposition of iron to Atlantic surface waters

The deposition and dissolution of atmospheric dust is considered the dominant source of Fe to remote Atlantic surface waters (Sarthou *et al.*, 2003; Jickells *et al.*, 2005; Baker *et al.*, 2006; Buck *et al.*, 2010a,b; Evangelista *et al.*, 2010; Ussher *et al.*, 2013).

The geographic variation in surface water dFe along *AMT*-19 must therefore, predominately reflect the balance between atmospheric inputs and removal processes.

Dust deposition models show that the North Atlantic Ocean receives approximately one order of magnitude more dust annually than the South Atlantic (Mahowald *et al.*, 1999; Jickells *et al.*, 2005) with the vast majority of this dust Saharan in origin. Using such model results, atmospheric dust deposition over the *AMT*-19 transect ranges from 10 g m^{-2} y^{-1} within the ITCZ to 0.01 g m^{-2} y^{-1} in the remote SATL (Jickells *et al.*, 2005). However, the fractional solubility of deposited Fe, hence the fraction of Fe available for phytoplankton growth, is largely dependent on a number of atmospheric and marine controls (Sedwick *et al.* 2007; Baker and Croot, 2010). Recently, an inverse relationship between atmospheric dust concentrations and Fe fractional solubility has been noted in Atlantic aerosols (Chen and Siefert., 2004; Baker and Jickells, 2006; Sedwick *et al.*, 2007), likely due to atmospheric mixing of low solubility lithogenic and high solubility anthropogenic aerosols (Sedwick *et al.*, 2007).

By using the upper and lower limits of dust deposition (Jickells *et al.*, 2005) and the median values of aerosol Fe solubility (Baker *et al.*, 2006) for the different Atlantic geographic provinces, assuming an Fe dust content of 3.5 % (Taylor and McLennan, 1985, McLennan, 2001), this study has estimated an annual flux rate of dFe from dust to Atlantic surface waters ranging from 1 to 282 µmol m^{-2} y^{-1} (Table 3.3).

Consistent with the findings of Ussher *et al.* (2013) and Sarthou *et al.* (2003) for Atlantic transects further to the east, the highest atmospheric dFe flux during *AMT*-19 was estimated for the WTRA (6 – 282 µmol m^{-2} y^{-1}). The AMBT's for the WTRA indicate that the air masses arriving within the marine boundary were Saharan in origin (Fig. 3.4D). Whilst the median aerosol Fe solubility of 4.5 % for the WTRA is lower

than most Atlantic provinces, the magnitude of the dust flux to this province is such that the atmospheric dFe flux (Table 3.3), hence surface dFe concentrations (Fig. 3.5) are highest. In addition, two rainfall events were recorded at ~ 9° N and 6° N, which support the argument for wet deposition within the ITCZ as the principle source of dFe to surface waters of the WTRA during *AMT*-19.

Table 3.3. Estimated atmospheric dissolved iron fluxes to Atlantic surface waters using the range of modelled dust deposition and median % iron solubility for individual provinces.

Province	**Dust flux lower limit ($g\ m^{-2}\ y^{-1}$)[a]**	**Dust flux upper limit ($g\ m^{-2}\ y^{-1}$)[a]**	**% Fe solubility[b]**	**dFe flux rate ($\mu mol\ m^{-2}\ y^{-1}$)**
NADR	0.5	1	15.0	47 – 94
NATL	0.5	2	7.8	24 – 98
NATR	0.5	10	1.7	5 – 107
WTRA	0.2	10	4.5	6 – 282
SATL	0.01	0.2	8.3	1 – 10
SSTC	0.2	0.5	4.7	6 – 29

[a] Values from Jickells *et al.* (2005)
[b] Median values from Baker *et al.* (2006)

Wet deposition can strongly influence the trace metal budget and chemistry of surface waters within the ITCZ by altering the fractional solubility of Fe in deposited aerosols (Jickells and Spokes, 2001; Sathou *et al.*, 2003). The fractional solubility of aerosol Fe deposited in rainwater is reported to be higher than that of Fe in aerosols deposited by dry deposition (Jickells and Spokes, 2001; Baker *et al.*, 2006), possibly due to the relatively low pH of rainwater (Baker and Croot, 2010). During the present study a small but perhaps significant pH decrease of 0.03 was observed within the centre of the ITCZ at ~ 9° N. This may go some way to explaining why this study observed a minimal difference between the dFe and TDFe size fractions for the ITCZ during *AMT*-19 (Fig. 3.5). Within the ITCZ, dFe represented 60 ± 26 % of TDFe

compared with 48 ± 26 % of TDFe in surface waters under the influence of dry deposition within the NATR/NATL. Thus, consistent with previous studies (*e.g.* Sarthou *et al.*, 2003; Bowie *et al.*, 2002a), this study concludes that wet deposition dominates the atmospheric dFe flux in the WTRA province.

Dry deposition of Saharan dust appears to be an important source of Fe to surface waters of the NATR with this study estimating a dFe flux of between 5 and 107 μmol m^{-2} y^{-1}. Whilst receiving a similar dust flux to the WTRA, it is the lower aerosol Fe solubility estimate for the NATR of 1.7 % that results in a maximum atmospheric dFe flux nearly one third of that received by the WTRA (Table 3.3). Within this NATR, the Saharan dust plume, which is transported away from the West African coast by northeasterly trade winds at heights up to 5 km (Prospero and Carlson, 1972), becomes entrained in the BAH at high altitude, forcing a clockwise reduction in plume elevation and subsequent intrusion into the marine boundary layer (Buck *et al.*, 2010a). The impact of the BAH on atmospheric transport of Saharan plume air masses during *AMT*-19 is clearly visible from 5-day AMBT's for the NATR (Fig. 3.4C).

The Fe data for the NADR (Fig. 3.5), along with the corresponding AMBT's (Fig. 3.4A), indicate that the slightly elevated surface dFe concentrations (≤ 0.58 nM) in this province may have originated from a previous atmospheric deposition event. Although dust inputs to the NADR (0.5 – 0.1 g m^{-2} y^{-1}) are lower in magnitude compared to other North Atlantic provinces (Table 3.3), estimated atmospheric dFe inputs to the NADR (47 - 94 μmol m^{-2} y^{-1}) are still highly variable, likely due to atmospheric interactions that influence aerosol Fe solubility (Buck *et al.*, 2010a). The AMBT's indicate that the aerosols would have originated over Northwest Europe and Scandinavia and were therefore likely influenced by anthropogenic combustion

products. Such mixing between natural and anthropogenic aerosols is reported to increase the fractional solubility of aerosol Fe (Sedwick *et al.*, 2007; Buck *et al.*, 2010a; Sholkovitz *et al.*, 2012). Iron in aerosols collected over the NADR is therefore often more soluble than that reported for aerosols elsewhere in the Atlantic open ocean (Baker *et al.*, 2006; Buck *et al.*, 2010a; Sholkovitz *et al.*, 2012). Thus, despite the low dust flux to the NADR, the elevated surface dFe concentrations in this province may be atmospheric in source.

The lowest atmospheric dFe flux (1 - 10 μmol m^{-2} y^{-1}) was estimated for the SATL (Table 3.3) where dFe concentrations were also at their lowest (Fig. 3.5). The ITCZ effectively forms a barrier between the North and South Atlantic basins that prevents the significant transport of Saharan dust southwards. With minimal atmospheric input, the low dFe concentrations throughout the upper water column of the remote SATL are likely to be sustained by rapid biological removal and downwelling. For example, Ussher *et al.* (2013) report downward vertical mixing across the SATL thermocline of 8 m^{-2} y^{-1} during *AMT*-15 and 16. Using this mixing rate, along with an average surface mixed layer TDFe concentration of 398 nmol m^{-3} for the SATL during *AMT*-19 (TDFe being representative of the combined dissolved and particulate Fe fractions), this study estimated a downward Fe flux of 3.2 μmol m^{-2} y^{-1} across the SATL thermocline (Table 3.4). This downward Fe flux is one to two orders of magnitude smaller than the mean seasonal atmospheric total Fe flux of 51 - 141 μmol m^{-2} y^{-1} reported for the SATL by Ussher *et al.* (2013) but compares remarkably well with the atmospheric dFe flux of 2.1 – 3.3 μmol m^{-2} y^{-1}. The fact that the downward flux of Fe compares more favourably with the atmospheric dFe input flux and not the atmospheric total Fe is not surprising given the temporal variability of lithogenic dust inputs to the

South Atlantic, the rapid sinking velocities of lithogenic particles (0.1 – 1.0 m d^{-1} for particles in the 1 - 2 µm diameter size fraction; Jannasch *et al*., 1996), and thus heterogeneity and highly variable residence times of lithogenic particles (100 – 1000 days) in the upper 100 m. It is therefore appropriate to assume that the SATL low surface mixed layer dFe inventory may be balanced in steady state by atmospheric soluble Fe inputs and the downward vertical transport of TDFe.

Further south, the estimated atmospheric dFe influx to surface waters of the SSTC of 6 – 29 µmol m^{-2} y^{-1} (Table 3.3) is higher than the 5 µmol m^{-2} y^{-1} reported for the SSTC in the eastern Atlantic (Klunder *et al.*, 2011). Modelled dust deposition to the western Atlantic SSTC, predominately Patagonian in origin (Evangilista *et al.*, 2010; Johnson *et al.*, 2010), is estimated to be between 0.2 and 5.0 g m^{-2} y^{-1}, roughly an order of magnitude higher than the flux to the eastern Atlantic SSTC (Mahowald *et al.,* 1999; Jickells *et al.*, 2005). However, the marginal difference between the surface water dFe and TDFe concentrations in this province (dFe represents 85 ± 5 % of TDFe) (Fig. 3.5) suggests that instead of atmospheric supply, the elevated dFe concentration likely arose from the mixing of sub-tropical gyre water with colder, fresher, relatively high Fe sub-Antarctic waters associated with the Brazil-Malvinas Current convergence.

Table 3.4. Estimated vertical iron fluxes between the mixed layer and below in Atlantic provinces during *AMT*-19 using iron data from this study and the calculated subduction rates of Ussher *et al.* (2013) for *AMT*-16. [a]Also shown is the mean seasonal atmospheric wet and dry dissolved iron flux from *AMT*-16 (Ussher *et al.*, 2013).

Province	Subduction rate ($m\ y^{-1}$)	Mean mixed layer dFe ($nmol\ m^{-3}$)	Mean mixed layer TDFe ($nmol\ m^{-3}$)	Mean dFe below mixed layer ($nmol\ m^{-3}$)	Mean TDFe below mixed layer ($nmol\ m^{-3}$)	Upward dFe flux ($\mu mol\ m^{-2}\ y^{-1}$)	Downward TDFe flux ($\mu mol\ m^{-2}\ y^{-1}$)	Wet and dry atmospheric dFe flux ($\mu mol\ m^{-2}\ y^{-1}$)[a]
NADR	-2.0	315	815	298	459	0.60	0.0	12.8
NATL	1.9	320	945	272	628	0.0	1.80	12.0
NATR	2.3	719	1163	501	855	0.0	2.67	14.2
WTRA	-14.3	415	778	421	747	6.03	0.0	38.3
SATL	8.0	305	398	260	298	0.0	3.18	3.3
SSTC	-3.0	489	581	420	466	1.26	0.0	9

3.4.3. Upward vertical flux of iron to Atlantic surface waters

Previous estimates suggest that upward vertical mixing from the North Atlantic OMZ provides a significant source of dFe to the WTRA surface mixed layer (≤ 27 % of the combined upward vertical mixing and atmospheric dFe flux; Ussher *et al.*, 2013). During *AMT-19*, dFe concentrations below the mixed layer in the WTRA averaged 421 nmol m^{-3} (Table 3.4). By using the upward vertical mixing rate of 14 m y^{-1} for the WTRA, reported by Ussher *et al.* (2013) for *AMT*-16, this study estimated an upward vertical dFe flux of 6.0 µmol m^{-2} y^{-1} (Table 3.4). Assuming a mean seasonal atmospheric dFe flux of 38.3 µmol m^{-2} y^{-1} to surface waters of the WTRA (Ussher *et al.*, 2013) this would suggest that upward vertical mixing provided approximately 14 % of the combined dFe input flux during *AMT*-19. If as suggested, the elevated dFe concentrations in these low oxygen waters are stable in location and magnitude (Ussher *et al.*, 2013; Fitzsimmons *et al.*, 2013) then future deoxygenation of this OMZ (Stramma *et al.*, 2009), and the subsequent stabilisation of soluble Fe(II) (Rue *et al.*, 1997), may increase the dFe inventory in sub-surface, and thus surface waters of the tropical North Atlantic. Similarly, upward vertical mixing has also been reported for the NADR and SSTC provinces (Ussher *et al.*, 2013). Within these provinces, the upward vertical dFe flux across the thermocline during *AMT*-19 was estimated to be 0.6 and 1.3 µmol m^{-2} y^{-1} respectively (Table 3.4), thus providing a source of dFe, albeit minimal, to the phytoplankton community at the base of the shallow mixed layer (Fig's 3.2 and 3.5).

3.4.4. Dissolved iron in sub-surface waters

The dFe maxima reported for the North Atlantic OMZ (0.75 - 1.50 nM: this study; Bergquist and Boyle, 2006; Measures *et al.*, 2008; Fitzsimmons *et al.*, 2013; Ussher *et al.*, 2013) are low in concentration compared with the values reported for the suboxic waters of the tropical Southeast Pacific near Chile (3.4 nM; Blain *et al.*, 2008), and near Peru (3.8 nM; Bruland *et al.*, 2005). In both of these cases, it is likely that Fe(II) contributed significantly to the measured dFe, stabilised by the extremely low oxygen concentrations (< 5 µM), and for the Chilean upwelling, cold water (< 9° C). In contrast, the oxygen concentrations in the North Atlantic OMZ during *AMT*-19 were at least 50 µM higher, reaching concentrations > 50 µM at 150 m, whilst water temperatures were warmer at > 12.2° C. Consistent with the redox conditions of Fe in hypoxic and suboxic waters (Rue *et al.*, 1997), the dFe in the North Atlantic OMZ is likely to be mainly Fe(III), with lower overall dFe concentrations.

The elevated dFe in the North Atlantic OMZ could result from a combination of inputs from (a) the dissolution of Fe from atmospheric dust particles, followed by the transfer of this signal to the OMZ via high rates of biological uptake and organic carbon (C_{org}) remineralisation, and (b) from the lateral mixing of dFe released from reducing sediments along the Northwest African shelf. The latter hypothesis however, has recently been rejected based on the distributions of dissolved manganese and its apparent minimum concentrations in the North Atlantic OMZ as opposed to maximum dFe concentrations (Measures *et al.*, 2008; Fitzsimmons *et al.*, 2013).

To investigate the role of remineralisation further, this study calculated Fe:C_{org} ratios below the mixed layer by converting apparent oxygen utilisation (AOU = $O_{2,sat} - O_{2,meas}$: calculated using Ocean Data View 4 software, Schlitzer, 2012), into

remineralised C_{org} (Feely *et al.*, 2004) using an $-O_2:C_{org}$ ratio of 1.6 typical of marine phytoplankton (Martin *et al.*, 1987). A direct comparison of dFe below the surface mixed layer and estimated C_{org} (Fig. 3.8) showed that $Fe:C_{org}$ ratio for the OMZ of 9.5 µmol mol^{-1} was within the range of 1.5 – 18 µmol mol^{-1} reported for oceanic phytoplankton (Sunda, 1997; Ho *et al.*, 2003).

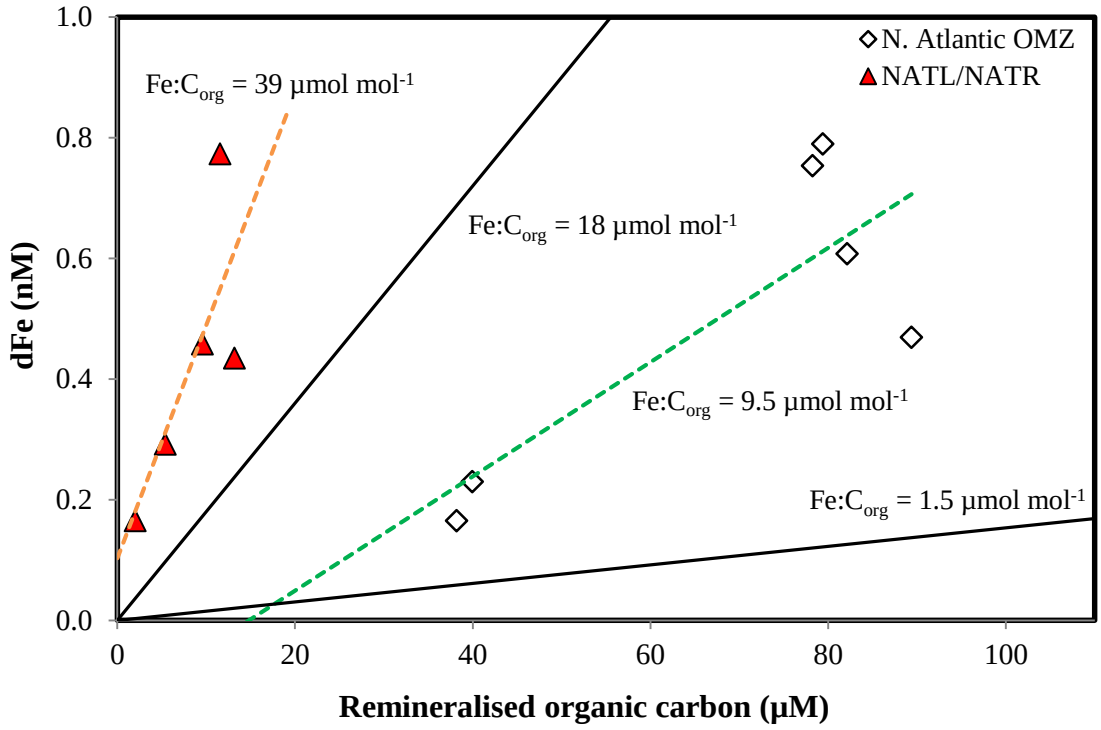

Figure 3.8. Relationship between dissolved iron and remineralised organic carbon (C_{org}) in the North Atlantic OMZ and NATR/NADR provinces. Also indicated are the upper and lower $Fe:C_{org}$ ratios reported for open ocean phytoplankton (Sunda, 1997; Ho *et al.*, 2003).

The $Fe:C_{org}$ ratio was in agreement with $Fe:C_{org}$ ratios reported by other workers (9.6 – 12.4 µmol mol^{-1}) and suggests that a significant fraction of the dFe in the North Atlantic OMZ would have been remineralised from biogenic matter. In contrast, this $Fe:C_{org}$ ratio is 4 – 6 times higher than the ratios observed in the Fe limited, HNLC

equatorial Pacific and Southern Oceans (Sunda, 1997). The enriched Fe:C_{org} ratios of the North Atlantic most likely reflect the differences in cellular Fe requirements of phytoplankton growing under Fe replete conditions compared to those in Fe deplete HNLC regions. For example, culture experiments have shown that cellular Fe:C_{org} ratios increase in oceanic phytoplankton with increasing external Fe concentration (Sunda and Huntsman, 1995b; Berman-Frank *et al.*, 2001). For *Trichodesmium*, a prevalent phytoplankton in surface waters of the tropical North Atlantic (Tyrrell *et al.*, 2003), an elevated Fe:C_{org} ratio of ~ 30 µmol mol^{-1} has been reported for cells growing at ~ 0.6 nM Fe (Berman-Frank *et al.*, 2001), reflecting the high cellular Fe demand for N_2 fixation. Thus, whilst the Fe:C_{org} signature of the OMZ may only reflect the Fe:C_{org} of the particulate sinking fraction (the largest cells) and the scavenging effect on this ratio is unknown, i.e. numerous carrier phases and types of associations are possible between trace metals and particles and therefore the fate of Fe associated with sinking particles is unclear (Planquette *et al*., 2009), the calculated Fe:C_{org} ratio suggests that the main source of Fe enrichment in the OMZ is the remineralisation of high Fe:C_{org} particulate matter.

Within the NATL/NATR between 22 – 28° N, an elevated Fe:C_{org} ratio of 39 µmol mol^{-1} (Fig. 3.8) was observed in sub-surface waters (< 100 m) indicating a potential lithogenic source of dFe. Here, the dFe fraction represented 69 ± 18 % of the TDFe pool. The most likely source of this elevated dFe is subduction out of the mixed layer. By using the subduction rates of 1.9 and 2.3 m^{-2} y^{-1} calculated by Ussher *et al.* (2013) for these provinces, this study estimated a downward vertical TDFe flux between the mixed layer (30 – 70 m) and the thermocline of 1.8 – 2.7 µmol m^{-2} y^{-1} (Table 3.4). Atmospheric deposition in the North Atlantic gyre is highly variable within timescales

shorter that surface water dFe residence times (Sarthou *et al.*, 2003; Ussher *et al.*, 2013) and therefore, the elevated sub-surface Fe:C_{org} ratio for this region could be a relic from a previous atmospheric deposition event.

3.4.5. The biological role of iron in Atlantic surface waters

The uptake of Fe by phytoplankton in surface waters and subsequent export is an important process for Fe removal from the euphotic zone (Martin and Gordon, 1988; Coale *et al.*, 2005). Consequently, sub-surface dFe minima are commonly associated with the chlorophyll-*a* maximum following the direct partitioning of Fe into living material (Measures *et al.*, 2008) as indicated by Fe:C_{org}. Along the *AMT*-19 transect, the sub-surface dFe minimum generally followed the chlorophyll-*a* maximum at the base of the mixed layer (Fig. 3.5). The exception to this was the SSTC province whereby elevated chlorophyll-*a* concentrations sat above elevated macronutrient concentrations but were in the direct vicinity of elevated dFe introduced with sub-Antarctic surface waters. The position of the chlorophyll-*a* maximum along the transect suggests that this feature is heavily dependent on the availability of nutrients, including Fe, and the flux of these nutrients across the thermocline, and effectively forms a barrier to the large-scale vertical diffusion of nutrients to the mixed layer.

Within the North Atlantic, mixed layer dFe concentrations were negatively correlated with chlorophyll-*a* within the NADR ($r^2 = 0.54$, $p < 0.01$, $n = 12$) and NATR ($r^2 = 0.72$, $p < 0.01$, $n = 11$), indicating that phytoplankton play an important role in removing dFe from sub-surface waters of these provinces. Primary productivity in North Atlantic provinces has been shown to be more dependent on phytoplankton

physiology than biomass (Marañón *et al.*, 1999), specifically at high latitudes, and it is therefore not surprising that low rates of primary productivity (< 2 mg m^{-3} d^{-1}) were associated with the NADR and NATR chlorophyll-*a* maximum during *AMT*-19. Instead, the highest rates of primary productivity in the North Atlantic were observed in the upper 5 - 25 m, particularly in the WTRA (> 10 mg m^{-3} d^{-1}).

It is estimated that picophytoplankton account for > 60 % of total photosynthesis in the Atlantic Ocean (Maranon *et al.*, 1999). Consistent with these findings, the concentration of the picophytoplankton *Synechococcus* in the North Atlantic was found to be highest (28 x 10^3 cells mL^{-1}) in the upper 25 m of the WTRA. It is well documented that *Synechococcus* are ubiquitous in the open ocean, even in regions where the Fe concentrations are extremely low and suspected to be limiting (Behrenfeld and Kolber, 1999). This phenomenon is reportedly through the adaptive expression of Fe stress-induced proteins (Webb *et al.*, 2001), and indeed, *Synechococcus* cellular concentrations were rarely below 1000 cells mL^{-1} during *AMT*-19. The elevated primary production and *Synechococcus* abundance within the WTRA are therefore likely linked to the elevated surface dFe concentrations that occur in this province (Fig. 3.5) through an increased atmospheric deposition flux to surface waters (Table 3.3).

In addition to surface dFe concentrations, the distribution of primary productivity may be linked to the nitrogen dynamics of *Synechococcus* and the distribution of N_2 fixing cyanobacteria. For example, the release of fixed nitrogen may have a direct impact on the surrounding phytoplankton community, especially in nitrogen limited regions. In the North Pacific, large blooms of *Trichodesmium* have been observed to exist concurrently with an abundance of *Synechococcus* (8 – 10 x 10^3 cell mL^{-1}) that is 3 – 4 times higher than is typically found in oceanic waters (Campbell

et al., 2005). In the Atlantic, the latitudinal distribution of *Trichodesmium* indicates maximum concentrations in the surface waters of the WTRA (Tyrrell *et al.*, 2003), a province for which the present study estimates high rates of atmospheric dFe flux (6 – 282 μmol m^{-2} y^{-1}; Table 3.3). Assuming that elevated dFe is supporting N_2 fixation in these surface waters (Moore *et al.*, 2009), the elevated primary productivity observed in the WTRA may be in part due to the elevated fixed nitrogen available to *Synechococcus*. The subsequent removal of dFe from surface waters would likely result in short residence times, on the order of months to years, in this highly productive province.

3.4.6. Iron residence times in the mixed layer

The major source for dFe to the mixed layer in the Atlantic Ocean is clearly through atmospheric dust deposition at the surface (Table 3.3). As shown in this study, Fe may also be supplied to the mixed layer by upwelling which, like the atmospheric flux, shows distinct regional differences between the North and South Atlantic (Table 3.4). To investigate this further, surface mixed layer residence times were calculated for the different Atlantic regions (Table 3.5).

Table 3.5. Estimated dissolved iron residence times in the mixed layer of Atlantic provinces during *AMT*-19.

Province	Mixed layer depth (m)	Mean mixed layer dFe (nmol m^{-3})	Integrated mixed layer dFe (nmol m^{-2})	Net input flux (μmol m^{-2} y^{-1})	Residence time (y)
NADR	40	315	12600	13.4	0.9
NATL	45	320	14400	12.0	1.2
NATR	36	719	25884	14.2	1.8
WTRA	58	415	24070	44.3	0.5
SATL1	68	305	20740	3.3	6.3
SATL2	30	489	14670	10.3	1.4

To calculate these residence times, the surface mixed layer integrated dFe inventory for each province was combined with the net dFe input flux (the sum of both seasonal atmospheric dFe fluxes (Ussher *et al.*, 2013) and the dFe fluxes to the surface mixed layer due to upward vertical mixing calculated during this study; see Table 3.4). Here, downward vertical fluxes are treated as null as residence times are steady state between the sum of input and output fluxes and therefore, if there is net downwelling, this becomes part of the output and need not be considered. The resulting residence times were estimated to be between 0.5 and 6.3 y along the transect (Table 3.5).

A marked difference in mixed layer residence times was observed between the North and South Atlantic gyres, from 1.2 – 1.8 y in the NATL and NATR provinces to 6.3 y in the SATL province. The difference in residence times between the northern and southern gyres is likely caused by the lower atmospheric Fe inputs and more efficient biological uptake and recycling in the SATL. For example, Ussher *et al*. (2013) suggested that the lower proportion of Fe associated with particles and colloids in the SATL, and the efficient biological recycling of soluble Fe, resulted in greater residence times relative to the North Atlantic gyre. This hypothesis is supported by observations of lower particle export in the South Atlantic relative to the North Atlantic (Charette and Moran, 1999).

In contrast, the lowest residence time was found in the WTRA due to high inputs of Fe (associated with lithogenic particles and colloids; Bergquist and Boyle, 2007; Ussher *et al.*, 2013) and a high particulate organic carbon flux (Charette and Moran, 1999). The overall north-south trend in mixed layer dFe residence times for the Atlantic Ocean was in agreement with the estimated 0.5 – 12.9 y by Ussher *et al.* (2013), and was also similar to that observed for ^{230}Th and ^{234}Th residence times in Atlantic surface

seawater which ranged from ~ 0.3 – 2.6 y in the sub-tropical gyres and decreased markedly to 0.4 – 1.6 y in the WTRA (Hsieh *et al.*, 2011).

3.5. Conclusions

This chapter presents dFe and TDFe data from the upper water column of the Atlantic Ocean as part of the *AMT*-19 time series programme. Surface water Fe distributions displayed distinct regional differences between the North and South Atlantic gyres with high Fe concentrations (dFe 1.65 nM) in waters underneath the influence of the Saharan dust belt (~ 4 – 29° N) and low Fe concentrations (dFe 0.14 nM) in the South Atlantic. The basin-scale differences in the Atlantic surface Fe inventory are consistent with the modelled ~ 10 fold difference in dust fluxes between the North and South Atlantic (Jickells *et al.*, 2005; Mahowald *et al.*, 2009).

Towards the northern extent of the dust belt, dFe represented only 48 ± 26 % of the TDFe pool indicating that atmospheric dry deposition of Fe-rich Saharan dust was the principal source of Fe to this region. Here, N_2 fixation rates were elevated (0.3 – 1.1 nmol L^{-1} d^{-1}) but decreased with decreasing dFe concentrations north of 29° N. These data suggest that the large variability in North Atlantic surface Fe concentrations were sufficient to influence N_2 fixation in the different Atlantic geographic provinces. At the southern extent of the dust belt, this study revealed wet deposition in the ITCZ as the principle source of Fe to surface waters. This hypothesis is supported by inverse linear Fe-salinity correlations, rainfall data and surface pH minima. Here, dFe represented 60 % of the surface TDFe pool indicating that the deposition of more soluble Fe in the ITCZ acts as an important source of bioavailable Fe to phytoplankton in this region, likely

influencing the increased surface water primary productivity. As such, the residence time for dFe in the WTRA was short at 0.5 y, consistent with a reported high particulate organic carbon flux (Charette and Moran, 1999).

By utilising AOU to calculate remineralised organic carbon, this study revealed the elevated dFe concentrations in the North Atlantic OMZ would indeed have largely arisen from remineralised organic matter, based on a $Fe:C_{org}$ ratio of 9.5 μmol mol^{-1} within the range reported for oceanic phytoplankton (Sunda, 1997; Ho *et al.*, 2003). Thus, the elevated dFe in the North Atlantic OMZ is fuelled by high atmospheric deposition fluxes. Conversely, this study showed that upward vertical mixing from the OMZ into the surface mixed layer was an important source of dFe providing ~ 6 μmol m^{-2} y^{-1}. If enhanced dFe concentrations in these low oxygen waters are stabilised, as suggested (Fitzsimmons *et al.*, 2013; Ussher *et al.*, 2013), then future deoxygenation of this OMZ (Stramma *et al.*, 2009) may significantly increase the dFe inventory in the tropical and sub-tropical North Atlantic.

The southern extent of the ITCZ effectively acted as a barrier to the atmospheric transport of Saharan dust, thus Fe, to the South Atlantic. The low surface concentrations of the South Atlantic gyre are therefore likely sustained by rapid biological removal, efficient recycling and downwelling. This study estimated a downward mixing TDFe flux of 3.2 μmol m^{-2} y^{-1} across the SATL thermocline that is comparable with the reported mean seasonal atmospheric dFe input of 2.1 – 3.3 μmol m^{-2} y^{-1} (Ussher *et al.*, 2013). The SATL low surface mixed layer dFe inventory may therefore be in steady state with a calculated residence time of 6.3 y consistent with low particulate organic carbon fluxes (Charette and Moran, 1999).

Chapter 4

Biogeochemical cycling of dissolved zinc along the GEOTRACES South Atlantic transect GA10 at 40º S

This chapter is based on a paper of the same name published in Global Biogeochemical Cycles (DOI: 10.1002/2013GB004637) by the following authors: Wyatt, N. J., Milne, A., Woodward, E. M. S., Rees, A. P., Browning, T. J., Bouman, H. A., Worsfold, P. J., Lohan, M. C.

As lead author, my contribution was to provide all the zinc measurements, drive the intellectual thought processes and to write the paper.

Abstract

The biogeochemical cycle of zinc (Zn) in the South Atlantic, at 40° S, was investigated as part of the UK GEOTRACES programme. To date there is little understanding of the supply of Zn, an essential requirement for phytoplankton growth, to this highly productive region. Vertical Zn profiles displayed nutrient-like distributions with distinct gradients associated with the water masses present. Surface Zn concentrations are among the lowest reported for the world's oceans (< 50 pM). Highest Zn concentrations were found in Antarctic Bottom Waters (> 8 nM). A strong Zn-Si linear relationship was observed (Zn (nM) = 0.065 Si (μM), r^2 = 0.97, *n* = 460). Our results suggest that the use of a global Zn-Si relationship would lead to an underestimation of dissolved Zn in deeper waters of the South Atlantic. By utilizing Si* as a tracer for Sub-Antarctic Mode Water (SAMW), our data indicate that the preferential removal of Zn in the Southern Ocean prevented a direct return path for dissolved Zn to the surface waters of the South Atlantic at 40° S, and potentially the thermocline waters of the South Atlantic sub-tropical gyre. The importance of Zn for phytoplankton growth was evaluated using the Zn-soluble reactive phosphorus (SRP) relationship and estimated free Zn^{2+} concentration. We hypothesize that the low Zn concentrations in the South Atlantic may select for phytoplankton cells with a lower Zn requirement. In addition, a much deeper kink at ~ 500m in the Zn:SRP ratio was observed compared to other oceanic regions.

4.1. Introduction

Trace metal micronutrients such as zinc (Zn) play a key role in the productivity of the oceans. Zinc is an essential co-factor in many phytoplankton enzymatic processes

(Anderson *et al.*, 1978; Vallee and Auld, 1990; Morel and Price, 2003), and as such is essential for phytoplankton growth. Zinc is used for the uptake of carbon dioxide (CO_2) via the enzyme carbonic anhydrase (Morel *et al.*, 1994; Tortell *et al.*, 2000; Hu *et al.*, 2003) and for organic phosphorus acquisition via the enzyme alkaline phosphatase (Shaked *et al.*, 2006). In addition, Zn is utilised in both nucleic acid transcription and repair proteins (Montsant *et al.*, 2007). The vertical profile of Zn in the world's oceans resembles those of the major nutrients due to biological uptake and utilization (Bruland, 1980; Ellwood, 2008; Lohan *et al.*, 2002; Croot *et al.*, 2011; Jakuba *et al.*, 2012). The Zn associated with biota and particulates can either be recycled in surface waters, or exported and remineralised at depth. As Zn is essential for phytoplankton growth, it has an impact on the global biological carbon pump. The stoichiometric relationship between Zn and the major nutrients, such as silicate and phosphate, is an important control on the efficiency and size of this pump.

In oceanic surface waters, Zn concentrations are < 0.1 nM, with approximately 98 % of this pool chelated by strong organic ligands (Bruland, 1989; Ellwood and van den Berg, 2000; Lohan *et al.*, 2005b). This reduces the bioavailable free Zn^{2+} to concentrations < 2 pM, which have been shown to limit phytoplankton growth in culture experiments (Anderson *et al.*, 1978; Brand *et al.*, 1983; Sunda and Huntsman, 1992; 1995a; de La Rocha *et al.*, 2000; Saito and Goepfert, 2008). A Zn concentration of 0.8 pM reduced the activity of carbonic anhydrase in phytoplankton, potentially limiting CO_2 uptake and growth (Morel *et al.*, 1994; Tortell *et al.*, 2000). Alkaline phosphatase plays an important role in allowing microorganisms to acquire phosphorus from organic compounds in oligotrophic regimes (Riegman *et al.*, 2000; Dyhrman and Palenik, 2003). The activity of alkaline phosphatase in phytoplankton was also reduced

when grown at 0.4 pM Zn (Shaked *et al.*, 2006). In diatoms, the uptake of silicate has also been shown to be inhibited by low Zn concentrations (Rueter and Morel, 1981; de La Rocha *et al.*, 2000) with possible changes to community structure as a result (Leblanc *et al.*, 2005). Diatoms are responsible for the majority of carbon exported from the surface to the deep ocean (Nelson *et al.*, 1995; Tortell *et al.*, 2000). Therefore a community shift, and/or change in silicification rates, under low Zn conditions may alter the silicate to carbon uptake ratio of the phytoplankton community. This in turn has clear implications for the efficiency of the biological carbon pump.

The low Zn concentrations found in open-ocean surface waters are low enough to limit phytoplankton growth based on results from laboratory culture studies (Sunda and Huntsman, 1992; 1995a; Saito and Goepfert, 2008). However, the relatively few shipboard incubation experiments that have been conducted with natural assemblages showed minimal effects of Zn additions on the bulk phytoplankton community (Coale *et al.*, 2003; Crawford *et al.*, 2003, Leblanc *et al.*, 2005; Lohan *et al.*, 2005b; Jakuba *et al.*, 2012). Consequently, the potential for Zn limitation of phytoplankton growth is still under debate. One possible explanation for the lack of observed Zn limitation during field studies is biochemical substitution. Some phytoplankton have been shown to have a requirement for Zn that can be largely alleviated by either cobalt (Co) or cadmium (Cd) in times of Zn stress (Sunda and Huntsman, 1995a; Yee and Morel, 1996; Lee and Morel, 1995; Saito and Goepfert, 2008). Furthermore, the evidence for Zn limitation in the oceans may be obscured by the more widespread occurrence of Fe limitation.

What is clear is that our understanding of the impact that dissolved Zn might have on open-ocean primary productivity levels has been hindered by the relative paucity of reliable Zn data. As Zn is a ubiquitous contaminant and frequently used on

marine vessels and equipment, accurate data can only be obtained by adopting strict ultra-clean precautions and protocols during both sampling and analytical procedures (Bruland *et al.*, 1979; de Baar *et al.*, 2008). Currently, there are no Zn data for the South Atlantic Ocean, although Croot *et al.* (2011) have reported Zn data from ten profiles along the Zero Meridian between the Antarctic continent and 46° S.

The present study focused on determining the biogeochemical cycle of dissolved Zn along 40° S in the Atlantic Ocean between South Africa and Uruguay. The South Atlantic is characterised by surface waters that are micronutrient deplete compared with the North Atlantic (Bowie *et al.*, 2002a; Ussher *at al*., 2013) and yet they exhibit considerable surface productivity at 40° S. The enhanced productivity along this Section is hypothesised to be derived from the mixing of macronutrient rich waters of the Antarctic Circumpolar Current (ACC) to the south with the phosphate enhanced but nitrate and silicate depleted Sub-Tropical Surface Water (STSW) of the South Atlantic Gyre to the north. However, there is little understanding of the supply of Zn in this region.

4.2. Materials and procedures

4.2.1. Sampling methods

Seawater samples were collected from 26 stations during two UK-GEOTRACES cruises between South Africa and South America (Section GA10, Fig. 4.1). The first cruise (D357) took place from 18th October – 22nd November 2010, on board the R.R.S. *Discovery*, whilst the second cruise (JC068) took place from 24th December 2011 – 27th January 2012 on the R.R.S. *James Cook*. For the D357 cruise,

only samples collected below 1000 m are presented due to the impact of seasonal biological uptake and regeneration processes on Zn concentrations in the upper water column.

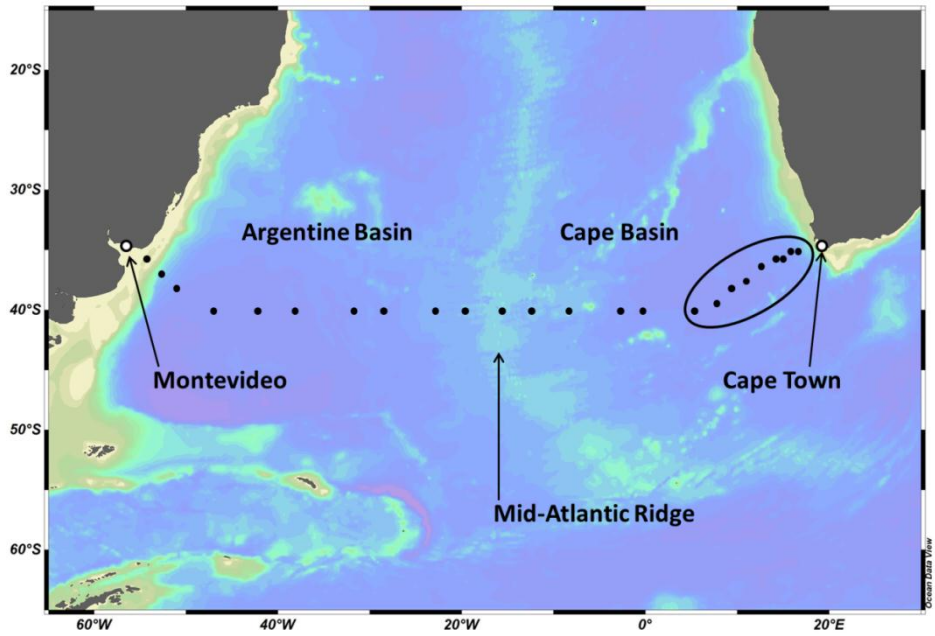

Figure 4.1. The stations sampled for dissolved zinc along Section GA10 during 2 UK GEOTRACES cruises D357 (circled) and JC068. The 3 stations closest to South Africa were reoccupied during JC068. Station metadata can be obtained from http://www.bodc.ac.uk/geotraces/. This figure was made using Ocean Data View (Schlitzer, 2012).

All sampling bottles were cleaned according to the procedures detailed in the GEOTRACES sample handling protocols (Cutter *et al.*, 2010). Seawater samples were collected using a titanium CTD frame fitted with twenty four, 10 L trace metal clean Teflon coated OTE (Ocean Test Equipment) samplers deployed on a plasma rope. Upon recovery, the OTE bottles were transferred into a class 1000 clean air container and lightly pressurized (1.7 bar) with high purity compressed air, which was filtered in-line using a 0.2 µm cellulose acetate filter capsule (Sartobran P-300, Sartorius). Samples for

dissolved Zn were filtered through 0.8/0.2 µm AcroPak Supor polyethersulfone membrane filter capsules (Pall) into 125 mL low density polyethylene bottles. Each sample was acidified to pH 1.7 (0.024 M) by addition of 12 M hydrochloric acid (HCl, UpA, Romil) under a class 100 laminar flow hood. Vertical profile sampling was augmented by high-resolution underway surface samples. Surface seawater was pumped into the trace metal clean laboratory using a Teflon diaphragm pump (Almatec A-15, Germany) connected by acid-washed braided PVC tubing to a towed 'fish' positioned at approximately 2 – 3 m. Underway samples were filtered in-line and acidified as described for samples collected from the titanium sampling system.

4.2.2. Determination of zinc in seawater

Dissolved Zn analysis was carried out in an over-pressurised class 1000 clean air container on-board ship. Dissolved Zn was determined using flow-injection with fluorimetric detection (FI-FL), as first described by Nowicki *et al.* (1994) and modified by Gosnell *et al.* (2012). Briefly, the sample was buffered in-line to pH 5.2 with 0.3 M ammonium acetate before being loaded onto a chelating iminodiacetic acid (IDA, Toyopearl AF-Chelate-650 M) pre-concentration column. The column was rinsed using 0.08 M ammonium acetate to remove the seawater matrix cations before Zn was eluted from the column with 0.08 M HCl (SpA, Romil). The HCl eluent entered the reaction stream where it mixed with a 40 µM p-tosyl-8-aminoquinoline (pTAQ: Aldrich) solution containing 2 M ammonium hydroxide and 0.5 M boric acid. The emission of the fluorescent complex was detected by a Shimadzu RF-10Axl fluorimeter with excitation and emission wavelengths set to 377 nm and 495 nm respectively.

Zinc concentrations were quantified using the method of standard additions to low-Zn (0.08 ± 0.05 nM, n = 10) seawater. Due to the large range of Zn concentrations observed (0.015 - 8.6 nM), it was necessary to use two separate calibration ranges. For samples collected from 0 to 900 m, a calibration range of 0.2 to 1 nM was used, whereas for depths ≥ 1000 m, Zn standards ranged from 1 to 10 nM. All samples and standards were analysed in triplicate.

The accuracy of the method was assessed by the quantification of Zn in surface water (S) and 1000 m water (D2) collected during the SAFe programme (Johnson *et al.*, 2007). The concentration of Zn measured in the SAFe reference samples during this study yielded values (± 1 std. dev.) of 0.060 ± 0.020 nM (n = 7) for S and 7.72 ± 0.09 nM (n = 12) for D2 and were in good agreement with the reported consensus values (S = 0.064 ± 0.019 nM; D2 = 7.54 ± 0.14 nM).

Cadmium is known to also form a fluorescent complex with the reagent pTAQ. The potential interference from this element on the observed Zn signal was therefore investigated using Cd additions to low-Zn seawater. The interference from Cd contributed up to 67 % of the Zn fluorescence signal. This is comparable to the 70 % reported by Nowicki *et al.* (1994) and higher than the 30 % reported by Gosnell *et al.* (2012). As dissolved Cd exists in seawater at approximately one-tenth the concentration of Zn (Bruland *et al.*, 1978; Bruland, 1980), this resulted in a correction factor of ~ 6.7 % being applied.

4.2.3. Nutrients, phytoplankton pigments, temperature and salinity

The dissolved macronutrients silicate, phosphate, nitrate (determined as nitrate + nitrite, but referred to throughout the paper as nitrate) were determined in all samples for which Zn was determined and in samples from the stainless steel rosette. These were determined on-board by Malcolm Woodward (PML) using an AA III segmented-flow AutoAnalyzer (Bran & Luebbe) following colorimetric procedures (Woodward and Rees, 2001). Clean sampling and analysis procedures were adopted according to international GO-SHIP protocols (Hydes *et al.*, 2010). Salinity, temperature and depth were measured using a CTD system (Seabird 911+). Dissolved O_2 was determined by a Seabird SBE 43 O_2 sensor. Salinity was calibrated on-board using discrete samples taken from the OTE bottles using an Autosal 8400B salinometer (Guildline) whilst dissolved O_2 was calibrated using a photometric automated Winkler titration system (Carrit and Carpenter , 1966). Biological data for this study was provided by Dr. Heather Bouman and Tom Browning (University of Oxford, UK). For chlorophyll-*a* analysis, samples were filtered (0.7 µm Whatman GF/F) and then the filters were extracted in 90 % acetone overnight (Holm-Hansen *et al.*, 1965). The chlorophyll-*a* extract was measured on a pre-calibrated (spinach chlorophyll-*a* standard, Sigma) Turner Designs Trilogy fluorimeter. Phytoplankton pigment samples (0.5 – 2 L) were filtered (0.7 µm Whatman GF/F), flash frozen in liquid nitrogen and stored at - 80°C prior to analysis using a Thermo HPLC system. The matrix factorization program CHEMTAX was used to interpret the contribution of taxonomic groups to total chlorophyll-*a* (Mackey *et al.*, 1996).

4.3. Results

4.3.1. Hydrographic setting and macronutrient distributions

The thermohaline structure of the South Atlantic water column at 40° S is determined largely by water masses that have their origins in the high-latitude regions of the Northern and Southern Hemispheres (Fig. 4.2A, B). It is at this latitude that the cold and fresh Sub-Antarctic Surface Water (SASW) meets the relatively warm and salty STSW of the South Atlantic gyre. Along the transect, SASW with potential temperature (Θ) < 15 °C and salinity < 35, occupies large areas within the Cape Basin whereas STSW with Θ > 15 °C and salinity > 35 is more prominent within the Argentine Basin (Fig. 4.2A, B). The SASW has higher macronutrient concentrations (nitrate > 2.5 µM and silicate > 1.2 µM) compared with those found within the STSW (< 0.1 µM nitrate and < 1 µM silicate) (Fig. 4.2C, D, E).

Between South Africa and 10° E, the leakage of warm (Θ 15 - 23 °C) and salty (S > 35) waters from the Agulhas Current (AC) was clearly visible at depths to 200 m (Fig. 4.2A, B). Nitrate and phosphate concentrations within the AC were extremely low (0.02 µM and 0.1 µM respectively) (Fig. 4.2C, D). The Brazil Current (BC) was also clearly distinguishable by the intrusion of warm (Θ 15 - 25 °C) and salty (S 35 - 37) water to depths of 200 m (Fig. 4.2A, B). The macronutrient concentrations in the BC were similar to those found within the STSW. Inshore from the BC at 54° W, salinity decreased to 28.5 due to freshwater discharge from the Rio de la Plata estuary. High silicate and nitrate concentrations (22.2 µM and 13.9 µM respectively) were observed within the vicinity of the low salinity signal.

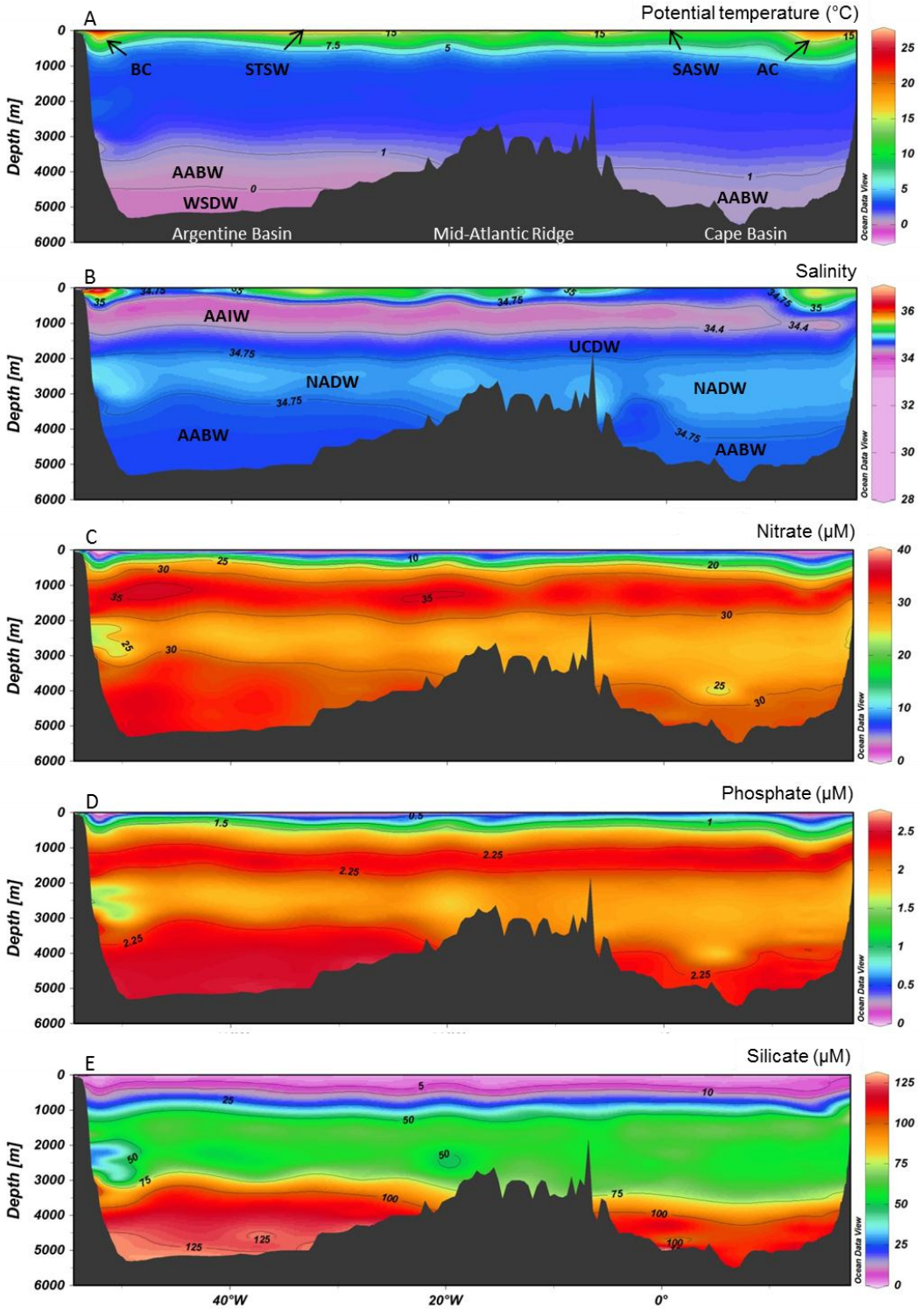

Figure 4.2. Distributions of (A) potential temperature, (B) salinity, (C) nitrate, (D) phosphate and (E) silicate used to indicate the major water masses at 40° S. Abbreviations in alphabetical order: AABW: Antarctic Bottom Water; AAIW: Antarctic Intermediate Water; AC: Agulhas Current; BC: Brazil Current; NADW: North Atlantic Deep Water; SASW: Sub-Antarctic Surface Water; STSW: Sub-Tropical Surface Water; UCDW: Upper Circumpolar Deep Water; WSDW: Weddell Sea Deep Water. This figure was made using Ocean Data View (Schlitzer, 2012).

The two primary intermediate water masses are Antarctic Intermediate Water (AAIW) and Upper Circumpolar Deep Water (UCDW) (Fig. 4.2A). AAIW is thought to be formed by upwelling of circumpolar deep water in either the southeast Pacific Ocean (McCartney, 1977; Talley, 1996) or in the winter waters of the Bellingshausen Sea (Santoso and England, 2004; Naveira Garabato *et al.*, 2009) and was identified along the transect by its salinity minimum ($S < 34.4$) between 500 and 1250 m. Below this, the UCDW, the upper branch of circumpolar deep water that arises from the mixing of upwelled water circulating in the ACC, was located at depths between 1250 and 1750 m. Nitrate and phosphate concentrations within these intermediate waters increased with depth to ~32 µM and ~2.25 µM respectively at 1750 m (Fig. 4.2C, D). It is these intermediate waters, along with the thermocline waters, that constitute the main return branch of the South Atlantic thermohaline overturning circulation (Donners and Drijfhourt, 2004; McDonagh and King, 2005).

The abyssal layer at this latitude was filled by cold, nutrient-rich bottom waters formed around Antarctica, often referred to collectively as Antarctic Bottom Water (AABW) (Fig. 4.2A - E). AABW macronutrient concentrations were the highest observed with nitrate, phosphate and silicate concentrations of ~36 µM, ~2.6 µM and ~129 µM respectively. Located between the AABW and the intermediate waters of the UCDW was the southward flowing NADW, identified by its deep salinity maximum ($S > 34.75$) and reduced macronutrient concentrations (Fig. 4.2A - E).

4.3.2. Distribution of dissolved zinc in the South Atlantic

The vertical profiles of dissolved Zn showed typical nutrient-like distributions for all stations with low Zn concentrations (0.015 - 0.90 nM) in the upper 500 m increasing to values around 8 nM in AABW (Fig. 4.3). Concentrations of Zn in NADW ranged from 4-5 nM. A slight reduction in Zn was observed within the core of the NADW compared with the Zn-enriched Southern Ocean waters that encompass it. This reduction varied between 0.1 and 0.5 nM along the Section with the exception of two stations in the west Argentine Basin where Zn concentrations decreased by 1.3 nM.

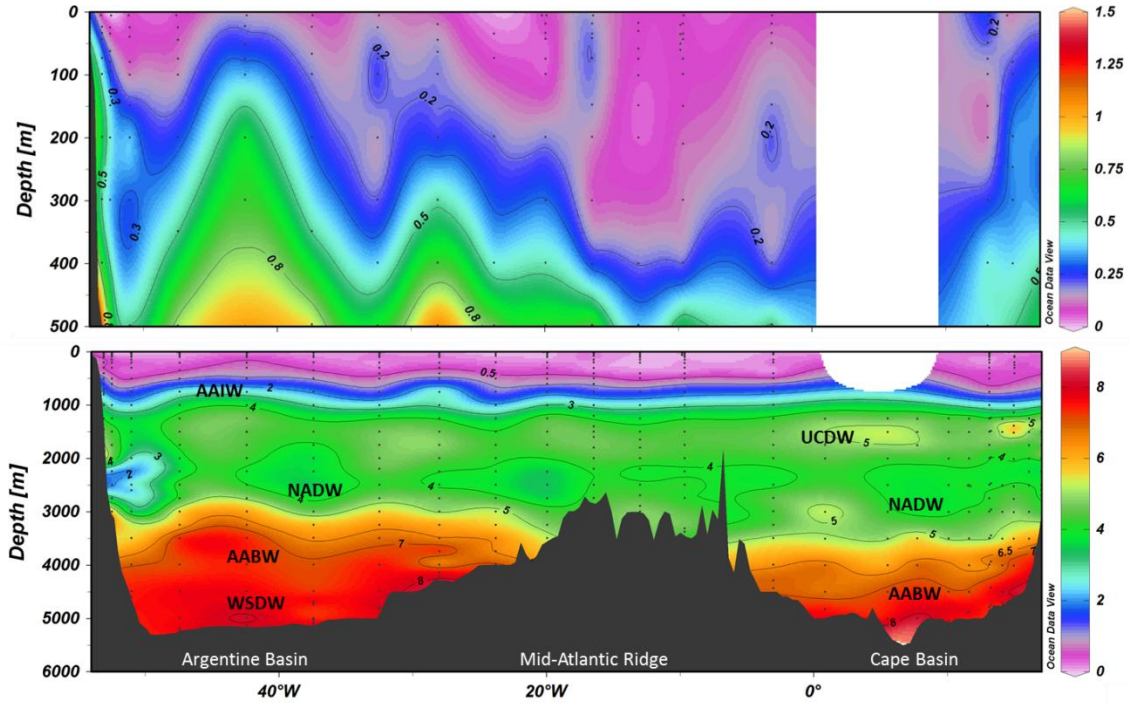

Figure 4.3. Concentrations of dissolved zinc in the upper 500 m (upper plot) and full depth (lower plot). Water mass abbreviations are outlined in Figure 4.2. This figure was made using Ocean Data View (Schlitzer, 2012).

The surface waters were sampled in late December and January and therefore represent austral summer conditions. The concentrations of Zn in the upper surface layer (10 – 25 m) averaged 0.13 ± 0.09 nM except for stations closest the South African

and South American continents where Zn concentrations of 0.40 nM and 1.15 nM respectively were observed. A sub-surface Zn minimum (0.090 ± 0.07 nM, $n = 15$) was observed at most stations at depths between 25 and 100 m. The Zn minimum was generally located within the vicinity of the chlorophyll-*a* maximum, but no relationship ($p > 0.05$) was observed between Zn and chlorophyll-*a* concentration in the Cape Basin. However, for the Argentine Basin, a significant negative correlation between Zn and chlorophyll-*a* concentration was observed ($r^2 = 0.91$, $p < 0.01$, $n = 11$).

Zinc concentrations obtained from the underway sampling system (2 - 5 m) were within the range of the averaged upper 25 m samples from the CTD. The highest Zn concentrations were found on the Uruguayan Shelf (0.70 - 1.25 nM) and coincided with elevated silicate concentrations and a decrease in salinity from 32.6 to 29.4, indicating that this region is influenced by freshwater inputs from the Rio de la Plata.

Within the Cape Basin, the stations closest the South African continent displayed the highest upper surface layer Zn concentrations, averaging 0.39 ± 0.01 nM, whilst surface concentrations for the open-ocean Cape Basin averaged 0.05 ± 0.04 nM. Below the upper surface layer, Zn concentrations at all stations increased to ~ 0.50 nM at 500 m, before increasing through the salinity minimum of AAIW to reach values of ~ 3 nM at 1000 m. Below the AAIW, Zn was elevated to ~ 4 nM within the UCDW and remained fairly constant (4 – 5 nM) throughout the underlying NADW. Below the NADW, the northward flowing, cold and nutrient rich AABW was channelled between the South African continental slope and the mid-Atlantic ridge, elevating the Zn concentrations to > 7 nM at all stations.

Within the Argentine Basin, the stations closest to the South American continent displayed the highest upper surface layer Zn concentrations for the entire transect (1.25

nM). Zinc concentrations for the open-ocean Argentine Basin averaged 0.15 ± 0.10 nM. The Argentine Basin sub-surface minimum of 0.11 ± 0.07 nM was more than double that of the Cape Basin. Unlike the Cape Basin, the Zn concentrations in the Argentine Basin did not increase uniformly to 0.5 nM at 500 m but instead were quite variable in their distribution, reaching concentrations between 0.6 and 0.9 nM (Fig. 4.3). Like the upper water column, the Zn distribution in the intermediate and deep waters of the Argentine Basin was not as longitudinally uniform as those in the east (Fig. 4.3). The Zn concentrations in the NADW and AABW were similar to those found in the Cape Basin. The introduction of Weddell Sea Deep Water (WSDW; Θ < 0° C, Fig. 4.2A), a form of AABW that originates from large-scale mixing in the Weddell Basin (Orsi *et al.*, 1999; Naveira Garabato *et al.*, 2002; Huhn *et al.*, 2008), to the Argentine Basin below 4500 m and the subsequent upwelling of NADW as AABW travelled north over the Southern Ocean ridge systems resulted in higher Zn concentrations at 3000 m relative to the Cape Basin (Fig. 4.3). At two stations above the South American continental slope, Zn concentrations as low as 1.7 nM were observed between 1750 and 3000 m (Fig. 4.3), which coincided with reduced potential temperature, salinity and macronutrient values (Fig. 4.2A - E), indicating the mixing of different water masses.

4.3.3. The zinc-silicate relationship in the South Atlantic

As widely reported for the ocean environment (Bruland and Franks, 1983; Martin *et al.*, 1989; Lohan *et al.*, 2002; Ellwood, 2008; Croot *et al.*, 2011), the full water column dissolved Zn profile is similar to that of dissolved silicate (Fig. 4.2E and 4.3). However, unlike Zn, which decreased to near-zero concentrations at the surface,

silicate concentrations at the majority of stations were homogenous within the top ~50 m, suggesting that Zn may become limiting to phytoplankton growth before silicate.

Using the complete data set, a significant Zn versus Si correlation, Zn (nM) = 0.065 Si (µM) + 0.209 (r^2 = 0.97, *n* = 460) was observed (Fig. 4.4). The highest Zn:Si ratios were observed in the intermediate waters (66 µmol mol^{-1}) that originate in the silicate-deplete regions of the Southern Ocean, whilst the lowest ratios were observed in the upper 500 m (25 µmol mol^{-1}), where Zn concentrations were extremely low, and in AABW (20 µmol mol^{-1}), where silicate concentrations were relatively high.

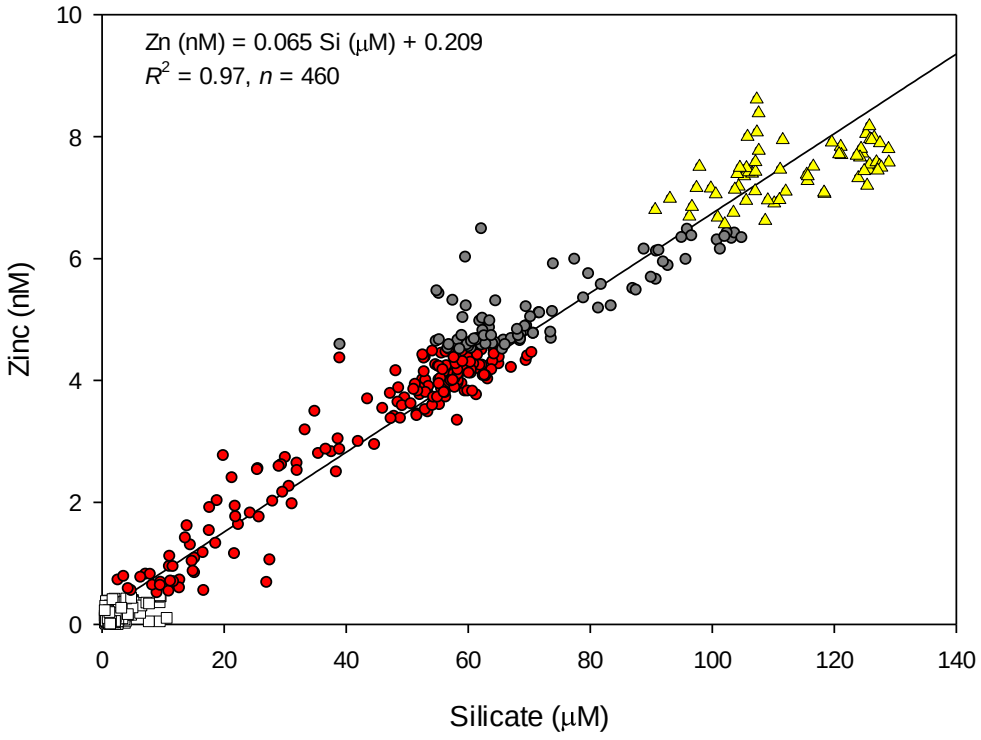

Figure 4.4. Concentrations of dissolved zinc versus dissolved silicate for the complete dataset. The Zn:Si ratio varies according to the water mass analysed: upper 500 m (squares: 0.025x + 0.111); the intermediate waters of AAIW and UCDW (red circles: 0.066x + 0.283); NADW (grey circles: 0.034x + 2.71); AABW (triangles: 0.020x + 5.129).

4.3.4. The zinc-soluble reactive phosphorus relationship in the South Atlantic

Similar to that observed for silicate, a relationship between dissolved Zn and SRP was observed for the complete data set (Fig. 4.5A), consistent with biological uptake and vertical export of Zn. The slope of the Zn to SRP ratio reflects the aggregate stoichiometry of biological processes (Saito *et al.*, 2010).

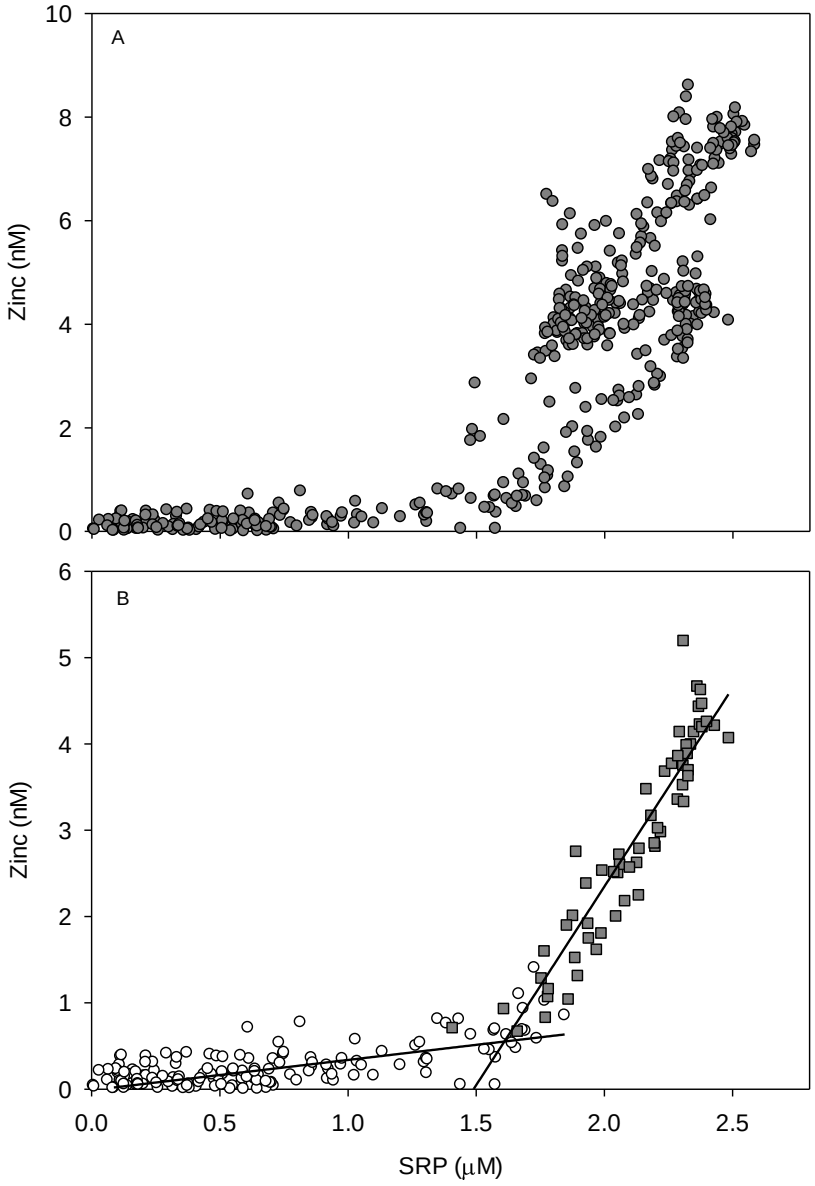

Figure 4.5. Concentrations of dissolved zinc versus soluble reactive phosphorus (SRP) for (A) the complete Section and (B) the upper 500 m (open circles) and between 500 and 1250 m (AAIW, filled squares).

As shown in Figure 4.5B, the Zn versus SRP relationship has a 'kink' at 500 m, (< 1.5 µM PO_4^{3-}) resulting in a Zn:SRP ratio of 349 µmol mol^{-1}. Whilst in the AAIW (500 - 1250 m) a Zn:SRP ratio of 4604 µmol mol^{-1} was observed.

4.4. Discussion

4.4.1. Zinc in South Atlantic surface waters

The concentrations of Zn in the upper 25 m of the open South Atlantic Ocean (0.13 ± 0.09 nM) are much lower than the 0.5 – 0.7 nM reported for both the open North East Atlantic and Atlantic sector of the Southern Ocean (Nolting *et al.*, 2000; Croot *et al.*, 2011), and are more typical of the concentrations reported for the North East Pacific (Lohan *et al.*, 2002; Jakuba *et al.*, 2012), the Pacific sector of the Southern Ocean (Coale *et al.*, 2005) and the Indian Ocean (Gosnell *et al.*, 2012). Zinc concentrations observed within the upper 25 m of the central Cape Basin are some of the lowest values reported for the world's oceans. Such low concentrations may be explained by a combination of the origins of the surface waters present at 40° S and the biological removal of Zn. As the SASW waters travel north into the South Atlantic, the concentrations of both Zn and silicate decrease due to the constant export of biogenic particles, including diatom frustules (Löscher, 1999). The incorporation of Zn and silicate into diatom opal (Ellwood and Hunter, 2000a; Anderson *et al.*, 2011) results in a deeper regeneration cycle than those of nitrate and phosphate (Bruland and Franks, 1983; Collier and Edmond, 1984). In the central Cape Basin, chlorophyll-*a* was > 0.5 mg m^{-3} in the upper 25 m. The sub-surface Zn minimum for the Cape Basin coincided with the chlorophyll-*a* maximum, indicating that uptake by phytoplankton, and export

from surface waters, is an important mechanism for Zn removal from the mixed layer. This observation is consistent with the findings of Löscher (1999) and Croot *et al.* (2011) who also reported low sub-surface Zn concentrations in the vicinity of elevated chlorophyll concentrations for the Southern Ocean.

In contrast to the Cape Basin, chlorophyll-*a* concentrations in the upper 25 m of the Argentine Basin were lower (~ 0.2 mg m^{-3}) whilst Zn concentrations were slightly higher, hence phytoplankton growth and productivity may have been primarily limited by the low macronutrient concentrations of the STSW. Another possible explanation for the slightly elevated Zn in the surface waters of the Argentine Basin is the deposition of atmospheric dust transported from the Patagonian Desert. Atmospheric sources are hypothesised to provide a minimal supply of soluble Zn to these waters (R. Chance, 2012, personal comm.). A second possible source of Zn is through the upwelling of Zn-rich waters from below. The upwelling of AAIW into the upper 500 m due to the introduction of WSDW in the deep Argentine Basin resulted in elevated Zn concentrations of 0.1 - 0.3 nM at 50 to 100 m (Fig. 4.3), which could potentially penetrate into the upper 25 m.

Coastal waters were enriched with Zn within the upper 25 m compared with the open-ocean. The South African coastal stations had upper surface Zn concentrations similar to those reported for surface waters of the AC in the Indian Ocean, off South Africa (Gosnell *et al.*, 2012). Reduced macronutrient and chlorophyll-*a* concentrations in the AC prevented the depletion of Zn in these waters. Higher Zn concentrations were observed on the Uruguayan Shelf and coincided with a decrease in salinity and an increase in temperature and macronutrient concentrations, most notably silicate. These

elevated Zn and silicate concentrations result from the discharge of freshwater from the Rio de la Plata estuary.

4.4.2. Zinc in South Atlantic deep waters

The distribution of Zn in the deep waters (> 1750 m) at 40˚ S is primarily influenced by the inflow of NADW and AABW. The intrusion of NADW is clearly identified by lower Zn (Fig. 4.3) and nitrate (Fig. 4.2C) concentrations as it moves southwards between 1750 - 3500 m depth in the Cape Basin and 1750 – 3000 m depth in the Argentine Basin. The Zn concentrations observed in the NADW are consistent with the values of 4.2 – 4.5 nM reported for the NADW by Croot *et al.* (2011), for a Southern Ocean station north of the Antarctic Polar Front at 50˚ S, 0˚ W.

High Zn concentrations averaging 7.2 nM were observed in the AABW of the Cape Basin below 3000 m (Fig. 4.3). Our data are higher than the values reported by Croot *et al.* (2011), who did not observe Zn concentrations above 6.2 nM, and compare more closely with the values of 7 – 8 nM, reported by Löscher (1999) for lower circumpolar deep water. Local enrichments in Zn concentration between 8 - 8.6 nM were observed within the deep Cape Basin at depths just above the sea floor, which coincided with elevated silicate concentrations of 107 µM. This suggests that the re-suspension of opal-rich sediments may be an important source of Zn and silicate to the water column in this region.

Within the Argentine Basin the introduction of WSDW (Fig. 4.2A) forces AABW to upwell and subsequently Zn concentrations were higher at 3000 m depth in the Argentine Basin compared with the Cape Basin (Fig. 4.3). Croot *et al.* (2011)

observed no elevation in deep water Zn concentration associated with the Bouvet Ridge system to the south of our transect which may have been a possible source of Zn to the deep waters of the Cape Basin at 40˚ S as it travelled north with AABW. Furthermore, we observed no Zn inputs from the mid-Atlantic Ridge, suggesting that hydrothermal activity is not a significant source of dissolved Zn to the South Atlantic Ocean and Atlantic sector of the Southern Ocean, as reported for Fe (Klunder *et al.*, 2011) and Mn (Middag *et al.*, 2011).

4.4.3. The zinc-silicate relationship in the South Atlantic

The overall Zn:Si ratio of 65 µmol mol^{-1} observed during this study (Fig. 4.4) is similar to the 77 µmol mol^{-1} reported for the Southern Ocean (Ellwood, 2008) and the 59 µmol mol^{-1} reported for both the Drake Passage (Martin *et al.*, 1990a) and Indian Ocean (Gosnell *et al.*, 2012). The ratio observed in the upper water column (25 µmol mol^{-1}) is similar to that reported for the highly-productive surface waters of the Ross Sea (17 µmol mol^{-1}) by Fitzwater *et al.* (2000). Culture studies have shown that the majority of Zn in diatoms is incorporated into organic material (> 97%), yet the Zn:Si ratio in the opal of diatom frustules is positively correlated with the availability of free Zn^{2+} in the growth media (Ellwood and Hunter, 2000a). The physiological mechanisms that determine why Zn and silicate should be correlated in the oceans are unclear. Initial studies have shown that silicate uptake by diatoms is inhibited by a Zn deficiency (Rueter and Morel, 1981; de La Rocha *et al.*, 2000). Recent studies have shown that Zn facilitates the uptake of silicate at low silicate concentrations by its presence in the active centre of silicon containing trans-membrane proteins (Grachev *et al.*, 2005, 2008). Danilovtseva *et al.* (2009) suggest that it may be polyamine-Zn complexes located

within the active centres of these transport proteins that aid the assimilation of silicate from seawater by silicifying organisms.

The observed trends in Zn:Si ratios from seawater have been used to estimate the changes in trace metal availability in surface waters (Ellwood and Hunter, 2000b; Hendry and Rickaby, 2008; Andersen *et al.*, 2011). Benthic foraminifera Zn:Ca ratios have been shown to reflect bottom water Zn concentrations and can therefore be used as a sensitive paleo-tracer for the glacial-interglacial interactions between NADW and the Southern Ocean derived deep waters (Marchitto *et al.*, 2000, 2002). However, owing to a lack of deep water Zn data, the validation of this hypothesis is dependent on the estimation of bottom water Zn concentrations using a global deep water (> 1000 m) Zn-silicate relationship (Zn = 0.052[Si] + 0.79) and measured silicate concentrations (Marchitto *et al.*, 2000). Our new, large data set suggests that this approach may result in an underestimation of Zn concentrations in the bottom waters of the South Atlantic and subsequently an underestimation of the Zn concentrations in past oceans. By applying our AABW relationship of Zn = 0.02[Si] + 5.13 to the measured silicate values, we estimate a mean AABW Zn concentration of 7.40 ± 0.21 nM compared with the measured concentration of 7.44 ± 0.44 nM. This is higher than the 6.69 ± 0.56 nM estimated by the global deep water relationship of Marchitto *et al.* (2000). Our data therefore highlights the requirement for more concomitant deep water Zn and silicate data to accurately determine the relationship between present and past ocean Zn biogeochemistry.

4.4.4. The biological control on zinc distribution in the South Atlantic

Correlations between Zn and SRP have been reported as evidence for biological uptake and remineralisation (Sunda and Huntsman, 1995a). Studies in the North Pacific, the Southern Ocean and the Ross Sea have shown that the Zn:SRP ratio exhibits a distinct kink in its profile between 20 and 150 m (1.2 – 1.5 µM PO_4^{3-}) (Sunda and Huntsman, 1995a; Saito *et al.*, 2010; Jakuba *et al.*, 2012). The Zn:SRP ratio in this study also showed a kink at ~1.5 µM SRP but at a much greater depth of ~ 500 m (Fig. 4.5B). The relationships found above and below the kink were similar to values from the sub-Arctic North Pacific, with a Zn:SRP ratio of 349 µmol mol^{-1} in waters above 500 m and 4604 µmol mol^{-1} in the AAIW that sits immediately below.

An explanation for the apparent kinks in these linear relationships is still under debate due to our limited knowledge of Zn biogeochemistry, which is hindered by a paucity of Zn data. The mechanisms proposed for this kink include: (1) the excess uptake of Zn by phytoplankton at the base of the euphotic zone followed by export and remineralisation of high Zn:SRP particulate material in deeper waters (Saito *et al.*, 2010). The presence of Zn-binding ligands in excess of the Zn concentration may also contribute to this effect as the free Zn^{2+} concentration will decrease concurrently, and (2) the influence of Fe limitation, which decreases P uptake whilst maintaining metal uptake rates, resulting in increased cellular metal:P ratios through a process termed 'growth-rate dilution' (Sunda and Huntsman, 2000; Cullen *et al.*, 2003; Cullen, 2006). Both mechanisms would result in elevated Zn:SRP ratios in phytoplankton that should consequently deplete Zn relative to SRP in the upper water column, followed by export and remineralisation below the euphotic zone.

According to the Redfield theory (Redfield *et al*., 1963), if phytoplankton are primarily responsible for the relative changes in Zn:SRP ratios then these values presumably reflect the Zn:SRP ratio in phytoplankton responsible for the removal of these elements. The Zn:SRP ratios observed in the South Atlantic can therefore be compared with the trace metal requirements of phytoplankton grown in cultures under growth-rate-limiting conditions (Sunda and Huntsman, 1992; 1995a) and subsequently used to interpret the biological impact that Zn concentrations have in this region. Based on analyses of pigment markers, the dominant phytoplankton species within the open South Atlantic Ocean during this study were estimated to be haptophytes (approx. 51 % of total chlorophyll-*a)*. In contrast, diatoms made up approximately 11 % of total chlorophyll-*a* in the open-ocean (approx. 13 – 23 % of total chlorophyll-*a*). Our upper 500 m Zn:SRP ratio of 349 µmol mol^{-1} was in excess of the minimum Zn concentration required for optimal growth by the small open-ocean diatom *Thalassiosira oceanica* (~ 110 µmol mol^{-1}) but not the haptophyte *Emiliania huxleyi* (~ 1100 µmol mol^{-1}).

Using the variations in Zn:SRP, we estimated free Zn^{2+} concentrations (Sunda and Huntsman, 1992; 1995a) of 0.6 – 80 pM, which are similar to the sub-Arctic North Pacific (Jakuba *et al.*, 2012) but lower than the Zn-ligand saturated, high Zn surface waters of the Southern Ocean (Zn^{2+} >100 pM) (Croot *et al.*, 2011). At free Zn^{2+} concentrations of 1 pM, the growth rate of the haptophytes *E. huxleyi* and *Phaeocystis antarctica* as well as the coastal diatoms *T. pseudonana* and *T. weissflogii* were limited in culture studies (Sunda and Huntsman, 1992; 1995a; de La Rocha *et al.*, 2000; Saito and Goepfert, 2008). These results suggest that the extremely low Zn concentrations in the South Atlantic Ocean may influence phytoplankton species composition by selecting for phytoplankton cells which have a lower cellular requirement for Zn. This is

in contrast to the observed phytoplankton distribution, where the highest haptophyte abundance corresponded with the lowest Zn concentrations. The haptophytes *E. huxleyi* and *P. antarctica*, as well as several diatoms, have been shown to substitute Co for Zn and vice versa in growth-limiting culture experiments (Sunda and Huntsman, 1995a; Saito and Goepfert, 2008). There is also evidence for this substitution in oceanic environments (Jakuba *et al.*, 2008) and may be occurring in this region.

During our study, a weak but significant relationship ($r^2 = 0.21$, $p < 0.05$, $n = 21$) was observed between the open-ocean Zn concentration and the marker pigment for diatom distribution (total chlorophyll-*a* normalized fucoxanthin). This may be in part due to the low cellular Zn requirement of open-ocean diatom species such as *T. oceanica* (Sunda and Huntsman, 1992; 1995a), which is a likely evolutionary adaptation to more oligotrophic and Zn-deplete waters. Only at the lowest Zn concentrations (~ 15 pM) observed for the South Atlantic would the estimated free Zn^{2+} concentration (~ 0.6 pM) be potentially growth limiting to *T. oceanica*.

4.4.5. The Southern Ocean control on zinc distribution in the upper 500 m

An intriguing result of this study is the extremely low Zn and silicate concentrations within the upper 500 m (Fig. 4.2E and 4.3). This is in contrast to both nitrate and phosphate (Fig. 4.2C, D) whose concentrations increase significantly below 50 m. One explanation for this may be that unlike nitrate and phosphate, Zn and silicate are not being returned to the upper 500 m at 40˚ S by Southern Ocean mode waters. The Southern Ocean is a critical region for the biological carbon pump, strongly influencing

both integrated global export (Sarmiento *et al.*, 2004; Palter *et al.*, 2010) and the overall efficiency of the pump (Sarmiento and Orr, 1991; Marinov *et al.* 2006, 2008).

Sub-Antarctic Mode Water (SAMW) has been identified as the main conduit returning nutrients from the surface waters of the frontal Southern Ocean to the thermocline waters of the Southern Hemisphere (Toggweiler *et al.*, 1991; Sarmiento *et al.*, 2004; Palter *et al.*, 2010), accounting for about three quarters of biological production north of 30˚ S (Sarmiento *et al.*, 2004). One unusual characteristic of SAMW are low silicate:nitrate ratios, generally attributed to the preferential removal of silicate by diatoms under Fe limitation (Franck *et al.*, 2000; Timmermans *et al.*, 2004). Given the high Zn requirement by diatoms for silicate uptake, and the strong oceanic Zn:Si relationship, it is reasonable to assume that the removal of silicate in the SAMW formation regions would also result in the removal of Zn from these surface waters.

In Figure 4.6, we have utilised the Si* tracer of SAMW (Si* = Si(OH) – NO_3^-), (Sarmiento *et al.*, 2004) to map this water mass at 40° S. Negative Si* values between 100 and 1000 m indicate that this tracer included the upper portion of AAIW, which is formed immediately to the south of SAMW in the Southern Ocean. Similar to Si, Zn concentrations in SAMW are extremely low, suggesting that SAMW was not a significant return path for Zn or silicate from the Southern Ocean. Instead, Zn was returned primarily within AAIW between 500 and 1250 m depth. This argument is strengthened by the kink in the Zn:SRP ratio being observed at 500 m rather than at the shallower depths reported for other oceanographic regions. Below 500 m, our AAIW Zn:SRP ratio of 4604 µmol mol^{-1} is slightly higher than the 3800 µmol mol^{-1} reported for the AAIW formation region of the Southern Ocean (Croot *et al.*, 2011).

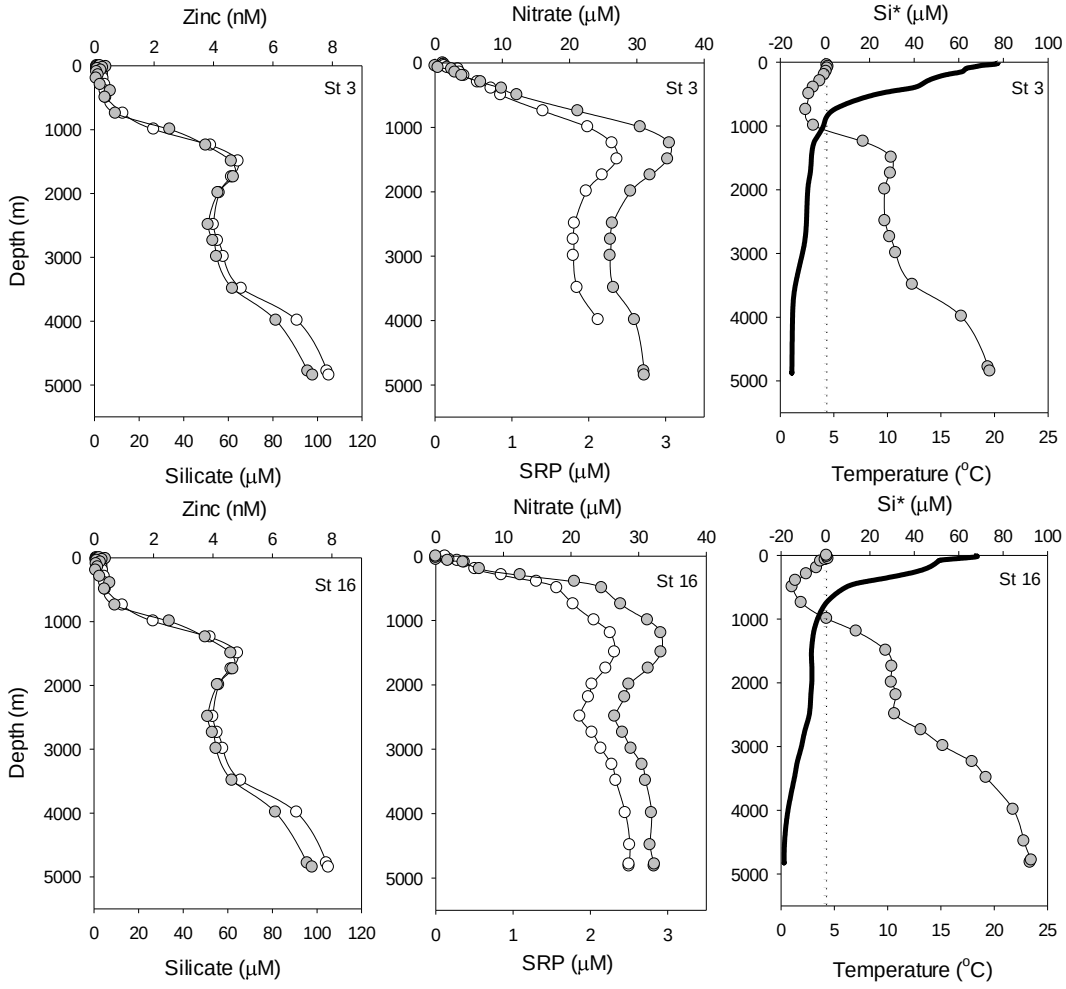

Figure 4.6. Vertical profiles of dissolved zinc (filled circles) and silicate (open circles), nitrate (filled circles) and soluble reactive phosphorus (SRP; open circles), Si* (filled circles) and temperature (black line) from stations 3 (Cape Basin) and 16 (Argentine Basin). SAMW is indicated by Si* < 0 (dashed line).

The difference between these ratios may reflect the export of Zn-rich biogenic particles out of SAMW as this water mass travels north and their subsequent remineralisation in the underlying AAIW, further reducing the potential for SAMW to return Zn efficiently to the upper thermocline waters of the South Atlantic Ocean.

The Si* tracer can also be used to provide further insight into the nutrient status of diatoms in the South Atlantic. Diatoms with adequate light and nutrients (including

Fe) are reported to contain silicate and nitrate in a mole ratio of about 1:1 (Ragueneau *et al.*, 2000), which requires Si* ≥ 0 (Sarmiento *et al.*, 2004). The presence of negative Si* SAMW at the base of the thermocline at non-coastal stations along this transect (Fig. 4.6) is associated with a Si:N ratio of ≤ 0.5, suggesting low diatom production. Using our data at 40º S we hypothesize that the potential for low diatom production in this region, and most likely throughout the open South Atlantic Ocean, may be in-part facilitated by the availability of dissolved Zn, which is maintained at extremely low concentrations by the lack of a significant Southern Ocean return path with SAMW.

4.5. Conclusions

We present dissolved Zn data for 556 discrete samples, the largest Zn data set reported to date. Surface Zn concentrations of 0.015 - 0.39 nM are among the lowest reported for the world's oceans, indicating the absence of a significant source of Zn to these waters and the potential for Zn limitation of phytoplankton growth. Here we suggest using the Si* tracer, that the low surface Zn concentrations are sustained by the lack of a return path from the Southern Ocean that returns high nitrate and phosphate concentrations to the thermocline waters at this latitude. Despite this, phytoplankton groups with cellular Zn requirements in excess of that available in the surface waters were dominant along the transect suggesting the potential co-substitution of Zn for alternative trace metals. The kink in the Zn-SRP relationship at ~ 500 m indicates that Zn is returned at this depth primarily by AAIW and that the kink is a result of the relative differences in biological utilization between water masses. A strong relationship between Zn and silicate, Zn (nM) = 0.065 Si (µM) + 0.209 (r^2 = 0.97, *n* = 460), was observed. Separate linear relationships observed between Zn and silicate for NADW

and AABW highlight the need for more deep Zn concentration data for estimating deep water Zn concentrations in paleo-oceanography.

Acknowledgments

The authors gratefully acknowledge the captains and crew of the RSS *Discovery* and *James Cook* for their excellent shipboard support. Our thanks to Bronwyn Wake, Rosie Chance, Christian Schlosser, Jessy Klar and Maxi Castrillejo for their help with trace metal sampling. This study was supported by a National Environmental Research Council (NERC) grant (NE/H004475/1) to M.C.L & E.M.S.W, and a NERC Studentship to N.J.W. (NE/G52388X/1).

Chapter 5

A seasonal study of cobalt and zinc biogeochemical cycling in the South Atlantic Ocean along the GEOTRACES Section GA10

5.1. Introduction

The trace metal micronutrient Co plays an important role in the productivity of ocean ecosystems. The role of Co in most phytoplankton is to serve as a metal centre in CA, which catalyses inorganic carbon acquisition (Morel *et al.*, 1994; Lane and Morel, 2000; Saito *et al.*, 2002) (Table 1.1 and Fig. 1.2). In addition, Co is a also required for the *de novo* biosynthesis of vitamin B_{12} by marine prokaryotes (Martens *et al.*, 2002; Bertrand *et al.*, 2007; Panzeca *et al.*, 2008), which is an essential requirement for up to 70 % of phytoplankton species (Swift, 1981; Croft *et al.*, 2005). Thus, the availability of Co in the oceans may influence the composition of phytoplankton assemblages in the oceans.

The vertical profile of dCo in the oceans generally falls into the hybrid-type category since its oceanic distributions are often controlled by a combination of nutrient-like processes in surface waters and scavenging processes in intermediate and deep waters (Noble *et al.*, 2008; Saito *et al.*, 2010; Bown *et al.*, 2011; Shelley *et al.*, 2012) (see Chapter 1.2.4.). The co-oxidation of Co by Mn-oxidising bacteria is reported to be one important scavenging mechanism for the removal of Co from seawater (Tebo *et al.*, 1984; Moffett and Ho, 1996). It is hypothesized that organic speciation may protect Co from scavenging in the interior ocean (Saito and Moffett, 2001; Saito *et al.*, 2005), particularly in low oxygen waters which may promote stabilisation of the Co(II) redox state (Bown *et al.*, 2012). Conservative Co behaviour has been reported for the Weddell Gyre, hypothesized to reflect a balance between the production and removal of Co-binding ligands in surface waters (Bown *et al.*, 2012). The sources of Co-binding ligands are not well characterised, but are suggested to be released as a by-product of

vitamin B_{12} biosynthesis by cyanobacteria (Saito and Moffett, 2001; Saito *et al.*, 2005; 2010), which are scarce in the Southern Ocean (Bertrand *et al.*, 2007).

In oceanic surface waters, dCo concentrations can be < 10 pM (*e.g.* Martin *et al.*, 1989; Bown *et al.*, 2011; Noble *et al.*, 2012). Moreover, between 60 and 99.9 % of the total dCo pool is organically complexed (Ellwood and van den Berg, 2001; Bown *et al.*, 2012) potentially reducing the bioavailable free Co ion (Co^{2+}) to concentrations < 0.01 pM. Consequently, low surface ocean dCo concentrations have been shown to limit phytoplankton growth in both culture experiments (Sunda and Huntsman, 1995a; Saito *et al.*, 2002; Saito and Goepfert, 2008) and field studies with natural assemblages (Bertrand *et al.*, 2007; Panzeca *et al.*, 2008). At Co^{2+} concentrations of 1 pM, the growth of the coastal diatom *Thalassiosira pseudonana* and the haptophyte *E huxleyi* was limited in culture, whereas for the oceanic diatom *T. oceanica* and the haptophyte *Phaeocystis antarctica* growth limiting Co^{2+} concentrations appear to be much lower at < 0.2 pM (Sunda and Huntsman, 1995a; Saito and Goepfert, 2008). Hence, the distribution and biogeochemistry of Co in the world's oceans is an area of marine trace metal research that is now receiving a great deal of attention.

The water column biogeochemistry of Co has been shown to be linked to that of Zn through similar biochemical functions in phytoplankton (Saito and Moffett, 2002; Jakuba *et al.*, 2008; Saito *et al.*, 2010). Both elements, as well as cadmium (Cd), are capable of biochemical substitution in the active centre of CA enzymes in phytoplankton in order to maintain enzymatic activity (Price and Morel, 1990; Yee and Morel, 1996; Lane and Morel, 2000; Saito *et al.*, 2008) (see Chapter 1.2.2.). Such biochemical substitution appears to be an important adaptation to life in trace metal depleted surface waters of the oceans. Physiological evidence of this Co-Zn substitution

has been demonstrated in the centric marine diatoms *T. weissflogii*, *T. oceanica* and *T. pseudonana* as well as the haptophytes *P. antarctica* and *E. huxleyi* with each having a preference for one element over the other (Price and Morel, 1990; Sunda and Huntsman, 1995a; Saito and Goepfert, 2008; Xu *et al.*, 2008). In stark contrast, the marine picocyanobacteria (*e.g. Prochlorococcus and Synechococcus*) have an absolute cellular Co requirement and appear to be incapable of Co-Zn biochemical substitution (Sunda and Huntsman, 1995a; Saito *et al.*, 2002). The relative proportion of Co to Zn may therefore favour the growth of certain species over others (Sunda and Huntsman, 1995a; Jakuba *et al.*, 2008; Saito and Goepfert, 2008; Saito *et al.*, 2010). This has clear implications for primary productivity, which is largely controlled by diatoms and cyanobacteria, and the efficiency of the oceanic biological carbon pump, which is largely controlled by the dominance of diatoms versus coccolithophores (Nelson *et al.*, 1995; de La Rocha, 2003).

Correlations between Co and soluble reactive phosphate (SRP) have been reported as evidence for biological uptake and remineralisation (*e.g.* Sunda and Huntsman, 1995a; Noble *et al.*, 2008; Saito *et al.*, 2004; 2010). These findings are similar to correlations observed between other trace metals and macronutrients, such as Zn or Cd with SRP or Zn with Si (*e.g.* Lohan *et al.*, 2002; Cullen *et al.*, 2003; Jakuba *et al.*, 2008; Saito *et al.*, 2010; Wyatt *et al.*, 2014). The slopes of these metal-SRP relationships in the upper water column reflect their relative biological utilisation and have proven useful in identifying the nutritional role of trace metals in diverse oceanic regimes including the Gulf of Alaska, the Peru upwelling region, the Northwest and Equatorial Atlantic, the Southern Ocean and the Ross Sea (Sunda and Huntsman, 1995a; Saito and Moffett, 2002; Jakuba *et al.*, 2008; Saito *et al.*, 2004; 2010; Bown *et al.*,

2011). Thus, metal-SRP vector analysis provides an important tool for determining the role of Co and/or Zn distributions for phytoplankton community structure.

The present study examines the temporal and spatial relationship between Co and Zn distributions and the subsequent impact on phytoplankton assemblages along the GEOTRACES Section GA10 in the South Atlantic Ocean. The surface waters of this region exhibit considerable productivity, hypothesised to be derived from the mixing of macronutrient rich Sub-Antarctic Surface Water (SASW) to the south with the macronutrient depleted waters of the Sub-Tropical Surface water (STSW) to the north. However, there is little to no understanding of trace metal cycling in this region. To date, the few published data sets from large-scale studies in the South Atlantic report low dCo concentrations ranging from ~ 6 to 110 pm (Table. 1.5) across diverse regimes such as the South Atlantic sub-tropical gyre, the Southeast Atlantic OMZ and the Atlantic sector of the Southern Ocean (Bowie *et al.*, 2002a; Pohl *et al.*, 2010; Bown *et al.*, 2011; Noble *et al.*, 2012). In contrast, the Zn data set presented here adds to that already reported by Wyatt *et al.* (2014) (see Chapter 4) and represents the only large–scale data set from the South Atlantic Ocean to date.

5.2. Materials and procedures

5.2.1. Sampling methods

Seawater samples were collected from 26 stations during two UK-GEOTRACES cruises between South Africa and South America (Section GA10, Fig. 5.1). The first cruise (D357) took place during austral spring 2010, sampling the Southeast Atlantic from 18th October to 22nd November 2010 on board the R.R.S.

Discovery. For the D357 cruise, two transects were completed between Cape Town, South Africa and the zero meridian that represent early austral spring (D357-1) and late austral spring (D357-2) respectively. The second cruise (JC068) took place during austral summer 2011/2012, sampling from Cape Town along the 40º S parallel to Montevideo, Uruguay between 24th December 2011 and 27th January 2012 on the R.R.S. *James Cook*.

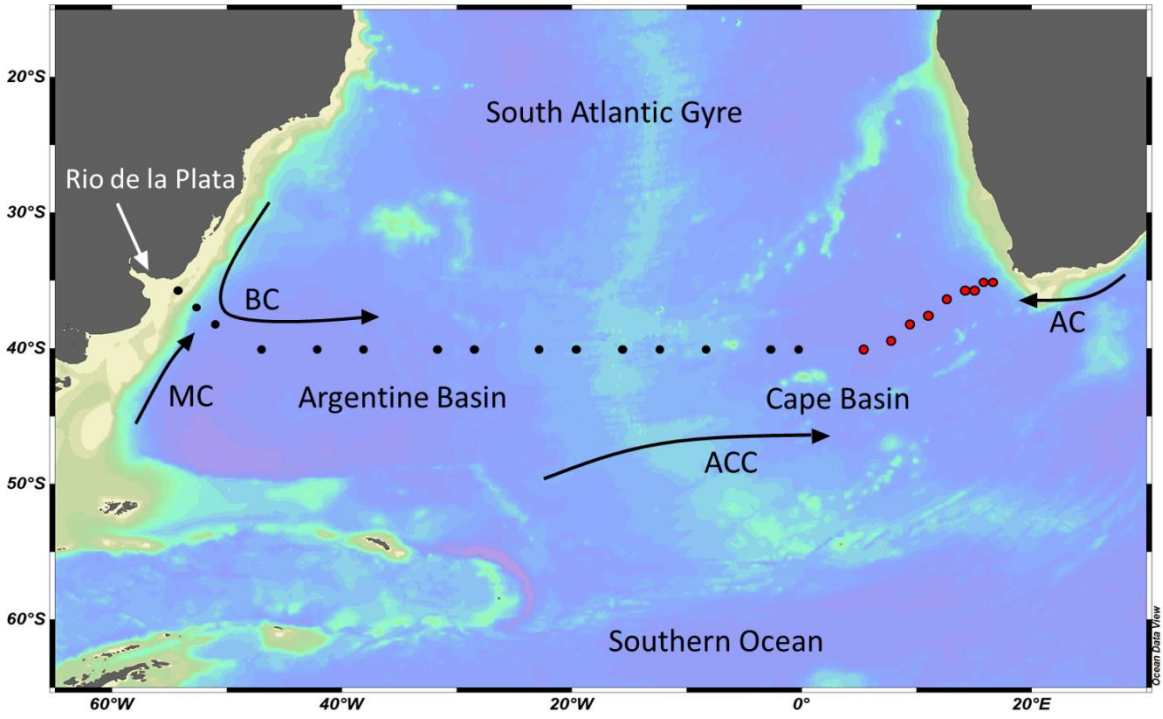

Figure 5.1. The stations sampled for dissolved cobalt and zinc along Section GA10 during 2 UK GEOTRACES cruises D357 (red circles) and JC068. The 3 stations closest to South Africa were reoccupied during JC068. The major South Atlantic currents influencing the hydrography of the Section are shown: AC: Agulhas current; ACC: Antarctic Circumpolar Current; BC: Brazil Current; MC: Malvinas Current. Station metadata can be obtained from http://www.bodc.ac.uk/geotraces/. This figure was made using Ocean Data View (Schlitzer, 2012).

All sampling bottles were cleaned according to the procedures detailed in the GEOTRACES sample handling protocols (Cutter *et al.*, 2010). Seawater samples were collected and treated using procedures described by Wyatt *et al.* (2014) (see Chapter 4).

Briefly, a titanium CTD frame fitted with twenty four trace metal clean Teflon coated OTE (Ocean Test Equipment) samplers were used to collect seawater. Upon recovery, the OTE bottles were transferred into a class 1000 clean air container and lightly pressurized (1.7 bar) with high purity compressed air. Samples for dissolved Co and Zn were filtered through 0.8/0.2 µm AcroPak Supor polyethersulfone membrane filter capsules (Pall) into 125 mL low density polyethylene bottles. Each sample was acidified to pH 1.7 (0.024 M; HCl, UpA, Romil) under a class 100 laminar flow hood.

5.2.2. Determination of cobalt and zinc in seawater

Dissolved Co (dCo) analysis was carried out within a Class 1000 clean room facility (ISO 9001) at the University of Plymouth, UK. Dissolved Co was determined in UV irradiated samples using FI-CL (see Chapter 2.6) as described by Shelley *et al.* (2012). The measurements are based on the catalytic oxidation of pyrogallol by hydrogen peroxide in the presence of Co. The samples were buffered in-line to pH 5.2 – 5.5 with 0.5 M ammonium acetate (SpA, Romil) before being loaded onto a Toyopearl AF-Chelate-650 M pre-concentration column (Fig. 2.8). The column was rinsed using 0.05 M ammonium acetate to remove the seawater matrix cations before Co was eluted from the column with 0.1 M HCl (SpA, Romil). The HCl eluent entered the reaction stream where it mixed with a 50 mM pyrogallol (1,2,3-trihydrobenzene) solution containing 0.025 M cetyltrimethylammonium (CTAB) and 10 % v/v hydrogen peroxide (30 %, Fisher Scientific). Chemiluminescence was detected by a Thorn EMI PMT. Cobalt concentrations were quantified using the method of standard additions (20 – 120 pM) to low-Co seawater (16.5 ± 5.2 nM, n = 15). All samples and standards were analysed in triplicate.

The accuracy of the analytical method was assessed by the quantification of dCo in surface (S) and 1000 m water (D1, D2) collected during the SAFe programme (Johnson *et al.*, 2007) and also 2000 m water (GD) collected as part of the international GEOTRACES programme (see Chapter 2.6.5). The concentrations of dCo (± 1 std. dev.) measured in reference samples during this study (S = 4.1 ± 0.4 pM, *n* = 3; D1 = 44.3 ± 1.0 pM, *n* = 4; D2 = 48.5 ± 0.04 pM, *n* = 2; GD = 73.0 ± 3.5 pM, *n* = 5) were in good agreement with the reported consensus values (S = 4.8 ± 1.2 pM; D1 = 45.4 ± 4.7 pM; D2 = 45.7 ± 2.9 pM; GD = 65.2 ± 1.2 pM, http://www.geotraces.org/science/intercalibration/322-standards-and-reference-materials).

Dissolved Zn (dZn) was determined using FI-FL, modified from the method of Nowicki *et al.* (1994) (see Chapter 2.7.), and described previously for this GEOTRACES Section by Wyatt *et al.* (2014) (see Chapter 4).

5.2.3. Pigment analyses and enumeration of phytoplankton groups

Biological data for this study was provided by Dr. Heather Bouman and Tom Browning (University of Oxford, UK). Phytoplankton pigment samples (0.5 – 2 L) were filtered (0.7 µm Whatman GF/F), flash frozen in liquid nitrogen and stored at - 80°C. Pigments were then extracted into 90 % acetone by sonification prior to analysis using a Thermo HPLC system. Pigments were identified using diagnostic retention times and comparison of individual pigment absorption spectra with a library of known spectra. Chlorophyll-*a* and pigment mixture standards were included in each run to calibrate retention times for the pigments. For the interpretation of metal pigment relationships, all pigments were normalised to total chlorophyll-*a*. The matrix factorization program

CHEMTAX was used to interpret the contribution of taxonomic groups to total chlorophyll-*a* (Mackey *et al.*, 1996). Starting pigment ratios for the different taxonomic groups were obtained from Wright *et al.* (1996) for Southern Ocean-type waters and Veldhuis and Kraay (2004) for gyre type waters present in the South Atlantic. Concentrations of eukaryotic nanophytoplankton, picophytoplankton, *Synechococcus and Prochlorococcus* were enumerated using a FACSort flow cytometer (Becton Dickenson, Oxford, UK) according to the methods described in Davey *et al.* (2008) and Zubkov *et al.* (2003). Initially 2 mL of seawater sample was fixed with 1 % paraformaldehyde and incubated in the dark at room temperature for 10 min before being flash frozen in liquid nitrogen and stored at - 80°C. Samples were analysed 4 to 5 months later by analytical flow cytometry using particle counts and measured chlorophyll fluorescence (> 650 nm), orange fluorescence (585 ± 21 nm), and side scatter. Samples were analysed twice for 3 minutes at a flow rate of ~170 μL min^{-1}. Phytoplankton cells were identified and enumerated using WinMDI Version 2.8 (Joseph Trotter) flow cytometry analysis software.

5.2.4. Nutrients, temperature and salinity

The dissolved macronutrients silicate, SRP, nitrate (determined as nitrate + nitrite) were determined in all samples for which dCo and dZn were determined. Analyses were determined on-board by Malcolm Woodward (PML) as described in Chapter 4. Clean sampling and analysis procedures were adopted according to international GO-SHIP protocols (Hydes *et al.*, 2010). Salinity, temperature and depth were measured using a CTD system (Seabird 911+) as described in Chapter 4.

5.3. Results

5.3.1. Hydrographic setting and biogeochemical features

The water masses along the D357 and JC068 transects were identified by their characteristic thermohaline, oxygen and macronutrient properties (Orsi *et al.*, 1995; Sarmiento *et al.*, 2004; Ansorge *et al.*, 2005; Johnson *et al.*, 2008; Naveira Garabato *et al.*, 2009). Figures 5.2 and 5.3 show these properties during D357-1 (early spring 2010) and D357-2 (late spring 2010) respectively along with the identified water masses. A detailed description of the hydrography during JC068 (summer 2011/12) is provided by Wyatt *et al.* (2014) (see Chapter 4) and the properties used to identify water masses along this transect shown in Figure 4.2.

Surface waters

During the two D357 (spring) transects, the surface waters at stations closest to South Africa were influenced by the Agulhas Current (AC) to depths of ~ 200 m with elevated potential temperature (Θ 15 – 18 ºC) and salinity (S 35 – 36) (Fig's 5.2A, B and 5.3A, B). These AC temperatures are lower than the Θ 15 – 23 ºC observed during JC068 (summer; Fig. 4.2A). Within offshore waters of the open Cape Basin, temperature and salinity decreased to $\Theta < 15^{o}$ C, $S < 35$ during all three transects due to mixing with SASW travelling north from the Antarctic Circumpolar Current (ACC) (Fig's 4.2A, B, 5.2A, B and 5.3A, B). The influence of the AC appears to extend further westward to ~ 9° E during D357-2 compared to ~ 14° E during D357-1 and JC068, likely a result of the rapid and marked intra-seasonal variability in the Agulhas retroflection and leakage regions (de Ruijter *et al.*, 1999; Lutjeharms, 2006).

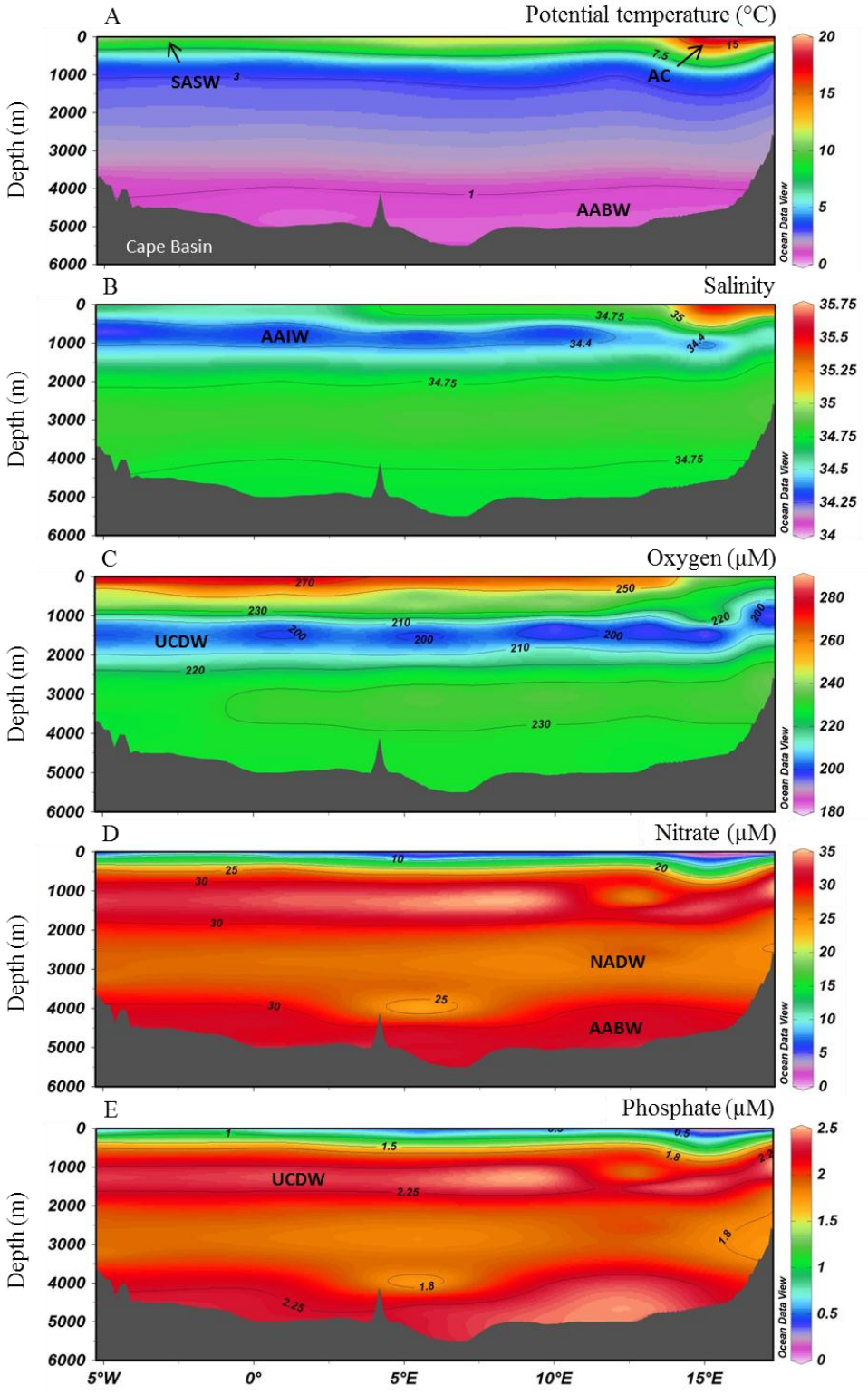

Figure 5.2. Distributions of (A) potential temperature, (B) salinity, (C) oxygen, (D) nitrate and (E) phosphate during D357-1 (early spring) used to indicate the major water masses. Abbreviations in alphabetical order: AABW: Antarctic Bottom Water; AAIW: Antarctic Intermediate Water; AC: Agulhas Current; NADW: North Atlantic Deep Water; SASW: Sub-Antarctic Surface Water; UCDW: Upper Circumpolar Deep Water. This figure was made using Ocean Data View (Schlitzer, 2012).

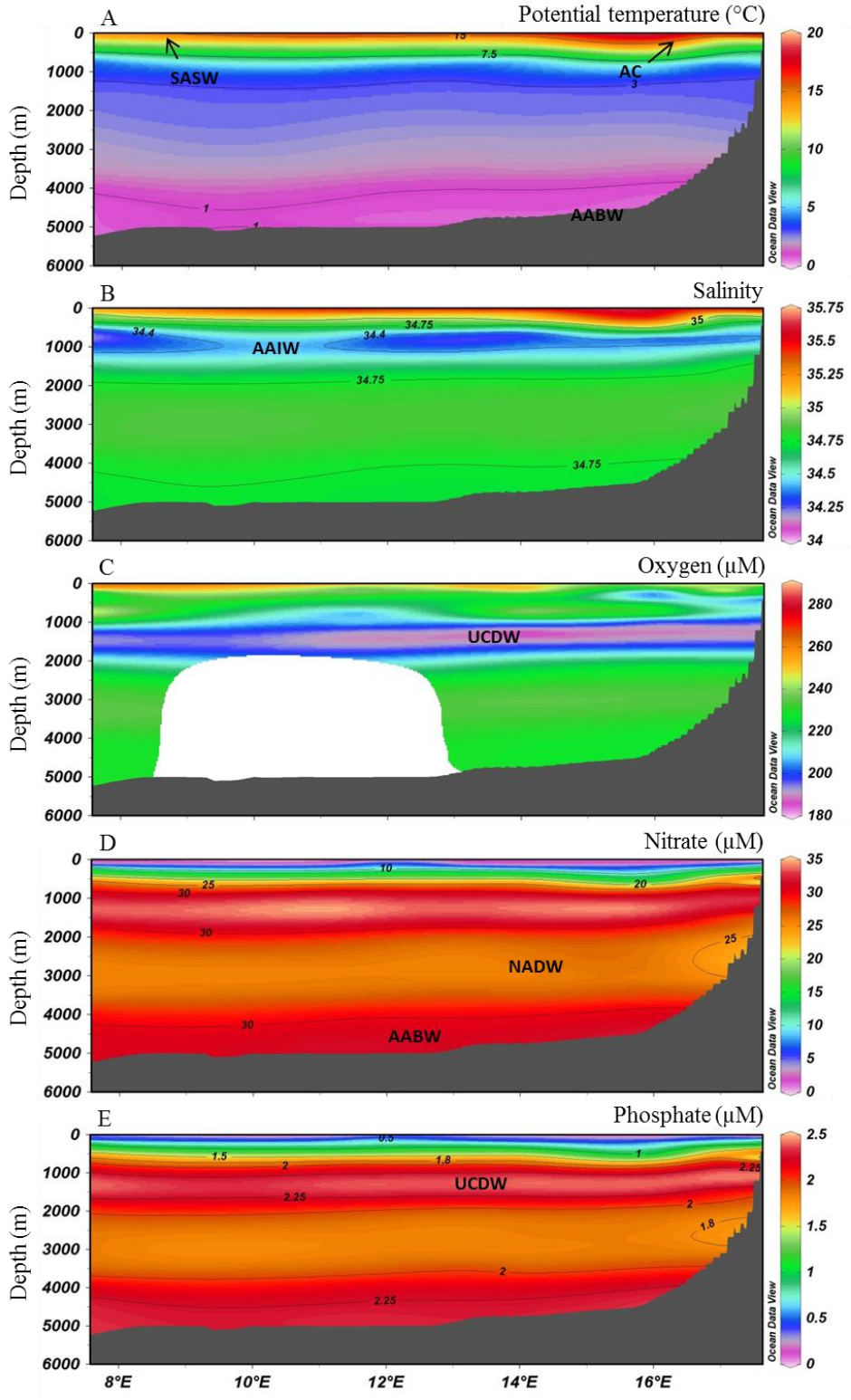

Figure 5.3. Distributions of (A) potential temperature, (B) salinity, (C) oxygen, (D) nitrate and (E) phosphate during D357-2 (late spring) used to indicate the major water masses. Abbreviations in alphabetical order: AABW: Antarctic Bottom Water; AAIW: Antarctic Intermediate Water; AC: Agulhas Current; NADW: North Atlantic Deep Water; SASW: Sub-Antarctic Surface Water; UCDW: Upper Circumpolar Deep Water. This figure was made using Ocean Data View (Schlitzer, 2012).

Within the Argentine Basin during JC068, the surface waters at stations closest South America were influenced by the Rio de la Plata estuary where salinity < 29 (Fig. 4.2B). Beyond the South American continental shelf margin the Brazil Current (BC: Θ 15 - 25º C, *S* 35 - 37) was observed to depths of ~ 200 m. Within offshore waters of the open Argentine Basin, surface water temperature (Θ >15 º C) and salinity (*S* > 35) was higher than its Cape Basin counterpart due to mixing with STSW travelling south from the South Atlantic sub-tropical gyre.

Sub-surface waters

Below the surface, Sub-Antarctic Mode Water (SAMW), the main conduit returning nutrients from the frontal Southern Ocean to the thermocline waters of the Southern Hemisphere (Sarmiento *et al.*, 2004; Palter *et al.*, 2010), was identified between 100 – 500 m during all three transects by a negative Si^* ($Si^* = Si(OH) – NO_3^-$). Between 500 and 1250 m, Antarctic Intermediate Water (AAIW) was identified by its salinity minimum (*S* < 34.4) (Fig's 5.2B and 5.3B), Θ 2.8 – 3.0º and SRP 1.25 – 2.25 µM. Located below Antarctic Intermediate Water, a layer of Upper Circumpolar Deep Water (UCDW: Θ 2.8 – 3.0º C, *S* 34.4 - 34.8) was found between 1250 and 1750 m, characterised by low oxygen (158 - 176 µmol kg^{-1}) (Fig's 5.2C and 5.3C) and a SRP maximum (> 2.25 µM) (Fig's 5.2E and 5.3E).

The abyssal layer at this latitude was occupied by cold and fresh Antarctic Bottom Water (AABW: Θ < 1º C, *S* < 34.8, SRP 2.25 - 2.60 µM) (Fig's 5.2A, B, E and 5.3A, B, E), which has its origins in the Southern Ocean. The AABW was located at depths of ~ 4500 m in the Cape Basin and ~ 4000 m in the Argentine Basin. Located between AABW and UCDW, North Atlantic Deep Water (NADW) is characterised by its deep salinity maximum (*S* > 34.8) and SRP minimum (< 2.25).

5.3.2. Dissolved cobalt and zinc in the upper water column: vertical profiles and spatial/temporal differences

The upper water column vertical profiles of dissolved Co and Zn from 6 stations during D357-1 (early spring), and 6 stations during D357-2 (late spring), are presented in Figure 5.4A – F and G – L respectively.

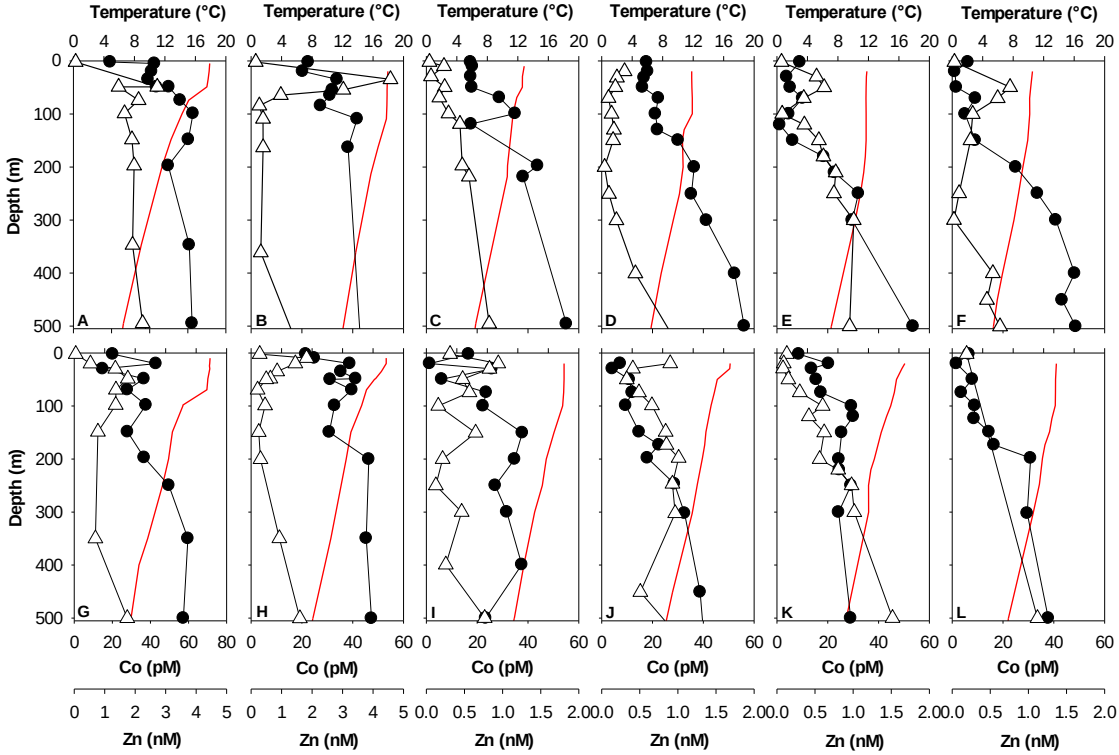

Figure 5.4. Vertical profiles of total dissolved cobalt (circles) and zinc (triangles) and temperature (red line) from early spring (D357-1; plots A – F) and late spring (D357-2; plots G – L) in the South Atlantic Ocean. Moving through the plots right to left is the equivalent to travelling along the D357 transect east to west. Plots A – B and G – I therefore represent stations sampled within the Agulhas Current during D357-1 and D357-2 respectively (note the different x axes), whilst plots C – F and J – L represent offshore stations.

During D357-1 (early spring), the concentrations of dissolved Co and Zn in the biologically active upper 150 m showed a distinct longitudinal gradient, with elevated

trace metal concentrations in AC waters (Co 20.2 - 62.8 pM and Zn 0.27 - 4.57 nM) (Fig. 5.4A – B) and markedly reduced concentrations in the open ocean (Co 1.0 - 34.9 pM and Zn 0.06 - 0.76 nM) (Fig. 5.4C – F). Previous observations of elevated Co and particulate aluminium within AC waters (Jeandel *et al.*, 2010; Bown *et al.*, 2011) indicate that these elevated metal concentrations could result from either atmospheric deposition and/or the transportation of particles from the Agulhas Bank.

Along the D357-1 (early spring) transect, both Co and Zn were positively correlated with salinity (r^2 = 0.38 and 0.31 respectively; n = 43, $p < 0.01$) in the upper 200 m (Fig. 5.5), the depth range of the AC Θ 15° C isotherm. This suggests that lateral, advective mixing of more-saline, high Co and Zn, AC waters with fresher, lower Co and Zn, open ocean waters may be an important control on the surface distributions of these metals within the Cape Basin prior to the on-set of the spring bloom.

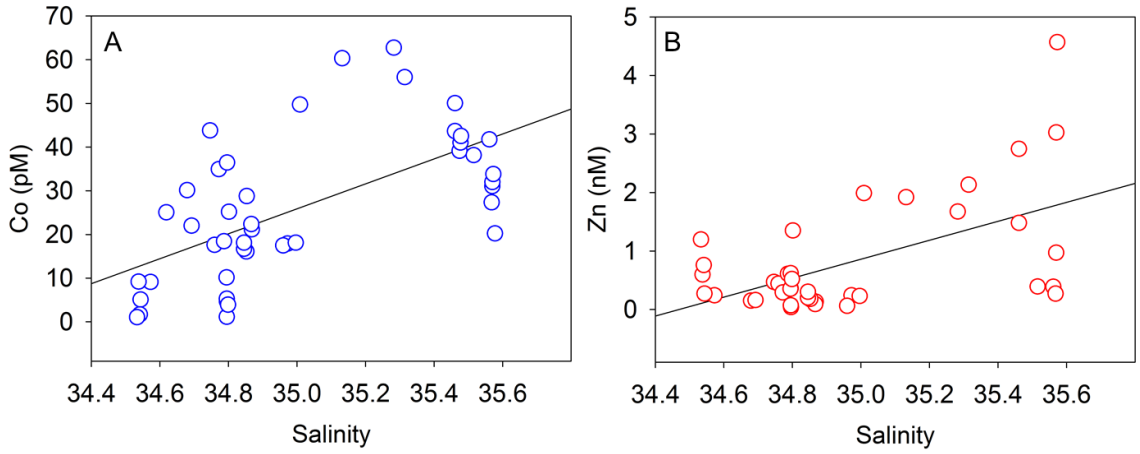

Figure 5.5. The relationship between salinity and dissolved (A) cobalt and (B) zinc in the upper 200 m of the Cape Basin during D357-1 (early spring). The correlation coefficients are 0.38 for Co vs salinity and 0.31 for Zn vs salinity (n = 43, $p < 0.01$).

During D357-2 (late spring), the longitudinal metal gradients were not as clearly defined owing to a reduction in surface Co and Zn concentrations within the AC (1.3 - 42.9 pM and 0.16 - 1.82 nM respectively) (Fig. 5.4G – I), whilst open ocean concentrations were similar to those observed during early spring (Co 1.7 - 30.1 pM and Zn 0.08 - 0.84 nM respectively) (Fig. 5.4J – L). The lower metal concentrations in the AC likely resulted from biological removal between the early and late spring by phytoplankton, with an estimated Co and Zn drawdown of 1.12×10^{-6} mol m^{-2} and 8.93×10^{-5} mol m^{-2} respectively over these 4 weeks.

During JC068 (summer), the concentrations of Co and Zn within the upper 150 m of the AC ranged 18 - 50 pM and 0.03 - 0.40 nM respectively. Despite a slightly higher concentration range, the integrated Co inventory for the upper 150 m of the AC was lower than that calculated for the D357-2 (late spring) transect. Similarly, the calculated Zn inventory for the AC was almost 7 fold lower than that calculated for the late spring transect. Whilst realising that other factors affect the Co and Zn concentrations in surface waters, if we assume that spring and summer metal concentrations were relatively constant between the D357 and JC068 cruises, then we can estimate a drawdown in the AC of 1.71×10^{-6} mol m^{-2} Co and 9.41×10^{-5} mol m^{-2} Zn between the D357-2 (late spring) and JC068 (summer) transects.

Within the Cape Basin open ocean, the JC068 (summer) Co concentrations ranged 2.8 – 37 pM, whilst Zn concentrations ranged 0.015 – 0.39 nM. The estimated drawdown of Co and Zn between the D357-2 and JC068 transects is 1.80×10^{-7} mol m^{-2} and 5.92×10^{-5} mol m^{-2} respectively. By using the ratio of Co and Zn to SRP from the Cape Basin open ocean to calculate metal:C ratios based on Redfield C:P stoichiometry of 106:1, and the robust relationship between metal:C ratios and the free metal ion

concentrations found in eukaryotic phytoplankton cultures (Sunda and Huntsman, 1995a), this study estimated maximum free Co^{2+} and Zn^{2+} concentrations for this region of ~ 10 and 70 pM respectively. The estimated minimum free Zn^{2+} concentration was ~ 0.1 pM, a concentration at which the growth rate of certain phytoplankton, with the exception of *T. oceanica*, have been limited in culture studies (Sunda and Huntsman, 1992, 1995a; de La Rocha *et al.*, 2000; Saito and Goepfert, 2008). Similarly, the estimated free Co^{2+} concentration of ~ 0.08 pM was below that required for the growth of certain eukaryotic phytoplankton but not the picocyanobacterium *Synechococcus*, which has an absolute but lower Co requirement (Sunda and Huntsman, 1995a). Following depletion of Co and Zn during the preceding months, the low concentrations observed in the Cape Basin open ocean during the summer may therefore co-limit phytoplankton growth.

In the Argentine Basin (JC068), similar to the Cape Basin, the concentrations of Co and Zn in the biologically active upper 150 m showed a distinct longitudinal gradient. Elevated metal concentrations were observed at stations closest South America (Co 106 pM and Zn 1.15 nM), associated with reduced salinity (S = < 29) from the Rio de la Plata estuary, whilst concentrations were markedly reduced in open ocean waters (Co 4.2 – 47.6 pM and Zn 0.015 - 0.42 nM). Concentrations of Zn were particularly low in offshore waters associated with the BC (0.015 – 0.23 nM), a western boundary current that transports warm, salty waters southwards from the South Atlantic sub-tropical gyre (Jullion *et al.*, 2010) (Fig. 5.1). Cobalt was negatively correlated with salinity in the upper 150 m throughout the BC and onto the South American continental shelf ($r^2 = 0.37$, $p < 0.01$, $n = 20$) with a stronger correlation observed for the top 5 m ($r^2 = 0.94$, $p < 0.01$, $n = 11$). This feature supports the hypothesis of marginal inputs,

dominated by the Rio de la Plata, and a degree of conservative mixing as reported for Co in the northeast and northwest Atlantic (Kremling and Streu, 2001; Saito and Moffett, 2002). Extrapolation of the surface salinity-Co regression to zero salinity provides an estimate of the Rio de la Plata Co concentration if mixing were completely conservative. The calculated zero salinity end member for Co had a value of 411 pM, almost half the estimated 790 pM Co for zero-salinity in the northwest Atlantic (Saito and Moffett, 2002). In contrast, whilst elevated Zn concentrations at South American coastal stations corresponded to reduced salinity and increased Si concentrations, and therefore likely arose from lithogenic inputs from the Rio de la Plata (Wyatt *et al.*, 2014) (see Chapter 4), Zn showed non-conservative behaviour due to rapid removal of Zn at coastal stations, coincident with a large diatom bloom.

The integrated 150 m Co and Zn inventories for the Argentine Basin open ocean (2.09×10^{-6} mol m^{-2} and 1.54×10^{-5} mol m^{-2} respectively), which exclude the low Zn concentrations in the BC, were higher than that of the Cape Basin open ocean (1.72×10^{-6} mol m^{-2} and 1.15×10^{-5} mol m^{-2} respectively). As well as fluvial inputs, other processes that may influence the inter-basin open ocean differences in metal concentrations include biological utilization (discussed further later), vertical/lateral mixing and atmospheric deposition. Previous studies have shown cross frontal mixing in the Argentine Basin at the SAMW/AAIW level associated with interaction within the Brazil-Malvinas confluence (Boebel *et al.*, 1999; Jullion *et al.*, 2010). These patches of mixing are discernible for extended periods and drift over long distances into the Argentine Basin. Thus, the elevated 150 m Co and Zn inventories for the Argentine Basin open ocean may result from the mixing of SAMW and AAIW with surface waters. This argument is supported by elevated Co and Zn concentrations observed in the upper

150 m at 28° W and 42° W that corresponded to salinity < 34.4 (AAIW) at 400 m and 300 m respectively and negative Si* (SAMW) at 63 m and 45 m respectively.

During the present study, the aerosol deposition flux of soluble Co and Zn to the South Atlantic open ocean ranged from 4 - 94 pmol m^{-2} d^{-1} and 4 - 21 nmol m^{-2} d^{-1} respectively (R. Chance, 2013, personal comm.), with slightly higher rates of deposition occurring in the Argentine Basin. However, these values are much lower than the deposition fluxes reported for other regions of the Atlantic Ocean (Jickells *et al.*, 1987; Bown *et al.*, 2011; Shelley *et al.*, 2012). In addition, such deposition over a 3 month period would only contribute for a maximum increase of 0.2 pM Co and 45 pM Zn in the mixed layer of the Argentine Basin, hence representing 0.2 % and 4.4 % of the mixed layer concentration measured. The contribution of dust dissolution to the mixed layer Co inventory of the Argentine open ocean is lower than the ≤ 2 % reported by Bown *et al.* (2011) for Southeast Atlantic stations close to South Africa and considerably lower than the ≤ 25 % estimated for the North Atlantic (Thuróczy *et al.*, 2010) where atmospheric dust inputs from Northwest Africa are high (see Chapter 1.3.2). Similarly, the contribution of dust dissolution to the mixed layer Zn inventory of the Argentine Basin of 4.4 % is significantly lower than the estimated ≤ 100 % in the North Atlantic (Thuróczy *et al.*, 2010). Atmospheric deposition therefore does not appear to be a significant source of Co and Zn to surface waters of the open Argentine Basin compared with inputs from the Rio de la Plata and upwelled water from below.

5.3.3. Dissolved cobalt and zinc in sub-surface waters

In Figure 5.6, the full water column dissolved Co and Zn data from D357-1 (early spring) (Fig. 5.6A, B) and D357-2 (late spring) (Fig. 5.6C, D), along with the full water column Co and Zn data from all 19 stations during JC068 (summer) (Fig. 5.6E, F), were used to create quasi-zonal sections.

The trace metal concentrations below the euphotic zone are largely controlled by the different water masses that occupy the South Atlantic at 40° S as shown for Zn by Wyatt *et al.* (2014) (see Chapter 4). The distributions of Co and Zn in sub-surface waters were therefore similar during all three transects. The concentrations of Co in the Cape Basin increased with depth to between 50 and 80 pM in the low-oxygenated UCDW (1250 and 1750 m) (Fig. 5.6A, C, E). Organic complexes are reported to represent more than 75 % of Co in these waters (Bown *et al.*, 2012), which would promote the stabilization of the soluble Co(II) redox state favoured by the low oxygen waters. Furthermore, elevated dCo concentrations have been reported in oxygen minimum zones of the South Atlantic/Benguela upwelling region (Noble *et al.*, 2012), the Costa Rica Dome and the Peru upwelling region (Saito *et al.* 2004; 2005), likely a result of reduced scavenging rates under low oxygen conditions (Noble *et al.*, 2012). At stations closest South Africa, elevated Co concentrations (50 – 70 pM) extended to 3000 m. Similar concentrations of dCo (45 – 55 pM) (Bown *et al.*, 2011), along with elevated dFe (Chever *et al.*, 2010) and particulate Al (Jeandel *et al.*, 2010), have previously been reported for similar depths within these waters and suggest a significant lithogenic source of Co from the South African continental margins.

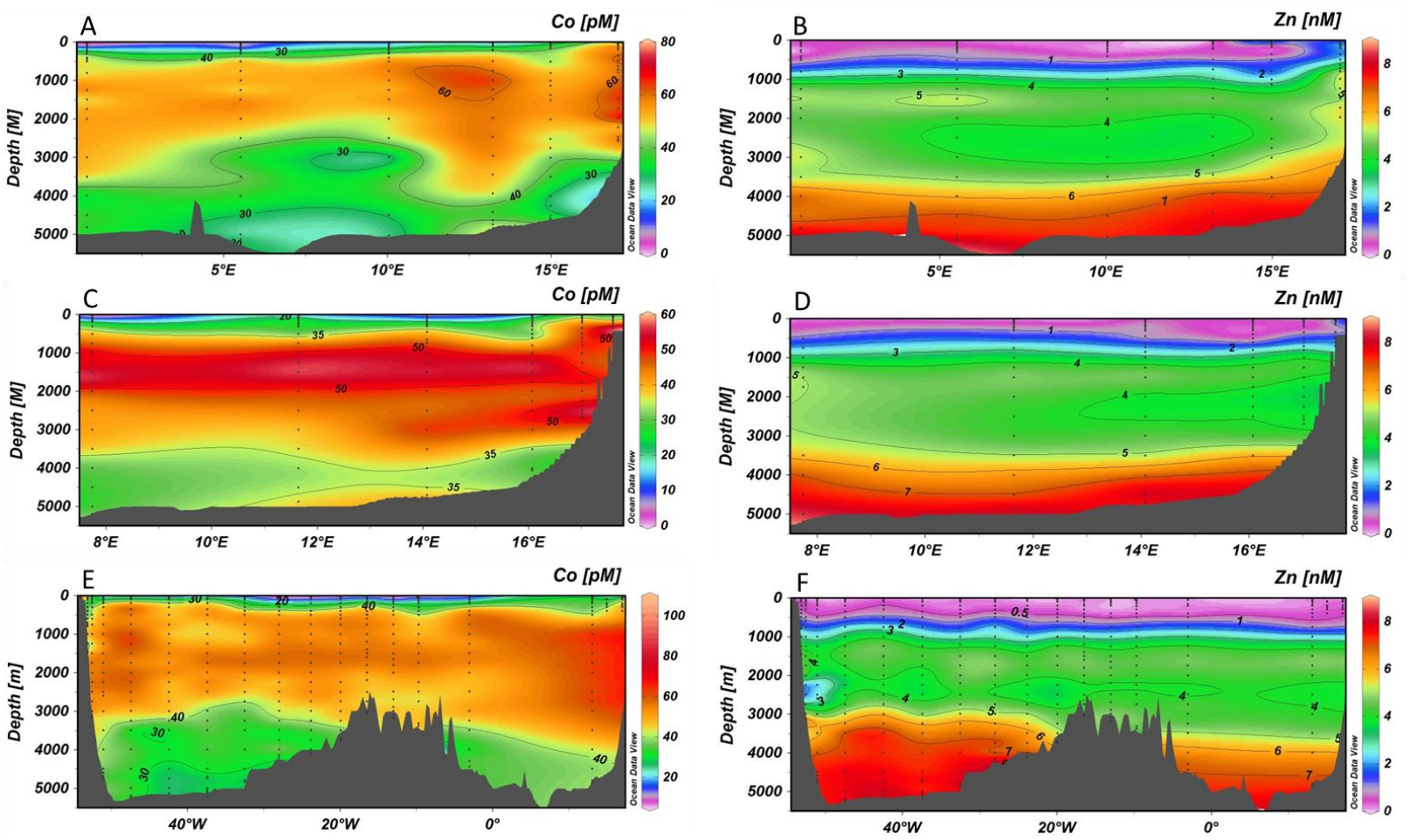

Figure 5.6. Zonal sections of dissolved cobalt and zinc during the early spring (D357-1; plots A and B), late spring (D357-2; plots C and D) and summer (JCO68; plots E and F). This figure was made using Ocean Data View (Schlitzer, 2012).

In the deep waters, Co concentrations during all three cruises displayed scavenged-like distributions. Cobalt concentrations decreased to between 30 and 40 pM below 3500 m in AABW, values which are in agreement those reported previously for the Southeast Atlantic (37 – 42 pM; Bown *et al.*, 2011) and the South Atlantic subtropical gyre (25 – 50 pM; Noble *et al.*, 2012).

The Zn concentrations below 150 m in the Cape Basin, during all three transects, did not increase significantly until 500 m (Fig. 5.6B, D, F). The biogeochemical cycle of Zn along the JC068 transect has indicated that the preferential removal of Zn with silicate by diatoms in the Southern Ocean may prevent a direct return path for Zn to the upper water column of the South Atlantic Ocean within SAMW (Wyatt *et al.*, 2014) (see Chapter 4). Below 500 m the Zn concentrations increased with depth in a typical nutrient fashion to maximum values of 6 – 8 nM in AABW.

The Co and Zn concentrations below 150 m in the Argentine Basin were broadly similar to that observed in the Cape Basin (Fig. 5.6E, F). However, the introduction of deep waters from the Weddell Gyre to the Argentine Basin (Naveira Garabato *et al.*, 2002; Huhn *et al.*, 2008) results in AABW nearer 3500 m compared to ~ 4000 m in the Cape Basin. Similarly, frontal mixing at the NADW/UCDW and AAIW/SAMW levels appears to result in elevated Co and Zn concentrations at depths of 500 m in the Argentine Basin compared to the Cape Basin (Fig. 5.6E, F).

5.3.4. Correlations of cobalt and zinc with soluble reactive phosphorus

Figure 5.7 shows the relationship between the complete vertical and horizontal distributions of SRP and dissolved Co and Zn in the South Atlantic Ocean at 40° S.

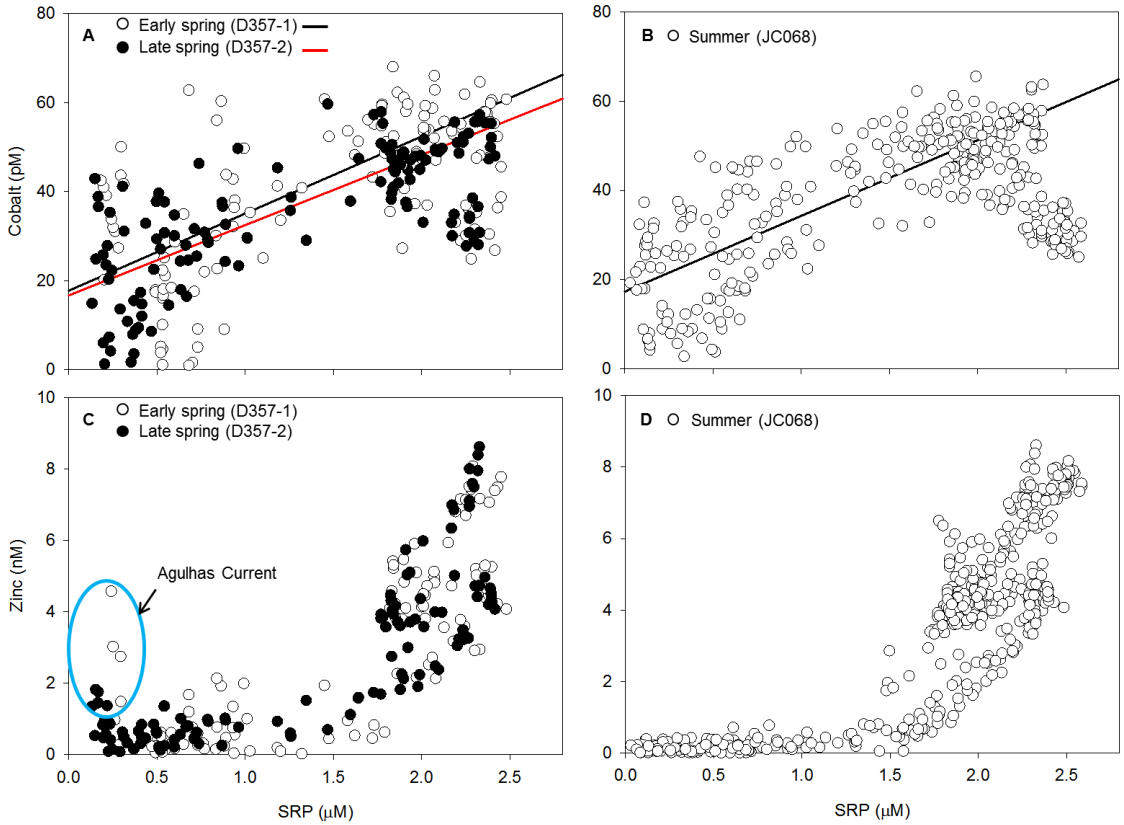

Figure 5.7. The relationship between soluble reactive phosphorus (SRP) and dissolved cobalt and zinc in the South Atlantic Ocean. Cobalt and SRP were linearly correlated in the upper 1250 m (< 1.7 - 2 µM SRP) during (A) the D357-1 (early spring; $r^2 = 0.46$; $n = 79$, $p < 0.01$) and D357-2 (late spring; $r^2 = 0.57$; $n = 84$, $p < 0.01$) transects and (B) the JC068 (summer; $r^2 = 0.62$; $n = 196$, $p < 0.01$) transect. Zinc and SRP are decoupled in the upper 500 m during (C) the D357-1 (early spring) and D357-2 (late spring) transects due to coastal zinc inputs to the Agulhas Current (highlighted). During JC068 (summer), zinc and SRP were correlated ($r^2 = 0.12$; $n = 57$, $p < 0.01$) in the upper 500 m (< 1.5 µM SRP). Note that the elevated zinc concentrations associated with the Rio de la Plata have been excluded.

Whilst the Co-SRP relationship was linear over the upper 1250 m during all three transects (Fig. 5.7A, B), for comparison with Zn further on, this study utilises the linear Co-SRP relationships from just the upper 500 m (Table 5.1).

Table 5.1. Regression slopes of Zn and Co versus PO_4^{3-} (µmol mol^{-1}) in the upper water column for different oceanic regimes.

Geographic location	Depth range (m)	Zn (nM)	ΔZn:ΔP (µmol mol^{-1})	r^2	Co (pM)	ΔCo:ΔP (µmol mol^{-1})	r^2	ΔZn:ΔCo	Reference
SE Atlantic (D357-1)	< 500	0.02 – 2.27[a]	550	0.25	1 - 65	17.9	0.20	30.7	This study
SE Atlantic (D357-2)	< 500	0.08 – 1.01[a]	407	0.19	1 - 60	22.0	0.26	18.5	This study
SE Atlantic (JC068)	< 500	0.01 – 0.67	127	0.12	2 – 66	17.5	0.27	7.3	This study
SW Atlantic (JC068)	< 500	0.01 – 1.41	390	0.57	4 - 76	20.4	0.52	19.1	This study
SE Atlantic	< 150				15 - 45	49.3	0.91		Bown *et al.* (2011)
NE Atlantic	20 - 150	0.25 – 0.61	593	0.91	40 - 49	9.94	0.91	59.7	Martin *et al.* (1993)
NE Atlantic	20 - 150	0.15 – 0.58	1885	0.99	21 - 44	45.0	0.78	41.9	Martin *et al.* (1993)
N Atlantic	Surface		7870						Bruland & Franks (1983)
N Atlantic	< 375		1861						Bruland & Franks (1983)
Equatorial Atlantic	5				5 - 87	560	0.63		Saito & Moffett (2002)
Sargasso Sea	10	0.07 – 1.32	1461	0.72	4 - 111	137	0.78	10.7	Jakuba *et al.* (2008)
NE Pacific	< 200	0.08 – 0.37	383	0.91					Bruland (1980)
NE Pacific (T5)	50 - 150	0.06 – 0.22	251	0.99	8 - 32	39.8	0.98	6.3	Sunda & Huntsman (1995a)[b]
NE Pacific (T6)	50 - 150	0.14 – 0.26	370	0.92	28 - 40	35.5	0.99	10.4	Sunda & Huntsman (1995a)[b]
NE Pacific (T8)	8 - 50	0.06 – 0.32	254	0.70	25 - 55	38.4	0.98	6.6	Sunda & Huntsman (1995a)[b]
NE Pacific	< 200					25.0			Martin & Gordon (1988)
Peru upwelling	5				21 - 315	248	0.83		Saito *et al.*, (2004)
Hawaiian Islands	< 250				11 – 47	37	0.91		Noble *et al.* (2008)
Hawaiian Islands	< 350				3 - 97	29	0.63		Noble *et al.* (2008)
S Ocean (Atlantic sector)	< 150				27 - 49	48.0	0.87		Bown *et al.* (2011)
S Ocean (Atlantic sector)	< 500		4857	0.73					Croot *et al.* (2011)
Ross Sea	0.5 - 40	0.24 – 3.95	509	0.95					Saito *et al.* (2010)[c]
Ross Sea	20 - 375	0.78 – 7.11	7580	0.72					Saito *et al.* (2010)[c]
Ross Sea	5 - 500				19 - 71	37.6	0.87	17[d]	Saito *et al.* (2010)

[a] Range excludes elevated Zn values for the AC.
[b] Data from Martin *et al.* (1989), stations T5, T6 and T8.
[c] Data from Fitzwater *et al.* (2000).
[d] ΔZn:ΔCo determined from linear Zn:P between 0.5 – 40 m and linear Co:P between 5 – 500 m.

The slopes of these relationships were 17.9 µmol mol^{-1} (r^2 = 0.20; *n* = 58, p < 0.01) for D357-1, 22.0 µmol mol^{-1} (r^2 = 0.26; *n* = 61, p < 0.01) for D357-2, 17.5 µmol mol^{-1} (r^2 = 27; *n* = 56, p < 0.01) for the Cape Basin during JC068 and 20.4 µmol mol^{-1} (r^2 = 0.52; *n* = 91, p < 0.01) for the Argentine Basin during JC068. These values are lower than the dissolved Co:P ratios of 25 – 41 µmol mol^{-1} reported for the Northeast Pacific, the Southeast Atlantic, the Ross Sea (Martin and Gordon, 1988, Sunda and Huntsman, 1995a, Noble *et al.*, 2008; Saito *et al.*, 2010; Bown *et al.*, 2011), and one order of magnitude lower than the 137 – 560 µmol mol^{-1} reported for the oligotrophic Sargasso Sea, the Eastern Tropical Pacific and the Equatorial Atlantic (Saito and Moffett, 2002; Saito *et al.*, 2004; Jakuba *et al.*, 2008; Table 5.1).

Below ~ 1750 m the Co-SRP relationship displayed a distinct curve during all three transects (Fig. 5.7A, B), where Co was removed, without stoichiometric removal of SRP, due to scavenging processes such as abiotic particle adsorption or biotic Mn co-oxidation (Tebo *et al.*, 1984; Moffett and Ho, 1996). This scavenging of Co occurred at a greater depth than the mesopelagic depths (500 – 800 m) reported for the Northeast Pacific (Martin *et al.*, 1989; Noble *et al.*, 2008), and compares more favourably with the Southeast Atlantic (Noble *et al.*, 2012), and the Atlantic sector of the Southern Ocean (Bown *et al.*, 2011). For the South Atlantic at 40° S, scavenging coincides with the lower boundary of low oxygen (158 - 176 µmol kg^{-1}) UCDW. Within the core of South Atlantic UCDW, 75 % of dCo is reported to be organically complexed (Bown *et al.*, 2012), which would result in only a quarter of labile Co being available for bacterial oxidation or passive scavenging. This suggests that the deeper depth at which scavenging is observed at 40° S is largely controlled by the presence of low oxygen UCDW and a high degree of organic complexation.

The Zn-SRP relationship for the South Atlantic during all three transects exhibited a number of distinct kinks in its linear profile (Fig. 5.7C, D). The shallowest kink in the Zn-SRP relationship during all three transects was observed at ~ 500 m (~ 1.5 µM SRP). This Zn-SRP kink was also observed in the North Pacific, the Southern Ocean and the Ross Sea (Martin *et al.*, 1989; Saito *et al.*, 2010; Jakuba *et al.*, 2012), but at much shallower depths between 20 and 150 m (1.2 – 1.5 µM PO_4^{3-}). The deeper depth of the South Atlantic Zn-SRP kink is hypothesized to reflect the extremely low Zn concentrations in the upper water column, and the lack of a direct return path for Zn, unlike SRP, from the Southern Ocean within SAMW between 100 and 500 m (Wyatt *et al.*, 2014) (see Chapter 4).

Within the Cape Basin, the Zn-SRP relationship in the upper 500 m during the D357 (spring) transects are decoupled, presumably due to the elevated coastal inputs of Zn compared to SRP. These values were therefore excluded from the Zn:SRP correlation. Subsequently, the Zn-SRP relationship was linear in the upper 500 m during D3571 (early spring; $r^2 = 0.25$; $n = 43$, $p < 0.01$), D357-2 (late spring; $r^2 = 0.19$; $n = 40$, $p < 0.01$) and JC068 (summer; $r^2 = 0.12$; $n = 57$, $p < 0.01$). The slopes of these relationships decreased between the transects from 550 µmol mol^{-1} to 407 µmol mol^{-1} and finally 127 µmol mol^{-1} respectively (Table 5.1). During JC068 (summer), Zn was tightly correlated with SRP in the upper 500 m of the Argentine Basin ($r^2 = 0.57$; $n = 75$, $p < 0.01$) with an elevated slope of 390 µmol mol^{-1} compared to the Cape Basin. These values are significantly lower than the 1460 – 7870 µmol mol^{-1} reported for the oligotrophic North Atlantic and Sargasso Sea (Bruland and Franks, 1983; Jakuba *et al.*, 2008; Table 5.1) and compare more favourably with the 250 – 509 µmol mol^{-1} reported for the Ross Sea and Northeast Pacific (Martin *et al.*, 1989; Saito *et al.*, 2010).

5.3.5. Phytoplankton community structure

During D357-1 (early spring), the highest concentrations of total chlorophyll-*a* were observed in AC waters (0.06 - 0.43 mg m^{-3}), whilst reduced concentrations were found in the Cape Basin open ocean (0.06 – 0.36 mg m^{-3}). Using pigment ratios for different taxonomic groups, the phytoplankton assemblage was estimated to be dominated by *Phaeocystis* type haptophytes, which contributed 79 ± 11 % and 53 ± 9 % towards chlorophyll-*a* in AC waters and open ocean waters respectively. *Emiliania huxleyi* type haptophytes were found to be extremely low in the AC (< 1 % chlorophyll-*a*) but contributed 19 ± 10 % towards chlorophyll-*a* in open ocean waters. In contrast, diatoms contributed 8 ± 5 % towards chlorophyll-*a* in AC waters but were extremely low offshore (< 1 % chlorophyll-*a*). Of the picocyanobacteria, *Synechococcus* was more abundant than *Prochlorococcus* in both the AC (6.6 – 25.9 x 10^3 cells mL^{-1} vs. 3.2 – 17.8 x 10^3 cells mL^{-1}) and open ocean waters (5.87 – 61.4 x 10^3 cells mL^{-1} vs. 3.2 – 31.5 x 10^3 cells mL^{-1}).

During D357-2 (late spring), total chlorophyll-*a* concentrations along the transect were elevated relative to those observed during the early spring (0.28 – 0.45 mg m^{-3} in the AC and 0.08 – 0.61 mg m^{-3} in the Cape Basin open ocean). The phytoplankton assemblage during this period was also by dominated by *Phaeocystis* type haptophytes, which contributed 69 ± 14 % and 79 ± 8 % towards chlorophyll-*a* within AC waters and open ocean waters respectively. Diatom contribution was elevated to 10 ± 8 % chlorophyll-*a* in AC waters and was 7 ± 5 % chlorophyll-*a* in open ocean waters, whilst *E. huxleyi* type haptophytes represented < 4 % chlorophyll-*a* along the transect. The abundance of *Prochlorococcus* varied little between the two D357 transects, whilst the abundance of *Synechococcus* was approximately 3 fold higher

within AC waters during D357-2 (2.61 – 79.1 x 10^3 cells mL^{-1}) but decreased in open ocean waters (3.0 – 43.8 x 10^3 cells mL^{-1}).

During JC068 (summer), total chlorophyll-*a* concentrations for the AC and the Cape Basin open ocean ranged between 0.03 and 1.02 mg m^{-3} and between 0.02 and 0.77 mg m^{-3} respectively, representing the highest chlorophyll concentrations observed for the Southeast Atlantic during this study. The contribution of *Phaeocystis* type haptophytes to the phytoplankton assemblage within AC waters was markedly reduced during JC068 (18 ± 8 % chlorophyll-*a*) and instead, a community shift towards *E. huxleyi* type haptophytes (20 ± 4 % chlorophyll-*a*), chrysophytes (20 ± 2 % chlorophyll-*a*) and diatoms (16 ± 4 % chlorophyll-*a*) was observed. This was also observed in the open ocean where the contribution of *Phaeocystis* type haptophytes was reduced to 41 % chlorophyll-*a*, whilst the contribution of *E. huxleyi* type haptophytes (37 ± 18 % chlorophyll-*a*), prasinophytes (9 ± 5 % chlorophyll-*a*) and dinoflagellates (8 ± 4 % chlorophyll-*a*) was elevated. The abundance of *Synechococcus* ranged between 0.2 x 10^2 cells mL^{-1} and 109.4 x 10^5 cells mL^{-1} along the transect with remarkably similar concentrations in both AC and open ocean waters. In contrast, *Prochlorococcus* was markedly higher during JC068 in both AC waters (1.3 x 10^2 cells mL^{-1} to 403.1 x 10^5 cells mL^{-1}) and open ocean waters (0.3 x 10^2 cells mL^{-1} to 9.7 x 10^4 cells mL^{-1}).

Within the Argentine Basin, the JC068 (summer) total chlorophyll-*a* concentrations were highest in the open ocean (0.02 – 1.46 mg m^{-3}). The phytoplankton assemblage of these open ocean waters was estimated to be dominated by *E. huxleyi* type haptophytes (24 % chlorophyll-*a*), whilst chrysophytes (20 % chlorophyll-*a*), diatoms (16 % chlorophyll-*a*), and *Phaeocystis* type haptophytes (15 % chlorophyll-*a*) also contributed significantly to the community structure. At stations closest South

America, total chlorophyll-*a* concentrations were 0.03 – 0.92 mg m^{-3}. Diatoms contributed 24 % to chlorophyll-*a*, with *Phaeocystis* and *E. huxleyi* type haptophytes contributing 19 % and 13 % respectively. In agreement with the known distribution and abundance of *Trichodesmium* in the Atlantic Ocean (Tyrell *et al.*, 2003), this cyanobacterium contributed 6 % to chlorophyll-*a* at coastal stations. The abundance of *Synechococcus* was elevated in both the open ocean and coastal regimes ranging 1.79 x 10^2 cells mL^{-1} to 2.4 x 10^5 cells mL^{-1}, whilst *Prochlorococcus* abundance was elevated to 0.3 x 10^2 cells mL^2 to 4.2 x 10^5 cells mL^{-1} in open ocean waters but was reduced to 1.1 x 10^3 cells mL^{-1} to 1.8 x 10^5 cells mL^{-1} in coastal waters.

5.4. Discussion

5.4.1. Metal-SRP vector analysis: the nutritional role for cobalt and zinc

The slopes of metal-SRP relationships can reflect the tug-of-war between biotic and abiotic processes on trace metal biogeochemistry (Cullen *et al.*, 2006; Noble *et al.*, 2008; Saito *et al.*, 2010; Wyatt *et al.*, 2014). Phytoplankton uptake and subsequent remineralisation of biomass would result in the removal and addition Zn, Co and SRP, and therefore would strengthen metal-SRP relationships. Abiotic trace metal inputs from the atmosphere or coastal sources, and the removal of metals from seawater by scavenging processes, may alter metal concentrations without a stoichiometric change in SRP, and therefore destroy metal-SRP correlations. This type of metal-SRP vector analysis has proven useful in identifying the biological utilisation of either Co or Zn in shallow waters of the Northeast and Equatorial Pacific (Sunda and Huntsman, 1995a;

Saito *et al.*, 2004; Noble *et al.*, 2008), the Southeast Atlantic (Bown *et al.*, 2011) and the Ross Sea (Saito *et al.*, 2010).

During this study, the Co:SRP ratio in the upper 500 m showed a temporal and spatial consistency ranging between 17.5 and 22.0 μmol mol^{-1}; Table 5.1. In contrast, the decrease in the upper water column Zn:SRP ratio of the Cape Basin between the D357-1 (early spring; 550 μmol mol^{-1}), D357-2 (late spring; 407 μmol mol^{-1}) and JC068 (summer; 127 μmol mol^{-1}) transects suggests that the nutritional demand for Zn may decline with decreasing Zn concentrations, whereby Co may have a greater relative nutritional value. This study represents the first investigation of phytoplankton nutritional stoichiometric plasticity in response to changes in Co and Zn concentrations over seasonal time scales. The biochemical substitution of Co and Zn within enzymes means that the phytoplankton community composition will likely change to reflect the changing metal concentrations and therefore the relative nutritional role of Co and Zn needs to be considered.

Within the Cape Basin, the metal-SRP ratios provide evidence for a greater nutritional reliance on Zn relative to Co. This is based on stoichiometric ratios for dissolved Zn:SRP/Co:SRP ($\Delta Zn{:}\Delta Co$) of 31:1, 19:1 and 7:1 for the three transects respectively (Table 5.1). In addition, these data suggest that on a seasonal basis, the nutritional reliance on these trace metals changes from a greater role for Zn to an environment where Co plays a relatively more important role. One explanation for this behaviour is the drawdown of Zn in the presence of phytoplankton with high Zn:SRP ratios followed by Zn depletion. This hypothesis is supported by a positive x-axis intercept for the D357-1 (early spring) Zn:SRP regression followed by positive y-axis intercept for both the D357-2 (late spring) and JC068 (summer) relationships. The

JC068 utilisation ratio of ΔZn:ΔCo 7:1 compares favourably with the ΔZn:ΔCo 6 – 10:1 reported for phytoplankton in the Zn deplete (0.06 – 0.32 nM) sub-Arctic Pacific (Sunda and Huntsman, 1995a). By contrast, higher Zn utilisation ratios of ΔZn:ΔCo 17 – 60:1 have been reported for Ross Sea and Northeast Atlantic phytoplankton (Martin *et al.*, 1993; Saito *et al.*, 2010) where surface Zn concentrations were in excess of 0.24 nM. Together, these data provide evidence that the removal of Zn between the D357 and JC068 transects results in a greater nutritional role for Co in the Cape Basin compared to that previously reported for the Atlantic Ocean. Cobalt may therefore play an extremely important role in controlling phytoplankton species composition and distribution within this region.

Within the Argentine Basin, the reliance on Zn relative to Co (ΔZn:ΔCo 19:1) during JC068 (summer) was almost 3 times greater than the 7:1 observed for the Cape Basin (Table 5.1). The South Atlantic east-west gradient in Zn and Co utilisation may be explained by the relative differences in surface metal concentration during this transect and the interdependent cellular Zn and Co requirements of phytoplankton. As stated earlier, the JC068 integrated 150 m Co and Zn inventories for the Argentine Basin open ocean were higher than that of the Cape Basin open ocean. However, the inter-basin difference for Zn (0.39×10^{-5} mol m^{-2}) is an order of magnitude greater than that of Co (0.37×10^{-6} mol m^{-2}). Laboratory based cultures studies have demonstrated that for eukaryotic phytoplankton, elevated free Zn^{2+} ion concentrations resulted in reduced Co^{2+} uptake rates and vice versa (Sunda and Huntsman, 1995a; Ho *et al.*, 2003). Thus, we should expect to see relatively high ΔZn:ΔCo utilisation ratios in the Argentine Basin compared to the Cape Basin. The nutritional role for Zn within the Argentine Basin was greater at coastal stations (ΔZn:ΔCo 57) compared to the open

ocean (ΔZn:ΔCo 16). At these coastal stations, marginal inputs from the Rio de la Plata resulted in a Zn:SRP ratio of 439 µmol mol^{-1} (r^2 = 0.60; *n* = 19, p < 0.01), a ratio that is comparable to the 509 µmol mol^{-1} reported for the Zn rich, diatom dominated Ross Sea (see above).

5.4.2. Cobalt and zinc controls on phytoplankton diversity in the South Atlantic

Culture studies have revealed that metal requirements differ amongst phytoplankton taxa (Sunda and Huntsman, 1995a; Webb *et al.*, 2001; Ho *et al.*, 2003) and that the dominance or limitation of certain phytoplankton species has implications for biological uptake and export of carbon (Nelson *et al.*, 1995; Tortell *et al.*, 2000; Poulton *et al.*, 2006). As such, the nutritional role for Co and Zn needs to be considered alongside phytoplankton diversity to determine how seasonal changes in metal concentration may favour the growth of certain species.

As stated above, this study observed a nutritional reliance on Zn relative to Co in the euphotic zone of the Cape Basin during the two D357 spring transects (Table 5.1). Despite this, no relationship was observed during either transect between Zn and *Phaeocystis* type haptophytes, phytoplankton with a cellular preference for Zn (Saito and Goepfert, 2008) and which dominated the phytoplankton assemblages. Instead, during D357-2 (late spring), both Co and Zn were positively correlated in the AC with fucoxanthin (r^2 = 0.55; *n* = 8, p < 0.05 and r^2 = 0.81; *n* = 6, p < 0.01 respectively) (Fig. 5.8E, F), a diatom indicator pigment that is also found in haptophytes. In addition, Zn and Si were inversely related within AC waters (r^2 = 0.26; *n* = 19, p < 0.05) during this period. These data suggest that the drawdown of Co and Zn from AC waters between

the two D357 transects may be predominantly associated with diatoms instead of *Phaeocystis*, as reported for the Ross Sea (Saito *et al.*, 2010). This hypothesis is supported by the work of Saito and Goepfert (2008) who report Co and Zn half-saturation constants for maximum growth of the coastal diatom *T. pseudonana* (1.2 x 10^{-12} pM and 3.6 x 10^{-12} pM respectively) that are approximately one order of magnitude greater than that of the haptophyte *P. antarctica* (9.5 x 10^{-13} pM and 1.9 x 10^{-13} pM respectively).

Whilst diatoms appear to play an important role in removing Co from the Cape Basin, this study suggests Co removal by picocyanobacteria, as well as other phytoplankton phyla may also occur. This hypothesis is based on an inverse relationship between Co and *Synechococcus* in both AC waters ($r^2 = 0.67$; $n = 10$, $p < 0.01$) (Fig 5.8A) and open ocean waters ($r^2 = 0.24$; $n = 17$, $p < 0.05$) during D357-1. Within AC waters, the abundance of *Synechococcus* increased between the two D357 transects and consequently. Consequently a stronger Co *Synechococcus* relationship was observed within this region during D357-2 ($r^2 = 0.76$; $n = 7$, $p < 0.01$) (Fig. 5.8B). In addition, Co and Zn within the AC during this period were strongly inversely correlated with violaxanthin ($r^2 = 0.94$; $n = 8$, $p < 0.01$ and $r^2 = 0.64$; $n = 6$, $p < 0.05$ respectively) (Fig. 5.8C, D), a diagnostic marker pigment for chlorophytes. *Synechococcus* has an absolute cellular Co requirement and a low Co:P ratio of ~ 13 µmol mol^{-1} required for maximum growth (Sunda and Huntsman, 1995a). Similarly low cellular Co:P ratios of ~ 10 µmol mol^{-1} and ~ 8 µmol mol^{-1} have been reported for the chlorophytes *Dunaliella tertiolecta* and *Nannochloris automus* respectively (Ho *et al.*, 2003). These values are well below the Co:SRP ratios of 17.9 – 22.0 µmol mol^{-1} reported here for the euphotic zone of the Cape Basin during the spring transects (Table 5.1).

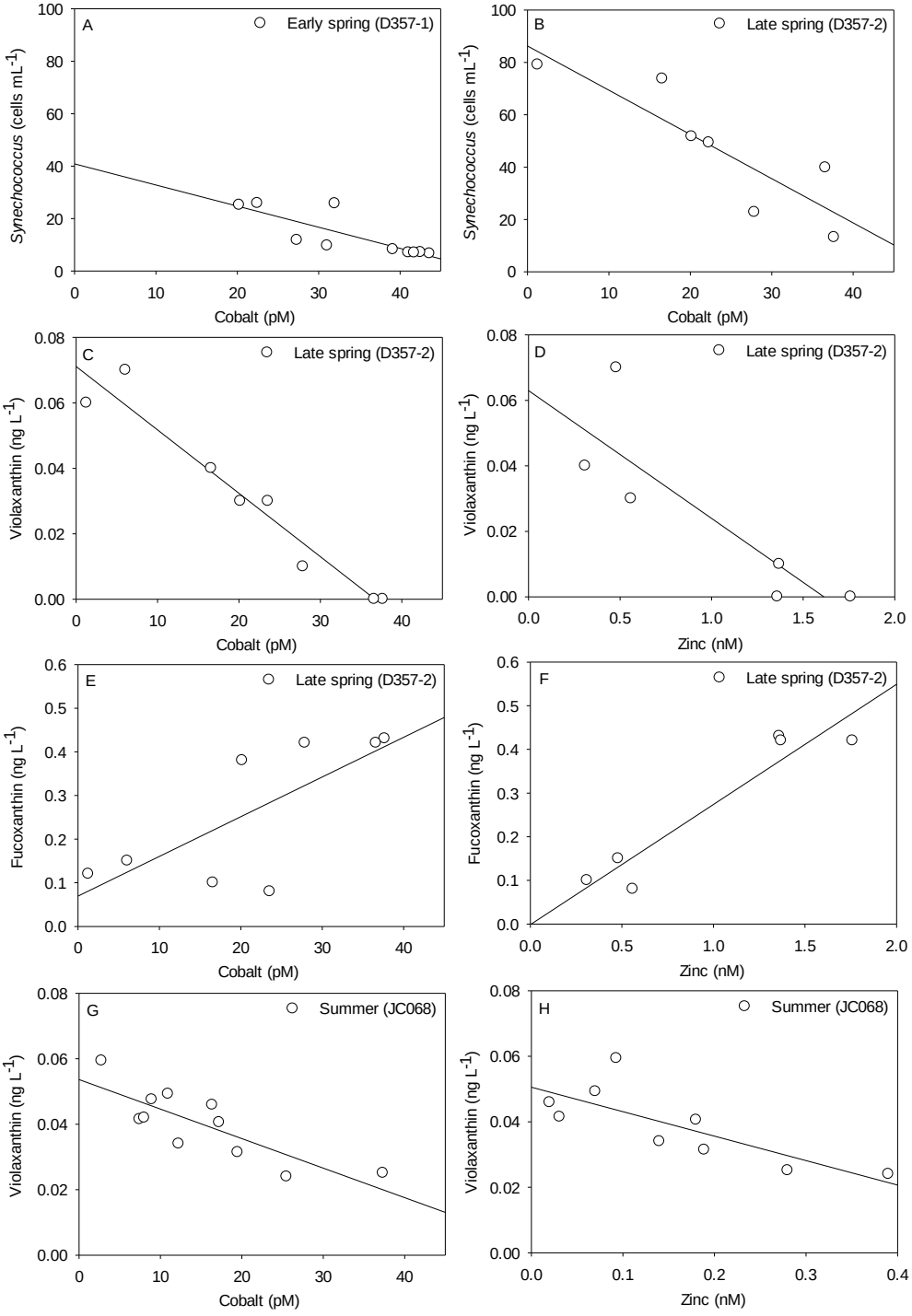

Figure 5.8. Comparison of total dissolved metals and phytoplankton signatures in the Cape Basin. (A - B) Co versus *Synechococcus* abundance in AC waters during D357-1 ($r^2 = 0.67$, $p < 0.01$) and D357-2 ($r^2 = 0.76$, $p < 0.01$). (C – D) Co and Zn versus the green algae indicator pigment chlorophyll-normalised violaxanthin within AC waters during D357-2 ($r^2 = 0.94$, $p < 0.01$ and $r^2 = 0.64$, $p < 0.05$ respectively). (E – F) Co and Zn versus the diatom indicator pigment chlorophyll-normalised fucoxanthin within AC waters during D357-2 ($r^2 = 0.55$, $p < 0.05$ and $r^2 = 0.81$, $p < 0.01$ respectively). (G – H) Co and Zn versus the green algae indicator pigment chlorophyll-normalised violaxanthin at open ocean stations during JC068 ($r^2 = 0.68$, $p < 0.01$ and $r^2 = 0.61$, $p < 0.05$ respectively).

These observations imply that picocyanobacteria, *Synechococcus* in particular, and chlorophytes may also play an important role in removing Co from the euphotic zone. Conversely, this suggests that low concentrations of Co may regulate growth rate and biomass of *Synechococcus* in the Southeast Atlantic, which may have implications for the primary productivity of this region.

During the JC068 (summer) transect, the nutritional reliance on Co is markedly increased within the Cape Basin (ΔZn:ΔCo 7, Table 5.1), possibly due to the removal of Zn by diatoms between the spring and summer months (*e.g.* 9.41 x 10^{-5} mol m^{-2} in AC waters) and a subsequent phytoplankton community shift to *E. huxleyi* type haptophytes, which have a cellular preference for Co (Sunda and Huntsman, 1995a). Despite this, no relationship between either metal and phytoplankton was observed within AC waters. In comparison to AC waters, Co in the Cape Basin open ocean was strongly inversely related with the fractional contributions of *E. huxleyi* type haptophytes ($r^2 = 0.50$; $n = 12$, $p < 0.05$) as well as *Synechococcus* abundance ($r^2 = 0.59$; $n = 10$, $p < 0.05$). In addition, both Co and Zn were strongly inversely correlated with violaxanthin ($r^2 = 0.68$; $n = 11$, $p < 0.01$ and $r^2 = 0.61$; $n = 9$, $p < 0.05$ respectively) in this region (Fig. 5.8G, H). Whilst being a diagnostic marker pigment for chlorophytes, violaxanthin, is also found in prasinophytes, which contributed almost 10 % towards the chlorophyll-*a* standing stock in the open ocean. The cellular metal ratios for these phytoplankton, bar the cyanobacterium that has an absolute Co requirement, have been reported between 1 and 10 µmol mol^{-1} Zn:Co, similar to the summer utilisation ratio of ΔZn:ΔCo 7:1 reported for the Cape Basin during this study. These data indicate that whilst we observed a small preference for Zn over Co in Cape Basin open ocean waters during JC068, the extremely low Zn concentrations appear to be driving phytoplankton community

structure towards that with primary cellular Co requirements, such as *E. huxleyi* and *Synechococcus* (Sunda and Huntsman, 1995a), and that with lower cellular Zn requirements such as oceanic prasinophytes and dinoflagellates (Ho *et al.*, 2003). This has clear implications for the efficiency of the oceanic biological carbon pump given that its efficiency is heavily influence by the dominance of *E. huxleyi* (Nelson *et al.*, 1995; de La Rocha, 2003).

Within the Argentine Basin, the ΔZn:ΔCo 57:1 utilisation ratio at coastal stations indicated that the nutritional role for Zn relative to Co was higher at these stations compared to any other part of the transect. At these stations, both chlorophyll-*a* concentration (0.92 mg m^{-3}) and the contribution of diatoms (24 % to chlorophyll-*a*) were elevated. Cobalt and Zn were positively correlated with chlorophyll-*a* ($r^2 = 0.67$; $n = 9$, $p < 0.01$ and $r^2 = 0.64$; $n = 7$, $p < 0.05$ respectively) (Fig. 5.9A, B) and the diatom marker pigment chlorophyll-normalised fucoxanthin ($r^2 = 0.63$; $n = 9$, $p < 0.05$ and $r^2 = 0.39$; $n = 7$, $p < 0.05$ respectively) (Fig. 5.9C, D). Note that the elevated 1.15 nM Zn sample at the station closest the South American continent corresponded to elevated Si concentration and appeared strongly influenced by the Rio de la Plata, hence this value did not fit the expected biological pattern and has been excluded from such relationships. The negative coastal relationships suggest that removal of Zn and Co by diatoms occurred in the time preceding our study. This is supported by satellite derived chlorophyll-*a* concentrations (NASA, MODIS; data not shown), which indicate post-bloom conditions at the time these coastal stations were sampled.

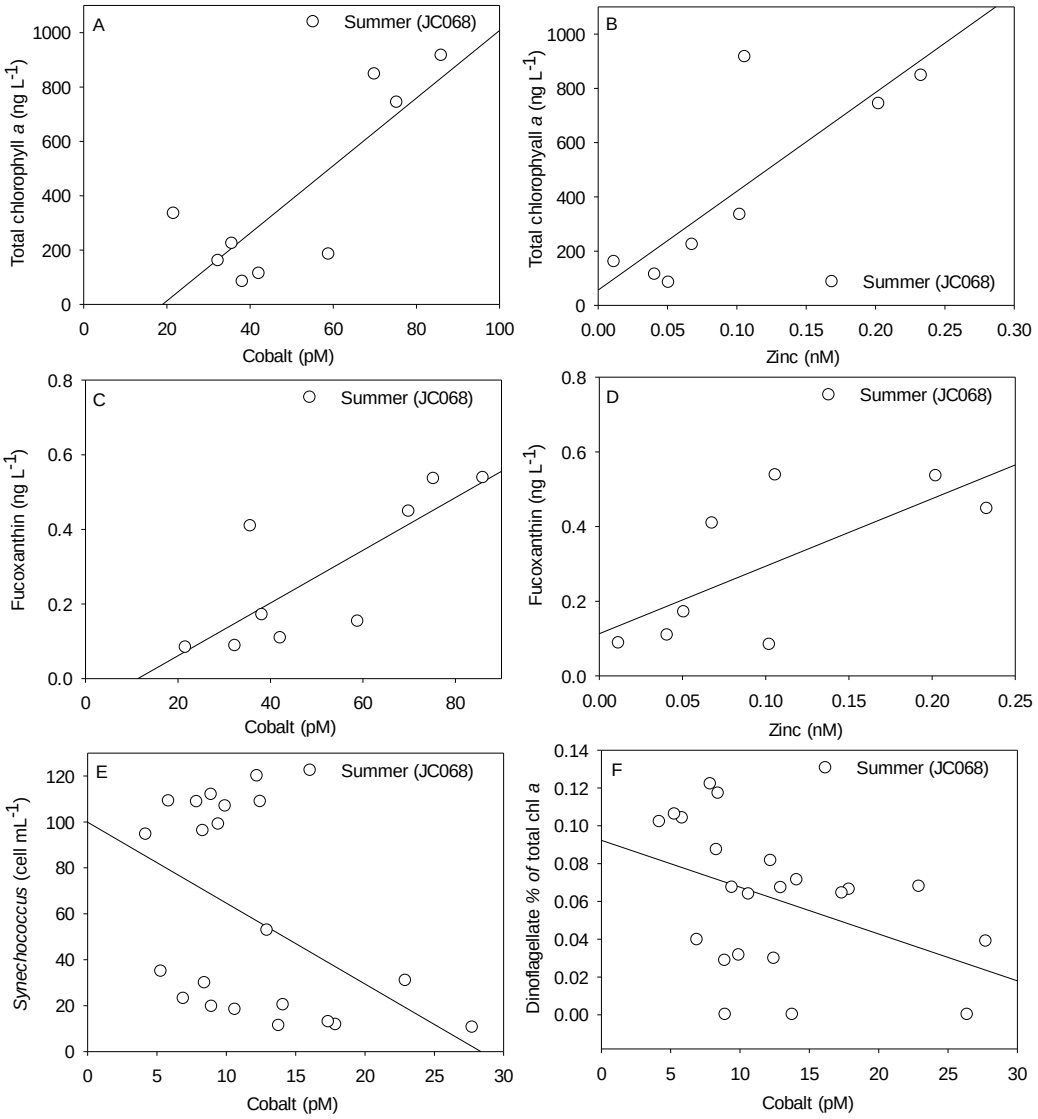

Figure 5.9. Comparison of total dissolved metals and phytoplankton signatures in the Argentine Basin during the summer transect (JC068). (A – B) Cobalt and zinc versus total chlorophyll-*a* at coastal stations (r^2 = 0.67, $p < 0.01$ and r^2 = 0.64, $p < 0.05$ respectively). (C –D) Cobalt and zinc versus the diatom indicator pigment chlorophyll-normalised fucoxanthin at coastal stations (r^2 = 0.63, $p < 0.05$ and r^2 = 0.39, $p < 0.05$ respectively). (E) Cobalt versus *Synechococcus* abundance at open ocean stations (r^2 = 0.22, $p < 0.05$). (F) Cobalt versus dinoflagellate contribution to total chlorophyll-*a* at open ocean stations (r^2 = 0.19, $p < 0.05$).

Stations in the Argentine Basin open ocean exhibited a similar pattern to stations in the Cape Basin open ocean. Despite a ΔZn:ΔCo 19:1 utilisation ratio in the euphotic

zone, Zn was not correlated with phytoplankton measurements. Instead, Co was weakly negatively correlated with *Synechococcus* abundance ($r^2 = 0.22$; $n = 21$, $p < 0.05$) (Fig. 5.9E) and dinoflagellate contribution to total chlorophyll-*a* ($r^2 = 0.19$; $n = 22$, $p < 0.05$) (Fig. 5.9F). Thus, despite the apparent nutritional reliance on Zn in the South Atlantic open ocean, it appears that the low Zn concentrations in the euphotic zone resulted in a phytoplankton community that have low or absent cellular Zn requirements, such as dinoflagellates and *Synechococcus* respectively, or the ability to co-substitute Co and Zn, such as *E. huxleyi*.

5.5. Conclusions

This chapter presents dissolved Co and Zn data for three transects in the South Atlantic Ocean and provides evidence that the biogeochemical cycle of Co in this region is linked with that of Zn. The highest Co and Zn concentrations (62.8 pM and 4.57 nM respectively) during this study were observed in AC waters during the early spring indicating the AC as a significant source of trace metals to surface waters of the Cape Basin during this period. This study suggests a drawdown of Zn in surface waters of the Cape Basin between the spring and summer transects (9.41×10^{-5} mol m^{-2} in AC waters and 5.92×10^{-5} mol m^{-2} in open ocean waters) that results in potentially growth limiting concentrations of Zn. Despite this, phytoplankton groups with cellular requirements in excess of that available in surface waters were dominant during the summer suggesting the potential for biochemical co-substitution, hence an increased biological role for Co.

This study observed a seasonal shift in the nutritional reliance on Co and Zn (defined by their linear stoichiometric relationship with SRP) from a large role for Zn in

the Cape Basin during the early spring to an environment where Co plays a relatively more important role during the summer. This change in nutritional reliance occurred in symmetry with a shift in phytoplankton community structure away from *Phaeocystis* type phytoplankton towards that with either an absolute or lower cellular Co requirement, such as *Synechococcus*, or phytoplankton with the ability to biochemically co-substitute Co and Zn, such as *E. huxleyi*. Subsequently, linear relationships between these phytoplankton and Co were observed in the Cape Basin during the summer JC068 transect indicating that when Zn concentrations are depleted, Co may play an important role in determining phytoplankton community structure in the Southeast Atlantic Ocean.

In the Argentine Basin, the nutritional reliance on Zn relative to Co was three fold greater than observed for the Cape Basin with the greatest role for Zn observed at diatom dominated coastal stations where coastal inputs were elevated. Inverse linear relationships observed between both Co and Zn and fucoxanthin at these stations indicated the removal of these trace metals occurred in the time preceding this study. Despite the larger nutritional role for Zn in the Argentine Basin open ocean compared to that of the Cape Basin, linear relationships between Zn and phytoplankton were absent. In contrast, Co was linearly related to phytoplankton with absent or low cellular Co requirements. Thus, it appears that, whilst there is an overall greater nutritional reliance on Zn in the South Atlantic at 40° S, the low Zn concentrations in open ocean surface waters may help control the distribution and dominance of key phytoplankton phyla such as diatoms, haptophytes and picocyanobacteria. This has clear implications for primary productivity and the efficiency of the oceanic biological carbon pump, which is largely controlled by the relative dominance of such phytoplankton.

Chapter 6

Conclusions, synthesis and future directions

6.1. Introduction

The trace metal micronutrients iron (Fe), zinc (Zn) and cobalt (Co) were the focus of this thesis. The diversity of roles for Fe, Zn and Co in phytoplankton biochemistry (Morel *et al.*, 2003; Morel and Price, 2003) has highlighted the need to bring together qualitative and quantitative studies on their biogeochemical cycling in the world's oceans. The research in this thesis has contributed to our knowledge of Fe cycling in the Atlantic Ocean in contrasting oceanographic regimes. This work has generated new data on Zn and Co distributions in the South Atlantic Ocean and has provided new insights into the physico-chemical and biological influences that interact to control their biogeochemistry where there was previous little understanding.

To achieve the objective of this research, the approach included trace metal clean sampling, analytical measurements of Fe, Zn and Co, incubation experiments to determine di-nitrogen (N_2) fixation rates, and data analysis, synthesis and interpretation. This work underlined the importance of integrating cross-disciplinary results (*e.g.* chemical, physical and biological measurements) to interpret the biogeochemistry of Fe, Zn and Co in the oceanographically diverse Atlantic Ocean.

During this research, samples were collected on three UK led research cruises to different regions of the Atlantic Ocean. *AMT*-19 was a large-scale, gyre centred cruise between 50° N to 40° S that also sampled across the temperate, sub-tropical and tropical North and South Atlantic. Here, dissolved Fe (dFe) and total dissolvable Fe (TDFe) were determined in samples from the upper water column to examine the biogeochemical cycling of Fe. The UK GEOTRACES Section A10 consisted of two separate research cruises located in the South Atlantic along the productive 40° S parallel where a there is little to no understanding of trace metal cycling. This research

provided the first large-scale exploration of the vertical and horizontal distributions of dissolved Zn and Co in this region.

6.2. Conclusions

6.2.1. Biogeochemistry of iron in the upper water column of the Atlantic Ocean: observations from the Atlantic Meridional Transect

Chapter 3 demonstrated that a number of distinct mechanisms interact to control the unique distributions of Fe in the upper water column (≤ 150 m) of the Atlantic Ocean. Such mechanisms include (1) dissolution of atmospheric Fe in surface waters, (2) biological uptake and internal recycling in the surface mixed layer, (3) remineralisation below the surface mixed layer and finally (4) vertical mixing across the thermocline.

Overall the data from this chapter showed distinct basin-scale differences in the Atlantic surface Fe inventory, with elevated dFe concentrations in the North Atlantic gyre (0.50 – 1.65 nM) compared with the South Atlantic gyre (0.14 – 0.32 nM) and a sharp dFe gradient observed at ~ 4° N. Such basin-scale differences are consistent with the ~ 10 fold difference in modelled atmospheric dust inputs between the North and South Atlantic (Jickells *et al.*, 2005; Mahowald *et al.*, 2009). Specifically, this study emphasised the importance of dry and wet Saharan dust deposition for the delivery of bioavailable dFe to the sub-tropical and tropical North Atlantic respectively, and showed that these mechanisms had a profound effect on climate relevant processes such as N_2 fixation in the North Atlantic.

Towards the southern extent of the Saharan dust belt, the converging wind systems of the northern and southern hemisphere in the Inter-Tropical Convergence Zone (ITCZ; 4 – 10° N) led to heavy rainfall and surface water dFe maxima. The wet deposition of more soluble Fe in the ITCZ was confirmed by a comparison between dFe and TDFe data in the vicinity of a salinity (S = 34.2) and pH (8.04) minimum. Here, dFe represented 60 ± 26 % of the TDFe pool compared with only 48 ± 26 % between 20 and 29° N where atmospheric dry deposition of Fe was elevated. It is therefore, not surprising that that the maximum rates of N_2 fixation in the Atlantic open ocean have been observed in the vicinity of the ITCZ (Moore *et al.*, 2009).

Whilst highlighting the importance of the ITCZ for the supply of Fe to surface waters of the tropical North Atlantic, the work in Chapter 3 also showed that the ITCZ acted as a barrier to the transport of lithogenic dust particles, thus Fe, to the South Atlantic. This work showed that the low surface concentrations of the South Atlantic gyre are therefore likely sustained by rapid biological removal, efficient recycling and a downwelling TDFe flux of 3.2 µmol m^{-2} y^{-1} comparable to atmospheric inputs. In that regard, the low surface mixed layer dFe inventory of the South Atlantic gyre may therefore be in steady state with a calculated residence time of 6.3 y consistent with low particulate organic carbon fluxes (Charette and Moran, 1999).

6.2.2. Biogeochemical cycling of dissolved zinc and cobalt along the GEOTRACES South Atlantic transect GA10 at 40° S

Chapters 4 and 5 provided for the first time the distribution and biogeochemistry of the key micronutrients Zn and Co along the productive 40° S parallel in the South

Atlantic. This work demonstrated that Zn and Co in the bioactive surface waters were elevated at stations closest to South Africa and South America due to marginal inputs from the Agulhas Current (AC) and Rio de la Plata estuary respectively. Within the open ocean, Zn and Co concentrations in the surface layer were observed at potentially growth limiting concentrations (15 pM and 3 pM respectively). Here, the vertical distributions of Zn and Co throughout the water column at 40° S were markedly different owing to their different chemistries in seawater. Zinc exhibited a nutrient-type vertical profile that resulted in maximum concentrations (7 – 8 nM) in AABW. In contrast, Co exhibited maximum concentrations (70 – 80 pM) in intermediate waters, associated with low oxygen, and was scavenged below ~ 1750 m.

In Chapter 4, the low Zn concentrations in the surface waters are shown to be sustained by the lack of a return path for Zn from the Southern Ocean that returns high nitrate and phosphate concentrations to the thermocline waters at this latitude. The research findings from this chapter indicate that the preferential removal of Zn and Si by diatoms in the frontal Southern Ocean may be responsible the low Zn concentrations in these Southern Ocean return waters based on strong Zn-Si relationships observed at both 40° S (Zn (nM) = 0.065 Si (µM) + 0.209; r^2 = 0.97, n = 460) and in the frontal Southern Ocean during previous studies. In addition, the kink in the 40° S Zn-SRP relationship at ~ 500 m indicates that Zn is being returned at this depth primarily by AAIW.

In Chapter 5, a particular focus was placed on the biological implications of Co and Zn availability in the South Atlantic. The research findings from this chapter showed that Co and Zn concentrations in the surface mixed layer varied over seasonal timescales often dropping below potential growth limiting concentrations. Despite this,

phytoplankton groups with cellular Co and Zn requirements in excess of that available were often dominant indicating the potential for biochemical co-substitution of these elements. With the concept of Co and Zn co-substitution becoming clearer, in part thanks to a greater understanding of the biochemical functions of these trace metals (Yee and Morel, 1996; Sunda and Huntsman, 1995a; Xu *et al.*, 2008; Saito *et al.*, 2008), Chapter 5 revealed how the availability of these trace metals over seasonal time scales played an essential role in structuring the phytoplankton community. Such plasticity of the phytoplankton community to changing trace metal concentrations has clear implications for primary productivity and the efficiency of the oceanic biological carbon pump, which is largely controlled by the relative dominance of certain phytoplankton. This work therefore represented a first step in our understanding of the role of trace metals for phytoplankton assemblages and subsequent primary productivity along the 40° S parallel in the South Atlantic.

6.3. GEOTRACES: synthesis and future directions

A principal focus of Chapters 4 and 5 was to determine the mechanisms that interact to control the low open ocean surface water concentrations of Zn and Co in the South Atlantic Ocean. Using the Zn and Co data from these chapters, as well as the soluble atmospheric trace metal flux data (Dr. Rosie Change; University of East Anglia) and the radium-228 (^{228}Ra) derived vertical mixing coefficients (Dr. Alan Hsieh; University of Oxford), a budget for Zn and Co in the South Atlantic at 40° S was calculated (Fig. 6.1) in order to quantify the importance of sources to this region.

The atmospheric input of soluble Zn to the South Atlantic open ocean showed no basin-scale difference (Fig. 6.1) with similar deposition rates for the Cape Basin (4 – 20 nmol m^{-2} d^{-1}) and the Argentine Basin (4 – 21 nmol m^{-2} d^{-1}). Similarly, the atmospheric input of soluble Co to the Cape Basin open ocean (0.004 – 0.094 nmol m^{-2} d^{-1}) was comparable to that of the Argentine Basin (0.0095 – 0.09 nmol m^{-2} d^{-1}).

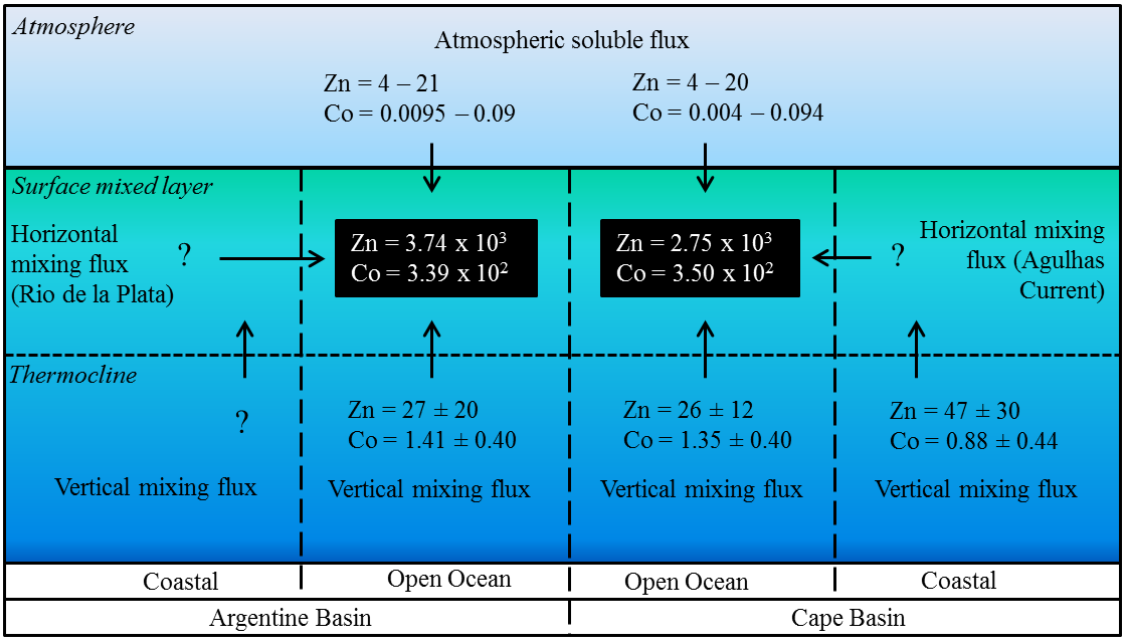

Figure 6.1. The principal mechanisms that transport zinc and cobalt to the South Atlantic open ocean at 40° S. Surface mixed layer concentrations of dissolved zinc and cobalt are in black boxes (nmol m^{-2}) and approximate flux values are expressed as nmol m^{-2} d^{-1}. The uncertainties associated to the vertical mixing fluxes represent 1 std. dev. of the mean vertical flux for each region.

The lack of an inter-basin difference in the atmospheric supply of both Zn and Co may be explained by the low atmospheric dust inputs to the south Atlantic open ocean compared with coastal regions (Mahowald et al., 1999; Jickells et al., 2005) and the low relative abundance of Zn and Co in mineral dust (0.0071 % and 0.0017 % respectively) (Taylor and McLennan, 1985; McLennan, 2001). It must be noted that stations closest South America had atmospheric soluble Zn inputs between 22 and 39

nmol m^{-2} d^{-1} where modelled dust inputs are elevated (Evangilista et al., 2010; Johnson et al., 2010). As expected, the atmospheric soluble Zn input is approximately three orders of magnitude higher than that of Co owing to its increased crustal abundance and the higher dust solubility for Zn in seawater (16 %) compared with Co (0.14 %) in natural particles (Thuróczy et al., 2010). Considering the maximum input of Zn and Co over a 30 day period, inputs of 600 and 3 nmol m^{-2} would represent 22 and 1 % of the surface mixed layer Zn and Co inventories respectively for the Cape Basin. Over the same period, maximum Zn and Co inputs of 630 and 3 nmol m^{-2} to the Argentine Basin would represent 17 and 1 % of the Zn and Co inventories respectively.

Chapters 4 and 5 have shown that horizontal and vertical mixing played important roles in the supply of Zn and Co to open ocean surface waters of the South Atlantic. A novel aspect to this study was the availability of ^{228}Ra data for the Cape Basin collected as part of the UK GEOTRACES D357 cruise (Dr. Alan Hsieh; University of Oxford). This naturally occurring isotope is produced be the decay of thorium-232 in shelf sediments, diffused into seawater and then transported into the open ocean. ^{228}Ra has a relatively short half-life of 5.75 years (Moore and Dymond, 1991) and its distributions can therefore be used as a geochemical tracer for lateral mixing from the coastal environment to the open ocean and vertical mixing through the upper water column (*e.g*. Yamada and Nozaki, 1986; van Beek *et al*., 2008; Hsieh et al. *in prep*). For example, Charette *et al*. (2007) used ^{228}Ra as a geochemical tracer for Fe delivered to the HNLC Crozet Plateau region from the Crozet Island system, and concluded that this source is sufficient to initiate and maintain an annual phytoplankton bloom.

By using the ^{228}Ra derived vertical diffusive mixing coefficients (K_z) for the upper 400 m of the Cape Basin (K_z ranged 0.9 to 2.1 cm^{-2} s^{-1}; Hsieh *et al. in prep*), this study estimated the vertical mixing flux of Zn and Co to the surface mixed layer (Fig. 6.1) based on Fick's first law of molecular diffusion in the following equation:

$$F_{metal} = K_z \left(\Delta\text{metal}/\Delta\text{z}\right) \qquad \text{Eq. 6.1.}$$

where F_{metal} is the diffusion flux (nmol m^{-2} d^{-1}) and Δmetal/Δz is the gradient of Zn and Co concentrations over the depth z below the surface mixed layer, which were obtained from the linear regression of the vertical metal profiles below the surface mixed layer to 400 m. Where ^{228}Ra vertical mixing coefficients were not available, for example in the remote open ocean where ^{228}Ra surface activity is low, an average K_z of 1.5 cm^{-2} s^{-1} assessed from tritium measurements in the South Atlantic was used (Li *et al.*, 1984). Vertical mixing fluxes for coastal stations closest to South America have not been estimated due to the level of uncertainty surrounding K_z estimates for the dynamic Malvinas-Brazil confluence region.

At stations closest to South Africa, the vertical mixing flux for Zn to the surface mixed layer was elevated (47 ± 30 nmol m^{-2} d^{-1}) compared with that of the open ocean Cape Basin (26 ± 12 nmol m^{-2} d^{-1}) and Argentine Basin (27 ± 20 nmol m^{-2} d^{-1}) (Fig. 6.1). The difference in the vertical Zn flux between the coastal and open ocean regimes reflects the elevated Zn concentrations below the mixed layer in the AC relative to the low Zn sub-pycnocline waters of the open ocean as shown in Chapter 4. In the open ocean, if vertical mixing occurred at the same rate over a 30 day period, upward Zn fluxes of 780 and 810 nmol m^{-2} to the Cape Basin and Argentine Basin respectively would represent Zn inputs equal to 28 and 22 % of the surface mixed layer Zn

inventories. The percentage contributions of vertical mixing to the mixed layer Zn inventories of both basins are only slightly elevated compared with the atmospheric Zn fluxes indicating that despite the low atmospheric dust fluxes to the South Atlantic compared with other oceanographic regimes, the relative contribution to the Zn inventories are broadly similar to that from upward mixing.

Whilst the mean vertical mixing fluxes for Zn are similar in both the Cape and Argentine Basins, the range of Zn inputs through vertical mixing is higher in the Argentine Basin. Here, the vertical mixing flux for Zn ranged from 10 to 68 nmol m^{-2} d^{-1} with the largest fluxes occurring in the vicinity of elevated sub-surface Zn concentrations (see Chapter 4, Figure 4.3). It is therefore likely that the elevated vertical Zn fluxes to the Argentine Basin open ocean, and hence the higher surface mixed layer Zn inventory compared with the Cape Basin, are in-part associated with cross frontal mixing at the intermediate water mass scale, as discussed in Chapter 5.

The vertical mixing flux for Co was similar for both the Cape Basin coastal and open ocean regimes (0.88 ± 0.44 nmol m^{-2} d^{-1} and 1.35 ± 0.40 nmol m^{-2} d^{-1} respectively) and the Argentine Basin (1.41 ± 0.40 nmol m^{-2} d^{-1}). In the open ocean, if vertical mixing occurred at the same rate over a 30 day period, upward Co fluxes of 41 and 42 nmol m^{-2} to the Cape Basin and Argentine Basin respectively would represent Co inputs equal to 11 and 12 % of the surface mixed layer Zn inventories. It is therefore clear that vertical mixing provides an important source of Co to the surface mixed layer of the South Atlantic relative to atmospheric fluxes (Fig. 6.1).

A large part of the open ocean mixed layer Zn and Co inventories is not explained by inputs from the atmospheric or vertical mixing. Horizontal mixing from the AC and Rio de la Plata to the open ocean likely contributes a significant fraction to

these inventories. The availability of ^{228}Ra data from the UK GEOTRACES Section GA10 cruises (Dr. Alan Hsieh; University of Oxford) will help constrain the horizontal diffusive mixing coefficients that can be applied to future calculations of horizontal Zn and Co fluxes in these highly dynamic regions. Such estimates would effectively close the box on external inputs to the surface mixed layer at 40° S and would allow the development of biogeochemical models that determine the role for Zn and Co in primary production and carbon export. This is critically important for this highly productive region and forms a key GEOTRACES objective.

The Southern Ocean nutrient supply accounts for about three-quarters of the biological production north of 30° S (Sarmiento *et al.*, 2004; Palter *et al.*, 2010). As shown in Chapter 4, Zn is markedly reduced in this return path through its preferential removal with silicate, most likely by diatoms, in the frontal Southern Ocean. The research findings from Chapter 4 have led to the development of a new tracer (Zn*) that can be used to map the low dissolved Zn concentrations delivered to pycnocline waters of the Southern Hemisphere by the upper branches of Meridional Overturning Circulation (MOC). By using the strong linear relationship between Zn and silicate reported in Chapter 4 (Zn (nM) = 0.065 Si (µM) + 0.029, $r^2 = 0.97$, $n = 460$), Zn* is calculated from the equation:

$$Zn^* = Zn\ (nM) - 0.065 \times Si\ (\mu M) + 0.029 \qquad \text{Eq. 6.2.}$$

where negative Zn* indicates the transport of low Zn values from the Antarctic Circumpolar Current to intermediate waters at 40° S and remains constant if sources (remineralisation) and sinks (uptake) of Zn and silicate occur at a ratio of Zn:Si (0.065), whilst the intercept of 0.029 fixes the deep water Zn* to zero.

At 40° S, negative Zn* values were observed to depths of ~ 900 m in the Cape Basin and ~ 600 – 800 m in the Argentine Basin (Fig. 6.2) confirming that Zn is only returned to this latitude with Antarctic Intermediate Water (AAIW) as shown in Chapter 4. The basin-scale difference in Zn* distribution further reflects cross-frontal mixing between AAIW and Sub-Antarctic Mode Water (SAMW) in the Argentine Basin.

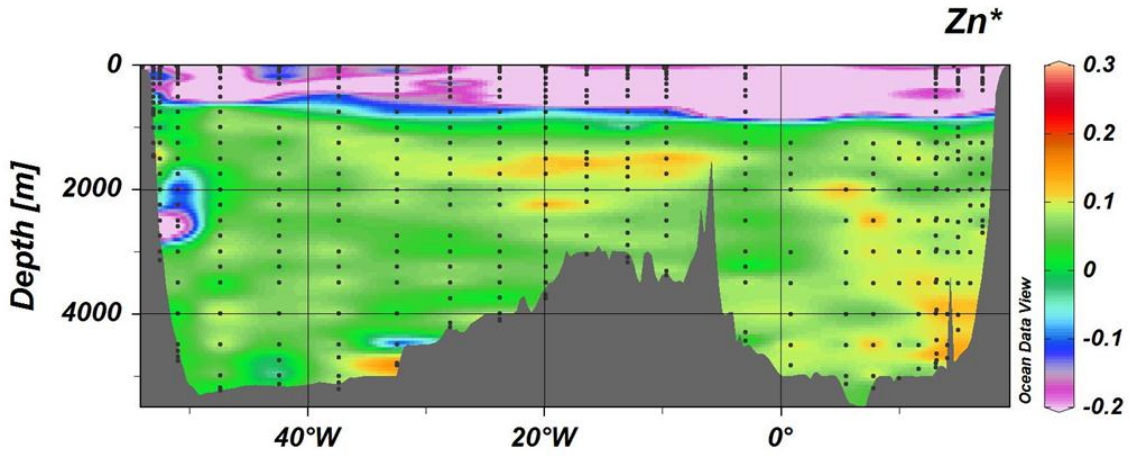

Figure 6.2. The tracer Zn* used to map low dissolved zinc concentrations delivered to the upper 1000 m of the South Atlantic from the Southern Ocean. This figure was made using Ocean Data View (Schlitzer, 2012).

This tracer has the potential to provide important quantitative information on the delivery of Zn from the Southern Ocean to the Southern hemisphere and subsequently the control of the Southern Ocean trace metal supply on the biological productivity of the world's oceans.

In order to gain a better understanding of the control of Zn and Co on phytoplankton assemblages, the extent to which SAMW and AAIW influence their distributions in this region and throughout the Southern Hemisphere over seasonal to inter-annual time-scales needs further investigation. The Zn* tracer provides such an opportunity and coupled with the seasonal Zn data from the GEOTRACES cruises

described in Chapters 4 and 5, may provide the first insights into the seasonal transport of Zn and Co from the Southern Ocean to bioactive surface waters of the South Atlantic. In addition, the Zn* tracer can be applied to other GEOTRACES Sections in the Atlantic Ocean to investigate the role of the Southern Ocean nutrient return path for Zn distributions throughout the Atlantic Ocean.

Recent estimates indicate marine sediments as a significant source of dissolved Fe to the world's oceans (Moore and Braucher, 2008; Homoky *et al*., 2012). In the South Atlantic, the Argentine Basin is a region of large lateral gradients and extremely high concentrations of particulate matter in the abyssal nepheloid layer (Richardson *et al.*, 1993). Particulate data from the UK GEOTRACES Section GA10 will provide a quantification of the magnitude and basin-scale differences in sedimentary supply of Zn and Co.

Chapters 4 and 5 provided the first insights into the potential for Zn and Co co-substitution in South Atlantic phytoplankton when either Zn or Co concentrations were growth limiting. Experiments with natural phytoplankton assemblages and ship-board incubations are required to investigate the physiological status of this regions phytoplankton. Such insights would afford us a great wealth of climate relevant information as it is the relative dominance of diatoms and coccolithophores that exert a primary control on the efficiency of the biological carbon pump.

6.4. Summary

There is a need to bring together quantitative and modelling studies that can improve our understanding of trace metal biogeochemistry in the world's oceans. Such

studies are crucial if we are to gain further understanding of how trace metals interact to influence marine primary productivity and the global carbon cycle. The research in this thesis addresses such issues by providing detailed examinations of the biogeochemical cycling of Fe, Zn and Co in the South Atlantic Ocean. This work prompts multiple avenues for future research that could be addressed during future research cruises and laboratory-based experiments.

References

Achterberg, E. P., T. W. Holland, A. R. Bowie, R. Fauzi, C. Mantoura, and P. J. Worsfold (2001), Determination of iron in seawater, *Analytica Chimica Acta*, *442*(1), 1-14.

Achterberg, E. P., C. M. Moore, S. A. Henson, S. Steigenberger, A. Stohl, S. Eckhardt, L. C. Avendano, M. Cassidy, D. Hembury, J. K. Klar, M. I. Lucas, A. I. Macey, C. M. Marsay, and T. J. Ryan-Keogh (2013), Natural iron fertilization by the Eyjafjallajokull volcanic eruption, *Geophysical Research Letters*, *40*(5), 921-926.

Aguilar-Islas, A. M., J. A. Resing, and K. W. Bruland (2006), Catalytically enhanced spectrophotometric determination of manganese in seawater by flow-injection analysis with a commercially available resin for on-line preconcentration, *Limnology and Oceanography-Methods*, *4*, 105-113.

Aiken, J., N. Rees, S. Hooker, P. Holligan, A. Bale, D. Robins, G. Moore, R. Harris, and D. Pilgrim (2000), The Atlantic Meridional Transect: overview and synthesis of data, *Progress in Oceanography*, *45*(3-4), 257-312.

Andersen, M. B., D. Vance, C. Archer, R. F. Anderson, M. J. Ellwood, and C. S. Allen (2011), The Zn adundance and isotopic composition of diatom frustules, a proxy for Zn availability in ocean surface seawater., *Earth and Planetary Science Letters*, *301*, 137-145.

Anderson, M. A., F. M. M. Morel, and R. R. L. Guillard (1978), Growth Limitation of a Coastal Diatom by Low Zinc Ion Activity, *Nature*, *276*(5683), 70-71.

Ansorge, I. J., S. Speich, J. R. E. Lutjeharms, G. J. Goni, C. J. D. Rautenbach, P. W. Froneman, M. Rouault, and S. Garzoli (2005), Monitoring the oceanic flow between Africa and Antarctica: Report of the first GoodHope cruise, *South African Journal of Science*, *101*(1-2), 29-35.

Arrigo, K. R. (2005), Marine microoganisms and global nutrient cycles, *Nature, 437*, 349-355.

Aumont, O., E. Maier-Reimer, S. Blain, and P. Monfray (2003), An ecosystem model of the global ocean including Fe, Si, P colimitations, *Global Biogeochemical Cycles*, *17*(2).

Averill, B. A. (1996), Dissimilatory nitrite and nitric oxide reductases, *Chemical Reviews*, *96*(7), 2951-2964.

Badger, M. (2003), The roles of carbonic anhydrases in photosynthetic CO2 concentrating mechanisms, *Photosynthesis Research*, *77*(2-3), 83-94.

Baker, A. R., and T. D. Jickells (2006), Mineral particle size as a control on aerosol iron solubility, *Geophysical Research Letters*, *33*(17).

Baker, A. R., and P. L. Croot (2010), Atmospheric and marine controls on aerosol iron solubility in seawater, *Marine Chemistry*, *120*(1-4), 4-13.

Baker, A. R., T. D. Jickells, M. Witt, and K. L. Linge (2006), Trends in the solubility of iron, aluminium, manganese and phosphorus in aerosol collected over the Atlantic Ocean, *Marine Chemistry*, *98*(1), 43-58.

Baker, A. R., K. Weston, S. D. Kelly, M. Voss, P. Streu, and J. N. Cape (2007), Dry and wet deposition of nutrients from the tropical Atlantic atmosphere: Links to primary productivity and nitrogen fixation, *Deep-Sea Research Part I-Oceanographic Research Papers*, *54*(10), 1704-1720.

Barnett, N., and P. Francis (2005a), Chemiluminescence: Liquid phase, in *Encyclopedia on Analytical Chemistry*, edited by P. J. Worsfold, A. Townshend and C. F. Poole, Elsevier, Oxford, England, pp. 511-521.

Barnett, N., and P. Francis (2005b), Chemiluminescence: Overview, in *Encyclopedia on Analytical Chemistry*, edited by P. J. Worsfold, A. Townshend and C. F. Poole, Elsevier, Oxford, England, pp. 506-511.

Barni, F., S. W. Lewis, A. Berti, G. M. Miskelly, and G. Lago (2007), Forensic application of the luminol reaction as a presumptive test for latent blood detection, *Talanta*, *72*(3), 896-913.

Behrenfeld, M. J., and Z. S. Kolber (1999), Widespread iron limitation of phytoplankton in the South Pacific Ocean, *Science*, *283*(5403), 840-843.

Behrenfeld, M. J., R. T. O'Malley, D. A. Siegel, C. R. McClain, J. L. Sarmiento, G. C. Feldman, A. J. Milligan, P. G. Falkowski, R. M. Letelier, and E. S. Boss (2006), Climate-driven trends in contemporary ocean productivity, *Nature*, *444*(7120), 752-755.

Behrenfeld, M. J., T. K. Westberry, E. S. Boss, R. T. O'Malley, D. A. Siegel, J. D. Wiggert, B. A. Franz, C. R. McClain, G. C. Feldman, S. C. Doney, J. K. Moore, G. Dall'Olmo, A. J. Milligan, I. Lima, and N. Mahowald (2009), Satellite-detected fluorescence reveals global physiology of ocean phytoplankton, *Biogeosciences*, *6*(5), 779-794.

Bennett, S. A., E. P. Achterberg, D. P. Connelly, P. J. Statham, G. R. Fones, and C. R. German (2008), The distribution and stabilisation of dissolved Fe in deep-sea hydrothermal plumes, *Earth and Planetary Science Letters*, *270*(3-4), 157-167.

Bergquist, B. A., and E. A. Boyle (2006), Dissolved iron in the tropical and subtropical Atlantic Ocean, *Global Biogeochemical Cycles*, *20*(1).

Berman-Frank, I., J. T. Cullen, Y. Shaked, R. M. Sherrell, and P. G. Falkowski (2001), Iron availability, cellular iron quotas, and nitrogen fixation in *Trichodesmium*, *Limnology and Oceanography*, *46*(6), 1249-1260.

Bertrand, E. M., M. A. Saito, J. M. Rose, C. R. Riesselman, M. C. Lohan, A. E. Noble, P. A. Lee, and G. R. DiTullio (2007), Vitamin B_{12} and iron colimitation of phytoplankton growth in the Ross Sea, *Limnology and Oceanography*, *52*(3), 1079-1093.

Bidigare, R. R., K. L. Hanson, K. O. Buesseler, S. G. Wakeham, K. H. Freeman, R. D. Pancost, F. J. Millero, P. Steinberg, B. N. Popp, M. Latasa, M. R. Landry, and E. A. Laws (1999), Iron-stimulated changes in ^{13}C fractionation and export by equatorial Pacific phytoplankton: Toward a paleogrowth rate proxy, *Paleoceanography*, *14*(5), 589-595.

Blain, S., G. Sarthou, and P. Laan (2008), Distribution of dissolved iron during the natural iron-fertilization experiment KEOPS (Kerguelen Plateau, Southern Ocean), *Deep-Sea Research Part II*, *55*(5-7), 594-605.

Boebel, O., C. Schmid, G. Podesta, and W. Zenk (1999), Intermediate water in the Brazil-Malvinas Confluence Zone: A Lagrangian view, *Journal of Geophysical Research-Oceans*, *104*(C9), 21063-21082.

Bowen, E. J. (1964), Chemiluminescence in solution, *Pure Applied Chemistry*, *9*(4), 473-480.

Bowie, A. R., and M. C. Lohan (2009), Determination of Iron in Seawater, in *Practical Guidelines For The Analysis of Seawater* edited by O. Wurl, Taylor and Francis Group, Boca Raton, FL, pp. 235-257.

Bowie, A. R., E. P. Achterberg, R. F. C. Mantoura, and P. J. Worsfold (1998), Determination of sub-nanomolar levels of iron in seawater using flow injection with chemiluminescence detection, *Analytica Chimica Acta*, *361*(3), 189-200.

Bowie, A. R., D. J. Whitworth, E. P. Achterberg, R. F. C. Mantoura, and P. J. Worsfold (2002a), Biogeochemistry of Fe and other trace elements (Al, Co, Ni) in the

upper Atlantic Ocean, *Deep-Sea Research Part I-Oceanographic Research Papers*, *49*(4), 605-636.

Bowie, A. R., E. P. Achterberg, P. N. Sedwick, S. Ussher, and P. J. Worsfold (2002b), Real-time monitoring of picomolar concentrations of iron(II) in marine waters using automated flow injection-chemiluminescence instrumentation, *Environmental Science & Technology*, *36*(21), 4600-4607.

Bown, J., M. Boye, and D. M. Nelson (2012), New insights on the role of organic speciation in the biogeochemical cycle of dissolved cobalt in the southeastern Atlantic and the Southern Ocean, *Biogeosciences*, *9*(7), 2719-2736.

Bown, J., M. Boye, A. Baker, E. Duvieilbourg, F. Lacan, F. Le Moigne, F. Planchon, S. Speich, and D. M. Nelson (2011), The biogeochemical cycle of dissolved cobalt in the Atlantic and the Southern Ocean south off the coast of South Africa, *Marine Chemistry*, *126*(1-4), 193-206.

Boyd, P. W., and M. J. Ellwood (2010), The biogeochemical cycle of iron in the ocean, *Nature Geoscience*, *3*(10), 675-682.

Boyd, P. W., T. Jickells, C. S. Law, S. Blain, E. A. Boyle, K. O. Buesseler, K. H. Coale, J. J. Cullen, H. J. W. de Baar, M. Follows, M. Harvey, C. Lancelot, M. Levasseur, N. P. J. Owens, R. Pollard, R. B. Rivkin, J. Sarmiento, V. Schoemann, V. Smetacek, S. Takeda, A. Tsuda, S. Turner, and A. J. Watson (2007), Mesoscale iron enrichment experiments 1993-2005: Synthesis and future directions, *Science*, *315*(5812), 612-617.

Boyd, P. W., A. J. Watson, C. S. Law, E. R. Abraham, T. Trull, R. Murdoch, D. C. E. Bakker, A. R. Bowie, K. O. Buesseler, H. Chang, M. Charette, P. Croot, K. Downing, R. Frew, M. Gall, M. Hadfield, J. Hall, M. Harvey, G. Jameson, J. LaRoche, M. Liddicoat, R. Ling, M. T. Maldonado, R. M. McKay, S. Nodder, S. Pickmere, R. Pridmore, S. Rintoul, K. Safi, P. Sutton, R. Strzepek, K. Tanneberger, S. Turner, A. Waite, and J. Zeldis (2000), A mesoscale phytoplankton bloom in the polar Southern Ocean stimulated by iron fertilization, *Nature*, *407*(6805), 695-702.

Boye, M., B. D. Wake, P. L. Garcia, J. Bown, A. R. Baker, and E. P. Achterberg (2012), Distributions of dissolved trace metals (Cd, Cu, Mn, Pb, Ag) in the southeastern Atlantic and the Southern Ocean, *Biogeosciences*, *9*(8), 3231-3246.

Boyle, E., and W. Jenkins (2008), Hydrothermal iron in the deep western South Pacific, *Geochimica Et Cosmochimica Acta*, *72*(12), A107-A107.

Boyle, E., R. Collier, A. T. Dengler, J. M. Edmond, A. C. Ng, and R. F. Stallard (1974), Chemical Mass Balance in Estuaries, *Geochimica Et Cosmochimica Acta*, *38*(11), 1719-1728.

Boyle, E. A., B. A. Bergquist, R. A. Kayser, and N. Mahowald (2005), Iron, manganese, and lead at Hawaii Ocean Time-series station ALOHA: Temporal variability and an intermediate water hydrothermal plume, *Geochimica Et Cosmochimica Acta*, *69*(4), 933-952.

Bozhevol'nov, E. A., and G. V. Serebriakova (1961), 8-p-(toluenesulfonilamino)-quinoline is a new fluorescent reagent for zinc and cadmium., *Khimicheskiie Reaktivy I Preparaty*, *24*, 36-42.

Brand, L. E., W. G. Sunda, and R. R. L. Guillard (1983), Limitation of Marine-Phytoplankton Reproductive Rates by Zinc, Manganese, and Iron, *Limnology and Oceanography*, *28*(6), 1182-1198.

Breitbarth, E., R. J. Bellerby, C. C. Neill, M. V. Ardelan, M. Meyerhofer, E. Zollner, P. L. Croot, and U. Riebesell (2010), Ocean acidification affects iron speciation during a coastal seawater mesocosm experiment, *Biogeosciences*, *7*(3), 1065-1073.

Brown, M. T., and K. W. Bruland (2008), An improved flow-injection analysis method for the determination of dissolved aluminum in seawater, *Limnology and Oceanography-Methods*, *6*, 87-95.

Bruland, K. W. (1980), Oceanographic Distributions of Cadmium, Zinc, Nickel, and Copper in the North Pacific, *Earth and Planetary Science Letters*, *47*(2), 176-198.

Bruland, K. W. (1989), Complexation of Zinc by Natural Organic-Ligands in the Central North Pacific, *Limnology and Oceanography*, *34*(2), 269-285.

Bruland, K. W., and R. P. Franks (1983), Mn, Ni, Cu, Zn and Cd in the western North Atlantic, in *Trace Metals in Seawater*, edited by C. S. Wong, K. W. Bruland, E. Boyle, D. Burton and E. D. Goldberg, NATO Conference Series IV; Marine Sciences, pp. 395-414.

Bruland, K. W., and M. C. Lohan (2003), Controls of Trace Metals in Seawater, in *The Oceans and Marine Geochemistry - Treatise on Geochemistry*, edited by H. Elderfield, Elsevier-Pergamon, Oxford, UK, pp. 81-103.

Bruland, K. W., G. A. Knauer, and J. H. Martin (1978), Zinc in Northeast Pacific Waters, *Nature*, *271*(5647), 741-743.

Bruland, K. W., J. R. Donat, and D. A. Hutchins (1991), Interactive Influences of Bioactive Trace-Metals on Biological Production in Oceanic Waters, *Limnology and Oceanography*, *36*(8), 1555-1577.

Bruland, K. W., K. J. Orians, and J. P. Cowen (1994), Reactive Trace-Metals in the Stratified Central North Pacific, *Geochimica Et Cosmochimica Acta*, *58*(15), 3171-3182.

Bruland, K. W., R. P. Franks, G. A. Knauer, and J. H. Martin (1979), Sampling and Analytical Methods for the Determination of Copper, Cadmium, Zinc, and Nickel at the Nanogram Per Liter Level in Sea-Water, *Analytica Chimica Acta*, *105*(1), 233-245.

Bruland, K. W., E. L. Rue, G. J. Smith, and G. R. DiTullio (2005), Iron, macronutrients and diatom blooms in the Peru upwelling regime: brown and blue waters of Peru, *Marine Chemistry*, *93*(2-4), 81-103.

Buck, C. S., W. M. Landing, J. A. Resing, and C. I. Measures (2010a), The solubility and deposition of aerosol Fe and other trace elements in the North Atlantic Ocean: Observations from the A16N CLIVAR/CO2 repeat hydrography section, *Marine Chemistry*, *120*(1-4), 57-70.

Buck, C. S., W. M. Landing, and J. A. Resing (2010b), Particle size and aerosol iron solubility: A high-resolution analysis of Atlantic aerosols, *Marine Chemistry*, *120*(1-4), 14-24.

Buck, K. N., and K. W. Bruland (2007), The physicochemical speciation of dissolved iron in the Bering Sea, Alaska, *Limnology and Oceanography*, *52*(5), 1800-1808.

Buesseler, K. O., J. E. Andrews, S. M. Pike, and M. A. Charette (2004), The effects of iron fertilization on carbon sequestration in the Southern Ocean, *Science*, *304*(5669), 414-417.

Campbell, L., E. J. Carpenter, J. P. Montoya, A. B. Kustka, and D. G. Capone (2005), Picoplankton community structure within and outside a *Trichodesmium* bloom

in the southwestern Pacific Ocean, *Vie Et Milieu-Life and Environment*, *55*(3-4), 185-195.

Cannizzaro, V., A. R. Bowie, A. Sax, E. P. Achterberg, and P. J. Worsfold (2000), Determination of cobalt and iron in estuarine and coastal waters using flow injection with chemiluminescence detection, *Analyst*, *125*(1), 51-57.

Capone, D. G., J. P. Zehr, H. W. Paerl, B. Bergman, and E. J. Carpenter (1997), Trichodesmium, a globally significant marine cyanobacterium, *Science*, *276*(5316), 1221-1229.

Carpenter, E. J., J. P. Montoya, J. Burns, M. R. Mulholland, A. Subramaniam, and D. G. Capone (1999), Extensive bloom of a N_2 fixing diatom/cyanobacterial association in the tropical Atlantic Ocean, *Marine Ecology Progress Series*, *185*, 273-283.

Carritt, D. E., and J. H. Carpenter (1966), Comparison and evaluation of currently employed modifications of the Winkler method for determining dissolved oxygen in seawater; a NASCO Report, *Journal of Marine Research*, *24*, 286 - 319.

Castrillejo, M., P. J. Statham, G. R. Phones, H. Planquette, F. Idrus, and K. Roberts (2013), Dissolved trace metals (Ni, Zn, Co, Cd, Al, and Mn) around the Crozet Islands, Southern Ocean, *Journal of Geophysical Research*, *118*, 5188-5201.

Charette, M. A., and S. B. Moran (1999), Rates of particle scavenging and particulate organic carbon export estimated using 234Th as a tracer in the subtropical and equatorial Atlantic Ocean, *Deep-Sea Research Part II*, *46*(5), 885-906.

Charette, M. A., M. E. Gonneea, P. J. Morris, P. Statham, F. Fones, H. Planquette, I. Salter, A. N. Garabato (2007), Radiam isotopes as traces of iron sources fueling a Southern Ocean phytoplankton bloom, *Deep Sea Research II*, *54*, 1989-1998.

Chen, Y., and R. L. Siefert (2004), Seasonal and spatial distributions and dry deposition fluxes of atmospheric total and labile iron over the tropical and subtropical North Atlantic Ocean, *Journal of Geophysical Research*, *109*(D9).

Chen, Y., A. Tovar-Sanchez, R. L. Siefert, S. A. Sanudo-Wilhelmy, and G. S. Zhuang (2011), Luxury uptake of aerosol iron by Trichodesmium in the western tropical North Atlantic, *Geophysical Research Letters*, *38*.

Chester, R. (2003), *Marine Geochemistry*, 2nd ed., Blackwell Science Ltd, 506 pp.

Chester, R., M. Nimmo, and S. Keyse (1996), The influence of Saharan and Middle Eastern desert-derived dust on the trace metal composition of Mediterranean aerosols and rainwaters: an overview., in *The Impact of Desert Dust across the Mediterranean*, edited by S. Guerzoni and R. Chester, Kluwer Academic Publishers, Dordrecht, pp. 253-273.

Chever, F., E. Bucciarelli, G. Sarthou, S. Speich, M. Arhan, P. Penven, and A. Tagliabue (2010), Physical speciation of iron in the Atlantic sector of the Southern Ocean along a transect from the subtropical domain to the Weddell Sea Gyre, *Journal of Geophysical Research-Oceans*, *115*.

Chiang, J. C. H., Y. Kushnir, and S. E. Zebiak (2000), Interdecadal changes in eastern Pacific ITCZ variability and its influence on the Atlantic ITCZ, *Geophysical Research Letters*, *27*(22), 3687-3690.

Chierici, M., A. Fransson, D. R. Turner, E. A. Pakhomov, and P. W. Froneman (2004), Variability in pH, fCO_2, oxygen and flux of CO_2 in the surface water along a transect in the Atlantic sector of the Southern Ocean, *Deep-Sea Research Part II*, *51*(22-24), 2773-2787.

Clayton, T. D., and R. H. Byrne (1993), Spectrophotometric Seawater Ph Measurements - Total Hydrogen-Ion Concentration Scale Calibration of M-Cresol Purple and at-Sea Results, *Deep-Sea Research Part I-Oceanographic Research Papers*, *40*(10), 2115-2129.

Coale, K. H., R. M. Gordon, and X. J. Wang (2005), The distribution and behavior of dissolved and particulate iron and zinc in the Ross Sea and Antarctic circumpolar current along 170 degrees W, *Deep-Sea Research Part I-Oceanographic Research Papers*, *52*(2), 295-318.

Coale, K. H., X. J. Wang, S. J. Tanner, and K. S. Johnson (2003), Phytoplankton growth and biological response to iron and zinc addition in the Ross Sea and Antarctic Circumpolar Current along 170 degrees W, *Deep-Sea Research Part Ii-Topical Studies in Oceanography*, *50*(3-4), 635-653.

Coale, K. H., K. S. Johnson, S. E. Fitzwater, R. M. Gordon, S. Tanner, F. P. Chavez, L. Ferioli, C. Sakamoto, P. Rogers, F. Millero, P. Steinberg, P. Nightingale, D. Cooper, W. P. Cochlan, M. R. Landry, J. Constantinou, G. Rollwagen, A. Trasvina, and R. Kudela (1996), A massive phytoplankton bloom induced by an

ecosystem-scale iron fertilization experiment in the equatorial Pacific Ocean, *Nature*, *383*(6600), 495-501.

Coale, K. H., K. S. Johnson, F. P. Chavez, K. O. Buesseler, R. T. Barber, M. A. Brzezinski, W. P. Cochlan, F. J. Millero, P. G. Falkowski, J. E. Bauer, R. H. Wanninkhof, R. M. Kudela, M. A. Altabet, B. E. Hales, T. Takahashi, M. R. Landry, R. R. Bidigare, X. J. Wang, Z. Chase, P. G. Strutton, G. E. Friederich, M. Y. Gorbunov, V. P. Lance, A. K. Hilting, M. R. Hiscock, M. Demarest, W. T. Hiscock, K. F. Sullivan, S. J. Tanner, R. M. Gordon, C. N. Hunter, V. A. Elrod, S. E. Fitzwater, J. L. Jones, S. Tozzi, M. Koblizek, A. E. Roberts, J. Herndon, J. Brewster, N. Ladizinsky, G. Smith, D. Cooper, D. Timothy, S. L. Brown, K. E. Selph, C. C. Sheridan, B. S. Twining, and Z. I. Johnson (2004), Southern ocean iron enrichment experiment: Carbon cycling in high- and low-Si waters, *Science*, *304*(5669), 408-414.

Coles, V. J., and R. R. Hood (2007), Modeling the impact of iron and phosphorus limitations on nitrogen fixation in the Atlantic Ocean, *Biogeosciences*, *4*(4), 455-479.

Collier, R., and J. Edmond (1984), The trace element geochemistry of marine biogenic particulate matter, *Progress in Oceanography*, *13*, 113-199.

Crawford, D. W., M. S. Lipsen, D. A. Purdie, M. C. Lohan, P. J. Statham, F. A. Whitney, J. N. Putland, W. K. Johnson, N. Sutherland, T. D. Peterson, P. J. Harrison, and C. S. Wong (2003), Influence of zinc and iron enrichments on phytoplankton growth in the northeastern subarctic Pacific, *Limnology and Oceanography*, *48*(4), 1583-1600.

Croft, M. T., A. D. Lawrence, E. Raux-Deery, M. J. Warren, and A. G. Smith (2005), Algae acquire vitamin B_{12} through a symbiotic relationship with bacteria, *Nature*, *438*(7064), 90-93.

Croot, P. L., O. Baars, and P. Streu (2011), The distribution of dissolved zinc in the Atlantic sector of the Southern Ocean, *Deep-Sea Res. Part II*, *58*(25-26), 2707-2719.

Cullen, J. T. (2006), On the Nonlinear Relationship between Dissolved Cadmium and Phosphate in the Modern Global Ocean: Could Chronic Iron Limitation of Phytoplankton Growth Cause the Kink?, *Limnology and Oceanography*, *51*, 1369-1380.

Cullen, J. T., Z. Chase, K. H. Coale, S. E. Fitzwater, and R. M. Sherrell (2003), Effect of iron limitation on the cadmium to phosphorus ratio of natural phytoplankton assemblages from the Southern Ocean, *Limnology and Oceanography*, *48*, 1079-1087.

Cutter, G., P. Anderssen, L. Codispoti, P. L. Croot, R. Francois, M. C. Lohan, H. Obata, and M. Rutgers van der Leoff (2010), Sampling and Sample-handling Protocols for GEOTRACES Cruises, geotraces.org

Dammshäuser, A., T. Wagener, and P. L. Croot (2011), Surface water dissolved aluminum and titanium: Tracers for specific time scales of dust deposition to the Atlantic?, *Geophysical Research Letters*, *38*(24).

Danilovtseva, E., V. Aseyev, M. Karesoja, and V. Annenkov (2009), Sorption of silicic acid from non-saturated aqueous solution by a complex of zinc ions with poly(vinylamine), *European Polymer Journal*, *45*, 1391-1396.

Davey, M., G. A. Tarran, M. M. Mills, C. Ridame, R. J. Geider, and J. LaRoche (2008), Nutrient limitation of picophytoplankton photosynthesis and growth in the tropical North Atlantic, *Limnology and Oceanography*, *53*(5), 1722-1733.

de Baar, H. J. W. (1994), von Liebig's Law of the Minimum and plankton ecology (1899-1991), *Progress in Oceanography*, *33*(4), 347-386.

de Baar, H. J. W., and C. L. de La Rocha (2003), Trace Metals in the Oceans: evolution, biology and global change, in *Marine Science Frontiers for Europe*, edited by G. Wefer, F. Lamy and F. Mantoura, Springer-Verlag, Berlin, Heidelberg, New York, Tokyo, pp. 79-105.

de Baar, H. J. W., P. M. Saager, R. F. Nolting, and J. Vandermeer (1994), Cadmium Versus Phosphate in the World Ocean, *Marine Chemistry*, *46*(3), 261-281.

de Baar, H. J. W., K. R. Timmermans, P. Laan, H. H. De Porto, S. Ober, J. J. Blom, M. C. Bakker, J. Schilling, G. Sarthou, M. G. Smit, and M. Klunder (2008), Titan: A new facility for ultraclean sampling of trace elements and isotopes in the deep oceans in the international Geotraces program, *Marine Chemistry*, *111*(1-2), 4-21.

de Baar, H. J. W., P. W. Boyd, K. H. Coale, M. R. Landry, A. Tsuda, P. Assmy, D. C. E. Bakker, Y. Bozec, R. T. Barber, M. A. Brzezinski, K. O. Buesseler, M. Boye, P. L. Croot, F. Gervais, M. Y. Gorbunov, P. J. Harrison, W. T. Hiscock, P. Laan, C. Lancelot, C. S. Law, M. Levasseur, A. Marchetti, F. J. Millero, J. Nishioka, Y.

Nojiri, T. van Oijen, U. Riebesell, M. J. A. Rijkenberg, H. Saito, S. Takeda, K. R. Timmermans, M. J. W. Veldhuis, A. M. Waite, and C. S. Wong (2005), Synthesis of iron fertilization experiments: From the iron age in the age of enlightenment, *Journal of Geophysical Research-Oceans*, *110*(C9).

de Jong, J. T. M., J. den Das, U. Bathmann, M. H. C. Stoll, G. Kattner, R. F. Nolting, and H. J. W. de Baar (1998), Dissolved iron at subnanomolar levels in the Southern Ocean as determined by ship-board analysis, *Analytica Chimica Acta*, *377*(2-3), 113-124.

de La Rocha, C. L. (2003), The Biological Pump, in *The Oceans and Marine Geochemistry - Treatise on Geochemistry*, edited by H. D. Holland and K. K. Turekian, Elsevier-Pergamon, Oxford, UK, pp. 83 - 111.

de La Rocha, C. L., D. A. Hutchins, M. A. Brzezinski, and Y. H. Zhang (2000), Effects of iron and zinc deficiency on elemental composition and silica production by diatoms, *Marine Ecology Progress Series*, *195*, 71-79.

de Ruijter, W. P. M., A. Biastoch, S. S. Drijfhout, J. R. E. Lutjeharms, R. P. Matano, T. Pichevin, P. J. van Leeuwen, and W. Weijer (1999), Indian-Atlantic interocean exchange: Dynamics, estimation and impact, *Journal of Geophysical Research-Oceans*, *104*(C9), 20885-20910.

Desboeufs, K. V., R. Losno, F. Vimeux, and S. Cholbi (1999), The pH-dependent dissolution of wind-transported Saharan dust, *Journal of Geophysical Research-Atmospheres*, *104*(D17), 21287-21299.

Desboeufs, K. V., A. Sofikitis, R. Losno, J. L. Colin, and P. Ausset (2005), Dissolution and solubility of trace metals from natural and anthropogenic aerosol particulate matter, *Chemosphere*, *58*(2), 195-203.

Diaz-Garcia, M. E., and R. Badia-Laiño (2005a), Fluorescence: Overview, in *Encyclopedia on Analytical Chemistry*, edited by P. J. Worsfold, A. Townshend and C. F. Poole, Elsevier, Oxford, England, pp. 97-106.

Diaz-Garcia, M. E., and R. Badia-Laiño (2005b), Fluorescence: Derivarization, in *Encyclopedia on Analytical Chemistry*, edited by P. J. Worsfold, A. Townshend and C. F. Poole, Elsevier, Oxford, England, pp. 138-148.

Diaz-Garcia, M. E., and R. Badia-Laiño (2005c), Fluorescence: Florescence Labelling, in *Encyclopedia on Analytical Chemistry*, edited by P. J. Worsfold, A. Townshend and C. F. Poole, Elsevier, Oxford, England, pp. 149-163.

Dickson, A. G., C. L. Sabine, and J. R. Christian (2007), Guide to best practices for ocean CO_2 measurements, *PICES Special Publication*, *3*, pp. 191.

Dierssen, H., W. Balzer, and W. M. Landing (2001), Simplified synthesis of an 8-hydroxyquinoline chelating resin and a study of trace metal profiles from Jellyfish Lake, Palau, *Marine Chemistry*, *73*(3-4), 173-192.

Dlugokencky, E., and P. P. Tans (2013), Trends in Atmospheric Carbon Dioxide - Mauna Loa NOAA/ESRL www.esrl.noaa.gov/gmd/ccgg/trends/.

Donat, J. R., and K. W. Bruland (1988), Direct Determination of Dissolved Cobalt and Nickel in Seawater by Differential Pulse Cathodic Stripping Voltammetry Preceded by Adsorptive Collection of Cyclohexane-1,2-Dione Dioxime Complexes, *Analytical Chemistry*, *60*(3), 240-244.

Donners, J., and S. S. Drijfhout (2004), The Lagrangian view of South Atlantic Interocean exchange in a global ocean model compared with inverse model results, *Journal of Physical Oceanography*, *34*(5), 1019-1035.

Draxler, R. R., and G. D. Rolph (2013), HYPLIT (Hybrid Single-Particle Langrangian Intergrated Trajectory) Model access via NOAA ARL READY Website (http://www.arl.noaa.gov/HYSPLIT.php). NOAA Air Resources Laboratory, College Park, MD

Droop, M. R. (1974), Nutrient Status of Algal Cells in Continuous Culture, *Journal of the Marine Biological Association of the United Kingdom*, *54*(4), 825-855.

Droop, M. R. (2007), Vitamins, phytoplankton and bacteria: symbiosis or scavenging?, *Journal of Plankton Research*, *29*(2), 107-113.

Duce, R. A., and N. W. Tindale (1991), Atmospheric Transport of Iron and Its Deposition in the Ocean, *Limnology and Oceanography*, *36*(8), 1715-1726.

Dyhrman, S. T., and B. Palenik (2003), Characterization of ectoenzyme activity and phosphate-regulated proteins in the coccolithophorid Emiliania huxleyi, *Journal of Plankton Research*, *25*(10), 1215-1225.

Elderfield, H., and A. Schultz (1996), Mid-ocean ridge hydrothermal fluxes and the chemical composition of the ocean, *Annual Review of Earth and Planetary Sciences*, *24*, 191-224.

Ellwood, M. J. (2004), Zinc and cadmium speciation in subantarctic waters east of New Zealand, *Marine Chemistry*, *87*(1-2), 37-58.

Ellwood, M. J. (2008), Wintertime trace metal (Zn, Cu, Ni, Cd, Pb and Co) and nutrient distributions in the Subantarctic Zone between 40-52 degrees S; 155-160 degrees E, *Marine Chemistry*, *112*(1-2), 107-117.

Ellwood, M. J., and C. M. G. van den Berg (2000), Zinc speciation in the Northeastern Atlantic Ocean, *Marine Chemistry*, *68*(4), 295-306.

Ellwood, M. J., and K. A. Hunter (2000a), The incorporation of zinc and iron into the frustule of the marine diatom Thalassiosira pseudonana, *Limnology and Oceanography*, *45*(7), 1517-1524.

Ellwood, M. J., and K. A. Hunter (2000b), Variations in the Zn/Si record over the last intergalcial glacial transition, *Paleoceanography*, *15*, 506-514.

Ellwood, M. J., and C. M. G. van den Berg (2001), Determination of organic complexation of cobalt in seawater by cathodic stripping voltammetry, *Marine Chemistry*, *75*, 33-47.

Elrod, V. A., W. M. Berelson, K. H. Coale, and K. S. Johnson (2004), The flux of iron from continental shelf sediments: A missing source for global budgets, *Geophysical Research Letters*, *31*(12).

Escoube, R., O. J. Rouxel, E. Sholkovitz, and O. F. X. Donard (2009), Iron isotope systematics in estuaries: The case of North River, Massachusetts (USA), *Geochimica Et Cosmochimica Acta*, *73*(14), 4045-4059.

Evangelista, H., J. Maldonado, E. A. dos Santos, R. H. M. Godoi, C. A. E. Garcia, V. M. T. Garcia, E. Jonhson, K. D. da Cunha, C. B. Leite, R. Van Grieken, K. Van Meel, Y. Makarovska, and D. M. Gaiero (2010), Inferring episodic atmospheric iron fluxes in the Western South Atlantic, *Atmospheric Environment*, *44*(5), 703-712.

Evmiridis, N. P., A. G. Vlessidis, and N. C. Thanasoulias (2007), Chemical analysis through CL-detection assisted by periodate oxidation, *Bioinorganic Chemistry and Applications.*

Fahrni, C. J., and T. V. O'Halloran (1999), Aqueous coordination chemistry of quinoline-based fluorescence probes for the biological chemistry of zinc, *Journal of the American Chemical Society*, *121*(49), 11448-11458.

Falcon, M., J. Guiteras, A. Izquierdo, and M. D. Prat (1993), Spectrofluorometric determination of zinc in foods with 8-(p-toluenesulphonamido)quinoline in micellar medium, *Talanta*, *40*(1), 17-20.

Falkowski, P., R. J. Scholes, E. Boyle, J. Canadell, D. Canfield, J. Elser, N. Gruber, K. Hibbard, P. Hogberg, S. Linder, F. T. Mackenzie, B. Moore, T. Pedersen, Y. Rosenthal, S. Seitzinger, V. Smetacek, and W. Steffen (2000), The global carbon cycle: A test of our knowledge of earth as a system, *Science*, *290*(5490), 291-296.

Falkowski, P. G. (1994), The Role of Phytoplankton Photosynthesis in Global Biogeochemical Cycles, *Photosynthesis Research*, *39*(3), 235-258.

Falkowski, P. G. (2002), The ocean's invisible forest - Marine phytoplankton play a critical role in regulating the earth's climate. Could they also be used to combat global warming, *Scientific American*, *287*(2), 54-61.

Falkowski, P. G., R. T. Barber, and V. Smetacek (1998), Biogeochemical controls and feedbacks on ocean primary production, *Science*, *281*(5374), 200-206.

Fan, S. M., W. J. Moxim, and H. Levy (2006), Aeolian input of bioavailable iron to the ocean, *Geophysical Research Letters*, *33*(7).

Feely, R. A., C. L. Sabine, R. Schlitzer, J. L. Bullister, S. Mecking, and D. Greeley (2004), Oxygen utilization and organic carbon remineralization in the upper water column of the Pacific Ocean, *Journal of Oceanography*, *60*(1), 45-52.

Feng, Y., C. E. Hare, J. M. Rose, S. M. Handy, G. R. DiTullio, P. A. Lee, W. O. Smith, J. Peloquin, S. Tozzi, J. Sun, Y. Zhang, R. B. Dunbar, M. C. Long, B. Sohst, M. Lohan, and D. A. Hutchins (2010), Interactive effects of iron, irradiance and CO2 on Ross Sea phytoplankton, *Deep-Sea Research Part I-Oceanographic Research Papers*, *57*(3), 368-383.

Field, C. B., M. J. Behrenfeld, J. T. Randerson, and P. Falkowski (1998), Primary production of the biosphere: Integrating terrestrial and oceanic components, *Science*, *281*(5374), 237-240.

Fitzsimmons, J. N., R. F. Zhang, and E. A. Boyle (2013), Dissolved iron in the tropical North Atlantic Ocean, *Marine Chemistry*, *154*, 87-99.

Fitzsimons, M. F., M. Lohan, G. E. Millwood, and A. D. Tappin (2011), The Role of Suspended Particles, in *Treatise on Estuarine and Coastal Science; Volume 4, Geochemistry of Estuaries and Coasts*, edited by G. Shimmield, Elsevier, pp. 71-114.

Fitzwater, S. E., K. S. Johnson, R. M. Gordon, K. H. Coale, and W. O. Smith (2000), Trace metal concentrations in the Ross Sea and their relationship with nutrients and phytoplankton growth, *Deep-Sea Research II*, *47*, 3159-3179.

Flynn, K. J., and C. R. Hipkin (1999), Interactions between iron, light, ammonium, and nitrate: Insights from the construction of a dynamic model of algal physiology, *Journal of Phycology*, *35*(6), 1171-1190.

Formenti, P., W. Elbert, W. Maenhaut, J. Haywood, and M. O. Andreae (2003), Chemical composition of mineral dust aerosol during the Saharan Dust Experiment (SHADE) airborne campaign in the Cape Verde region, September 2000, *Journal of Geophysical Research-Atmospheres*, *108*(D18).

Fouquet, Y., U. Vonstackelberg, J. L. Charlou, J. Erzinger, P. M. Herzig, R. Muhe, and M. Wiedicke (1993), Metallogenesis in Back-Arc Environments - the Lau Basin Example, *Economic Geology and the Bulletin of the Society of Economic Geologists*, *88*(8), 2154-2181.

Franck, V. M., M. A. Brzezinski, K. H. Coale, and D. M. Nelson (2000), Iron and silicic acid concentrations regulate Si uptake north and south of the Polar Frontal Zone in the Pacific Sector of the Southern Ocean, *Deep-Sea Reseach II*, *47*, 3315-3338.

Frederickson, C. J., E. J. Kasarskis, D. Ringo, and R. E. Frederickson (1987), A quinoline fluorescence method for visualizing and assaying the histochemically reactive zinc (bouton zinc) in the brain, *Journal of Neuroscience Methods*, *20*(2), 91-103.

Fu, F. X., M. R. Mulholland, N. S. Garcia, A. Beck, P. W. Bernhardt, M. E. Warner, S. A. Sanudo-Wilhelmy, and D. A. Hutchins (2008), Interactions between changing pCO_2, N_2 fixation, and Fe limitation in the marine unicellular cyanobacterium *Crocosphaera*, *Limnology and Oceanography*, *53*(6), 2472-2484.

GEOTRACES (2006), *GEOTRACES Science Plan*, Mayland: Scientific Committee on Oceanic Research, pp.

German, C. R., and K. L. Von Damm (2003), Hydrothermal Processes in *The Oceans and Marine Geochemistry - Treatise on Geochemistry*, edited by H. Elderfield, Elsevier-Pergamon, Oxford, UK, pp. 181-222.

Gist, N., P. Serret, E. M. S. Woodward, K. Chamberlain, and C. Robinson (2009), Seasonal and spatial variability in plankton production and respiration in the Subtropical Gyres of the Atlantic Ocean, *Deep-Sea Research Part Ii-Topical Studies in Oceanography*, *56*(15), 931-940.

Gosnell, K. J., W. M. Landing, and A. Milne (2012), Fluorometric detection of total dissolved zinc in the southern Indian Ocean, *Marine Chemistry*, *132*, 68-76.

Grachev, M. A., V. V. Annenkov, and Y. V. Likhoshway (2008), Silicon nanotechnologies of pigmented henterokonts, *Bioessays*, *30*, 328-337.

Grachev, M. A., T. A. Sherbakova, Y. A. Masyukova, and Y. V. Likhoshway (2005), A potential zinc-binding motif in silicic acis transport proteins of diatoms, *Diatom Res.*, *20*, 409-411.

Gran, H. H. (1931), On the conditions for the production of plankton in the sea, *Rapports et Proces-Verbaux des Reunions du Conseil International Permanent pour l'Exploration de la Mer*, *75*, 37-46.

Gunderman, K. D., and F. McCapra (1987), *Chemiluminescence in orgainc chemistry*, Springer-Verlag, Berlin, 217 pp.

Hardardóttir, V., K. L. Brown, T. Fridriksson, J. W. Hedenquist, M. D. Hannington, and S. Thorhallsson (2009), Metals in deep liquid of the Reykjanes geothermal system, southwest Iceland: Implications for the composition of seafloor black smoker fluids, *Geological Society of America - Geology*, *37*, 1103-1106.

Hart, T. J. (1934), On the Phytoplankton of the South-west Atlantic and the Bellingshausen Sea. 1929 - 31, 268 pp, Cambridge University Press, Discovery reports vol. 8.

Hastenrath, S., and J. Merle (1987), Annual Cycle of Subsurface Thermal Structure in the Tropical Atlantic Ocean, *Journal of Physical Oceanography*, *17*(9), 1518-1538.

Helmers, E., and O. Schrems (1995), Wet Deposition of Metals to the Tropical North and the South-Atlantic Ocean, *Atmospheric Environment*, *29*(18), 2475-2484.

Hendry, K. R., and E. M. Rickaby (2008), Opal (Zn/Si) ratios as a nearshore geochemical proxy in coastal Antarctica, *Paleoceanography*, *23*, 2.

Ho, T. Y., A. Quigg, Z. V. Finkel, A. J. Milligan, K. Wyman, P. G. Falkowski, and F. M. M. Morel (2003), The elemental composition of some marine phytoplankton, *Journal of Phycology*, *39*(6), 1145-1159.

Holm-Hansen, O., C. J. Lorenzen, and J. D. H. Holmes (1965), Fluorometric determination of chlorophyll, *J. Const. Int. Explor. Mer., 30*, 3-15.

Homoky, W. B., S. G. John, T. M. Conway, and R. A. Mills (2013), Distinct iron isotopic signatures and supply from marine sediment dissolution, *Nature Communications, 4*.

Hopkinson, B. M., and K. A. Barbeau (2007), Organic and redox speciation of iron in the eastern tropical North Pacific suboxic zone, *Marine Chemistry, 106*(1-2), 2-17.

Hsieh, Y. T., G. M. Henderson, and A. L. Thomas (2011), Combining seawater ^{232}Th and ^{230}Th concentrations to determine dust fluxes to the surface ocean, *Earth and Planetary Science Letters*, *312*(3-4), 280-290.

Hsieh, Y. T., W. Geibert, E. M. S. Woodward, and G. M. Henderson (2013), Ra isotopes as tracers for ocean mixing and nutrient supply, *Marine Chemistry, in press*.

Hu, H. H., Y. J. Shi, W. Cong, and Z. L. Cai (2003), Growth and photosynthesis limitation of marine red tide alga Skeletonema costatum by low concentrations of Zn2+, *Biotechnology Letters*, *25*(22), 1881-1885.

Huhn, O., H. H. Hellmer, M. Rhein, C. Rodehacke, W. Roether, M. P. Schodlok, and M. Schroder (2008), Evidence of deep- and bottom-water formation in the western Weddell Sea, *Deep Sea Reseach II, 55*, 1098-1116.

Hurst, M. P., and K. W. Bruland (2008), The effects of the San Francisco Bay plume on trace metal and nutrient distributions in the Gulf of the Farallones, *Geochimica Et Cosmochimica Acta, 72*(2), 395-411.

Hutchins, D. A., and K. W. Bruland (1994), Grazer-Mediated Regeneration and Assimilation of Fe, Zn and Mn from Planktonic Prey, *Marine Ecology Progress Series, 110*(2-3), 259-269.

Hutchins, D. A., G. R. Ditullio, and K. W. Bruland (1993), Iron and regenerated production: evidence for biological iron recycling, *Limnology and Oceanography*, *38*(6), 1242-1255.

Hydes, D. J., M. Aoyama, A. Aminot, K. Bakker, S. Becker, S. Coverly, A. Daniel, A. G. Dickson, O. Grosso, R. Kerouel, J. van Ooijen, K. Sato, T. Tanhua, E. M. S. Woodward, and J. Z. Zhang (2010), The GO-SHIP Repeat Hydrography Manual:

A collection of Expert Reports and Guidlines, IOCCP Report No. 14, ICPO Publication Series No. 134, Version 1.

Inman, S. M., P. M. Thibado, E. J. Stromvall, and S. H. Lieberman (1989), Use of micellularized P-Tosyl-8-Aminoquinoline for Direct Detection of Nanomolar Levels of Zinc and Cadmium in Aqueous Solutions, in *Pittsburgh Conference and Exposition on Analytical Chemistry and Applied Spectroscopy*, edited, Naval Oceans Systems Center.

Jakuba, R. W., J. W. Moffett, and S. T. Dyhrman (2008), Evidence for the linked biogeochemical cycling of zinc, cobalt, and phosphorus in the western North Atlantic Ocean, *Global Biogeochemical Cycles*, *22*, GB4012.

Jakuba, R. W., M. A. Saito, J. W. Moffett, and Y. Xu (2012), Dissolved zinc in the subarctic North Pacific and Bering Sea: Its distribution, speciation, and importance to primary producers, *Global Biogeochemical Cycles*, *26*.

Jannasch, H. W., B. D. Honeyman, and J. W. Murray (1996), Marine scavenging: The relative importance of mass transfer and reaction rates, *Limnology and Oceanography*, *41*(1), 82-88.

Jeandel, C., F. Lacan, and M. Labatut (2010), trace element concentrations of the suspended particles in the Southern Ocean (Bonus/GoodHope transect), paper presented at AGU OS10 Scientific Program, Ocean Sciences Conference (AGU/ASLO), Portland, USA.

Jickells, T. D., and L. Spokes (2001), Atmospheric iron inputs to the oceans, in *The Biogeochemistry of Iron in Seawater*, edited by K. Hunter and D. Turner, John Wiley, New York, pp. 85-122.

Jickells, T. D., T. M. Church, and W. G. Deuser (1987), A comparison of atmospheric inputs and deep-ocean particle fluxes for the Sargasso Sea, *Global Biogeochemical Cycles*, *1*, 117-130.

Jickells, T. D., Z. S. An, K. K. Andersen, A. R. Baker, G. Bergametti, N. Brooks, J. J. Cao, P. W. Boyd, R. A. Duce, K. A. Hunter, H. Kawahata, N. Kubilay, J. laRoche, P. S. Liss, N. Mahowald, J. M. Prospero, A. J. Ridgwell, I. Tegen, and R. Torres (2005), Global iron connections between desert dust, ocean biogeochemistry, and climate, *Science*, *308*(5718), 67-71.

Johnson, G. C. (2008), Quantifying Antarctic Bottom Water and North Atlantic Deep Water volumes, *Journal of Geophysical Research-Oceans*, *113*(C5).

Johnson, K. S., R. M. Gordon, and K. H. Coale (1997), What controls dissolved iron concentrations in the world ocean?, *Marine Chemistry*, *57*(3-4), 137-161.

Johnson, K. S., V. Elrod, S. Fitzwater, J. Plant, E. Boyle, B. Bergquist, K. Bruland, A. Aguilar-Islas, K. Buck, M. Lohan, G. J. Smith, B. Sohst, K. Coale, M. Gordon, S. Tanner, C. Measures, J. Moffett, K. Barbeau, A. King, A. Bowie, Z. Chase, J. Cullen, P. Laan, W. Landing, J. Mendez, A. Milne, H. Obata, T. Doi, L. Ossiander, G. Sarthou, P. Sedwick, S. Van den Berg, L. Laglera-Baquer, J.-f. Wu, and Y. Cai (2007), Developing standards for dissolved iron in seawater, *Eos, Transactions American Geophysical Union*, *88*(11), 131-132.

Johnson, M. S., N. Meskhidze, F. Solmon, S. Gasso, P. Y. Chuang, D. M. Gaiero, R. M. Yantosca, S. L. Wu, Y. X. Wang, and C. Carouge (2010), Modeling dust and soluble iron deposition to the South Atlantic Ocean, *Journal of Geophysical Research-Atmospheres*, *115*.

Judson, S. (1968), Erosion of the land, or What's Happening to Our Continents?, *American Scientist*, *56*(4), 356-374.

Jullion, L., K. J. Heywood, A. C. N. Garabato, and D. P. Stevens (2010), Circulation and Water Mass Modification in the Brazil-Malvinas Confluence, *Journal of Physical Oceanography*, *40*(5), 845-864.

Kallos, G., A. Papadopoulos, P. Katsafados, and S. Nickovic (2006), Transatlantic Saharan dust transport: Model simulation and results, *Journal of Geophysical Research-Atmospheres*, *111*(D9).

Karl, D., R. Letelier, L. Tupas, J. Dore, J. Christian, and D. Hebel (1997), The role of nitrogen fixation in biogeochemical cycling in the subtropical North Pacific Ocean, *Nature*, *388*(6642), 533-538.

Karl, D., A. Michaels, B. Bergman, D. Capone, E. Carpenter, R. Letelier, F. Lipschultz, H. Paerl, D. Sigman, and L. Stal (2002), Dinitrogen fixation in the world's oceans, *Biogeochemistry*, *57*(1), 47-+.

Karstensen, J., L. Stramma, and M. Visbeck (2008), Oxygen minimum zones in the eastern tropical Atlantic and Pacific oceans, *Progress in Oceanography*, *77*(4), 331-350.

Kaufman, Y. J., I. Koren, L. A. Remer, D. Tanre, P. Ginoux, and S. Fan (2005), Dust transport and deposition observed from the Terra-Moderate Resolution Imaging

Spectroradiometer (MODIS) spacecraft over the Atlantic ocean, *Journal of Geophysical Research-Atmospheres*, *110*(D10).

Kearns, D. R. (1971), Physical and Chemical Properties of Singlet Molecular Oxygen, *Chemical Reviews*, *71*(4), 395-&.

Kimura, E., and S. Aoki (2001), Chemistry of zinc(II) fluorophore sensors, *Biometals*, *14*(3-4), 191-204.

Kirchman, D. L. (1996), Oceanography - Microbial ferrous wheel, *Nature*, *383*(6598), 303-304.

Klunder, M. B., P. Laan, R. Middag, H. J. W. De Baar, and J. C. Ooijen (2011), Dissolved iron in the Southern Ocean (Atlantic sector), *Deep-Sea Reseach II*, *58*, 2678-2694.

Knauer, G. A., J. H. Martin, and R. M. Gordon (1982), Cobalt in Northeast Pacific Waters, *Nature*, *297*(5861), 49-51.

Kremling, K., and P. Streu (2001), The behaviour of dissolved Cd, Co, Zn, and Pb in North Atlantic near-surface waters (30 degrees N/60 degrees W-60 degrees N/2 degrees W), *Deep-Sea Research Part I-Oceanographic Research Papers*, *48*(12), 2541-2567.

Küpper, H., I. Šetlik, S. Seibert, O. Prášil, E. Šetlikova, M. Strittmatter, O. Levitan, J. Lohscheider, I. Adamska, and I. Berman-Frank (2008), Iron limitation in the marine cyanobacterium Trichodesmium reveals new insights into regulation of photosynthesis and nitrogen fixation, *New Phytologist*, *179*(3), 784-798.

Kupriyanova, E. V., and N. A. Pronina (2011), Carbonic Anhydrase: Enzyme That Has Transformed the Biosphere, *Russian Journal of Plant Physiology*, *58*(2), 197-209.

Kuss, J., and K. Kremling (1999a), Spatial variability of particle associated trace elements in near-surface waters of the North Atlantic (30 degrees N/60 degrees W to 60 degrees N/2 degrees W), derived by large-volume sampling, *Marine Chemistry*, *68*(1-2), 71-86.

Kuss, J., and K. Kremling (1999b), Particulate trace element fluxes in the deep northeast Atlantic Ocean, *Deep-Sea Research Part I-Oceanographic Research Papers*, *46*(1), 149-169.

Kustka, A., S. Sanudo-Wilhelmy, E. J. Carpenter, D. G. Capone, and J. A. Raven (2003a), A revised estimate of the iron use efficiency of nitrogen fixation, with

special reference to the marine cyanobacterium Trichodesmium spp. (Cyanophyta), *Journal of Phycology*, *39*(1), 12-25.

Kustka, A. B., S. A. Sanudo-Wilhelmy, E. J. Carpenter, D. Capone, J. Burns, and W. G. Sunda (2003b), Iron requirements for dinitrogen- and ammonium-supported growth in cultures of Trichodesmium (IMS 101): Comparison with nitrogen fixation rates and iron: carbon ratios of field populations, *Limnology and Oceanography*, *48*(5), 1869-1884.

Laes, A., S. Blain, P. Laan, S. J. Ussher, E. P. Achterberg, P. Treguer, and H. J. W. de Baar (2007), Sources and transport of dissolved iron and manganese along the continental margin of the Bay of Biscay, *Biogeosciences*, *4*(2), 181-194.

Lai, X., K. Norisuye, M. Mikata, T. Minami, A. R. Bowie, and Y. Sohrin (2008), Spatial and temporal distribution of Fe, Ni, Cu and Pb along 140 degrees E in the Southern Ocean during austral summer 2001/02, *Marine Chemistry*, *111*(3-4), 171-183.

Landing, W. M., and K. W. Bruland (1987), The Contrasting Biogeochemistry of Iron and Manganese in the Pacific-Ocean, *Geochimica Et Cosmochimica Acta*, *51*(1), 29-43.

Landing, W. M., C. Haraldsson, and N. Paxeus (1986), Vinyl Polymer Agglomerate Based Transition-Metal Cation Chelating Ion-Exchange Resin Containing the 8-Hydroxyquinoline Functional-Group, *Analytical Chemistry*, *58*(14), 3031-3035.

Lane, E. S., D. M. Semeniuk, R. F. Strzepek, J. T. Cullen, and M. T. Maldonado (2009), Effects of iron limitation on intracellular cadmium of cultured phytoplankton: Implications for surface dissolved cadmium to phosphate ratios, *Marine Chemistry*, *115*(3-4), 155-162.

Lane, T. W., and F. M. M. Morel (2000), Regulation of carbonic anhydrase expression by zinc, cobalt, and carbon dioxide in the marine diatom *Thalassiosira weissflogii*, *Plant Physiology*, *123*(1), 345-352.

Lane, T. W., M. A. Saito, G. N. George, I. J. Pickering, R. C. Prince, and F. M. M. Morel (2005), A cadmium enzyme from a marine diatom, *Nature*, *435*(7038), 42-42.

Laws, E. A., P. G. Falkowski, W. O. Smith, H. Ducklow, and J. J. McCarthy (2000), Temperature effects on export production in the open ocean, *Global Biogeochemical Cycles*, *14*(4), 1231-1246.

Leblanc, K., C. E. Hare, P. W. Boyd, K. W. Bruland, B. Sohst, S. Pickmere, M. C. Lohan, K. Buck, M. Ellwood, and D. A. Hutchins (2005), Fe and Zn effects on the Si cycle and diatom community structure in two contrasting high and low-silicate HNLC areas, *Deep-Sea Research Part I - Oceanographic Research Papers*, *52*(10), 1842-1864.

Lee, J. G., and F. M. M. Morel (1995), Replacement of Zinc by Cadmium in Marine-Phytoplankton, *Marine Ecology Progress Series*, *127*(1-3), 305-309.

Lewis, E., and D. W. R. Wallace (1998), Program developed for CO_2 system calculations ORNL/CDIAC-IOS, edited, Carbon Dioxide Information Analysis Center, Oak Ridge National Laboratory, US Department for Energy, Oak Ridge, Tennessee.

Li, Y. H., and L. H. Chan (1979), Desorption of Ba and ^{226}Ra from River-Borne Sediments in the Hudson Estuary, *Earth and Planetary Science Letters*, *43*(3), 343-350.

Li, Y. H., L. Burkhardt, and H. Teraoka (1984a), Desorption and Coagulation of Trace-Elements during Estuarine Mixing, *Geochimica Et Cosmochimica Acta*, *48*(10), 1879-1884.

Li, Y. H., T. H. Peng, W. S. Broecker, and H. G. Ostlund (1984b), The Average Vertical Mixing Coefficient for the Oceanic Thermocline, *Tellus Series B-Chemical and Physical Meteorology*, *36*(3), 212-217.

Lin, J. M., and M. Yamada (2003), Microheterogeneous systems of micelles and microemulsions as reaction media in chemiluminescent analysis, *Trac-Trends in Analytical Chemistry*, *22*(2), 99-107.

Lippiatt, S. M., M. T. Brown, M. C. Lohan, and K. W. Bruland (2011), Reactive iron delivery to the Gulf of Alaska via a Kenai eddy, *Deep-Sea Research Part I-Oceanographic Research Papers*, *58*(11), 1091-1102.

Lohan, M. C., and K. W. Bruland (2008), Elevated Fe(II) and dissolved Fe in hypoxic shelf waters off Oregon and Washington: An enhanced source of iron to coastal upwelling regimes, *Environmental Science & Technology*, *42*(17), 6462-6468.

Lohan, M. C., P. J. Statham, and D. W. Crawford (2002), Total dissolved zinc in the upper water column of the subarctic North East Pacific, *Deep-Sea Research Part Ii-Topical Studies in Oceanography*, *49*(24-25), 5793-5808.

Lohan, M. C., A. M. Aguilar-Islas, and K. W. Bruland (2006), Direct determination of iron in acidified (pH 1.7) seawater samples by flow injection analysis with catalytic spectrophotometric detection: Application and intercomparison, *Limnology and Oceanography-Methods*, *4*, 164-171.

Lohan, M. C., A. M. Aguilar-Islas, R. P. Franks, and K. W. Bruland (2005a), Determination of iron and copper in seawater at pH 1.7 with a new commercially available chelating resin, NTA Superflow, *Analytica Chimica Acta*, *530*(1), 121-129.

Lohan, M. C., D. W. Crawford, D. A. Purdie, and P. J. Statham (2005b), Iron and zinc enrichments in the northeastern subarctic Pacific: Ligand production and zinc availability in response to phytoplankton growth, *Limnology and Oceanography*, *50*(5), 1427-1437.

Longhurst, A. R. (1998), *Ecological Geography of the Sea*, Academic Press, San Diego and London, 398 pp.

Löscher, B. M. (1999), Relationships among Ni, Cu, Zn and major nutrients in the Southern Ocean, *Marine Chemistry*, *67*, 67-102.

Löscher, B. M., J. van der Meer, H. J. W. de Baar, P. M. Saager, and J. T. M. de Jong (1997), The global Cd/phosphate relationship in deep ocean waters and the need for accuracy, *Marine Chemistry*, *59*(1-2), 87-93.

Lunvongsa, S., M. Oshima, and S. Motomizu (2006), Determination of total and dissolved amount of iron in water samples using catalytic spectrophotometric flow injection analysis, *Talanta*, *68*(3), 969-973.

Lutjeharms, J. R. E. (2006), The ocean environment off southeastern Africa: a review, *South African Journal of Science*, *102*(9-10), 419-426.

Mackey, M. D., D. J. Mackey, H. W. Higgins, and S. W. Wright (1996), CHEMTAX - a program for estimating class abundances from chemical markers: application to HPLC measurements of phytoplankton, *Marine Ecology Progress Series*, *144*, 265-283.

Mahowald, N., K. Kohfeld, M. Hansson, Y. Balkanski, S. P. Harrison, I. C. Prentice, M. Schulz, and H. Rodhe (1999), Dust sources and deposition during the last glacial maximum and current climate: A comparison of model results with paleodata from ice cores and marine sediments, *Journal of Geophysical Research-Atmospheres*, *104*(D13), 15895-15916.

Mahowald, N. M., S. Engelstaedter, C. Luo, A. Sealy, P. Artaxo, C. Benitez-Nelson, S. Bonnet, Y. Chen, P. Y. Chuang, D. D. Cohen, F. Dulac, B. Herut, A. M. Johansen, N. Kubilay, R. Losno, W. Maenhaut, A. Paytan, J. A. Prospero, L. M. Shank, and R. L. Siefert (2009), Atmospheric Iron Deposition: Global Distribution, Variability, and Human Perturbations, *Annual Review of Marine Science*, *1*, 245-278.

Maldonado, M. T., and N. M. Price (2001), Reduction and transport of organically bound iron by Thalassiosira oceanica (Bacillariophyceae), *Journal of Phycology*, *37*(2), 298-309.

Marañón, E., and P. M. Holligan (1999), Photosynthetic parameters of phytoplankton from 50 degrees N to 50 degrees S in the Atlantic Ocean, *Marine Ecology Progress Series*, *176*, 191-203.

Marañón, E., M. J. Behrenfeld, N. González, B. Mouriño, and M. V. Zubkov (2003), High variability of primary production in oligotrophic waters of the Atlantic Ocean: uncoupling from phytoplankton biomass and size structure, *Marine Ecology Progress Series*, *257*, 1-11.

Marchitto, T. M., W. B. Curry, and D. W. Oppo (2000), Zinc concentrations in benthic foraminifera reflect seawater chemistry, *Paleoceanography*, *15*(3), 299-306.

Marchitto, T. M., D. W. Oppo, and W. B. Curry (2002), Paired benthic foraminiferal Cd/Ca and Zn/Ca evidence for a greatly increased presence of Southern Ocean Water in the glacial North Atlantic, *Paleoceanography*, *17*(3).

Maret, W. (2002), Optical methods for measuring zinc binding and release, zinc coordination environments in zinc finger proteins, and redox sensitivity and activity of zinc-bound thiols, *Protein Sensors and Reactive Oxygen Species, Pt B, Thiol Enzymes and Proteins*, *348*, 230-237.

Maring, H., D. L. Savoie, M. A. Izaguirre, L. Custals, and J. S. Reid (2003), Mineral dust aerosol size distribution change during atmospheric transport, *Journal of Geophysical Research-Atmospheres*, *108*(D19).

Marinov, I., A. Gnanadesikan, J. R. Toggweiler, and J. L. Sarmiento (2006), The Southern Ocean biogeochemical divide, *Nature*, *441*, 964-967.

Marinov, I., A. Gnanadesikan, J. L. Sarmiento, J. R. Toggweiler, M. Follows, and B. K. Mignone (2008), Impact of oceanic circulation on biological carbon storage in the ocean and atmospheric pCO_2, *Global Biogeochemical Cycles*, *22*.

Martens, J. H., H. Barg, M. J. Warren, and D. Jahn (2002), Microbial production of vitamin B_{12}, *Applied Microbiology and Biotechnology*, *58*(3), 275-285.

Martin, J. H. (1990), Glacial-Interglacial CO_2 Change: The Iron Hypothesis, *Paleoceanography*, *5*(1), 1-13.

Martin, J. H., and R. M. Gordon (1988), Northeast Pacific Iron Distributions in Relation to Phytoplankton Productivity, *Deep-Sea Research Part a-Oceanographic Research Papers*, *35*(2), 177-196.

Martin, J. H., S. E. Fitzwater, and R. M. Gordon (1990a), Iron deficiency limits phytoplankton productivity in Antarctic waters, *Global Biogeochemical Cycles*, *4*(1), 5-12.

Martin, J. H., R. M. Gordon, and S. E. Fitzwater (1990b), Iron in Antarctic Waters, *Nature*, *345*(6271), 156-158.

Martin, J. H., R. M. Gordon, and S. E. Fitzwater (1991), The Case for Iron, *Limnology and Oceanography*, *36*(8), 1793-1802.

Martin, J. H., G. A. Knauer, D. M. Karl, and W. W. Broenkow (1987), VERTEX: Carbon cycling in the northeast Pacific, *Deep-Sea Research*, *34*, 267-285.

Martin, J. H., R. M. Gordon, S. Fitzwater, and W. W. Broenkow (1989), VERTEX: phytoplankton/iron studies in the Gulf of Alaska, *Deep-Sea Research*, *36*, 649-680.

Martin, J. H., S. E. Fitzwater, R. M. Gordon, C. N. Hunter, and S. J. Tanner (1993), Iron, Primary Production and Carbon Nitrogen Flux Studies during the JGOFS North Atlantic Bloom Experiment, *Deep-Sea Research Part Ii-Topical Studies in Oceanography*, *40*(1-2), 115-134.

Martin, J. H., K. H. Coale, K. S. Johnson, S. E. Fitzwater, R. M. Gordon, S. J. Tanner, C. N. Hunter, V. A. Elrod, J. L. Nowicki, T. L. Coley, R. T. Barber, S. Lindley, A. J. Watson, K. Vanscoy, C. S. Law, M. I. Liddicoat, R. Ling, T. Stanton, J. Stockel, C. Collins, A. Anderson, R. Bidigare, M. Ondrusek, M. Latasa, F. J. Millero, K. Lee, W. Yao, J. Z. Zhang, G. Friederich, C. Sakamoto, F. Chavez, K. Buck, Z. Kolber, R. Greene, P. Falkowski, S. W. Chisholm, F. Hoge, R. Swift, J. Yungel, S. Turner, P. Nightingale, A. Hatton, P. Liss, and N. W. Tindale (1994), Testing the Iron Hypothesis in Ecosystems of the Equatorial Pacific-Ocean, *Nature*, *371*(6493), 123-129.

Mason, R. P. (2013), *Trace Metals in Aquatic Systems*, Wiley-Blackwell, Chichester, UK, 440 pp.

Mather, R. L., S. E. Reynolds, G. A. Wolff, R. G. Williams, S. Torres-Valdes, E. M. S. Woodward, A. Landolfi, X. Pan, R. Sanders, and E. P. Achterberg (2008), Phosphorus cycling in the North and South Atlantic Ocean subtropical gyres, *Nature Geoscience*, *1*(7), 439-443.

MBARI (2013), The MBARI Chemical Sensor Program: Peridoc Table of elements in the Ocean, www.mbari.org/chemsensor/pteo.htm.

McCartney, M. S. (1977), Subantarctic Mode Water, *Deep Sea Research*, *24*, 103-119.

McDonagh, E. L., and B. A. King (2005), Oceanic fluxes in the South Atlantic, *Journal of Physical Oceanography*, *35*(1), 109-122.

McLennan, S. M. (2001), Relationships between the trace element composition of sedimentary rocks and upper continental crust, *Geochemistry Geophysics Geosystems*, *2*, art. no.-2000GC000109.

Measures, C. I., and S. Vink (2001), Dissolved Fe in the upper waters of the Pacific sector of the Southern Ocean, *Deep-Sea Research Part Ii-Topical Studies in Oceanography*, *48*(19-20), 3913-3941.

Measures, C. I., J. Yuan, and J. A. Resing (1995), Determination of Iron in Seawater by Flow Injection-Analysis Using in-Line Preconcentration and Spectrophotometric Detection, *Marine Chemistry*, *50*(1-4), 3-12.

Measures, C. I., M. Hatta, and M. M. Grand (2012), Bioactive Trace Metal Distributions and Biogeochemical Controls in the Southern Ocean, *Oceanography*, *25*(3), 122-133.

Measures, C. I., W. M. Landing, M. T. Brown, and C. S. Buck (2008), High-resolution Al and Fe data from the Atlantic Ocean CLIVAR-CO(2) repeat hydrography A16N transect: Extensive linkages between atmospheric dust and upper ocean geochemistry, *Global Biogeochemical Cycles*, *22*(1).

Meeusen, J. W., H. Tomasiewicz, A. Nowakowski, and D. H. Petering (2011), TSQ (6-methoxy-8-p-toluenesulfonamido-quinoline), a common fluorescent sensor for cellular zinc, images zinc proteins, *Inorganic Chemistry*, *50*(16), 7563-7573.

Merenyi, G., J. Lind, and T. E. Eriksen (1990), Luminol chemiluminescence: chemistry, excitation, emitter, *Journal of Bioluminescence and Chemiluminescence*, *5*(1), 53-56.

Middag, R., H. J. W. de Baar, P. Laan, P. H. Cai, and J. C. Ooijen (2011), Dissolved manganese in the Atlantic sector of the Southern Ocean, *Deep-Sea Reseach II*, *58*, 2661-2677.

Miller, R. J., and J. D. Ingle (1981), Determination of cobalt by pyrogallol chemiluminescence, *Talanta*, *29*, 303-311.

Mills, M. M., C. Ridame, M. Davey, J. La Roche, and R. J. Geider (2004), Iron and phosphorus co-limit nitrogen fixation in the eastern tropical North Atlantic, *Nature*, *429*(6989), 292-294.

Milne, A., W. Landing, M. Bizimis, and P. Morton (2010), Determination of Mn, Fe, Co, Ni, Cu, Zn, Cd and Pb in seawater using high resolution magnetic sector inductively coupled mass spectrometry (HR-ICP-MS), *Analytica Chimica Acta*, *665*(2), 200-207.

Moffett, J. W., and J. Ho (1996), Oxidation of cobalt and manganese in seawater via a common microbially catalyzed pathway, *Geochimica Et Cosmochimica Acta*, *60*(18), 3415-3424.

Mohr, W., T. Grosskopf, D. W. R. Wallace, and J. LaRoche (2010), Methodological Underestimation of Oceanic Nitrogen Fixation Rates, *Plos One*, *5*(9).

Montoya, J. P., M. Voss, P. Kahler, and D. G. Capone (1996), A simple, high-precision, high-sensitivity tracer assay for N-2 fixation, *Applied and Environmental Microbiology*, *62*(3), 986-993.

Montsant, A., A. E. Allen, S. Coesel, A. De Martino, A. Falciatore, M. Mangogna, M. Siaut, M. Heijde, K. Jabbari, U. Maheswari, E. Rayko, A. Vardi, K. E. Apt, J. A. Berges, A. Chiovitti, A. K. Davis, K. Thamatrakoln, M. Z. Hadi, T. W. Lane, J. C. Lippmeier, D. Martinez, M. S. Parker, G. J. Pazour, M. A. Saito, D. S. Rokhsar, E. V. Armbrust, and C. Bowler (2007), Identification and comparative genomic analysis of signaling and regulatory components in the diatom Thalassiosira pseudonana, *Journal of Phycology*, *43*(3), 585-604.

Moore, C. M., M. M. Mills, R. Langlois, A. Milne, E. P. Achterberg, J. La Roche, and R. J. Geider (2008), Relative influence of nitrogen and phosphorus availability on phytoplankton physiology and productivity in the oligotrophic sub-tropical North Atlantic Ocean, *Limnology and Oceanography*, *53*(1), 291-305.

Moore, C. M., M. M. Mills, A. Milne, R. Langlois, E. P. Achterberg, K. Lochte, R. J. Geider, and J. La Roche (2006), Iron limits primary productivity during spring

bloom development in the central North Atlantic, *Global Change Biology*, *12*(4), 626-634.

Moore, C. M., M. M. Mills, E. P. Achterberg, R. J. Geider, J. LaRoche, M. I. Lucas, E. L. McDonagh, X. Pan, A. J. Poulton, M. J. A. Rijkenberg, D. J. Suggett, S. J. Ussher, and E. M. S. Woodward (2009), Large-scale distribution of Atlantic nitrogen fixation controlled by iron availability, *Nature Geoscience*, *2*(12), 867-871.

Moore, J. K., and O. Braucher (2008), Sedimentary and mineral dust sources of dissolved iron to the world ocean, *Biogeosciences*, *5*(3), 631-656.

Moore, J. K., S. C. Doney, D. M. Glover, and I. Y. Fung (2002), Iron cycling and nutrient-limitation patterns in surface waters of the World Ocean, *Deep-Sea Research Part Ii-Topical Studies in Oceanography*, *49*(1-3), 463-507.

Moore, W. S., and J. Dymond (1991), Fluxes of Ra-226 and Barium in the Pacific-Ocean - the Importance of Boundary Processes, *Earth and Planetary Science Letters*, *107*(1), 55-68.

Morel, F. M. M. (2008), The co-evolution of phytoplankton and trace element cycles in the oceans, *Geobiology*, *6*(3), 318-324.

Morel, F. M. M., and N. M. Price (2003), The biogeochemical cycles of trace metals in the oceans, *Science*, *300*(5621), 944-947.

Morel, F. M. M., A. J. Milligan, and M. A. Saito (2003), Marine bioinorganic chemistry: the role of trace metals in the oceanic cycles in *The Oceans and Marine Geochemistry - Treatise on Geochemistry*, edited by H. D. Holland and K. K. Turekian, Elsevier-Pergamon, Oxford, UK, pp.

Morel, F. M. M., J. R. Reinfelder, S. B. Roberts, C. P. Chamberlain, J. G. Lee, and D. Yee (1994), Zinc and Carbon Co-Limitation of Marine-Phytoplankton, *Nature*, *369*(6483), 740-742.

Mulholland, M. R., P. W. Bernhardt, J. L. Blanco-Garcia, A. Mannino, K. Hyde, E. Mondragon, K. Turk, P. H. Moisander, and J. P. Zehr (2012), Rates of dinitrogen fixation and the abundance of diazotrophs in North American coastal waters between Cape Hatteras and Georges Bank, *Limnology and Oceanography*, *57*(4), 1067-1083.

NASA (2003), Ocean Plant Life Slows Down and Absorbs Less Carbon, www.nasa.gov/centers/goddard/news/top-story/2003/0815oceancarbon.html.

Nasir, M. S., C. J. Fahrni, D. A. Suhy, K. J. Kolodsick, C. P. Singer, and T. V. O'Halloran (1999), The chemical cell biology of zinc: structure and intracellular fluorescence of a zinc-quinolinesulfonamide complex, *Journal of Biological Inorganic Chemistry*, *4*(6), 775-783.

Naveira Garabato, A. C., E. L. McDonagh, D. P. Stevens, K. J. Heywood, and R. J. Sanders (2002), On the export of Antarctic Bottom water from the Weddell Sea, *Deep Sea Reseach II*, *49*, 4715-4742.

Naveira Garabato, A. C., L. Jullion, D. P. Stevens, K. J. Heywood, and B. A. King (2009), Variability of Subantarctic Mode Water and Antarctic Intermediate Water in the Drake Passage during the Late-Twentieth and Early-Twenty-First Centuries, *Journal of Climate*, *22*(13), 3661-3688.

Nelson, D. M., P. Treguer, M. A. Brzezinski, A. Leynaert, and B. Queguiner (1995), Production and Dissolution of Biogenic Silica in the Ocean - Revised Global Estimates, Comparison with Regional Data and Relationship to Biogenic Sedimentation, *Global Biogeochemical Cycles*, *9*(3), 359-372.

Nishioka, J., H. Obata, and D. Tsumune (2013), Evidence of an extensive spread of hydrothermal dissolved iron in the Indian Ocean, *Earth and Planetary Science Letters*, *361*, 26-33.

Noble, A. E., M. A. Saito, K. Maiti, and C. R. Benitez-Nelson (2008), Cobalt, manganese, and iron near the Hawaiian Islands: A potential concentrating mechanism for cobalt within a cyclonic eddy and implications for the hybrid-type trace metals, *Deep-Sea Research Part Ii-Topical Studies in Oceanography*, *55*(10-13), 1473-1490.

Noble, A. E., C. H. Lamborg, D. C. Ohnemus, P. J. Lam, T. J. Goepfert, C. I. Measures, C. H. Frame, K. L. Casciotti, G. R. DiTullio, J. Jennings, and M. A. Saito (2012), Basin-scale inputs of cobalt, iron, and manganese from the Benguela-Angola front to the South Atlantic Ocean, *Limnology and Oceanography*, *57*(4), 989-1010.

Nolting, R. F. H., M., J. T. M. de Jong, K. R. Timmermans, and H. J. W. de Baar (2000), The determination and distribution of Zn in surface water samples collected in the northeast Atlantic Ocean, *J. Environ. Monit.*, *2*, 534-538.

Nowakowski, A. B., and D. H. Petering (2011), Reactions of the fluorescent sensor, zinquin, with the zinc-proteome: adduct formation and ligand substitution, *Inorganic Chemistry*, *50*(20), 10124-10133.

Nowicki, J. L., K. S. Johnson, K. H. Coale, V. A. Elrod, and S. H. Lieberman (1994), Determination of Zinc in Seawater Using Flow-Injection Analysis with Fluorometric Detection, *Analytical Chemistry*, *66*(17), 2732-2738.

Nuester, J., S. Vogt, and B. S. Twining (2012), Localization of Iron within Centric Diatoms of the Genus *Thalassiosira*, *Journal of Phycology*, *48*(3), 626-634.

O'sullivan, D. W., A. K. Hanson, and D. R. Kester (1995), Stopped-Flow Luminol Chemiluminescence Determination of Fe(Ii) and Reducible Iron in Seawater at Subnanomolar Levels, *Marine Chemistry*, *49*(1), 65-77.

Obata, H., H. Karatani, and E. Nakayama (1993), Automated-Determination of Iron in Seawater by Chelating Resin Concentration and Chemiluminescence Detection, *Analytical Chemistry*, *65*(11), 1524-1528.

Orsi, A. H., T. Whitworth, and W. D. Nowlin (1995), On the Meridional Extent and Fronts of the Antarctic Circumpolar Current, *Deep-Sea Research Part I*, *42*(5), 641-673.

Orsi, A. H., G. C. Johnson, and J. L. Bullister (1999), Circulation, mixing, and production of Antarctic Bottom Water, *Progress in Oceanography*, *43*, 55-109.

Owens, N. J. P., and A. P. Rees (1989), Determination of N-15 at Submicrogram Levels of Nitrogen Using Automated Continuous-Flow Isotope Ratio Mass-Spectrometry, *Analyst*, *114*(12), 1655-1657.

Palter, J. B., J. L. Sarmiento, A. Gnanadesikan, J. Simeon, and R. D. Slater (2010), Fueling export production: nutrient return pathways from the deep ocean and their dependence on the Meridional Overturning Circulation, *Biogeosciences*, *7*(11), 3549-3568.

Panzeca, C., A. J. Beck, K. Leblanc, G. T. Taylor, D. A. Hutchins, and S. A. Sanudo-Wilhelmy (2008), Potential cobalt limitation of vitamin B(12) synthesis in the North Atlantic Ocean, *Global Biogeochemical Cycles*, *22*(2).

Perry, K. D., T. A. Cahill, R. A. Eldred, D. D. Dutcher, and T. E. Gill (1997), Long-range transport of North African dust to the eastern United States, *Journal of Geophysical Research-Atmospheres*, *102*(D10), 11225-11238.

Planquette, H., P. J. Statham, G. R. Fones, M. A. Charette, C. M. Moore, I. Salter, F. H. Nedelec, S. L. Taylor, M. French, A. R. Baker, N. Mahowald, and T. D. Jickells (2007), Dissolved iron in the vicinity of the Crozet Islands, Southern Ocean, *Deep-Sea Research Part Ii-Topical Studies in Oceanography*, *54*(18-20), 1999-2019.

Planquette, H., G. R. Fones, P. J. Statham, and P.J. Morris (2009), Origin of iron and aluminium in large particles (> 53 μm) in the Crozet region, Southern Ocean, *Marine Chemistry*, *115*, 21-42.

Pluth, M. D., E. Tomat, and S. J. Lippard (2011), Biochemistry of Mobile Zinc and Nitric Oxide Revealed by Fluorescent Sensors, *Annual Review of Biochemistry, Vol 80*, *80*, 333-355.

Pohl, C., G. Kattner, and M. Schulzbaldes (1993), Cadmium, Copper, Lead and Zinc on Transects through Arctic and Eastern Atlantic Surface and Deep Waters, *Journal of Marine Systems*, *4*(1), 17-29.

Pohl, C., P. L. Croot, U. Hennings, T. Daberkow, G. Budeus, and M. Rutgers v.d. Leoff (2010), Synoptic transects on the distribution of trace elements (Hg, Pb, Cd, Cu, Ni, Zn, Co, Mn, Fe, and Al) in surface waters of the Northern- and Southern East Atlantic, *Journal of Marine Systems*, *84*, 28-41.

Pollard, R. T., I. Salter, R. J. Sanders, M. I. Lucas, C. M. Moore, R. A. Mills, P. J. Statham, J. T. Allen, A. R. Baker, D. C. E. Bakker, M. A. Charette, S. Fielding, G. R. Fones, M. French, A. E. Hickman, R. J. Holland, J. A. Hughes, T. D. Jickells, R. S. Lampitt, P. J. Morris, F. H. Nedelec, M. Nielsdottir, H. Planquette, E. E. Popova, A. J. Poulton, J. F. Read, S. Seeyave, T. Smith, M. Stinchcombe, S. Taylor, S. Thomalla, H. J. Venables, R. Williamson, and M. V. Zubkov (2009), Southern Ocean deep-water carbon export enhanced by natural iron fertilization, *Nature*, *457*(7229), 577-U581.

Poulton, A. J., P. M. Holligan, A. Hickman, Y. N. Kim, T. R. Adey, M. C. Stinchcombe, C. Holeton, S. Root, and E. M. S. Woodward (2006), Phytoplankton carbon fixation, chlorophyll-biomass and diagnostic pigments in the Atlantic Ocean, *Deep-Sea Research Part II*, *53*(14-16), 1593-1610.

Powell, R. T., and A. Wilson-Finelli (2003), Importance of organic Fe complexing ligands in the Mississippi River plume, *Estuarine Coastal and Shelf Science*, *58*(4), 757-763.

Price, G. D., and M. R. Badger (1989), Isolation and Characterization of High Co2-Requiring-Mutants of the Cyanobacterium Synechococcus Pcc7942 - 2 Phenotypes That Accumulate Inorganic Carbon but Are Apparently Unable to Generate Co2 within the Carboxysome, *Plant Physiology*, *91*(2), 514-525.

Price, N. M., and F. M. M. Morel (1990), Cadmium and Cobalt Substitution for Zinc in a Marine Diatom, *Nature*, *344*(6267), 658-660.

Prospero, J. M., and T. N. Carlson (1972), Vertical and Areal Distribution of Saharan Dust over Western Equatorial North-Atlantic Ocean, *Journal of Geophysical Research*, *77*(27), 5255-&.

Prospero, J. M., and P. J. Lamb (2003), African droughts and dust transport to the Caribbean: Climate change implications, *Science*, *302*(5647), 1024-1027.

Prospero, J. M., R. A. Glaccum, and R. T. Nees (1981), Atmospheric Transport of Soil Dust from Africa to South-America, *Nature*, *289*(5798), 570-572.

Radic, A., F. Lacan, and J. W. Murray (2011), Iron isotopes in the seawater of the equatorial Pacific Ocean: New constraints for the oceanic iron cycle, *Earth and Planetary Science Letters*, *306*(1-2), 1-10.

Ragueneau, O., P. Treguer, A. Leynaert, R. F. Anderson, M. A. Brzezinski, D. J. DeMaster, R. C. Dugdale, J. Dymond, G. Fischer, R. Francois, C. Heinze, E. Maier-Reimer, V. Martin-Jezequel, D. M. Nelson, and B. Queguiner (2000), A review of the Si cycle in the modern ocean: recent progress and missing gaps in the application of biogenic opal as a paleoproductivity proxy, *Global and Planetary Change*, *26*, 317-365.

Raven, J. A. (1990), Predictions of Mn and Fe Use Efficiencies of Phototrophic Growth as a Function of Light Availability for Growth and of C Assimilation Pathway, *New Phytologist*, *116*(1), 1-18.

Raven, J. A., B. Wollenweber, and L. L. Handley (1992), A Comparison of Ammonium and Nitrate as Nitrogen-Sources for Photolithotrophs, *New Phytologist*, *121*(1), 19-32.

Redfield, A. C., B. H. Ketchum, and F. A. Richards (1963), The influence of organisms on the composition of seawater, in *The composition of seawater. The Sea.*, edited by M. N. Hill, Wiley, New York, pp. 26-27.

Richardson, M. J., G. L. Weatherly, and W. D. Gardner (1993), Benthic Storms in the Argentine Basin, *Deep-Sea Research Part Ii-Topical Studies in Oceanography*, *40*(4-5), 975-987.

Riegman, R., W. Stolte, A. A. M. Noordeloos, and D. Slezak (2000), Nutrient uptake, and alkaline phosphate (EC 3 : 1 : 3 : 1) activity of Emiliania huxleyi (Prymnesiophyceae) during growth under N and P limitation in continuous cultures, *Journal of Phycology*, *36*(1), 87-96.

Roberts, S. B., T. W. Lane, and F. M. M. Morel (1997), Carbonic anhydrase in the marine diatom Thalassiosira weissflogii (Bacillariophyceae), *Journal of Phycology*, *33*(5), 845-850.

Robinson, C., A. J. Poulton, P. M. Holligan, A. R. Baker, G. Forster, N. Gist, T. D. Jickells, G. Malin, R. Upstill-Goddard, R. G. Williams, E. M. S. Woodward, and M. V. Zubkov (2006), The Atlantic Meridional Transect (AMT) Programme: A contextual view 1995-2005, *Deep-Sea Research Part II*, *53*(14-16), 1485-1515.

Rolph, G. D. (2013), Real-time Environmental Applications and Display System (READY) Website (http://www.ready.noaa.gov). NOAA Air Resources Laboratory, College Park, MD

Rose, A. L., and T. D. Waite (2001), Chemiluminescence of luminol in the presence of iron(II) and oxygen: oxidation mechanism and implications for its analytical use, *Analytical Chemistry*, *73*(24), 5909-5920.

Rue, E. L., and K. W. Bruland (1995), Complexation of Iron(III) by Natural Organic-Ligands in the Central North Pacific as Determined by a New Competitive Ligand Equilibration Adsorptive Cathodic Stripping Voltammetric Method, *Marine Chemistry*, *50*(1-4), 117-138.

Rue, E. L., G. J. Smith, G. A. Cutter, and K. W. Bruland (1997), The response of trace element redox couples to suboxic conditions in the water column, *Deep-Sea Research Part I*, *44*(1), 113-134.

Rueter, J. G., and F. M. M. Morel (1981), The Interaction between Zinc-Deficiency and Copper Toxicity as It Affects the Silicic-Acid Uptake Mechanisms in Thalassiosira-Pseudonana, *Limnology and Oceanography*, *26*(1), 67-73.

Sachs, J. P., and C. L. Myhrvold (2011), A Shifting Band of Rain, *Scientific American*, *304*(3), 60-65.

Sachs, J. P., D. Sachse, R. H. Smittenberg, Z. H. Zhang, D. S. Battisti, and S. Golubic (2009), Southward movement of the Pacific intertropical convergence zone AD 1400-1850, *Nature Geoscience*, *2*(7), 519-525.

Saito, M. A., and J. W. Moffett (2001), Complexation of cobalt by natural organic ligands in the Sargasso Sea as determined by a new high-sensitivity electrochemical cobalt speciation method suitable for open ocean work, *Marine Chemistry*, *75*(1-2), 49-68.

Saito, M. A., and J. W. Moffett (2002), Temporal and spatial variability of cobalt in the Atlantic Ocean, *Geochimica Et Cosmochimica Acta*, *66*(11), 1943-1953.

Saito, M. A., and T. J. Goepfert (2008), Zinc-cobalt colimitation of Phaeocystis antarctica, *Limnology and Oceanography*, *53*(1), 266-275.

Saito, M. A., J. W. Moffett, and G. R. DiTullio (2004), Cobalt and nickel in the Peru upwelling region: A major flux of labile cobalt utilized as a micronutrient, *Global Biogeochemical Cycles*, *18*(4).

Saito, M. A., G. Rocap, and J. W. Moffett (2005), Production of cobalt binding ligands in a Synechococcus feature at the Costa Rica upwelling dome, *Limnology and Oceanography*, *50*(1), 279-290.

Saito, M. A., T. J. Goepfert, and J. T. Ritt (2008), Some thoughts on the concept of colimitation: Three definitions and the importance of bioavailability, *Limnology and Oceanography*, *53*(1), 276-290.

Saito, M. A., J. W. Moffett, S. W. Chisholm, and J. B. Waterbury (2002), Cobalt limitation and uptake in Prochlorococcus, *Limnology and Oceanography*, *47*(6), 1629-1636.

Saito, M. A., A. E. Noble, T. J. Goepfert, C. H. Lamborg, and W. J. Jenkins (2013), Slow-spreading submarine ridges in the South Atlantic as a significant oceanic iron source *Nature Geoscience, in press*.

Saito, M. A., T. J. Goepfert, A. E. Noble, E. M. Bertrand, P. N. Sedwick, and G. R. DiTullio (2010), A seasonal study of dissolved cobalt in the Ross Sea, Antarctica: micronutrient behavior, absence of scavenging, and relationships with Zn, Cd, and P, *Biogeosciences*, *7*(12), 4059-4082.

Sakamoto-Arnold, C. M., and K. S. Johnson (1987), Determination of Picomolar Levels of Cobalt in Seawater by Flow Injection Analysis with Chemiluminescence Detection, *Analytical Chemistry*, *59*(14), 1789-1794.

Santoso, A., and M. H. England (2004), Antarctic intermediate water circulation and variability in a coupled climate model, *Journal of Physical Oceanography*, *34*(10), 2160-2179.

Santschi, P. H., J. J. Lenhart, and B. D. Honeyman (1997), Heterogeneous processes affecting trace contaminant distribution in estuaries: The role of natural organic matter, *Marine Chemistry*, *58*(1-2), 99-125.

Sanudo-Wilhelmy, S. A., A. B. Kustka, C. J. Gobler, D. A. Hutchins, M. Yang, K. Lwiza, J. Burns, D. G. Capone, J. A. Raven, and E. J. Carpenter (2001), Phosphorus limitation of nitrogen fixation by Trichodesmium in the central Atlantic Ocean, *Nature*, *411*(6833), 66-69.

Sarmiento, J. L., and J. C. Orr (1991), Three-dimensional simulations of the impact of the Southern Ocean nutrients depletion on atmospheric CO_2 and ocean chemistry, *Limnology and Oceanography*, *36*(8), 1928-1950.

Sarmiento, J. L., N. Gruber, M. A. Brzezinski, and J. P. Dunne (2004), High-latitude controls of thermocline nutrients and low latitude biological productivity, *Nature*, *427*(6969), 56-60.

Sarthou, G., A. R. Baker, J. Kramer, P. Laan, A. Laes, S. Ussher, E. P. Achterberg, H. J. W. de Baar, K. R. Timmermans, and S. Blain (2007), Influence of atmospheric inputs on the iron distribution in the subtropical North-East Atlantic Ocean, *Marine Chemistry*, *104*(3-4), 186-202.

Sarthou, G., A. R. Baker, S. Blain, E. P. Achterberg, M. Boye, A. R. Bowie, P. Croot, P. Laan, H. J. W. de Baar, T. D. Jickells, and P. J. Worsfold (2003), Atmospheric iron deposition and sea-surface dissolved iron concentrations in the eastern Atlantic Ocean, *Deep-Sea Research Part I-Oceanographic Research Papers*, *50*(10-11), 1339-1352.

Schlitzer, R. (2012), Ocean Data View, http://odv.awi.de/en/home/.

Sedwick, P. N., and G. R. DiTullio (1997), Regulation of algal blooms in Antarctic shelf waters by the release of iron from melting sea ice, *Geophysical Research Letters*, *24*(20), 2515-2518.

Sedwick, P. N., E. R. Sholkovitz, and T. M. Church (2007), Impact of anthropogenic combustion emissions on the fractional solubility of aerosol iron: Evidence from the Sargasso Sea, *Geochemistry Geophysics Geosystems*, *8*.

Sedwick, P. N., A. R. Bowie, and T. W. Trull (2008), Dissolved iron in the Australian sector of the Southern Ocean (CLIVAR SR3 section): Meridional and seasonal trends, *Deep-Sea Research Part I-Oceanographic Research Papers*, *55*(8), 911-925.

Serebriakova, G. V., I. A. Krasavin, E. A. Bozhevol'nov, and V. M. Dziomko (1964), Study of selected 8-(arensulfonilamino)-quinolines as reagents for luminescent determination of zinc and cadmium, *Khimicheskiie Reaktivy I Preparaty*, *26*, 97-108.

Shaked, Y., A. B. Kustka, and F. M. M. Morel (2005), A general kinetic model for iron acquisition by eukaryotic phytoplankton, *Limnology and Oceanography*, *50*(3), 872-882.

Shaked, Y., Y. Xu, K. Leblanc, and F. M. M. Morel (2006), Zinc availability and alkaline phosphatase activity in Emiliania huxleyi: Implications for Zn-P co-limitation in the ocean, *Limnology and Oceanography*, *51*(1), 299-309.

Shelley, R. U. (2011), Cobalt biogeochemistry in the Atlantic ocean using Flow-Injection Chemiluminecence, 261 pp, University of Plymouth.

Shelley, R. U., B. Zachhuber, P. N. Sedwick, P. J. Worsfold, and M. C. Lohan (2010), Determination of total dissolved cobalt in UV-irradiated seawater using flow injection with chemiluminescence detection, *Limnology and Oceanography-Methods*, *8*, 352-362.

Shelley, R. U., P. N. Sedwick, T. S. Bibby, P. Cabedo-Sanz, T. M. Church, R. J. Johnson, A. I. Macey, C. M. Marsay, E. R. Sholkovitz, S. J. Ussher, P. J. Worsfold, and M. C. Lohan (2012), Controls on dissolved cobalt in surface waters of the Sargasso Sea: Comparisons with iron and aluminum, *Global Biogeochemical Cycles*, *26*.

Sherrell, R. M., and E. A. Boyle (1992), The trace metal composition of suspended particles in the oceanic water column near Bermuda, *Earth and Planetary Science Letters*, *111*(1), 155-174.

Sholkovitz, E. R., and D. Copland (1981), The Coagulation, Solubility and Adsorption Properties of Fe, Mn, Cu, Ni, Cd, Co and Humic Acids in a River Water, *Geochimica Et Cosmochimica Acta*, *45*(2), 181-189.

Sholkovitz, E. R., P. N. Sedwick, T. M. Church, A. R. Baker, and C. F. Powell (2012), Fractional solubility of aerosol iron: Synthesis of a global-scale data set, *Geochimica Et Cosmochimica Acta*, *89*, 173-189.

Slawinska, D., and J. Slawinski (1975), Chemiluminescent flow method for determination of formaldehyde, *Analytical Chemistry*, *47*(13), 2101-2109.

Slemons, L. O., J. W. Murray, J. Resing, B. Paul, and P. Dutrieux (2010), Western Pacific coastal sources of iron, manganese, and aluminum to the Equatorial Undercurrent, *Global Biogeochemical Cycles*, *24*.

Smetacek, V. (1999), Diatoms and the ocean carbon cycle, *Protist*, *150*(1), 25-32.

Smetacek, V., C. Klaas, V. H. Strass, P. Assmy, M. Montresor, B. Ciewski, N. Savoye, A. Webb, F. d'Ovidio, J. M. Arrieta, U. Bathmann, R. Bellerby, G. M. Berg, P. Croot, S. Gonzalez, J. Henjes, G. J. Herndl, L. J. Hoffmann, H. Leach, M. Losch, M. M. Mills, C. Neill, I. Peeken, R. Rottgers, O. Sachs, E. Sauter, M. M. Schmidt, J. Schwarz, A. Terbruggen and D. Wold-Gladrow (2012), Deep carbon export from a Southern Ocean iron-fertilized diatom bloom, *Nature*, *487*, 313-319.

Snitsarev, V., T. Budde, T. P. Stricker, J. M. Cox, D. J. Krupa, L. Geng, and A. R. Kay (2001), Fluorescent detection of Zn^{2+}-rich vesicles with zinquin: mechanism of action in lipid environments, *Biophysical Journal*, *80*(3), 1538-1546.

Sohrin, Y., and K. W. Bruland (2011), Global status of trace elements in the ocean, *Trac-Trends in Analytical Chemistry*, *30*(8), 1291-1307.

Sohrin, Y., S. Urushihara, S. Nakatsuka, T. Kono, E. Higo, T. Minami, K. Norisuye, and S. Umetani (2008), Multielemental determination of GEOTRACES key trace metals in seawater by ICPMS after preconcentration using an ethylenediaminetriacetic acid chelating resin, *Analytical Chemistry*, *80*(16), 6267-6273.

Sohrin, Y., S. Iwamoto, S. Akiyama, T. Fujita, T. Kugii, H. Obata, E. Nakayama, S. Goda, Y. Fujishima, H. Hasegawa, K. Ueda, and M. Matsui (1998), Determination of trace elements in seawater by fluorinated metal alkoxide glass-immobilized 8-hydroxyquinoline concentration and high-resolution inductively coupled plasma mass spectrometry detection, *Analytica Chimica Acta*, *363*(1), 11-19.

Spokes, L. J., and T. D. Jickells (1996), Factors controlling the solubility of aerosol trace metals in the atmosphere and on mixing into seawater, *Aquatic Geochemistry*, *1*, 355-374.

Statham, P. J., C. R. German, and D. P. Connelly (2005), Iron(II) distribution and oxidation kinetics in hydrothermal plumes at the Kairei and Edmond vent sites, Indian Ocean, *Earth and Planetary Science Letters*, *236*(3-4), 588-596.

Stieg, S., and T. A. Nieman (1977), Determination of Trace Concentrations of Cobalt(Ii) and Other Metals by Chemiluminescent Oxidation of Gallic Acid, *Analytical Chemistry*, *49*(9), 1322-1325.

Stramma, L., M. Visbeck, P. Brandt, T. Tanhua, and D. Wallace (2009), Deoxygenation in the oxygen minimum zone of the eastern tropical North Atlantic, *Geophysical Research Letters*, *36*.

Stramma, L., P. Brandt, J. Schafstall, F. Schott, J. Fischer, and A. Kortzinger (2008), Oxygen minimum zone in the North Atlantic south and east of the Cape Verde Islands, *Journal of Geophysical Research-Oceans*, *113*(C4).

Sunda, W. G. (1997), Control of dissolved iron concentrations in the world ocean: A comment, *Marine Chemistry*, *57*(3-4), 169-172.

Sunda, W. G., and S. A. Huntsman (1992), Feedback Interactions between Zinc and Phytoplankton in Seawater, *Limnology and Oceanography*, *37*(1), 25-40.

Sunda, W. G., and S. A. Huntsman (1995a), Cobalt and zinc interreplacement in marine phytoplankton: Biological and geochemical implications, *Limnology and Oceanography*, *40*(8), 1404-1417.

Sunda, W. G., and S. A. Huntsman (1995b), Iron Uptake and Growth Limitation in Oceanic and Coastal Phytoplankton, *Marine Chemistry*, *50*(1-4), 189-206.

Sunda, W. G., and S. A. Huntsman (2000), Effect of Zn, Mn, and Fe on Cd accumulation in phytoplankton: Implications for oceanic Cd cycling, *Limnology and Oceanography*, *45*(7), 1501-1516.

Swift, D. G. (1981), Vitamin levels in the gulf of maine and ecological significance of vitamin B_{12} there, *Journal of Marine Research*, *39*(2), 375-403.

Tagliabue, A., T. Mtshali, O. Aumont, A. R. Bowie, M. B. Klunder, A. N. Roychoudhury, and S. Swart (2012), A global compilation of dissolved iron measurements: focus on distributions and processes in the Southern Ocean, *Biogeosciences*, *9*(6), 2333-2349.

Tagliabue, A., L. Bopp, J. C. Dutay, A. R. Bowie, F. Chever, P. Jean-Baptiste, E. Bucciarelli, D. Lannuzel, T. Remenyi, G. Sarthou, O. Aumont, M. Gehlen, and C. Jeandel (2010), Hydrothermal contribution to the oceanic dissolved iron inventory, *Nature Geoscience*, *3*(4), 252-256.

Talley, L. D. (1996), Antarctic Intermediate Water in the South Atlantic, in *The South Atlantic: Present and Past Circulation*, edited by G. Wefer, W. Berger, H., G. Siedler and D. Webb, Springer-Verlag, Berlin Heidelberg, pp. 219-238.

Taylor, G. T., and C. W. Sullivan (2008), Vitamin B-12 and cobalt cycling among diatoms and bacteria in Antarctic sea ice microbial communities, *Limnology and Oceanography*, *53*(5), 1862-1877.

Taylor, S. R., and S. M. McLennan (1985), *The Continental Crust: It's Composition and Evolution*, Blackwell Scientific, Oxford, London, Edinburgh, Boston, Palo Alto, Melbourse, 312 pp.

Tebo, B. M., K. H. Nealson, S. Emerson, and L. Jacobs (1984), Microbial mediation of Mn(II) and Co(II) precipitation at the O_2/H_2 interfaces in two anoxic fjords, *Limnology and Oceanography*, *29*(6), 1247-1258.

Thuróczy, C. E., M. Boye, and R. Losno (2010), Dissolution of cobalt and zinc from natural and anthropogenic dusts in seawater, *Biogeosciences*, *7*(6), 1927-1936.

Timmermans, K. R., B. van den Wagt, and H. J. W. de Baar (2004), Growth rates, half-saturation constants, and silicate, nitrate, and phosphate depletion in relation to iron availability of four large, open-ocean diatoms from the Southern Ocean, *Limnology and Oceanography*, *49*, 2141-2151.

Tivey, M. K. (2007), Generation of Seafloor Hydrothermal Vent Fluids and Associated Mineral Deposits, *Oceanography*, *20*(1), 50-65.

Toggweiler, J. R., K. Dixon, and W. S. Broecker (1991), The Peru upwelling and the ventilation of the South Pacific thermocline, *J. Geophys. Res.*, *96*, 20467-20497.

Toner, B. M., S. C. Fakra, S. J. Manganini, C. M. Santelli, M. A. Marcus, J. Moffett, O. Rouxel, C. R. German, and K. J. Edwards (2009), Preservation of iron(II) by carbon-rich matrices in a hydrothermal plume, *Nature Geoscience*, *2*(3), 197-201.

Tortell, P. D., M. T. Maldonado, and N. M. Price (1996), The role of heterotrophic bacteria in iron-limited ocean ecosystems, *Nature*, *383*(6598), 330-332.

Tortell, P. D., G. H. Rau, and F. M. M. Morel (2000), Inorganic carbon acquisition in coastal Pacific phytoplankton communities, *Limnology and Oceanography*, *45*(7), 1485-1500.

Tosoh-Bioscience (2010), Process Media Products, http://www.separations.eu.tosohbioscience.com/Products/ProcessMedia/ByMode/AFC/ToyopearlAF-Chelate-650.htm.

Trautz, M., and P. Z. Schorigin (1905), Ueber Chemilumineszenz, *Wiss. Photog. Photochem.*, *3*, 121-130.

Trojanowicz, M. (2000), *Flow Injection Analysis: Instrumentation and Applications*, World Scientific Publishing, Singapore, 481 pp.

Tsuda, A., S. Takeda, H. Saito, J. Nishioka, Y. Nojiri, I. Kudo, H. Kiyosawa, A. Shiomoto, K. Imai, T. Ono, A. Shimamoto, D. Tsumune, T. Yoshimura, T. Aono, A. Hinuma, M. Kinugasa, K. Suzuki, Y. Sohrin, Y. Noiri, H. Tani, Y. Deguchi, N. Tsurushima, H. Ogawa, K. Fukami, K. Kuma, and T. Saino (2003), A mesoscale iron enrichment in the western Subarctic Pacific induces a large centric diatom bloom, *Science*, *300*(5621), 958-961.

Tsuda, A., S. Takeda, H. Saito, J. Nishioka, I. Kudo, Y. Nojiri, K. Suzuki, M. Uematsu, M. L. Wells, D. Tsumune, T. Yoshimura, T. Aono, T. Aramaki, W. P. Cochlan, M. Hayakawa, K. Imai, T. Isada, Y. Iwamoto, W. K. Johnson, S. Kameyama, S. Kato, H. Kiyosawa, Y. Kondo, M. Levasseur, R. J. Machida, I. Nagao, F. Nakagawa, T. Nakanish, S. Nakatsuka, A. Narita, Y. Noiri, H. Obata, H. Ogawa, K. Oguma, T. Ono, T. Sakuragi, M. Sasakawa, M. Sato, A. Shimamoto, H. Takata, C. G. Trick, Y. W. Watanabe, C. S. Wong, and N. Yoshie (2007), Evidence for the grazing hypothesis: Grazing reduces phytoplankton responses of the HNLC ecosystem to iron enrichment in the western subarctic pacific (SEEDS II), *Journal of Oceanography*, *63*(6), 983-994.

Turner, A., and G. E. Millward (2002), Suspended particles: Their role in estuarine biogeochemical cycles, *Estuarine Coastal and Shelf Science*, *55*(6), 857-883.

Tyrrell, T. (1999), The relative influences of nitrogen and phosphorus on oceanic primary production, *Nature*, *400*(6744), 525-531.

Tyrrell, T., E. Maranon, A. J. Poulton, A. R. Bowie, D. S. Harbour, and E. M. S. Woodward (2003), Large-scale latitudinal distribution of Trichodesmium spp. in the Atlantic Ocean, *Journal of Plankton Research*, *25*(4), 405-416.

Uchida, R., K. Kuma, A. Omata, S. Ishikawa, N. Hioki, H. Ueno, Y. Isoda, K. Sakaoka, Y. Kamei, and S. Takagi (2013), Water column iron dynamics in the subarctic North Pacific Ocean and the Bering Sea, *Journal of Geophysical Research-Oceans*, *118*(3), 1257-1271.

Ussher, S. J., E. P. Achterberg, and P. J. Worsfold (2004), Marine Biogeochemistry of Iron, *Environmental Chemistry*, *1*(2), 67-80.

Ussher, S. J., M. Yaqoob, E. P. Achterberg, A. Nabi, and P. J. Worsfold (2005), Effect of model ligands on iron redox speciation in natural waters using flow injection with luminol chemiluminescence detection, *Analytical Chemistry*, *77*(7), 1971-1978.

Ussher, S. J., P. J. Worsfold, E. P. Achterberg, A. Laes, S. Blain, P. Laan, and H. J. W. de Baar (2007), Distribution and redox speciation of dissolved iron on the European continental margin, *Limnology and Oceanography*, *52*(6), 2530-2539.

Ussher, S. J., E. P. Achterberg, C. Powell, A. R. Baker, T. D. Jickells, R. Torres, and P. J. Worsfold (2013), Impact of atmospheric deposition on the contrasting iron biogeochemistry of the North and South Atlantic Ocean, *Global Biogeochemical Cycles*, *in press*.

Vallee, B. L., and D. S. Auld (1990), Zinc Coordination, Function, and Structure of Zinc Enzymes and Other Proteins, *Biochemistry*, *29*(24), 5647-5659.

van Beek, P., M. Bourquin, J. L. Reyss, M. Souhaut, M. A. Charette, and C. Jeandel (2008), Radium isotopes to investigate the water mass pathways on the Kerguelen Plateau (Southern Ocean), *Deep-Sea Research Part Ii-Topical Studies in Oceanography*, *55*(5-7), 622-637.

Van den Berg, C. M. G. (1995), Evidence for Organic Complexation of Iron in Seawater, *Marine Chemistry*, *50*(1-4), 139-157.

van der Weijden, C. H., M. J. H. L. Arnoldus, and C. J. Meurs (1977), Desorption of metals from suspended material in the Rhine estuary, *Netherlands Journal of Sea Research*, *11*, 130-145.

Vega, M., and C. M. G. van den Berg (1997), Determination of cobalt in seawater by catalytic adsorptive cathodic stripping voltammetry, *Analytical Chemistry*, *69*(5), 874-881.

Veldhuis, M. J. W., and G. W. Kraay (2004), Phytoplankton in the subtropical Atlantic Ocean: towards a better assessment of biomass and composition, *Deep-Sea Research Part I-Oceanographic Research Papers*, *51*(4), 507-530.

Villareal, T. A., and E. J. Carpenter (1990), Diel buoyancy regulation in the marine diazotrophic cyanobacterium *Trichodesmium thiebautii*, *Limnology and Oceanography*, *35*(8), 1832-1837.

Vink, S., and C. I. Measures (2001), The role of dust deposition in determining surface water distributions of Al and Fe in the South West Atlantic, *Deep-Sea Research Part Ii-Topical Studies in Oceanography*, *48*(13), 2787-2809.

Vraspir, J. M., and A. Butler (2009), Chemistry of Marine Ligands and Siderophores, *Annual Review of Marine Science*, *1*, 43-63.

Warnken, K. W., D. G. Tang, G. A. Gill, and P. H. Santschi (2000), Performance optimization of a commercially available iminodiacetate resin for the determination of Mn, Ni, Cu, Cd and Pb by on-line preconcentration inductively coupled plasma-mass spectrometry, *Analytica Chimica Acta*, *423*(2), 265-276.

Watson, A. J., D. C. E. Bakker, A. J. Ridgwell, P. W. Boyd, and C. S. Law (2000), Effect of iron supply on Southern Ocean CO_2 uptake and implications for glacial atmospheric CO_2, *Nature*, *407*(6805), 730-733.

Watson, A. J., P. W. Boyd, S. M. Turner, T. D. Jickells, and P. S. Liss (2008), Designing the next generation of ocean iron fertilization experiments, *Marine Ecology Progress Series*, *364*, 303-309.

Webb, E. A., J. W. Moffett, and J. B. Waterbury (2001), Iron stress in open-ocean cyanobacteria (*Synechococcus*, *Trichodesmium*, and *Crocosphaera* spp.): Identification of the IdiA protein, *Applied and Environmental Microbiology*, *67*(12), 5444-5452.

Weeks, D. A., and K. W. Bruland (2002), Improved method for shipboard determination of iron in seawater by flow injection analysis, *Analytica Chimica Acta*, *453*(1), 21-32.

Welschmeyer, N. A. (1994), Fluorometric Analysis of Chlorophyll-a in the Presence of Chlorophyll-B and Pheopigments, *Limnology and Oceanography*, *39*(8), 1985-1992.

White, E. H., and M. M. Bursey (1964), Chemiluminescence of luminol and related hydrazides. The light emission step, *Journal of the American Chemical Society*, *86*, 941-942.

White, E. H., O. Zafiriou, H. H. Kägi, and J. H. M. M. Hill (1964), Chemiluminescence of luminol: the chemical reaction, *Journal of the American Chemical Society*, *86*, 940-941.

Wilhelm, S. W., A. L. King, B. S. Twining, G. R. LeCleir, J. M. DeBruyn, R. F. Strzepek, C. L. Breene, S. Pickmere, M. J. Ellwood, P. W. Boyd, and D. A. Hutchins (2013), Elemental quotas and physiology of a southwestern Pacific Ocean plankton community as a function of iron availability, *Aquatic Microbial Ecology*, *68*(3), 185-194.

Willie, S. N., J. W. H. Lam, L. Yang, and G. Tao (2001), On-line removal of Ca, Na and Mg from iminodiacetate resin for the determination of trace elements in seawater and fish otoliths by flow injection ICP-MS, *Analytica Chimica Acta*, *447*(1-2), 143-152.

Wilson, S. T., D. Bottjer, M. J. Church, and D. M. Karl (2012), Comparative Assessment of Nitrogen Fixation Methodologies, Conducted in the Oligotrophic North Pacific Ocean, *Applied and Environmental Microbiology*, *78*(18), 6516-6523.

Witt, M., A. R. Baker, and T. D. Jickells (2006), Atmospheric trace metals over the Atlantic and South Indian Oceans: Investigation of metal concentrations and lead isotope ratios in coastal and remote marine aerosols, *Atmospheric Environment*, *40*(28), 5435-5451.

Wolfe-Simon, F., D. Grzebyk, O. Schofield, and P. G. Falkowski (2005), The role and evolution of superoxide dismutases in algae, *Journal of Phycology*, *41*(3), 453-465.

Wong, G. T. F., S. C. Pai, and S. W. Chung (1995), Cobalt in the western Philippine Sea, *Oceanologica Acta*, *18*(6), 631-638.

Woodward, E. M. S., and A. P. Rees (2001), Nutrient distributions in an anticyclonic eddy in the northeast Atlantic Ocean, with reference to nanomolar ammonium concentrations, *Deep-Sea Research Part Ii-Topical Studies in Oceanography*, *48*(4-5), 775-793.

Wright, S. W., D. P. Thomas, H. J. Marchant, H. W. Higgins, M. D. Mackey, and D. J. Mackey (1996), Analysis of phytoplankton of the Australian sector of the Southern Ocean: Comparisons of microscopy and size frequency data with interpretations of pigment HPLC data using the 'CHEMTAX' matrix factorisation program, *Marine Ecology Progress Series*, *144*(1-3), 285-298.

Wu, J. F., E. Boyle, W. Sunda, and L. S. Wen (2001), Soluble and colloidal iron in the olgotrophic North Atlantic and North Pacific, *Science*, *293*(5531), 847-849.

Wyatt, N. J., A. Milne, E. M. S. Woodward, A. P. Rees, T. J. Browning, H. A. Bouman, P. J. Worsfold, and M. C. Lohan (2014), Biogeochemical cycling of dissolved zinc along the GEOTRACES South Atlantic transect GA10 at 40^{o} S, *Global Biogeochemical Cycles*, DOI: 10.1002/2013GB004637.

Xu, W. H., R. C. Sandford, P. J. Worsfold, A. Carlton, and G. Hanrahan (2005), Flow injection techniques in aquatic environmental analysis: Recent applications and technological advances, *Critical Reviews in Analytical Chemistry*, *35*(3), 237-246.

Xu, Y., L. Feng, P. D. Jeffrey, Y. G. Shi, and F. M. M. Morel (2008), Structure and metal exchange in the cadmium carbonic anhydrase of marine diatoms, *Nature*, *452*(7183), 56-U53.

Yamada, M., and Y. Nozaki (1986), Radium Isotopes in Coastal and Open Ocean Surface Waters of the Western North Pacific, *Marine Chemistry*, *19*(4), 379-389.

Yamada, M., T. Komatsu, S. Nakahara, and S. Suzuki (1983), Improved chemiluminescence determination of traces of cobalt(II) by continuous flow and flow injection methods, *Analytica Chimica Acta*, *155*(Dec), 259-262.

Yee, D., and F. M. M. Morel (1996), In vivo substitution of zinc by cobalt in carbonic anhydrase of a marine diatom, *Limnology and Oceanography*, *41*(3), 573-577.

Zagatto, E. A. G., C. C. Oliveira, A. Townshend, and P. J. Worsfold (2012), *Flow Analysis with Spectrophotometric and Luminometric Detection*, Elsevier, Massachusetts, Oxford, Amsterdam, 472 pp.

Zubkov, M. V., B. M. Fuchs, G. A. Tarran, P. H. Burkill, and R. Amann (2003), High rate of uptake of organic nitrogen compounds by Prochlorococcus cyanobacteria as a key to their dominance in oligotrophic oceanic waters, *Applied and Environmental Microbiology*, *69*(2), 1299-1304.